Soil moisture dynamics and evapotranspiration at the fringe of the Botswana Kalahari, with emphasis on deep rooting vegetation

Obolokile Thothi Obakeng

Cover page: Shows vegetation in the Kalahari and the escarpment area during the dry season.

VRIJE UNIVERSITEIT

Soil moisture dynamics and evapotranspiration at the fringe of the Botswana Kalahari, with emphasis on deep rooting vegetation

door

Obolokile Thothi Obakeng

geboren te Letlhakane, Botswana

Examining committee

Prof.dr.ir. R.A. Feddes (Wageningen Universiteit, The Netherlands)

Prof.dr. W.H.O. Ernst (Vrije Universiteit Amsterdam, The Netherlands)

Prof.dr. A.M.J. Meijerink (International Institute for Geo-information Science and Earth Observation, The Netherlands)

Dr. A. van de Griend (Vrije Universiteit Amsterdam, The Netherlands)

Dr. L.N. Molwalefhe (University of Botswana, Botswana)

To my mother

Preface and acknowledgements

This thesis study was undertaken within the framework of the Kalahari Research Project (KRP) that was initiated in September 2000 by the Botswana Geological Survey (BGS) and the International Institute for Geo-information Science and Earth Observation (ITC), in The Netherlands. The main objective of KRP project was spatio-temporal assessment of subsurface fluxes for better management of groundwater resources in the Botswana Kalahari. The project is a follow up of earlier studies which were undertaken by the Groundwater Recharge and Evaluation Study (GRES) projects. The GRES phase I project was conducted in the eastern part of Botswana from 1987-1992, and mainly concentrated on the quantification of recharge rates and associated processes in areas where the Precambrian Basement is exposed or close to the surface (Gieske, 1992). The GRES phase II project was conducted in the part of Botswana covered by Kalahari sediments from 1992-1997, and was mainly focused on improving the understanding of groundwater recharge mechanisms in areas with thick sand cover and deep groundwater tables (Selaolo, 1998). Both the GRES I and II projects were joint ventures of the BGS, Vrije Universiteit Amsterdam (VUA) and University of Botswana (UB).

The present study is an initiative of BGS that was carried out by BGS and ITC, with the scientific assistance of the Vrije Universiteit Amsterdam (VUA). I am grateful to all organizations for all the support that was given to me. I am particularly indebted to the following persons for providing much needed assistance in various ways during my thesis work and in the general project implementation;

- Prof. dr. J.J. de Vries (Promotor) was always responsive to my work and I am very grateful for his advice on my thesis work. During his visit to my study area, he always entertained me with many stories.
- Dr. ir. M. Lubczynski (Co-promotor) gave valuable technical and scientific assistance on my draft manuscripts. He also contributed in the design and set-up of the monitoring network within the framework of the KRP.
- Prof. dr. A.M.J. Meijerink for initiating the KRP project and his valuable scientific advice. I will always remember his comments regarding the difficulty of dealing with unsaturated zone processes.
- Prof. dr. Z. Su for monitoring the progress of my thesis work and giving valuable scientific advice.
- Dr. A. van de Griend for his advice on meteorological aspects of my thesis work.

Table of Contents

vi

Abbreviations and Acronyms

ADAS	Automated Data Acquisition System
AGTR	Automated Groundwater Table Recorders
BGS	Botswana Geological Survey
BNWMPR	Botswana National Water Master Plan Review
BRGM	*Bureau de Recherches Geologiques et Minieres*
BSEB	Bowen ratio-Surface Energy Balance approach
BUF	Biometric Upscaling Functions
CTO	Central Transport Organisation
CK-MWL	Central Kalahari Meteoric Water Line
CSIR	Council for Scientific and Industrial Research
DK	Superficial deposit or Kalahari beds
DMS	Department of Meteorological Services
EARTH	Extended model for Aquifer Recharge and soil moisture Transport through the unsaturated Hard rock
G-MWL	Global Meteoric Water Line
GRES	Groundwater Recharge and Evaluation Study
ITC	International Institute for Geo-information Science and Earth Observation
ITCZ	Inter-Tropical Convergence Zone
KRP	Kalahari Research Project
LB	Letlhakeng-Botlhapatlou
LINRES	Linear reservoir
m a. g. s	m above ground surface
m a. s. l.	m above sea level
m b. g. s.	m below ground surface
mp	matric pressure
NS	Ntane sandstone
NTG	Natural Thermal Gradient

P-M	Penman-Monteith
PWP	permanent wilting point
QUADRU	Quaternary Dating Research Unit
RH/T	Relative humidity and temperature
SB	Stormberg basalt
SGC	Swedish Geological Company
TDP	Thermal Dissipation Probe
TNO	*Nederlandse Organisatie voor toegepast- natuurwetenschappelijk onderzoek*
TP	Temperature Profile
TSEB	Temperature profiles-Surface Energy Balance
UB	University of Botswana
UP	*Umweltanalytische Produkte*
V-SMOW	Vienna Standard Mean Ocean Water
VUA	Vrije Universiteit Amsterdam
WCS	Wellfield Consulting services
WTF	Water Table Fluctuation

List of Frequently used Symbols

Symbol	Interpretation	Units/Dimensions
AET	actual evapotranspiration	$[LT^{-1}]$ or
		$(MJ\ m^{-2}day^{-1})$
α	albedo	$[-]$
α_c	reaction factor or reservoir outflow	
	recession constant	$[T^{-1}]$
α_d	adiabatic lapse rate	$(k\ m^{-1})$
A_C	projected ground area of	
	tree crown	$[L^2]$
A_p	plot area	$[L^2]$
A_s	stem area	$[L^2]$
$A_s{}^p$	plot-total stem area	$[L^2]$
$A_c{}^p$	plot-total crown area	$[L^2]$
A_x	sap wood area	$[L^2]$
B^{-1}	dimensionless inverse	
	Stanton number	$[-]$
β	Bowen ratio	$[-]$
C_p	specific heat capacity of air	$(kJ\ Kg^{-1}\ ^oC^{-1}$
		or $J\ Kg^{-1}\ ^oC^{-1})$
C_s	heat capacity per unit	
	volume of soil	$(MJ\ m^3\ ^oC^{-1})$
d_o	zero plane displacement height	$[L]$
ΔW	change in vadose zone storage	$[L]$
Δ_T	rate of change of the saturation	
	vapour pressure with temperature	$(kPa\ ^oC^{-1})$

Symbol	Interpretation	Units/Dimensions
D_L	distance between the divide and the drainage base	[L]
Δh	recharge related change in water table height	[L]
Δt	time interval	[T]
ΔT	temperature difference between two sensor probes	(^{o}C)
ΔT_{max}	maximum temperature difference between two probes	(^{o}C)
E	vapour flux density	(Kg m^{-2} s^{-1})
e_a	actual vapour pressure	(kPa)
e_s	saturation vapour pressure	(kPa)
E_s	soil or surface evaporation	[LT^{-1}]
ET	evapotranspiration	[LT^{-1}]
ε	ratio of molecular weight of water vapour to that of dry air	[-]
g	acceleration due to gravity	[LT^{-2}]
G_o	soil heat flux	(Wm^{-2} or MJ m^{-2} day^{-1})
H	sensible heat flux	(W m^{-2} or MJ m^{-2} day^{-1})
$\bar{h}$	average head above the discharge base at the divide	[L]
h_{eff}	effective height of roughness elements	[L]
h_v	vegetation height	[L]
I	interception	[LT^{-1}]
I_c	intercerption capacity	[L]
k	von Karman's constant	(-)

x

Symbol	Interpretation	Units/Dimensions
kB^{-1}	excess resistance to heat transfer	[-]
K_s	saturated hydraulic conductivity	$[LT^{-1}]$
L	Monin-Obukhov length	[L]
$L{\downarrow}$	down-welling longwave radiation	(W m^{-2} or MJ m^{-2} day^{-1})
$L{\uparrow}$	up-welling longwave radiation	(W m^{-2} or MJ m^{-2} day^{-1})
LAI	leaf area index	(-)
λ	latent heat of vaporization of water	(J Kg^{-1} or MJ Kg^{-1})
λE	latent heat flux	(W m^{-2} or MJ m^{-2} day^{-1})
λE_p	total latent heat for potential evapotranspiration	(MJ m^{-2} day^{-1})
MSE	mean square error	$[L^2T^{-1}]$
n	number of observations	[-]
n_o^p	total number of trees per species and per plot	[-]
n_r	number of reservoirs	[-]
P	rainfall	$[LT^{-1}]$
P_α	atmospheric pressure	(kPa)
PET	potential evapotranspiration	$[LT^{-1}]$ or (MJ m^{-2}day^{-1})
ρ	air density	(Kg m^{-3})
ρ_a	mean air density at constant pressure	(Kg m^{-3})

Symbol	Interpretation	Units/Dimensions
Q_s	sap flow	$[L^3T^{-1}]$
Q_n	normalised sap flow	$[LT^{-1}]$
γ	psychrometric constant	(kPa °C^{-1})
Ψ_s	soil matric pressure	(kPa or bar)
ψ_h	stability correction function for heat transfer	[-]
ψ_m	stability correction function for momentum transfer	[-]
γ_d	specific groundwater drainage resistance	[T]
q_d	groundwater discharge	$[LT^{-1}]$
q_r	groundwater recharge	$[LT^{-1}]$
r	correlation coefficient	[-]
r_a	aerodynamic resistance	$[TL^{-1}]$
RH	relative humidity	(%)
RH_{min}	daily minimum relative humidity	(%)
RH_{max}	daily maximum relative humidity	(%)
r_s	surface resistance	$[TL^{-1}]$
R^2	coefficient of determination	[-] or (%)
R_i	Richardson number	[-]
R_l	ratio of the heavy isotope to the light isotope in a sample	[-]
R_n	net radiation	(W M^{-2} or MJ m^{-2} day^{-1})
R_{nl}	net longwave outgoing radiation	(MJ m^{-2} day^{-1})
R_s	measured solar radiation	(MJ m^{-2} day^{-1})
R_{so}	calculated clear-sky radiation	(MJ m^{-2} day^{-1})
R_{std}	ratio of the heavy isotope to the light isotope in V-SMOW	[-]

Symbol	Interpretation	Units/Dimensions
S	storage coefficient	[-]
S_y	specific yield	[-]
$S\downarrow$	down-welling shortwave radiation	(W M^{-2} or MJ m^{-2} day^{-1})
$S\uparrow$	up-welling shortwave radiation	(W m^{-2} or MJ m^{-2} day^{-1})
S_{fc}	soil moisture at field capacity	[L]
S_i	initial soil moisture content	[L]
S_m	maximum soil moisture content	[L]
S_r	residual soil moisture content	[L]
SRC	soil retention capacity	[L]
$SUST_{max}$	maximum surface storage	[L]
σ	Stefan-Boltzmann constant	(MJ K^{-4}M^{-2} day^{-1})
t	time	[T]
t_{da}	duration of water level rise	[T]
t_{dr}	duration of the recession	[T]
T	temperature	(^{o}C)
T_a or T_a	air temperature	(^{o}C or ^{o}K)
T_g	transpiration due to grass	[LT^{-1}]
T_{min}	minimum daily temperature	(^{o}C or ^{o}K)
T_{max}	maximum daily temperature	(^{o}C or ^{o}K)
T_p	tree transpiration or plot tree transpiration or plot level tree transpiration	[LT^{-1}]
T_s	surface temperature	(^{o}C)
T_{sat}	transpired water from the saturated zone	[LT^{-1}]
T_{sh}	transpiration due to shrubs	[LT^{-1}]

Symbol	Interpretation	Units/Dimensions
T_{sp}	species plot transpiration	$[LT^{-1}]$
T_{ss}	average regional transmissivity	$[L^2 T^{-1}]$
T_u	transpired water derived from vadose zone	$[LT^{-1}]$
T_v	mean air temperature near the surface	$[^oC]$
τ_o	surface shear stress	$(N\ m^{-2})$
θ_o	potential temperature at the surface	$[^oK]$
θ_a	potential temperature at height z	$[^oK]$
θ_s	volumetric soil moisture content	$[L^3 L^{-3}]$
u	wind speed	$[LT^{-1}]$
u_z	wind speed at z above the canopy	$[LT^{-1}]$
u_*	friction velocity	$[LT^{-1}]$
v	sap velocity	$[LT^{-1}]$
WS	wind speed	$[LT^{-1}]$
z	measurement height above the canopy	$[L]$
z_{oh}	roughness length for heat transfer	$[L]$
z_{om}	roughness length for momentum transfer	$[L]$
z_s	soil depth which responds to temperature change	$[L]$
Z	elevation above sea level	$[L]$

Chapter 1 General introduction

1.1   General framework

Botswana lies in the centre of the Southern African Plateau at a mean altitude of 1000 m above sea level (m a.s.l.). The Botswana Kalahari is a tectonic basin filled with unconsolidated sandy deposits of Cretaceous to recent age, which extends over 75% of Botswana representing nearly 500 000 km^2 of total surface area (Scholes et al., 1997). In the northwest Kalahari, the Okavango River drains inland from Angola into an extensive swamp area (Okavango delta; see Figure 1.2), but the remaining part is characterized by the absence of perennial water at the surface; flooding of dry valleys and depressions (pans) only occurs after heavy rainfall. Groundwater is mainly found in the Karoo rocks (sandstones, shales and basalts) below a mantle of Kalahari sand that ranges in thickness from 20 m near the fringe of the Kalahari to more than 100 m towards the centre. The groundwater tables more or less follow the top of the Karoo sediments and thus also range from depths of 20 m to more than 100 m. The main regional groundwater flow is from the water divide in the southwest at a surface elevation of 1250 m towards the lowest depression called the Makgadikgadi pans, some 600 km in north-easterly direction, with a surface elevation of 925 m. Thus, the regional hydraulic gradient is very small. No forms of groundwater outcrops exist under the current climate. Therefore, the Kalahari as such forms an almost closed basin with an internal groundwater drainage system at the Makgadikgadi pans. The Kalahari sandy deposits under present climatic conditions do not form extensive aquifers. Instead, perched water bodies occur locally in areas with large pans, which are associated with episodic ponding and rapid infiltration through fractured duricrusts.

Despite a moderate rainfall of about 400 mm/yr (on average) and the scarcity of surface water, the Kalahari supports extensive savanna vegetation that consists of shrubs, grass and trees. This can be explained by the combination of a high infiltration capacity and a high retention storage in the upper sandy sediments. This means that

almost all rainwater is taken up by the vegetation and therefore recharge to the deep aquifers is only a small proportion of the total precipitation. True desert conditions that are characterised by sparse vegetation and unstable moving sands are prevalent in the south-western part of Botswana where rainfall is in the order of 250 mm/yr. The annual potential evapotranspiration[1] amounts to 1350-1450 mm (Choudhury, 1997) whereas the actual evapotranspiration[2] has never been directly assessed, but could, of course, be not much less than the rainfall on an annual basis. A comprehensive account of the Kalahari environment is given by Thomas and Shaw (1991).

The Botswana National Water Master Plan Review estimates that 65% of Botswana's water supply depends on groundwater resources (BNWMPR, 2006: vol. 2). Most of the investigations on groundwater resources evaluation in Botswana have largely concentrated in the eastern part, where the majority of the people live (e.g. Farr et al., 1981; the Swedish Geological Company (SGC), 1988; the Bureau de Recherches Geologiques et Minieres (BRGM), 1991; BRGM, 1993 and Wellfield Consulting services (WCS), 1998). More recently, the Kalahari has come under increased pressure from land use change driven by technology, government policies and human and livestock population growth (Arntzen et al., 1996). Borehole drilling and pastoral policies have opened up the Kalahari to livestock farming outside wildlife management areas. Therefore, it is without doubt, that water is vital to the development of Botswana, most of which must be derived from groundwater, since surface water resources are scarce (Gaabake, 1997). In light of this, it is therefore imperative to undertake groundwater resources studies that do not only emphasize on exploration and assessment of available resources, but should also pay attention to the evaluation of the dynamics of groundwater recharge and groundwater discharge, as well as on the water use by the vegetation.

---

[1] *Potential evapotranspiration* refers to the maximum evaporative loss under existing atmospheric conditions when water supply is not limited.
[2] *Actual evapotranspiration* refers to the rate of evapotranspiration that depends on the prevailing moisture regimes in the soil, vegetation development and atmospheric conditions.

Groundwater recharge as used in this study is defined as water that passes through the unsaturated zone and reaches the groundwater table. The groundwater discharge as used in this study is the regional outflow to the drainage base. This groundwater discharge thus equals net groundwater recharge and represents the maximum amount of water that can be used in a sustainable way. Net groundwater recharge is the groundwater recharge minus any groundwater extraction by deep rooting vegetation and/or upward liquid/vapour flow of water from the aquifer (i.e. losses that occur subsequent to infiltration to the groundwater). The definitions are illustrated in Figure 1.1.
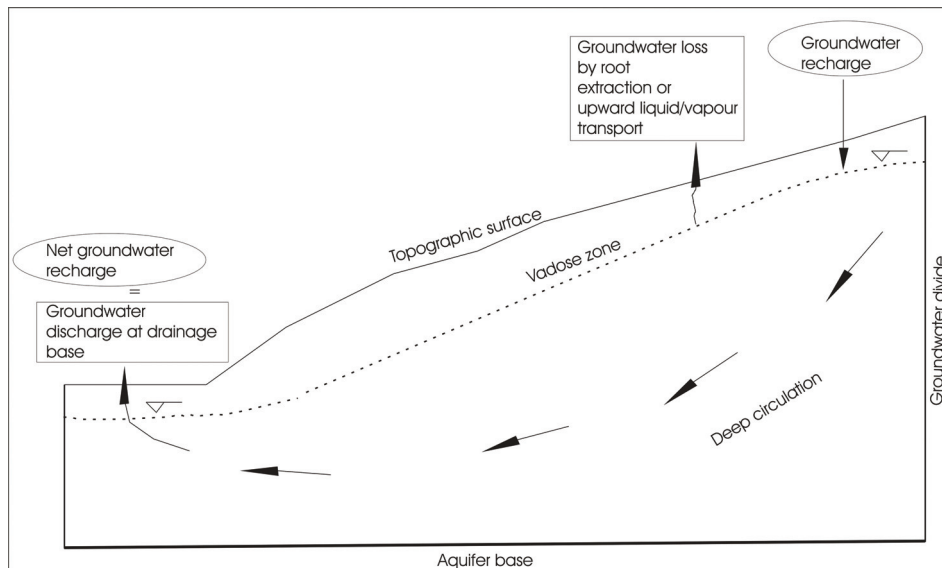
Figure 1.1: A schematic diagram illustrating groundwater recharge and groundwater discharge as defined in this study

Groundwater recharge and discharge in arid and semi-arid regions are usually very low and therefore difficult to assess. A simple estimation of groundwater recharge as the difference between rainfall and evapotranspiration in semi-arid regions is normally not suitable since the amount of groundwater recharge is much smaller than the collective errors in rainfall and evapotranspiration determinations.

The occurrence of groundwater recharge from rainwater by infiltration through the Kalahari sediments has been a controversial issue for more than hundred years (Selaolo, 1998). Some investigators concluded that virtually no rain recharge was occurring in the Kalahari, because of "seasonal moisture retention in the sands and complete loss by subsequent evapotranspiration" (Van Straten, 1955; Foster et al., 1982; De Vries and Von Hoyer, 1988). De Vries (1984) further substantiated this view through a numerical study of declining regional groundwater levels since the last pluvial period (12 000 yr. ago) and concluded that present day discharge was at most 1 mm/yr and could (partly) be explained as residual from an earlier pluvial period. According to this viewpoint, the present day recharge is either in equilibrium with current discharge of about 1 mm, or is less so that groundwater could be subjected to continuous depletion under present day climatic conditions. However, increasing evidence of the occurrence of substantial rain recharge through the Kalahari sands emerged from a variety of tracer studies such as Jennings (1974), Mazor et al. (1974), Verhagen et al. (1974), Mazor et al. (1977), Mazor et al. (1982), Verhagen (1990), Selaolo (1998), De Vries et al. (2000), Obakeng (2000) and more recently by Magombedze et al. (2004). However, there seems to be a discrepancy between this substantial recharge and the discharge, due to the absence of visible discharge areas in the Kalahari and the low regional discharge flow (outflow) to Makgadikgadi drainage base (De Vries, 1984). The paramount question thus is: *What happens to the substantial recharge, since the regional discharge flow is low and there are no visible discharge areas in the Kalahari? Could (as hypothesised by De Vries et al., 2000) groundwater be removed from the saturated zone through extraction by deep rooting trees?*

1.2   Scope of the study

The study area (also referred to hereafter as Serowe area) is located in the Central District (S 22°16.992', E 26°39.283') region of Botswana, at the eastern fringe of the Kalahari basin. It covers a total area of about 2693 km^2 and receives an average annual rainfall in the order of 440 mm. The main reason for the choice of Serowe as a pilot area is the accessibility of the area, and the availability of existing

information on meteorology, geology and hydrogeology as background to the data acquisition for the present study.

To solve the question of the fate of the water that percolates through the unsaturated zone and the groundwater recharge, the present study focuses on: (1) the investigation of rooting depths and water extraction by common Kalahari trees and (2) the seasonal behaviour of the different components of the water balance.

1.2.1 Research objectives

The main objective of this study is to explore if soil water and groundwater can possibly be extracted by deep rooting trees, from below the main root zone. This main root zone stretches to a depth of 4 m and forms a zone with extensive exchange of infiltrating rainwater and evapotranspiration. The question thus is whether percolating water that has escaped from evapotranspiration in this zone, might be subsequently subjected to water extraction through deep rooting trees, so that the flux to the groundwater table (groundwater recharge) could be higher than the resulting regional groundwater discharge.

To resolve this problem, the following steps were undertaken:

1. An investigation to establish if the roots of Kalahari tree species can reach great depths; tracers (lithium chloride) were injected at various depths, up till 73 m and subsequently (in consecutive days) small tree branches (twigs) and leaves were analysed to verify if the trees extracted water labelled with lithium chloride from the deep horizons.
2. Sap flow measurements were carried out in various deep rooting tree species (including some tree species that were investigated in step one), to determine transpiration.
3. The distribution of stable water isotope concentrations in sap (xylem water), in the unsaturated zone water and groundwater were analysed; in an attempt to detect the zones from which the deep rooting trees extract their water throughout the season.

5

Closely related to the main objective, actual evapotranspiration (AET), potential evapotranspiration (PET), rainfall, soil moisture regime and groundwater level fluctuations were monitored and analysed to obtain information on regional and seasonal behaviour and variability of the different components of the water balance.

1.2.2 Methods and instruments

In order to achieve the study objectives the following methods and instrumentation were used in the Serowe area.

1. The rooting depth investigation using the artificial tracer was undertaken at 18 experimental (drill-holes) sites in which 19 Kalahari trees belonging to seven tree species were sampled and analysed to ascertain if the water and tracer has been taken up at various depths.
2. Sap velocity was monitored continuously in 41 trees from November 2001 to January 2004 using sap flow sensors at seven sites. At these seven sites data acquisition was maintained and stored by data loggers. The monitored 41 trees represented nine species. The obtained sap velocity measurements were up-scaled into eight randomly selected 30 by 30 m plots to give an estimation of areal transpiration by trees.
3. Sampling for isotopes of xylem water and groundwater was undertaken at four experimental sites within the framework of the present study. In total there were six tree species sampled for xylem water extraction. Additionally, soil samples were collected to various depths ranging from 3.1- 10.1 m at the four experimental sites.
4. To obtain information and data for various components of the water balance a hydrological monitoring network was established between 2001 and 2003 in the study area. Ten monitoring sites consisting of various instruments such as rain gauges, anemometers, relative humidity and temperature sensors were established. Out of the ten sites only three sites were equipped with radiometers. Additionally, soil heat flux and soil temperature were also monitored at four of the ten monitoring sites. Soil moisture was continually being monitored at various depths using

soil moisture sensors at seven of the ten monitoring sites. Additionally, soil matric pressure was continually monitored at eight locations using *gypsum* blocks and in one location using *watermark* sensors. In all cases the data acquisition was controlled and stored by data loggers. Groundwater level monitoring was carried out at 17 boreholes equipped with automated groundwater table recorders between September 2001 and March 2005.

1.3   Outline of chapters

Chapter 1:   gives a general introduction of the thesis work and study area.

Chapter 2:   focuses on the spatial and temporal distribution of rainfall within the study area.

Chapter 3:   describes the spatial and temporal variability of evapotranspiration in the study area.

Chapter 4:   assesses the long term spatial and temporal variability of tree transpiration in eight selected plots across the study area.

Chapter 5:   discusses rooting depth investigation of savanna vegetation (mainly trees) using lithium as a chemical tracer.

Chapter 6:   focuses on the determination of the origin of water used by savanna vegetation using the stable environmental isotopes ^{2}H and ^{18}O.

Chapter 7:   presents the dynamics of soil moisture and groundwater levels, and presents a tentative approach of groundwater recharge in the study area on the basis of the observations of evapotranspiration and groundwater levels.

Chapter 8:   gives a summary and conclusions of the study.

1.4   Description of the study area

1.4.1 Geomorphology, topography, climate and vegetation

The selected Serowe study area consists of two contrasting parts: the Kalahari sandveld, to the west, and the hardveld, to the east. (Figure 1.2). The two parts are divided by a prominent, geomorphic, escarpment feature that represents the eastern limit of the Kalahari sand (Smith, 1984). The sandveld part slopes gently to the west, and is fairly flat and featureless without prominent drainage lines. In contrast, the hardveld slopes steeper to the east and there is a drainage system indicating courses of ephemeral streams, discharging water mainly after heavy showers. The present study mainly refers to the western sandveld; the Kalahari proper.

Rocks of the Karoo formations (sandstone, shale and basalt) at the western sandveld area are overlain by 60-100 m of Kalahari sand cover, whereas the eastern hardveld area is covered by only 0-5 m of superficial deposits. Rock outcrops are found mainly at the escarpment and along river valleys below the escarpment. Elsewhere Kalahari sands and superficial deposits overlie rocks.

The mean annual temperature is 20 ^{o}C. The summer temperatures can be in excess of 30 ^{o}C during the day, whilst winter temperatures can drop to below 0 ^{o}C at night. The long-term daily rainfall record since 1925 from Serowe meteorological station indicates high annual rainfall variation, ranging from 119-970 mm/yr, with a mean annual figure of 437 mm (see Chapter 2).The rainy season is between October and April, when ambient temperatures are at their highest values and rainfall occurs in the form of isolated, high intensity storms which produce a substantial proportion of the annual rainfall. These infrequent storms often constitute the principal source of groundwater replenishment in the study area. The dry winter season begins in May and ends in August.
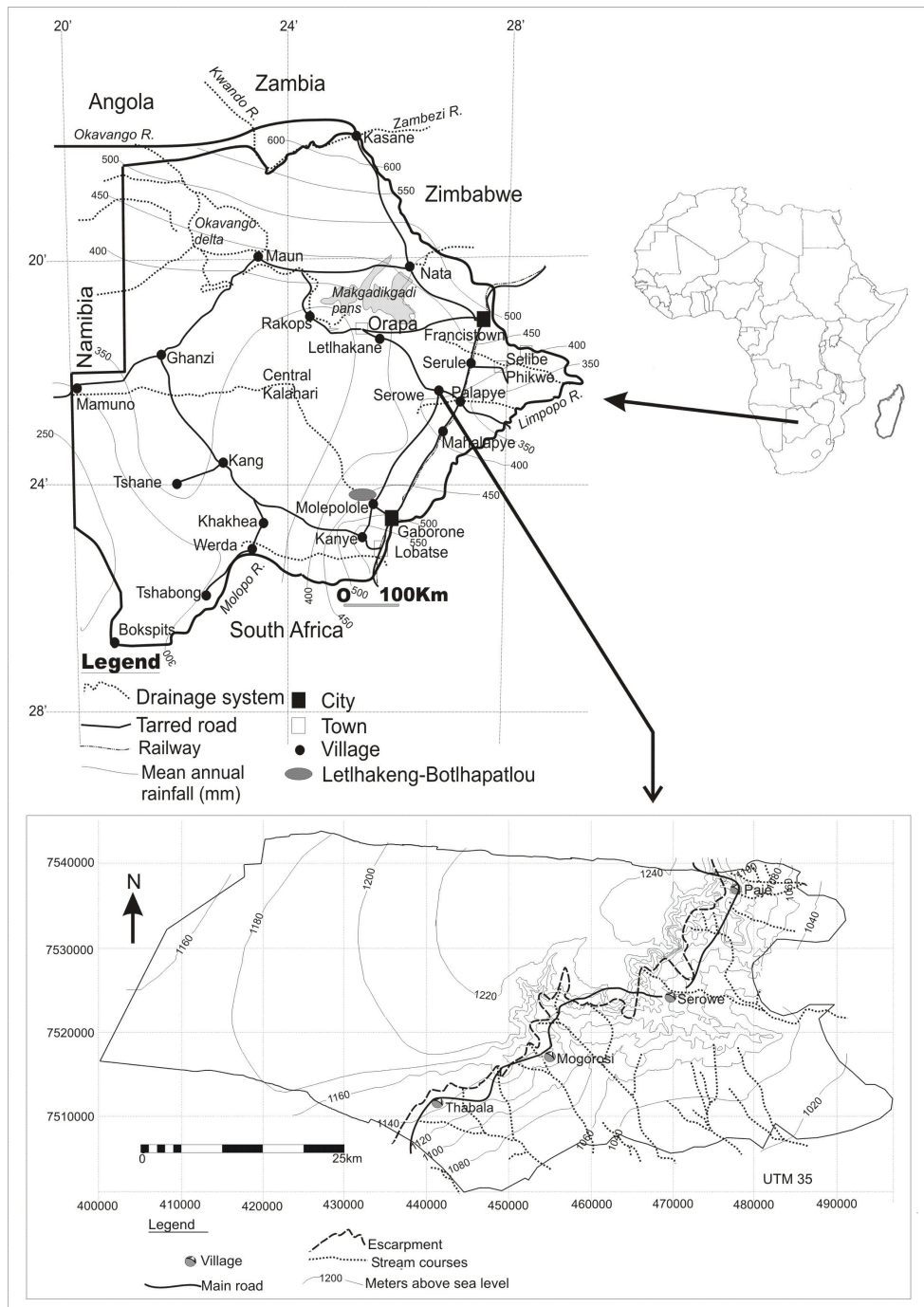
Figure 1.2. Location of the study area; (rainfall distribution after Bhalotra, 1987)

The hardveld is dominated by acacia savanna type of vegetation, which can vary from dense shrubland to tree savanna. The Kalahari sandveld is represented by open savanna vegetation type, characterized by continuous grass and a discontinuous sparse tree and bush cover. It is noticeable that in the eastern area, vegetation remains green even at the peak of the dry season in contrast to the western part, which is generally dry except for sparse evergreen trees. This perhaps stems from shallow groundwater tables (<20 m) found along the drainage lines and the possible existence of deeply rooted trees (Jennings, 1974).

The sandveld area is quite flat and is dominated by free draining coarse to loamy fine Kalahari sands with high permeability, high infiltration rate and high retention storage capacity because of the thick sand layer. Therefore surface runoff is negligible. In the hardveld part, the surface runoff is more pronounced due to the relief, rock outcrops and less permeable soils enriched in clay materials that originated from weathering of basalt and dolerite outcrops. Surface runoff only occurs after heavy rainfall events or relatively long-term periods of precipitation.

Within the Serowe study area, Ecosurv Botswana (1998) and Hernandez (2002) identified 4-10 vegetation communities. The western part of the study area (sandveld) is quite homogeneous with regard to species composition. Species such as *Acacia fleckii, Boscia albitrunca, Burkea africana, Ochna pulchra, Securidaca longipedunculata* and *Terminalia sericea* are strongly represented there. In the eastern part of the study area (hardveld) the vegetation is generally taller particularly along and in the vicinity of river courses and depressions. Species such as *Acacia karoo, Acacia tortilis, Acacia mellifera and Ziziphus mucronata* are widespread in the hardveld. At the escarpment edge where vegetation is taller, denser and more diverse than in the rest of the study area, species like *Combretum apiculatum, Croton gratissimus* and *Ricinodendron rautanenii* are strongly represented. Species such as *Acacia erioloba, Combretum apiculatum, Dichrostachys cinerea, Grewia retinervis, Lonchocarpus nelsii* and *Terminalia sericea* are found everywhere across the study area.

The description of the tree species is given by Coates-Palgrave (2002).

1.4.2 Geology

The geology of Botswana, including that of the Serowe area, is described in detail by Carney et al. (1994), of which most of it, is based on geophysical interpretations and cores from exploration works. This is mainly due to the absence of surface outcrops created by an extensive Kalahari sediment cover. The geological succession for the study area is summarized in Table 1.1.

Pre-Karoo strata

Archean Basement rocks of the study area consist of an assemblage of gneisses, migmatites and other plutonic rocks with varying degrees of foliation. Outcrops of the Palapye Group rocks belonging to the Proterozoic Shoshong Formation strata are found east of Serowe village, where they are represented by quartzites, siltstones, shales and sandstones with various shades of grey and pink colours. Pre-Karoo and post Palapye Group intrusions occur as coarse grained dolerite dykes which intruded into the Palapye Group or Basement rocks.

Karoo strata

The Dwyka Group is a basal unit of the Karoo Supergroup in southern Africa (Carney et al., 1994), which was deposited during a Permo-Carboniferous glacial episode. It consists of tillites and fine laminated mudstones that were deposited on a pre-Karoo topography. It is represented by the Dukwi Formation in the study area. As a result of the great depths of burial and the lack of borehole evidence, little is known about the hydrogeological characteristics of this lowermost unit of the Karoo.

The Ecca Group is mainly composed of sandstone, mudstones and carbonaceous shales that were deposited in lakes and deltas after the retreat of Dwyka glaciers. During Ecca deposition, plants colonised

inland sea shores in which coal seams developed (Carney et al., 1994).

Table 1.1. Lithostratigraphy of the study area (adapted from WCS, 1998)

Age	Supergroup	Group	Formation	Lithological descriptions
Cainozoic		Kalahari	Kalahari beds	Sand, silt, clay and duricrust
Mesozoic	Karoo	Stormberg Lava		Crystalline, massive, amygdaloidal basalts
Upper Palaeozoic		Lebung	Ntane	Aeolian sandstone, medium to fine grained with minor mudstone intercalations, white, pink, red, brown, grey, green, yellow, partially fluviatile towards base
			Mosolotsane	Fluvial red beds, siltstones, fine grained sandstone, red mudstones
		Beaufort	Thabala	Non-carbonaceous mudstones and siltstones with minor sandstones
		Ecca	Serowe	Carbonaceous mudstones, coals,siltstones, coally carbonaceous mudstones, fine sandstone
			Morupule	Coal seams, black carbonaceous mudstone, subordinate non-carbonaceous mudstones
			Kamotaka	White, massive, coarse to medium grained sandstone, subordinate siltstones, micaceous
			Makoro	Post glacial lacustrine mudstones and siltstones marking the base of Ecca Group
		Dwyka	Dukwi	Base of Karoo sequence, tillites and shales, varved siltstones and mudstones
Proterozoic		Palapye	Shoshong	Dolerite, siltstones,Shales and quartzite
Archean		Basement		Granite, gniess and amphibolite

Within the study area, the Ecca is represented by four formations, listed from old to young, they are: Makoro, Kamotaka, Morupule and

Serowe formations. Makoro Formation largely consists of non-carbonaceous, silty mudstones with micas becoming more abundant at the base of the formation whereas its upper part is comprised of interbedded fine-grained sandstone and mudstone. The Kamotaka Formation is characterized by massive feldspathic sandstone with minor micas, and mudstone clasts and conglomeratic bands that occurs locally at its base. In addition, sedimentary structures such as cross bedding and graded beds are also common in the formation. The Morupule Formation is largely made up of coal seams and carbonaceous mudstones. The Serowe Formation is the uppermost unit of the Ecca in the study area. It is for most part siltstones, fine-grained sandstones, carbonaceous mudstones with thin dull and bright coal lenses that follows conformably from the Morupule Formation. Few boreholes intersect the Ecca within the study area, and as such their hydrogeological significance will not be treated in the current study.

The Beaufort Group is represented by the Thabala Formation in the investigation area. It consists mainly of massive non-carbonaceous silty mudstones with minor coal streaks, calcareous mudstones and bands of concretion nodules.

The sediments of the Lebung Group represent the end phase of the Karoo sedimentation and suggest a progression from a lacustrine deposition to alluvial fan (Thomas and Shaw, 1991). The Lebung is made up of the Mosolotsane and Ntane formations. The Mosolotsane Formation consists of red (or grey) fine grained sandstone, siltstone and mudstone often with a conglomerate at its base. The Ntane Formation consists of fine to medium grained light brown to light orange sandstone. The Ntane is usually friable and poorly cemented except where it has been subjected to contact metamorphism. Therefore, it is sometimes difficult to differentiate it from Kalahari sand. Its thickness is highly variable in the study area, with an average total thickness of about 70-100 m (Swedish Geological Company (SGC), 1988).

A division in the Ntane Formation is usually made between the upper more arenaceous Massive Member and the lower more argillaceous

Transition Member. Outcrops of the Ntane sandstone occur where gully erosion has removed most of the overburden in the eastern part of the study area.

Above the Ntane are tholeiitic basalt lavas, which belong to the Stormberg Group. The thickness of the basalt is highly variable as a result of uneven Ntane topography on which it was extruded; thickness ranges from about 10 to greater than 40 m in the study area. Fresh surface exposures are mainly confined to river courses in the eastern part of the escarpment. West of the escarpment basalt occurrence beneath the Kalahari sediments was revealed by the aeromagnetic method (which is regarded as a suitable geophysical method for revealing basalt by virtue of its magnetic susceptibility).

Post Karoo strata

The Karoo rocks are mostly overlain by Kalahari Group sediments in most parts of Botswana (Farr et al., 1981) that comprise a sequence of predominantly terrestrial sediments of Cretaceous to recent age. The Kalahari deposits are of aeolian to fluvio-deltaic and lacustrine nature. Lithologies of the Kalahari beds consist of conglomerates, gravels, sandstones, mudstones, siltstones and duricrusts (calcretes, ferricretes and silcretes). The overall thickness of the Kalahari is extremely variable, ranging from about 60-100 m in the Serowe area.

Additionally, post Karoo dolerite dykes are known to occur within the study area, most of which have been emplaced along WNW-ESE trending faults (refer to Figure 1.3).

1.4.3 Hydrogeology

Groundwater occurrence and aquifer description

The hydrogeology of the study area has been extensively investigated by SGC (1988) and Wellfield Consulting Services (WCS), 1998. Their reports indicate that majority of boreholes in the study area penetrate the Kalahari succession and terminate in the upper Karoo rocks (Basalt, Ntane and Mosolotsane) e.g. boreholes 4743, 5309, 5310,

14

5336 etc. (refer to Figure 1.3). Duricrust horizons buried within the Kalahari sands can also promote lateral moisture fluxes as opposed to vertical fluxes, and as such may initiate surface runoff, and when situated at relatively shallow depths may create, good chances for moisture escape by evapotranspiration, thereby resulting in reduced replenishment to the underlying aquifers. On the other hand, fractured and dissolved calcrete facilitate fast infiltration and concentrated recharge. In combination with pans, this can result in perched aquifers (Dekker et al., 1997).

At the sandveld area the groundwater table is deep, ~60-100 m below ground surface (m b. g. s.); at the hardveld area depths are much shallower being ~8-40 m b. g. s. At the eastern side of the escarpment line as well as along the drainage lines at the eastern hardveld, the groundwater table is shallowest (<20 m). The majority of the villages in the study area are concentrated along this eastern edge of the escarpment (see Figure 1.2) where until some decades ago, springs were supplying water to the habitants.
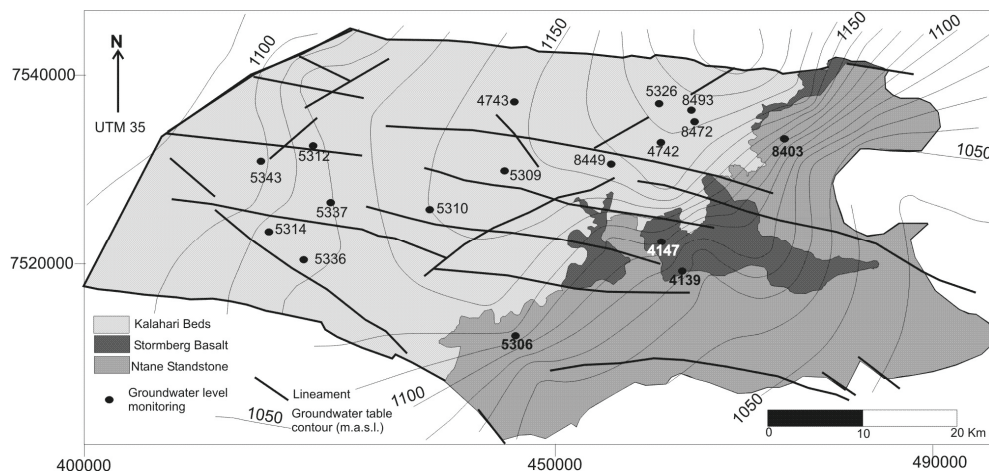
Figure 1.3. Geology, piezometric map and location of groundwater level monitoring points in the study area

The Ntane Formation (mainly sandstone) is regarded as a principal aquiferous unit, favoured by its primary porosity and a system of

fractures that enhances its porosity. Because of a high proportion of mudstones and siltstones, and typically low borehole yields obtained in the Mosolotsane Formation, this formation is considered as an aquiclude that forms the base of a more promising Ntane aquifer (WCS, 1998). This Ntane sandstone is overlain in some places by fractured Stormberg Basalts and Kalahari sediments having variable thickness. The basalt has low primary porosity, and therefore their hydrogeological characteristics depend on the presence of shear and vertical fractures.

Structurally the area is characterized by a dominant WNW-ESE trending fault system (Figure 1.3), often intruded by dolerite dykes, which break up the Karoo formations into a series of compartments. A structurally controlled groundwater system flows west and east from the groundwater divide which is located more or less in the centre part of the study area (Figures 1.3 and 1.4). The westerly directed flow regime has a gentle gradient, whereas the one to the east has a steeper gradient.
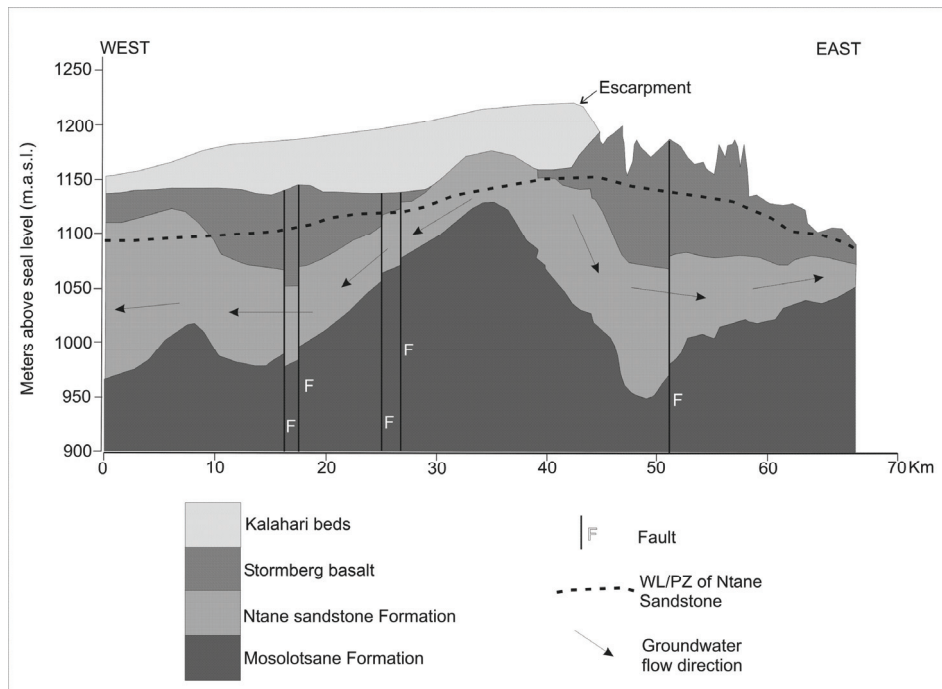
Figure 1.4. West–East hydrogeological cross section of the study area (redrawn from SGC, 1988); WL/PZ is water or piezometric level

Within the Serowe study area three types of hydrodynamic conditions of the Ntane aquifer can be identified as illustrated by Figure 1.5: (A) Kalahari beds or superficial deposits overlying the Ntane sandstone representing unconfined flow conditions; (B) Ntane aquifer covered by Stormberg basalt, with a hydraulic head above the top of the sandstone (confined conditions) and (C) Ntane sandstone covered by Stormberg basalt, but with a hydraulic head below the top of the sandstone (free water table conditions in a confined aquifer).
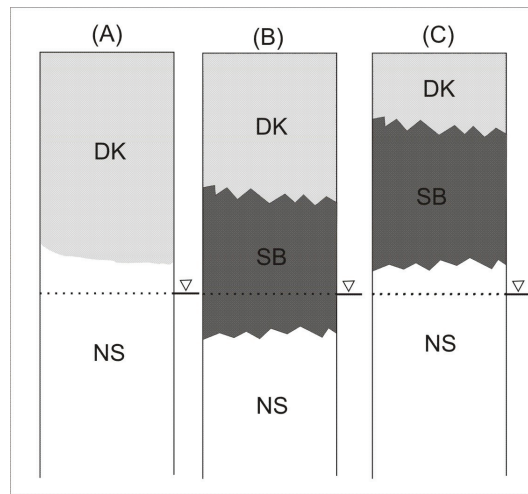
Figure 1.5. Hydrodynamic conditions of the Serowe study area; (DK is superficial deposit or Kalahari beds, NS is Ntane sandstone and SB is Stormberg basalt)

Hydraulic properties of the Ntane aquifer

Within the study area Farr et al. (1981), SGC (1988) and WCS (1998) conducted several pumping tests to describe the hydraulic behaviour of the Ntane aquifer. Table 1.2 contains a summary of ranges of hydraulic parameters obtained by these studies.

Table 1.2. Hydraulic parameters of the Ntane sandstone aquifer

Hydraulic parameter	Units	Ranges
Hydraulic conductivity	m/day	0.03-28
Transmissivity	m^2/day	1.5-199
Storage coefficient	(dimensionless)	1.3×10^{-5} -0.07
Borehole yields	m^3/day	127-1385

It is clear from Table 1.2 that hydraulic parameters of the Ntane aquifer vary remarkably. The broad variations in transmissivity (and/or hydraulic conductivity) values are partly explained by variations in fracture density and Ntane thickness, which have been indicated to vary across the study area. Variation in storage coefficient values can be partly explained by variations in primary porosity within the sandstone aquifer, and partly by the rate of

confinement. For example, where the sandstone is partly metamorphosed extremely low storage values can be expected as opposed to those found in unaffected parts of the aquifer, since metamorphism destroys primary structures in sedimentary rocks including primary porosity. Variations in borehole yields depend to a large extent (but not exclusively) on secondary permeability and possible leakage from overlying sediments such as Kalahari and basalt.

1.4.4 Vadose zone water balance

The vadose zone water balance of the Kalahari is mainly formed by rainfall and evapotranspiration since there is barely any surface runoff because of the high infiltration capacity of the sand cover. Figure 1.6 illustrates the water balance components of the Kalahari vadose zone system. To clarify the situation a preface of the order of magnitude of the water balance components of the study area is presented here.
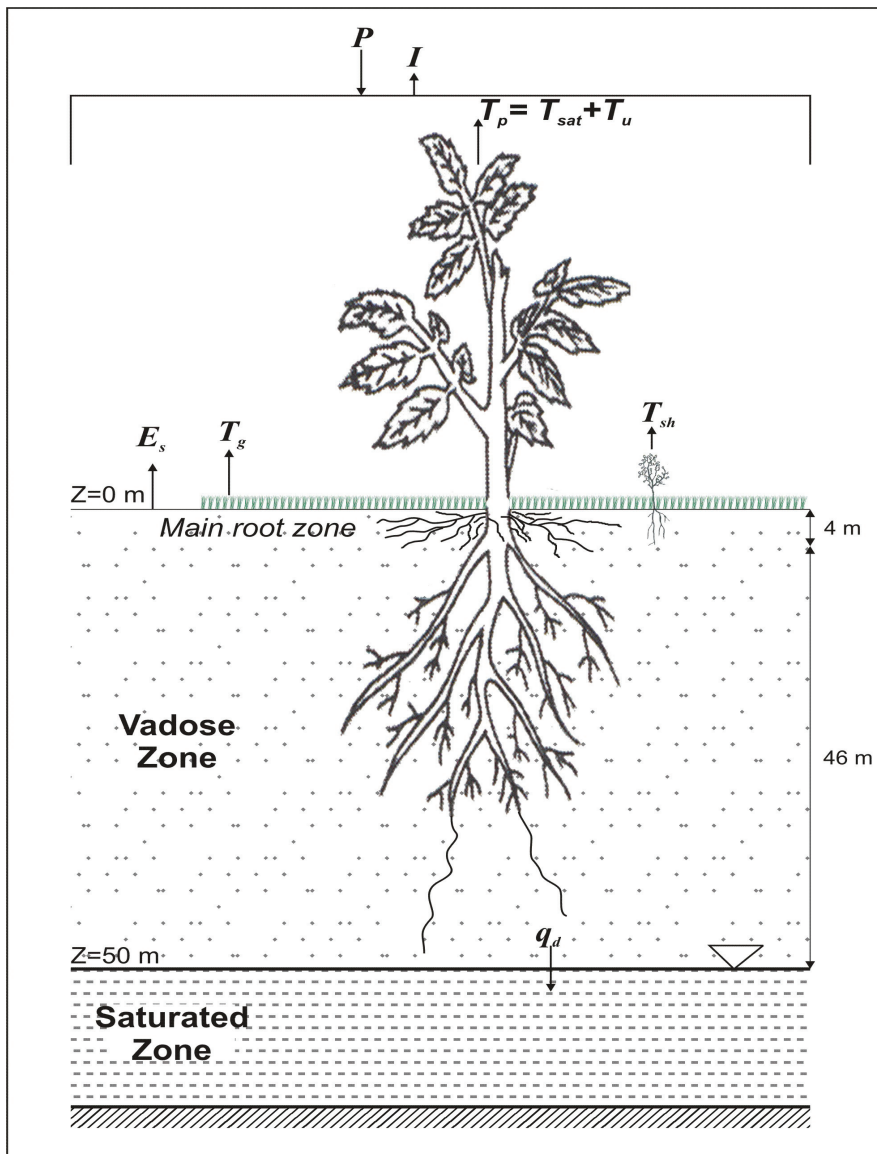
Figure 1.6. Schematic diagram illustrating the average conditions of the Kalahari vadose zone water balance components; P represent rainfall, I is interception, E_s is soil or surface evaporation, T_{sh} is transpiration due to shrubs, T_g is transpiration due to grass, q_d is groundwater discharge which is equal to the net groundwater recharge, T_p is tree transpiration consisting of T_{sat} and T_u transpiration components, in which T_{sat} and T_u represents transpiration water derived from the saturated and vadose zone respectively.

The schematisation of Figure 1.6 assumes that the water fluxes are vertical within the vadose zone and allows for horizontal flow in the saturated zone as illustrated in Figure 1.1. The vadose zone water balance of the Kalahari can be expressed as

$$q_d = P\text{-}AET \pm \Delta W \qquad (1.1)$$

where AET is actual evapotranspiration which is equal to the sum of the interception (I), surface or soil evaporation (E_s) and transpiration ($T_{sh} + T_g + T_p$), ΔW is change in vadose zone storage. Because the annual rainfall on average is in the order of 440 mm in the study area (Chapter 2) and q_d is in the order of 4 mm/yr (Chapter 7) and since $\Delta W=0$ on an annual time scale, the annual AET should be about 436 mm/yr. Because T_p is in the order of 12 mm/yr on average (Chapter 4, Table 4.5; excluding GS04), then about 424 mm/yr of the AET component is due to a combination of interception, soil or surface evaporation, grass transpiration and shrub transpiration components.

Chapter 2 Rainfall analysis

In this chapter rainfall data from long-term records and short-term records within the Serowe study area are presented in addition to the correlation of daily rainfall between rain gauges. This information is important for the estimation of areal rainfall.

2.1   Introduction

Rainfall is a primary component of the water balance in the semi-arid Kalahari. The variability in space and time of rainfall is fundamental to the rate of accumulation of water above and below ground levels and to the rate of evapotranspiration in an area. The entire circulation of water in an area is thus governed by the spatial and temporal distribution of rainfall. Rainfall in the semi-arid tropics is characterised by low annual averages but with high intensity showers. The long-term average annual rainfall is generally between 300 mm and 800 mm (Zhou et al., 2005).

The coefficient of variation of annual rainfall in Botswana increases from 30% in the northeast to more than 55% in the southwest in a similar pattern as annual rainfall decreases from about 600 mm to 250 mm (Bhalotra, 1987). According to Bhalotra (1987) for most parts of Botswana rainfall is predominantly convective but also influenced by a shift of the Inter-Tropical Convergence Zone (ITCZ) to the south. Average rainfall in the study area is 437 mm (1925-2004). See Table 2.1.

2.2   Instrumentation

 The study area was instrumented with 10 *Wallingford ARG100* tipping bucket rain gauges at selected sites of GS00-08 and GS10 (Figure 2.1), each having an orifice diameter of 25.4 cm and rainfall measurement resolution of 0.2 mm per tip. The rainfall monitoring started between 1999 and 2003 until March 2005. The rainfall data at GS01-08 were controlled and stored by *Skye Datahog2* loggers while the rainfall data at GS00 and GS10 were controlled and stored by

Delta-2e loggers. All rain gauges were installed at a height of 1.2 m above ground surface (m a. g. s.). The data were retrieved from the loggers every two weeks at GS01-08 gauge sites and every three months at GS00 and GS10 sites by a *laptop* computer. Additionally, there was already an existing collector type of rain gauge with an orifice diameter of 12.7 cm, installed at a height of 1.14 m a. g. s. by the Department of Meteorological Services (DMS). This rain gauge is referred to as MS in Figure 2.1. However, in the case of the MS rain gauge, rainfall was measured (in mm) every day at 0800 hours by DMS using a graduated measuring glass. All gauges were not equipped with heating devices and therefore were only capable of measuring precipitation in a liquid state.

Daily rainfall data were available from September 1999 to March 2005 for GS08 site, and from April 2000 to March 2005 for GS00 site. All rainfall data obtained before September 2001 at these two sites were acquired from the ITC rainfall monitoring network that existed prior to the current project. Except for GS08 and GS00 sites other sites of GS01-07 and GS10 recorded data after September 2001. The MS site provided monthly rainfall data from January 1925 to December 2004.
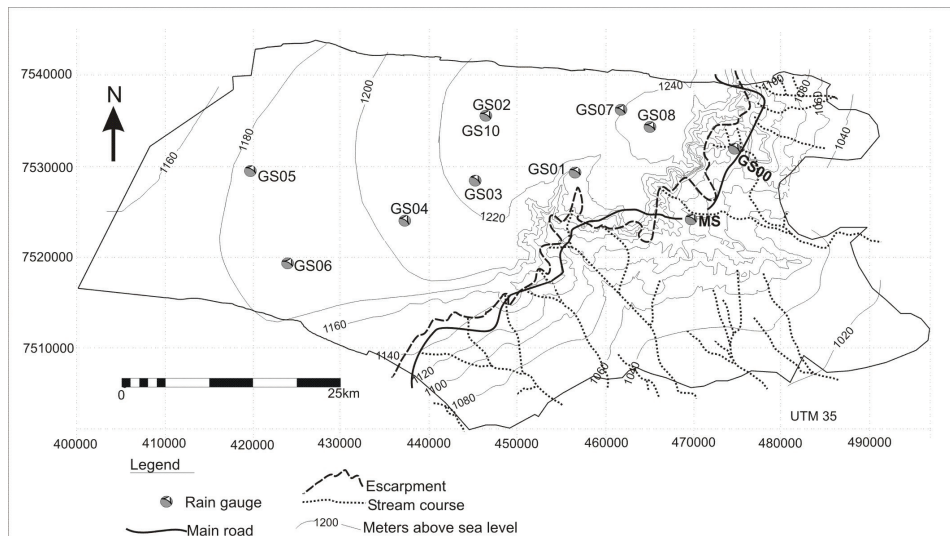
Figure 2.1. Topographic map and spatial distribution of rain gauges in the study area

During field visits rain gauges were inspected and cleaned to minimize failures that can be caused by a malfunctioning of the tipping bucket reed-switches and partial clogging of the rain gauge funnel by debris. Additionally, the integrity of rainfall records was checked with neighbouring gauges to ensure good quality of rainfall data.

2.3   Annual and monthly rainfall series

Figure 2.2 shows yearly rainfall recorded at the MS site for a period spanning from 1925-2004. Clearly there are years with exceptionally high (>800 mm/yr) rainfall such as 1940, 1955, 1988, 1995 and 2000. The corresponding statistics of the long-term data are presented in Table 2.1. Figure 2.3 shows the monthly rainfall for Serowe study area for three years (2002-2004) with pronounced seasonality, in which 90-100% of rainfall occurs during summer months (October-April). In Figure 2.4 the short-term record clearly highlights the wetter period of 2004 as compared to the years 2002 and 2003.

Table 2.1. Rainfall statistics based on long-term MS rainfall record (1925-2004); ±174 mm/yr is the standard deviation

Average annual rainfall (1925-2004)	437±174 mm/yr
Minimum annual rainfall (1927)	119 mm/yr
Maximum annual rainfall (2000)	970 mm/yr
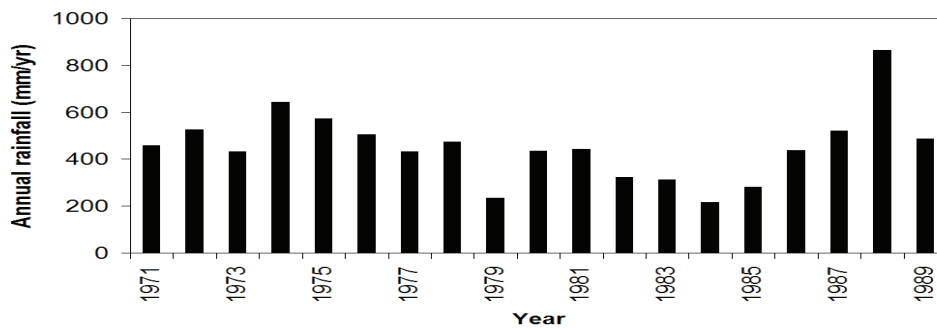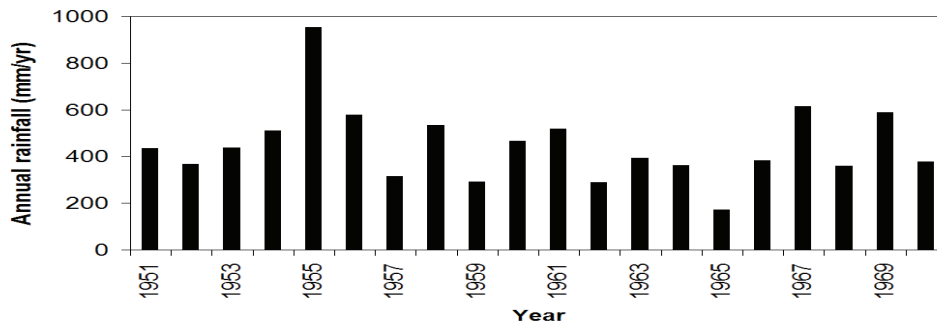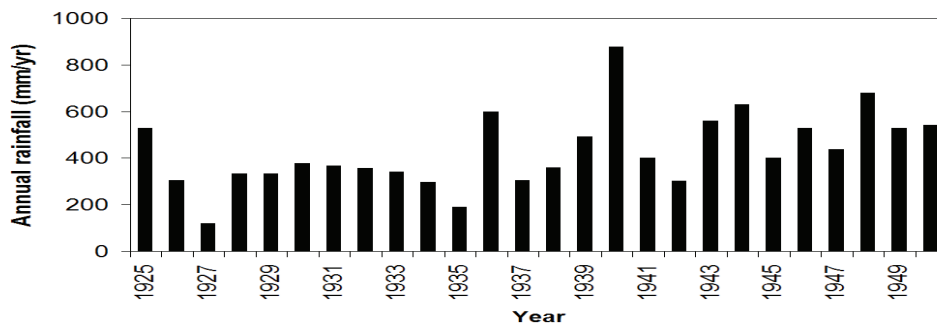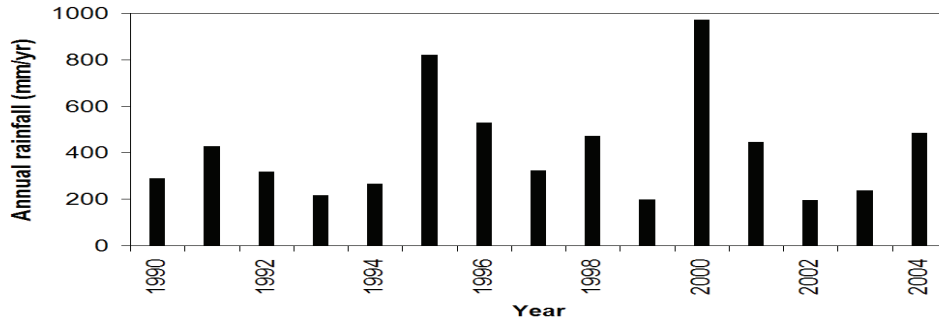
Figure 2.2. Yearly rainfall from 1925-2004 recorded at the MS site
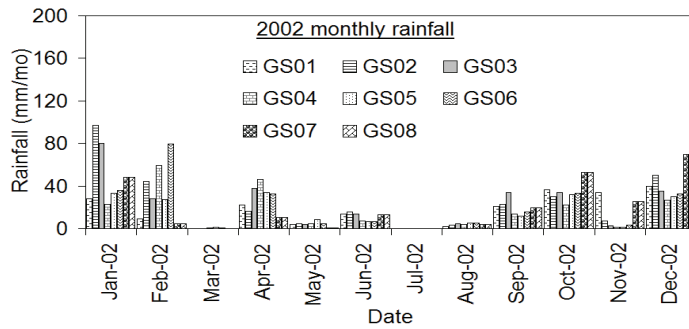
Years with incomplete data have been omitted e.g. 1999-2001 and 2005

Figure 2.3. Monthly rainfall for 2002-2004 recorded at various rain gauge sites

27

Figure 2.4. Yearly rainfall from 2002-2004 recorded at various rain gauge sites

2.4   Rain-days and daily rainfall correlations

Tables 2.2-2.3 show the number of rain-days with at least 10 mm of rainfall and the number of rain-days with less than 10 mm of rainfall respectively. The tables show that the majority of rain-days is associated with rainfall less than 10 mm. It can also be observed from these tables that most of the annual rainfall is provided by rain-days with at least 10 mm, the majority of which is usually associated with high intensity showers of the order of 20-50 mm.

Table 2.2. Rain-days with at least 10 mm of rainfall;

Year	Statistics	GS01	GS02	GS03	GS04	GS05	GS06	GS07	GS08
2002	Average	15	30	19	22	18	20	24	24
	Maximum	20	74	41	53	28	43	43	43
	Minimum	11	15	10	11	10	10	13	13
	Standard deviation	3	23	9	16	8	12	12	12
	no. of rain days	8	6	11	6	4	7	7	7
2003	Average	22	30	22	22	19	18	25	25
	Maximum	39	63	31	30	33	36	53	53
	Minimum	10	11	10	12	11	11	10	10
	Standard deviation	8	18	7	7	8	8	13	13
	no. of rain days	12	8	11	7	7	10	9	9
2004	Average	25	24	26	24	25	22	21	21
	Maximum	65	48	60	55	53	41	64	64
	Minimum	11	11	10	10	10	10	11	11
	Standard deviation	16	12	15	13	11	10	14	14
	no. of rain days	21	16	16	17	18	14	14	14

Table 2.3. Rain-days with less than 10 mm of rainfall

Year	Statistics	GS01	GS02	GS03	GS04	GS05	GS06	GS07	GS08
2002	Average	2	2	2	1	2	2	2	2
	Maximum	8	9	10	8	9	9	9	9
	Minimum	0.2	0.2	0.2	0.2	0.2	0.2	0.2	0.2
	Standard deviation	2	3	2	2	3	3	3	3
	no. of rain days	52	53	42	52	54	59	34	34
2003	Average	2	2	2	2	2	2	2	2
	Maximum	10	10	8	9	9	10	8	8
	Minimum	0.2	0.2	0.2	0.2	0.2	0.2	0.2	0.2
	Standard deviation	2	2	2	3	3	2	2	2
	no. of rain days	59	63	49	49	51	54	45	46
2004	Average	1	2	2	1	1	1	1	1
	Maximum	10	10	10	9	9	10	10	10
	Minimum	0.2	0.2	0.2	0.2	0.2	0.2	0.2	0.2
	Standard deviation	2	2	2	2	2	2	2	2
	no. of rain days	72	77	92	81	64	89	87	87

A correlation analysis is normally performed to reveal the direction and strength of the relationship between two variables. Figure 2.5 depicts the correlation coefficients (r) between daily rainfall recorded at specific rain gauges and daily rainfall recorded by other rain gauges within the study area. The following observation can be made:

- With a few exceptions such as Figure 2.5(a), 2.5(g) and 2.5(h) rainfall from rain gauges which are in the immediate neighbourhood is usually highly correlated.
- Correlation coefficients range from 0.4-1, with the lowest correlation coefficient being found between rainfall data of GS10 and GS00 rain gauges with an inter-gauge distance of 29 km, while the highest rainfall data correlation coefficient is found between rain gauge pairs GS07/GS08 and GS02/GS10. The inter-gauge distance between the paired gauges is 3 km and 30 m for GS07/GS08 and GS02/GS10 respectively.

In general terms, spatial trends of rainfall correlations between the gauges decreases with increasing distance from the gauge. The decline in correlations with increasing distance from measurement point may be attributed to both the local nature of convective rainfall and, may be to some extent, to the effects of site conditions at the gauge.
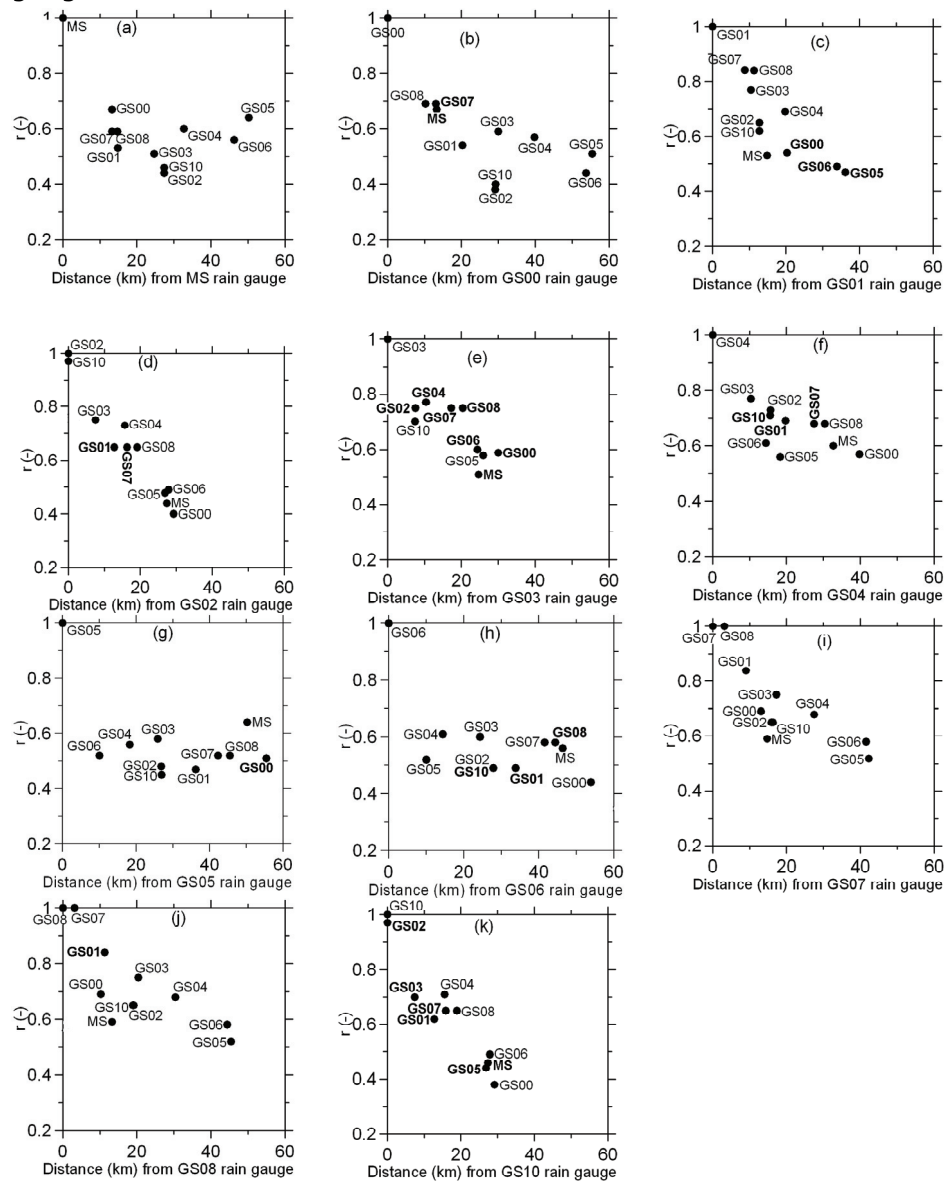
Figure 2.5. Correlation coefficients between daily rainfall at individual rain gauges as a function of inter gauge distance

2.5 Conclusions

1. The average long-term annual rainfall for the period 1925- 2004 is 437 mm with a minimum of 119 mm (in 1927) and a maximum of 970 mm (in 2000).

2. Rainfall is mainly of convective nature occurring mainly during the hot season, producing showers in the order of 20-50 mm.

3. A spatial correlation study of daily rainfall at individual rain gauges reveals that in general, spatial trends of rainfall correlations between gauges decreases with increasing separation distance between the gauges.

Chapter 3 Monitoring of evapotranspiration

3.1   Introduction

Evapotranspiration (*ET*) is a major component of the water cycle, particularly in arid and semi-arid areas like the Kalahari where, the annual potential evapotranspiration is much greater than the annual rainfall. Evapotranspiration plays an important role not only in the general water cycle but also in groundwater balances as was shown by Lubczynski (2000) for the Serowe study area. It has either direct or indirect impact on groundwater resources. The direct impact relates to groundwater evapotranspiration attributed to groundwater water extraction (close to the capillary fringe) by deep root systems of savanna vegetation called groundwater transpiration and/or by evaporation from the groundwater table. The indirect impact relates to the evapotranspiration of water from the surface and from the unsaturated zone (i.e. the water that has not reached the water table). The latter one is related to moisture uptake by plant root systems in the unsaturated zone and by evaporation from unsaturated zone. It has been proved that under dry climatic conditions, groundwater uptake by roots may take place even from more than 50 m depth (Phillips, 1963) whereas evaporation from the groundwater table by vapour and capillary transport may take place from more than 20 m depth (Walvoord et al., 2002a,b). Both fluxes can be significant in the overall groundwater balance.

The separate measurements (for partitioning purpose) of the unsaturated and groundwater components of the actual evapotranspiration still remain a problem. The most successful in that field is a combination of methods such as micrometeorology (for actual evapotranspiration), sap flow measurements (for transpiration) and tracer methods (for either transpiration or evaporation estimates) although these methods do not allow for complete experimental separation of each component of evapotranspiration. Such separation is theoretically possible only by modelling of fluxes and subsequent validation.

Before considering the various components, this chapter presents the results of an attempt to determine the actual evapotranspiration by using surface energy balance methods.

Average annual actual evapotranspiration in the Kalahari is obviously not much less than the average annual rainfall. The direct determination of this component of the water balance, and its seasonal variations has not yet been carried out. This problem has been taken up as a challenge within the framework of the present study, in which an automated monitoring network was established in the Serowe area. The installation of the automated micrometeorological monitoring network had the following objectives that also match the objective of the present research: (1) to improve the understanding of the hydrological regime of fluxes specific for the Kalahari sandveld and hardveld regions; (2) to provide input for modelling subsurface fluxes; (3) to define the most suitable and cost effective micrometeorological evapotranspiration monitoring scheme for future groundwater assessment in the Kalahari.

It should be emphasized that the idea of the described micrometeorological monitoring was not to present the most accurate, complex and expensive evapotranspiration solution such as e.g. eddy covariance technique but to define an optimal and cost effective evapotranspiration monitoring solution for groundwater assessment. Such a solution was expected to be less hardware demanding than the complex solutions used in surface hydrology and therefore, with a given cost of instrumentation of reasonable accuracy, was also expected to provide the maximum spatio-temporal output coverage. It is also expected that such an approach at least gives information on the fluctuations of evapotranspiration throughout the year and inter-annually since evapotranspiration on an annual basis is well known.

3.2   Literature overview and selection of methods for the present study

Depending on the focus of the study and the instrumentation available, the evapotranspiration can be either assessed as potential

evapotranspiration (*PET*) or as actual evapotranspiration (*AET*). There are numerous methods for estimating *PET* e.g. Penman (1948), Thornthwaite (1948), Blaney-Criddle (1950), Makkink (1957), Jensen and Haise (1963), Penman-Monteith (Monteith, 1965), Priestley and Taylor (1972), Thom and Oliver (1977), Hamon (1961), Hargreaves and Samani (1985) and Abtew (1996). Many good overviews of these methods are found in the hydrological literature (Brutsaert, 1982; Jensen et al., 1990; Dingman, 1994; Morton, 1994; Allen et al., 1998; Xu and Singh, 2002; Gieske, 2003).

The *PET* assessment methods vary in data demands, from very simple (more empirically based), requiring only information on monthly average temperatures, to complex (more physically based), requiring data on maximum and minimum temperature, solar radiation, humidity, wind speed, as well as characteristics of the vegetation. Several studies such as for example by Jensen et al. (1990) and Vörösmarty et al. (1998), have dealt with the search of the best formulae to compute *PET*. Jensen et al. (1990) recommended the Penman-Monteith method as presented by Allen et al. (1998) as the preferred method. However, Vörösmarty et al. (1998) compared *PET* estimates given by 11 different methods and found that the temperature based Hamon method gave the best performance followed by several variations of Penman-Monteith approaches. The combination method of Penman (1948) is usually considered as the most physically based (Shuttleworth, 1993). Although many authors have compared several *PET* methods there is no commonly accepted choice. However, many agree on the validity of the Penman-Monteith method which will be used here.

AET is perhaps the most difficult hydrological flux to measure. The evaporative component can be measured directly by evaporation pans although such measurements do not represent vegetative controls on moisture loss. Such controls in direct (*in situ*) measurement of *AET* can be provided by lysimeters (e.g. Conway and Van Bavel, 1967; Black et al., 1969; Kocke et al., 1985). Direct lysimetric measurements of *AET* are however time consuming and expensive and therefore they are rather seldomly applied, except for the calibration of empirical and analytical *AET* models. Estimating actual

evapotranspiration using analytical and empirical equations, typically based on the auxiliary field measurements, is by far more common. Most of such equations were developed by correlating measured evapotranspiration with measured microclimatic weather parameters that directly or indirectly affect evapotranspiration.

Since there are many factors affecting evapotranspiration, it was and still is difficult to formulate an equation that can produce reliable estimates of *ET* under different (sets of) conditions. The most known in this regard are the Bowen-ratio (Bowen, 1926; Tillman, 1972), the eddy correlation (Wallace et al., 1993) and the scintillometry approaches (McAneney et al., 1995 and De Bruin et al., 1995). Other approaches that are also used to derive actual evapotranspiration estimates are the Temperature Fluctuation Energy Balance Method (Lloyd et al., 1991) and its modification, the Temperature Variation Energy Balance Method (Vugts et al., 1993). Some of these methods have found applications in a wide variety of studies under different environments (Gash and Stewart, 1975; Hatton and Vertessy, 1990; Thiermann and Grassl, 1992; De Bruin et al., 1995; Gehrels, 1999). Recently it was also proved that the energy balance algorithms for assessment of *AET* can be applied not only from data of microclimatic stations but also spatially, using satellite, multi-spectral (remote sensing) data (e.g. Peters, 1995; Bastiaanssen et al., 1998a,b; Kustas and Norman, 1999; French et al., 2000 and Su, 2002).

Actual evapotranspiration (considered as a component of the water balance) can also be determined using other principles. For example, approaches based on diurnal fluctuation of the groundwater table (Freeze and Cherry, 1979) or from the isotopic composition of water (Walker and Brunel, 1990) can provide useful estimates of *AET*. Additionally, other commonly used approaches are those that are based on soil moisture modelling. This type of approach typically uses the relation of *AET* with the measured *PET* as expressed by the coefficient of evapotranspiration (*AET/PET*) which is controlled by temporal soil moisture availability. A good example could be the one dimensional (1-D) lumped parameter model called EARTH (Van der Lee and Gehrels, 1990) or more sophisticated 1-D models based on the Richard's equation such as SWAP (Van Dam et al., 1997) or

36

HYDRUS (Šimůnek et al., 1998). The Richard's algorithm was also built into distributed unsaturated zone water balance models such as SWAT (Arnold et al., 1998) and HELP3 (Schroeder et al., 1994) for example. The advantage of this approach is that AET is derived in combination with other water balance components. The main problem for the present study is the difficulty in proper parameterization of the root water uptake zone which for Kalahari savanna vegetation extends down to more than 60 m depth (see Chapter 5). Additionally the mechanism of water exchange between plants and soil is complicated by the less known phenomenon of hydraulic lift[3] (Dawson, 1993; 1996 and Burgess et al., 1998).

For the present study the Bowen ratio, temperature fluctuation (profile) and Penman- Monteith methods were selected and used for evapotranspiration assessment.

3.3   Monitoring network

The microclimatic evapotranspiration-monitoring network was established in 2001. It consisted of 11 automated data acquisition system (ADAS) towers of various sensor configurations and mast heights. There were two primary/reference, 18 m high, *galaxy* ADAS towers, one called GS00 in the eastern hardveld part and the other called GS10 in the western sandveld part (Figure 3.1), eight secondary 2 m high ADAS towers called GS01-GS08 and one GS09 10 m high ADAS mobile retractable tower.

---

[3] Hydraulic lift is the vertical transfer of water from wet deep layers to relatively dry shallow layers resulting from root water transport and efflux to the soil.
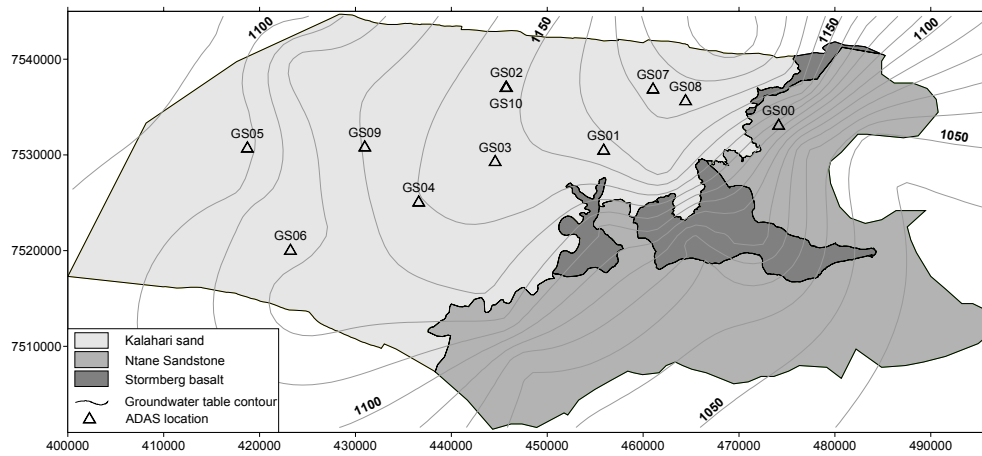
Figure 3.1. Serowe study area and microclimatic monitoring network

The two primary towers were meant to provide a reference temporal variability of *AET* and *PET*. The GS00 was installed in September 2001 whereas the GS10 was installed in November 2003. Both primary towers were equipped with one *Kipp&Zonen CNR1* net radiometer installed at the top of the tower construction, three *Vector A100L2* anemometers and three *Eijkelkamp capacitive* relative humidity & *PT100* temperature (*RH/T*) sensors at 2 m, 13 m, and 18 m heights at GS00 and at 2 m, 10 m and 18 m heights at GS10. In addition, at each primary tower there were also: one *TNO* soil heat flux plate buried at the depth of 2 cm, two *Eijkelkamp* soil temperature *Fenwall thermistor* sensors (*Th2-f*) buried at depths of 2 cm and 15 cm, and the *Wallingford* type of tipping bucket rain gauge with resolution 0.2 mm/tip, placed at a height of 1.2 m a. g. s. as presented in Chapter 2.

The data acquisition and the data storage were controlled by the multi-channel *Delta-2e* loggers. Both loggers were programmed for variable, sensor dependent sampling time but uniform data storage of 0.5 hour (hr). The eight 2 m high secondary towers were meant for the assessment of *PET* only. Out of these eight towers, seven GS01-GS07 (Figure 3.1) were equipped with one *Skye SKH 2011 RH/T* unit attached to a mast at the height of 2 m a. g. s. and one *Wallingford* type of tipping bucket rain gauge placed at a height of 1.2 m above the ground.

The GS08 ADAS tower was installed to provide *PET* input data and to act as a backup of the GS00 tower in case of its failure. It consisted of the *Vector A100R* anemometer, the *Skye RH/T* unit and the *Kipp&Zonen CM3* pyranometer for measuring incoming short-wave radiation all mounted at the height of 2 m a. g. s. Other instruments at GS08 included the two *Skye* soil temperature thermistor sensors buried at depths of 2 cm and 15 cm below the ground surface and the *Wallingford* type of tipping bucket rain gauge. All eight secondary ADAS towers, i.e. GS01-08 were controlled by *Skye DataHog2* loggers, sampling data at various, sensor-dependent sampling times and storing data with a uniform interval of half an hour.

Apart from the permanent towers there was also one mobile tower, GS09, constructed on a retractable 10 m high mast. This tower was equipped with two *Vector A100R* anemometers and two *Skye RH/T* sensors, normally installed at 2 m and 10 m heights, a pair of *Skye* soil temperature sensors normally buried at depths of 2 cm and 15 cm in the soil. The GS09 mobile tower was equipped with *Skye DataHog2* logger sampling data at various sensor-dependent sampling times and storing data with a uniform interval of half an hour. During field campaigns, GS09 was moved between stations GS01-GS08 every ten-days, otherwise it was fixed at its semi-permanent location marked as GS09 (Figure 3.1).

3.4 Micrometeorological variables

3.4.1 Net radiation

The net radiation (R_n) variable is required for *PET* and *AET* calculation. R_n can be computed from Equation 3.1, provided all the components of incoming and outgoing radiation on the earth surface are known as this was the case for GS00 and GS10 reference towers.

$$R_n = S \downarrow - S \uparrow + L \downarrow - L \uparrow \qquad [\text{W m}^{-2}] \qquad (3.1)$$

where $S\downarrow$ and $S\uparrow$ are down-welling and up-welling shortwave radiations respectively, and $L\downarrow$ and $L\uparrow$ are down-welling and up-welling longwave radiations respectively.

All the other towers in the study area (GS01-GS09) were not sufficiently instrumented to measure R_n directly. Therefore for those tower locations, R_n was estimated on the basis of the nearest location - assuming spatially invariable shortwave incoming radiation ($S\downarrow$) and using the Allen et al. (1998) procedure, defined as

$$R_n = \left[(1-\alpha)S\downarrow\right] - R_{nl} \tag{3.2}$$

where α [-] is the albedo and R_{nl} [MJ m^{-2} day^{-1}] is the net longwave outgoing radiation given by

$$R_{nl} = \sigma\left[\frac{T_{max} + T_{min}}{2}\right]\left[\left(0.34 - 0.14\sqrt{e_a}\right)\right]\left[1.35\frac{R_s}{R_{so}} - 0.35\right] \tag{3.3}$$

Here, σ is the Stefan-Boltzmann constant (4.903x10^{-9} MJ K^{-4}M^{-2} day^{-1}), T_{max} [^{o}K] and T_{min} [^{o}K] are maximum and minimum daily temperatures respectively, e_a [kPa] is the actual vapour pressure derived from the relative humidity (*RH*) as $0.005[e^o(T_{min})RH_{max} + e^o(T_{max})RH_{min}]$, where RH_{max} [%] and RH_{min} [%] represent daily maximum and minimum relative humidity respectively, $e^o(T_{min})$ [kPa] is given by $0.6108exp\{(17.27T_{min}/(T_{min}+237.3)\})/(T_{min}+237.3)$ and $e^o(T_{max})$ [kPa] is given by $0.6108exp\{(17.27T_{max}/(T_{max}+237.3)\})/(T_{max}+237.3)$), in which T_{min} and T_{max} are expressed in ^{o}C and R_s [MJ m^{-2} day^{-1}] and R_{so} [MJ m^{-2} day^{-1}] are measured solar radiation and calculated clear-sky radiation respectively.

The definition of R_{so} was based on the calculation of extraterrestrial radiation (Allen et al., 1998) and on an estimate of the tower site altitude. Then Equation 3.3 was used for the determination of R_{nl} to facilitate Equation 3.2 and calculate R_n for all the monitoring sites of GS01-GS09 that did not have net radiometers.

Figure 3.2 illustrates a typical example of the diurnal course of the clear-sky radiation components and the post-processed net radiation for 1 April 2002 at the GS00 site. It can be observed that $S\downarrow$ and R_n reached their maxima slightly after 12 pm (local time) whilst $S\uparrow$ and $L\uparrow$ reached their minima at approximately the same time. The $L\downarrow$ was more or less stable throughout the day.
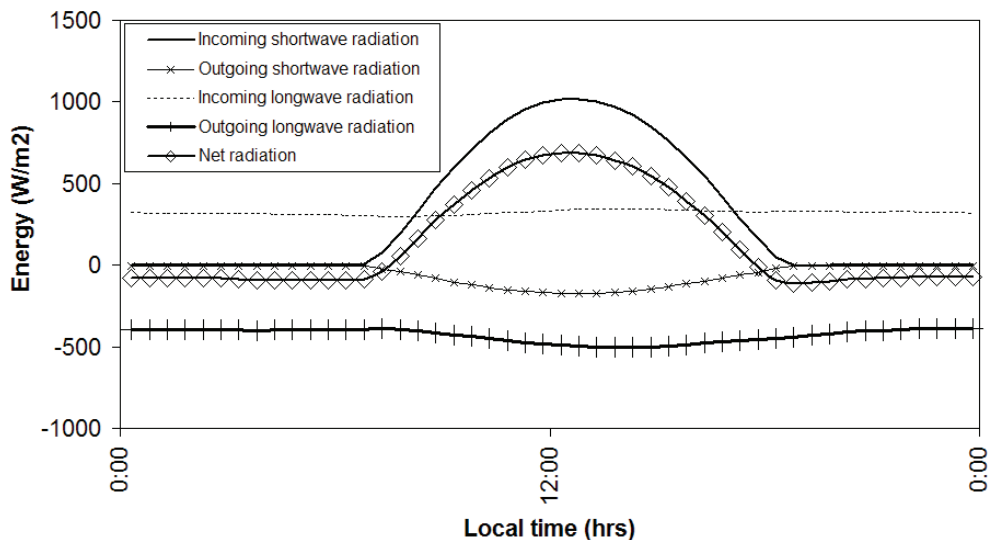
Figure 3.2. An example of diurnal, clear-sky radiation for GS00 monitoring site on 1 April 2002

3.4.2 Temperature and relative humidity

The calculation of PET according to Equation 3.4, requires air temperature and relative humidity (RH) measurements above the canopy (Dingman, 1994). Such measurements were carried out at GS00 and GS10 monitoring sites. However, in eight other monitoring sites of GS01-GS08, RH and air temperature were measured only at a 2 m height. In order to extrapolate 2 m measurements to above-canopy measurements, at each of the eight monitoring sites, periodic measurements with the mobile 10 m tower (originally located at GS09) equipped with RH/T sensors at 2 and 10 m heights were made. These measurements were carried out between September 2002 and September 2003 in four series with ten day intervals, so each location was visited four times a year, every time in different hydrological

41

conditions. Table 3.1 presents the regression models that were developed as a result of that experiment. The quality of fit ($R^2 \geq 0.9$) of these regression models was good, so they were finally used to provide the above-canopy *RH/T* data demanded for *PET* assessment.

Table 3.1. Regression models for estimation of air temperature and relative humidity at 10 m height using site specific temperature and relative humidity measurements at 2 m. T_2 and T_{10} represent air temperature at 2 m and 10 m respectively. RH_{10} and RH_2 represent relative humidity at 10 m and 2 m respectively and n represent number of observations

Site	Temperature Regression model	R^2	n	Relative humidity Regression model	R^2	n
GS01	$T_{10}=0.93\ T_2+1.17$	0.98	405	$RH_{10}=1.00\ RH_2-0.25$	0.98	405
GS02	$T_{10}=0.80\ T_2+4.42$	0.95	865	$RH_{10}=0.90\ RH_2+2.43$	0.95	865
GS03	$T_{10}=0.85\ T_2+3.60$	0.96	736	$RH_{10}=0.90\ RH_2+2.49$	0.97	736
GS04	$T_{10}=0.82\ T_2+4.07$	0.95	1267	$RH_{10}=0.86\ RH_2+3.59$	0.94	1267
GS05	$T_{10}=0.90\ T_2+2.13$	0.98	1258	$RH_{10}=0.95\ RH_2+1.45$	0.98	1258
GS06	$T_{10}=0.85\ T_2+3.04$	0.97	843	$RH_{10}=0.91\ RH_2+2.66$	0.97	843
GS07	$T_{10}=0.77\ T_2+5.21$	0.91	847	$RH_{10}=1.89\ RH_2\hat{}0.84$	0.90	847
GS08	$T_{10}=0.75\ T_2+5.92$	0.92	1138	$RH_{10}=0.82\ RH_2+0.06$	0.92	420

In order to demonstrate typical diurnal courses of *RH* and air temperature in the Serowe study area during the end of summer and winter time, two clear-sky daily records of 1 April 2002 and 19 June 2002 at a 2 m height at GS00 site were selected and presented respectively in Figure 3.3. In both daily records the *RH* has a parabolic shape characterized by large *RH* values in the nights and a decline starting ≈07:00 am until a minimum at ≈15:00 pm. The air temperature depicts an opposite trend, being characterized by a rise (at ≈07:00 am) to a maximum (also at ≈15:00 pm), followed by a decrease again. The main differences between the measurements in the selected two (example) days is the longer time of low relative humidity in the day and lower temperatures in June than in April.
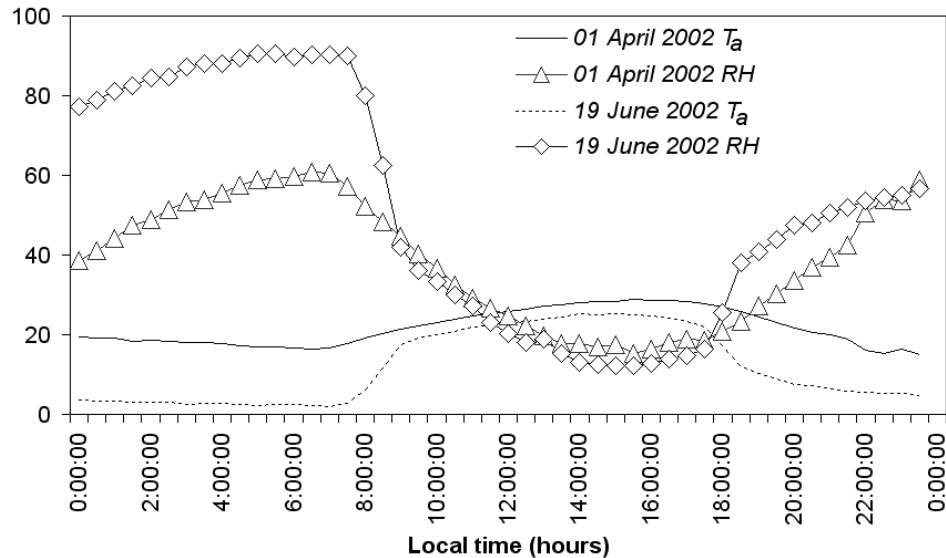
Figure 3.3. Examples of diurnal relative humidity (*RH* in %) and air temperature (*T~a~* in °C) on the 1 April 2002 and on the 19 June 2002 at GS00 site

3.4.3 Wind speed

As mentioned, the wind speed (*WS*) monitoring in the study area was only available in the three ADAS stations, at GS00 (at 2 m, 13 m and 18 m height), GS08 (at 2 m height) since 2001 and at GS10 (at 2 m, 10 m and 18 m heights) since 2003. In order to provide wind speed characteristics for evapotranspiration calculations at the sites of GS01-07, which were not equipped with wind speed meters, at each of these sites, periodic, serial measurements were made with the mobile (10 m) tower (originally located at GS09) equipped with two wind speed meters, one at 2 m and the second at 10 m height. The first field campaign was carried out between September 2002 and September 2003 in four series with ten days intervals, so each location was accessed four times, every time in different hydrological conditions. The main purpose of that experiment was to correlate the wind speed at the sites which are permanently monitored (GS00 and GS08) with wind speed recorded at the mobile tower which was moved between the locations of GS01-07 for *PET* assessment. The second field campaign was carried out between January 2004 and

February 2004 when each location was accessed once for a period of three days. The objective of that experiment was to correlate the wind speed of the mobile tower when moved between the locations of GS01-08 with the wind speed at the recently installed permanent station of GS10. The results of these experiments are summarized in Figure 3.4 and Table 3.2.
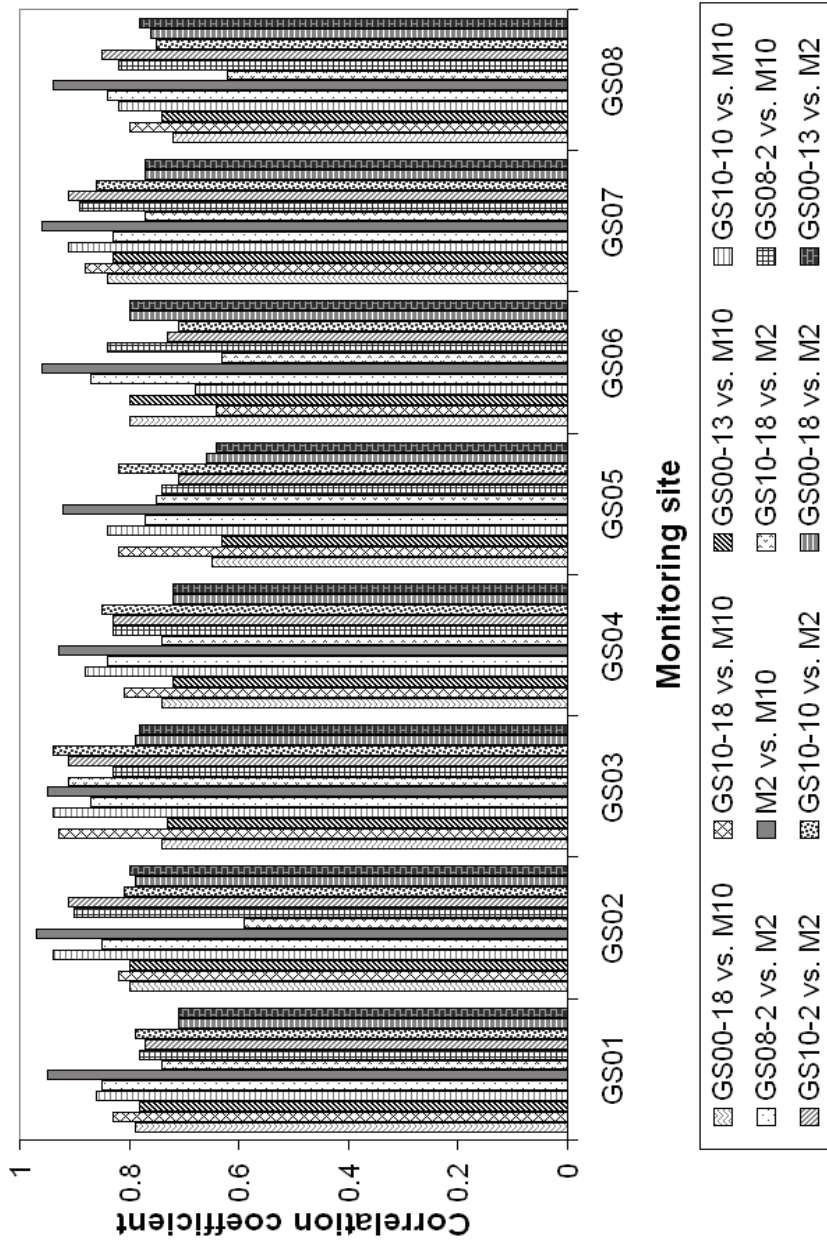
Figure 3.4. A bar diagram depicting correlation coefficients between mobile mast wind speed (*WS*) measurements at GS01-08 locations and permanent wind speed measurements at GS00, GS08 and GS10 sites; *M10* and *M2* represent *WS* at heights of 10 m and 2 m respectively. GS08-2 represents *WS* at 2 m height at GS08 site. GS10-2, GS10-10 and GS10-18 represent *WS* at 2 m, 10 m and 18 m heights at GS10 site

respectively and GS00-2, GS00-13 and GS00-18 represent *WS* at 2 m, 13 m and 18 m, heights at GS00 site respectively

Figure 3.4 depicts variation of correlation of the mobile tower half-hourly wind speed measurements at the sites of GS01-08 with the continuous wind speed measurements at GS00, GS08 and GS10 tower sites. The correlations for GS08 and GS10 were substantially better than for GS00. This was because GS00 in contrast to all Kalahari sandveld towers, is located on the hardveld side (Figure 3.1) characterized by different wind speed characteristics due to the taller and differing vegetation and shielding effect of the adjacent escarpment. As a result the GS00 data was not used for wind speed extrapolation. While analyzing mobile tower wind speed measurements, comparatively better correlations were obtained for 2 m and 10 m heights at the same location than between different locations but at the same heights of measurements. GS02 site indicated the highest correlation coefficient (0.97) and GS05 lowest correlation coefficient of 0.87.

Table 3.2. Regression models for estimation of wind speed at 2 and 10 m heights at various locations across study area; *WS2* represent wind speed at 2 m, *GS08_WS2* represent 2 m height GS08 wind speed, *WS10* represent wind speed at 10 m and *GS10_WS10* represent 10 m height GS10 wind speed and *n* represent number of observations

Site	GS08 Regression model no.1 (*WS2_WS2* at different sites)	R^2	*n*	GS10 Regression model no.2 (*WS10_WS10* at different sites)	R^2	*n*	Regression model no.3 (*WS2_WS10* at same site)	R^2	*n*
GS01	*WS2*=0.89 *GS08_WS2* +0.39	0.72	1222	*WS10*=0.79 *GS10_WS10* +0.25	0.74	187	*WS10*=1.71 *WS2*+1.51	0.77	1647
GS02	*WS2*=1.19 *GS08_WS2* +0.17	0.82	865	*WS10*=0.95 *GS10_WS10* +0.05	0.88	190	*WS10*=1.51 *WS2*+1.19	0.92	441
GS03	*WS2*=1.11 *GS08_WS2* +0.46	0.76	736	*WS10*=0.86 *GS10_WS10* +0.22	0.88	178	*WS10*=1.54 *WS2*+1.00	0.90	736
GS04	*WS2*=0.93 *GS08_WS2* +0.26	0.73	1267	*WS10*=0.80 *GS10_WS10* +0.07	0.77	188	*WS10*=1.41 *WS2*+1.48	0.86	1267
GS05	*WS2*=0.91 *GS08_WS2* +0.67	0.70	1200	*WS10*=0.96 *GS10_WS10* +0.29	0.71	188	*WS10*=1.56 *WS2*+1.25	0.85	1258
GS06	*WS2*=1.08 *GS08_WS2* +0.45	0.76	843	*WS10*=0.77 *GS10_WS10* +0.70	0.46	331	*WS10*=1.52 *WS2*+1.17	0.93	843
GS07	*WS2*=0.69 *GS08_WS2* +1.30	0.79	847	*WS10*=0.86 *GS10_WS10*	0.83	96	*WS10*=1.99 *WS2*+1.28	0.76	847
GS08	-	-	-	*WS10*=0.85 *GS10_WS10* +0.32	0.78	1218	*WS10*=1.57 *WS2*+1.76	0.89	1137

The three types of regression models as specified in Table 3.2 were developed to provide the missing, above-canopy, wind speed data of 10 m heights at GS01-08 sites for *PET* calculation. The quality of fit of these models is described by R^2. The type 1 wind speed regression models were established between the permanent 2 m high wind

speed measurements at GS08 and the simultaneous 2 m height wind speed measurements at the GS01-07 mobile tower locations. The R^2 of these models varies between 0.70 at GS05 and 0.82 at GS02. The type 2 wind speed regression models were established between the permanent 10 m high wind speed measurements at GS10 and the simultaneous 10 m height wind speed measurements at the GS01-08 mobile tower locations. All the R^2 are above 0.70 except for GS06 location where $R^2 = 0.46$ which is difficult to explain. The type 3 wind speed regression models (Table 3.2) were established at GS01-08 locations using simultaneous 2 m and 10 m height mobile mast wind speed measurements. The R^2 of these models is generally ≥ 0.85 except for GS01 and GS07 where R^2 were 0.77 and 0.76 respectively. Those lower R^2 values can be explained by clustering of tall trees at these locations, which is not observed at the other sites.

The calculation of *PET* requires wind speed measurements above the canopy. Before 2003, when the fully equipped (wind profile available) GS10 was setup in the Kalahari sandveld, the only permanent sandveld wind speed measurement was available at GS08 and only at a height of 2 m. These GS08 measurements were extrapolated to 10 m wind speed measurements at each GS01-08 sites where *PET* was to be defined, first by using the type 1 regression model and finally by using the type 3 regression model (Table 3.2). After installation of GS10 the type 2 regression model was used.

The extrapolated half-hourly estimates of wind speed at 10 m were finally averaged to daily values for use in *PET* calculation according to Equation 3.4.

3.5 Theoretical background of evapotranspiration determination

This section provides a background for evapotranspiration methods used in the present study and the simplifications that were made due to data deficiency problems and also the specific groundwater related focus of this study.

3.5.1 Potential evapotranspiration

PET represents water demand (stress) of the atmospheric system being also the upper limit of evapotranspiration. In the study area, the potential evapotranspiration (*PET*) was determined with the Penman-Monteith (*P-M*) formula (Monteith, 1965) by assuming a surface resistance (r_s) of zero (wet conditions) which leads to the following *P-M PET* formulation

$$\lambda E_p = \frac{\Delta_T (R_n - G_o) + \rho_a C_p \left(\dfrac{e_s - e_a}{r_a} \right)}{\Delta_T + \gamma} \tag{3.4}$$

where λE_p [MJ m^{-2} day^{-1}] is the total latent heat (for potential evapotranspiration), R_n [MJ m^{-2} day^{-1}] is net radiation, G_o [MJ m^{-2} day^{-1}] is soil heat flux, γ [kPa ^{o}C^{-1}] is the psychrometric constant, C_p [kJ Kg^{-1} ^{o}C^{-1}] is the specific heat capacity of air taken as 1013 kJ Kg^{-1} ^{o}C^{-1}, ρ_a [Kg m^3] is mean air density at constant pressure, Δ_T [kPa ^{o}C^{-1}] is the rate of change of the saturation vapour pressure with temperature expressed as 4098(0.6108exp{(17.27T_a/(T_a+237.3)})/ (T_a+237.3), where T_a [^{o}C] is air temperature, e_s [kPa] is the saturation vapour pressure approximated by 0.5[$e^o(T_{min})$+$e^o(T_{max})$], where $e^o(T_{min})$ is given by 0.6108exp{(17.27T_{min}/(T_{min}+237.3)})/(T_{min}+237.3) and $e^o(T_{max})$ is given by 0.6108exp{(17.27T_{max}/(T_{max}+237.3)})/(T_{max}+237.3), in which T_{min} [^{o}C] and T_{max} [^{o}C] represent minimum and maximum daily air temperature respectively, e_a [kPa] is the actual vapour pressure derived from relative humidity (*RH*) as 0.005[$e^o(T_{min})RH_{max}$+ $e^o(T_{max})RH_{min}$], where RH_{max} [%] and RH_{min} [%] represent daily maximum and minimum relative humidity respectively, and r_a [s m^{-1}] is the aerodynamic resistance. *Subsequently, the PET in mm/day is expressed as PET=0.408 λE_p, in which 0.408 is a conversion factor and λE_p is express by* Equation 3.4.

Most of the parameters necessary to calculate *PET* according to Equation 3.4 were either monitored in the study area or could be defined by regression analysis. The most difficult to define in Equation 3.4 was r_a.

$$r_a = \frac{\left[\ln\left(\dfrac{z-d_o}{z_{om}}\right)-\psi_m\right]\left[\ln\left(\dfrac{z-d_o}{z_{oh}}\right)-\psi_h\right]}{k^2 u_z}$$

(3.5)

where d_o [m] is the zero plane displacement height, u_z [m s^{-1}] is wind speed at the measurement height z [m] above the canopy, z_{oh} [m] is the roughness length for heat transfer and water vapour, z_{om} [m] is the roughness length for momentum transfer, k is von Karman's constant (0.41), ψ_m and ψ_h are stability correction functions for momentum and heat transfer respectively.

r_a is a spatio-temporal variable, which regulates the transfer of heat, momentum and water vapour from an evaporating surface into the air above the vegetation canopy. r_a is inversely proportional to wind speed and changes with height above the ground.

In calculating r_a, three simplifying assumptions were made: 1) Brutsaert's (1982) aerodynamic roughness parameterization in which $z_{om} \approx 0.13 h_v$ and $d_o \approx 2h_v/3$; 2) the thermal roughness parameterization in which $z_{oh} \approx 0.1 z_{om}$ where h_v is vegetation height and 3) prevalence of neutral atmospheric conditions i.e. $\psi_m = \psi_h = 0$. These assumptions finally allowed the assessment of *PET* at GS01-GS08 ADAS locations. For GS00 and GS10 with wind speed profile measurements, r_a was calculated in a more sophisticated way, without simplifying assumptions 2 and 3.

3.5.2 Actual evapotranspiration

In this study, three methods of actual evapotranspiration assessment where attempted: 1) Bowen ratio-surface energy balance approach (BSEB); 2) temperature profiles-surface energy balance (TSEB) approach and; (3) Penman-Monteith (*P-M*) approach.

Bowen ratio-surface energy balance approach

The surface energy balance over land can be expressed as

$$R_n = G_o + H + \lambda E \qquad \text{[W m}^{-2}\text{]} \qquad (3.6)$$

where R_n, G_o, H and λE are net radiation, soil heat flux, sensible heat flux and latent heat flux respectively. λ [J Kg^{-1}] is the latent heat of vaporization of water and E [Kg m^{-2} s^{-1}] is the vapour flux density. The energy stored and used by vegetation is often negligible and is normally ignored in Equation 3.6. Partitioning the available energy (R_n-G_o) into latent heat (λE) and sensible heat (H) exchanges is of paramount importance in the energy balance equation, if the objective is to determine evaporation. If the fraction of influx energy (R_n-G_o) used to evaporate water can be separated from that used in heating the atmosphere, then λE can be easily calculated from the available energy. This energy partitioning can be achieved through the so-called Bowen ratio (β), which by definition (Bowen, 1926), is a ratio of sensible heat flux (H) to latent heat flux (λE) expressed as

$$\frac{H}{\lambda E} = \beta = \gamma \frac{\partial T_a}{\partial e_a} \qquad (3.7)$$

where ∂T_a and ∂e_a are vertical air temperature and actual vapour pressure gradients respectively, with T_a [^{o}C] representing air temperature and e_a [kPa] representing actual vapour pressure. γ [kPa^{-1} ^{o}C^{-1}] is the psychrometric constant given by: $\gamma = C_p P_a \lambda^{-1} \varepsilon^{-1}$ where C_p [J Kg^{-1} ^{o}C^{-1}] is specific heat at constant pressure for moist air usually taken as 1.013×10^{-3} MJ Kg^{-1} ^{o}C^{-1}, λ [MJ Kg^{-1}] is latent heat of vaporization, which is a function of the temperature (T in ^{o}C) of an evaporating surface given by $2.501 - 2.36 \times 10^{-3} T$ and ε [-] is the ratio of molecular weight of water vapour to that of dry air (0.622). P_a [kPa] is the atmospheric pressure given by $P_a = P_o [(T_o - \alpha_d (Z - Z_o))/T_o]^{5.25}$ where values for T_o [K] and P_o [kPa] and Z_o [m] are commonly taken as 293 K, 101.3 kPa and 0 m respectively. Z [m] is the elevation of the location in meters above the mean sea level, α_d [k m^{-1}] is the adiabatic lapse rate, normally taken as 0.0065 k m^{-1} for saturated air and 0.01 k m^{-1} for unsaturated air. Once β is known then λE can be calculated from measured R_n and G_o according to

$$\lambda E = \frac{R_n - G_o}{\beta + 1} \qquad (3.8)$$

51

R_n can be computed from Equation 3.1, provided that all components of incoming and outgoing radiation on the earth surface are known. G_o can be determined by monitoring soil temperature changes of a soil profile through time as described by

$$G_o = C_s \int_0^{z_s} \frac{\partial T_s}{\partial t} dz \qquad (3.9)$$

where C_s is the heat capacity per unit volume of soil, t is time, z_s is the soil depth which responds to temperature change and T_s is surface temperature.

According to Brutsaert (1982), the Bowen ratio surface energy balance (BSEB) method is more accurate when β is small. However, the BSEB method has a problem of numerical instabilities when β approaches −1. Angus and Watts (1984) through extensive experiments showed the error potential when β drops below −0.2. In an attempt to circumvent this problem, the values of β between −1.1 and −0.2 were fixed, in this study, but the calculation of actual evapotranspiration on some particular days still remained suspicious.

If not directly measured, soil heat flux (G_o), which is a component of the surface energy balance can be estimated from R_n with no dependence on soil properties according to De Bruin and Holtslag (1982) and Stull (1988) as follows, for daytime conditions: $G_o=0.1R_n$ and for night time conditions: $G_o=0.5R_n$.

Temperature profiles-surface energy balance approach

The temperature profiles-surface energy balance (TSEB) approach is based on deriving AET as latent heat flux (λE) from the surface energy balance (Equation 3.6) under the assumptions that G_o and R_n are considered as known (usually measured at least partially) and that the sensible heat flux (H) is derived from the temperature profile (TP) method. The theoretical basis of TP is given below.

In the atmospheric surface layer, the similarity relationships for the profiles of the mean wind speed u_z and the mean temperature difference θ_o-θ_a are usually expressed as

$$u_z = k^{-1} u_* \left[\ln\left(\frac{z-d_o}{z_{om}}\right) - \psi_m\left(\frac{z-d_o}{L}\right) + \psi_m\left(\frac{z_{om}}{L}\right) \right] \tag{3.10}$$

$$\theta_o - \theta_a = (ku_* C_p \rho)^{-1} H \left[\ln\left(\frac{z-d_o}{z_{oh}}\right) - \psi_h\left(\frac{z-d_o}{L}\right) + \psi_h\left(\frac{z_{oh}}{L}\right) \right] \tag{3.11}$$

where height z [m] is measured above the surface, u_* is the friction velocity, C_p is the specific heat capacity of air taken as 1.013 kJ Kg^{-1} $^{\circ}$C^{-1}, ρ [kg m^{-3}] is air density, k is von Karman's constant (0.41), d_o is the zero plane displacement height, z_{om} is the roughness height for momentum transfer, z_{oh} is the scalar roughness length for heat transfer, θ_o is the potential temperature at the surface, θ_a is the potential temperature at height z, L [m] is the Monin-Obukhov length, ψ_m and ψ_h are stability correction functions for momentum and heat transfer respectively. It is best if ψ_m and ψ_h are derived through field experiments. In this study however we adopted the Businger-Dyer integrated stability functions, because no field experiments were carried out in this regard.

For unstable conditions ($L<0$), ψ_h and ψ_m can be estimated from Equation 3.12 and 3.13 respectively

$$\psi_h = 2 \ln\left[\frac{(1+x^2)}{2}\right] \tag{3.12}$$

$$\psi_m = 2 \ln\left[\frac{(1+x)}{2}\right] + \ln\left[\frac{(1+x^2)}{2}\right] - 2\arctan(x) + \frac{\pi}{2} \tag{3.13}$$

where x is given by

$$x = \left(1 - 16\frac{z-d_o}{L}\right)^{1/4} \tag{3.14}$$

For stable atmospheric conditions ($L>0$), ψ_m and ψ_h are given by

$$\psi_h = \psi_m = \left[-5 \left(\frac{z - d_o}{L} \right) \right]$$ (3.15)

The effect of the modification of forced convection by temperature gradients on momentum and heat (and water vapour) transfer can be corrected by dimensionless parameters. One of the widely used stability parameter is known as the Monin-Obukhov correction factor. The Monin-Obukhov length L [m] is given by

$$L = -\frac{\rho C_p u * T_v}{kgH}$$ (3.16)

where, g [m s^{-2}] is acceleration due to gravity and T_v [^{o}C] is mean air temperature near the surface. When L is greater than 0 stable atmospheric conditions exist and when L is less than 0 unstable atmospheric conditions prevail otherwise the conditions are neutral. The derivation of H is obtained by solving a system of non-linear Equations 3.10-3.16 iteratively, until the value of H do not change significantly (< 5%). Essentially, the derivation of H only requires, wind speed and temperature at the reference height (e.g. 18 m for GS00 and GS10) as well as surface temperature and is independent of other surface energy terms. This scheme is referred hereafter as the temperature profile (*TP*) method.

In the above derivations, the aerodynamic and thermal roughness parameters need to be known. In a region of the earth close to the surface when wind speed and vegetation parameters (height and *LAI*) are available, the within canopy turbulent model of Massman (1997) can be used to estimate aerodynamic parameters (z_{om} and d_o). Su et al. (2001) have applied the Massman (1997) model to three different environments (cotton, shrubs and grass), and obtained fairly reasonable aerodynamic parameters for all those environments. Reasonable estimates of z_{om} and d_o for vegetation have also been obtained by using empirical relationships over fairly flat and uniform surfaces as for example with Brutsaert's (1982) relationships of $z_{om} \approx 0.13 h_v$ and $d_o \approx 2 h_v / 3$ where h_v is vegetation height. However, both z_{om} and d_o for vegetation are known to be a function of wind speed (Kustas et al., 1989) and as such are spatially and temporally

54

variable. A further complication arises, when the surface is partially covered by vegetation. Then vegetation density becomes important as well as the shape (Raupach, 1994). If a detailed land cover classification exists, then the tabulated values of Wieringa (1986; 1993) can be used. When all other information is unavailable then the aerodynamic parameters can be deduced from vegetation indices obtained from satellite data. However, since the aerodynamic parameters depend on wind speed and wind direction as well as on surface characteristics any simplification scheme should be used only if data is lacking (Su, 2002) and the uncertainty of such an assessment should be emphasized. As mentioned, the simplified Brutsaert assumptions can be used for a rough estimate of the aerodynamic roughness parameters (z_{om} and d_o) when data availability is limited. However, in the case of more extensive monitoring schemes, the more reliable concept of effective height of roughness elements (h_{eff}) can be applied.

For a homogeneous region of the earth close to the earth surface (but at some distance above the roughness elements), under steady state conditions, the wind profile is generally accepted to be logarithmic

$$u = \frac{u_*}{k} \ln\left[\left(\frac{z - d_o}{z_{om}}\right)\right] \tag{3.17}$$

where, u is wind speed at height z, $u_* = (\tau_o/\rho)^{0.5}$ is the friction velocity, τ_o is the surface shear stress and ρ is the air density.

Due to data deficiency, in this study it was assumed that the logarithmic wind profile was already satisfied i.e. Equation 3.17 is valid. With this assumption in mind, and by using simple expressions of Brutsaert (1982) and with wind speed measurements at two heights above the canopy, a system of simultaneous equations was developed to determine the effective height of roughness elements (vegetation, huts, hills etc.) at near-neutral conditions according to

$$u_1 = \frac{u_*}{k} \ln\left[\left(\frac{z_1 - 2/3 h_{eff}}{0.13 h_{eff}}\right)\right] \tag{3.18}$$

$$u_2 = \frac{u_*}{k} \ln\left[\left(\frac{z_2 - 2/3h_{eff}}{0.13h_{eff}}\right)\right] \qquad (3.19)$$

where u_1 and u_2 are wind speed measurements at heights z_1 and z_2 respectively and h_{eff} is the effective height of roughness elements which can be understood as equivalent height that will produce an observed roughness. However, before such an approach can be applied, data under near-neutral conditions must be selected from the entire dataset.

With gradients of wind speed and temperature relatively close to the surface, stability can be estimated from the Richardson number R_i, which indicates that near–neutral conditions prevail when, R_i tends to zero.

$$R_i = \frac{g}{T_a} \frac{\partial T_a}{\partial z} \Bigg/ \left(\frac{\partial u}{\partial z}\right)^2 \qquad (3.20)$$

where g is acceleration due to gravity and T_a is air temperature. To obtain profiles with reliable wind speeds at near-neutral conditions, R_i should meet the criterion $|R_i| \leq 0.015$. Due to the lack of wind direction measurements in our monitoring sites, h_{eff} values were averaged for each month. The underlying assumption was that the average effective height of roughness elements was consistent over the whole fetch area on a monthly basis. In essence, by calculation of effective roughness height, an attempt was made to lump the influence of those parameters that are unavailable or are impossible to obtain reliably and accurately e.g. one-sided leaf area index (*LAI)* and vegetation height of the whole fetch area. In situations where, h_{eff} could not be determined because of absence of near-neutral conditions, z_{om} and d_o were obtained directly from the mean vegetation height, according to Brutsaert (1982). However, this approach does not account for the influence of tree leaves. The influence of damage to tree leaves due to herbivory has been reported by Warrington et al. (1989), Vanderklein et al. (2004) and Katjiua and Ward (2006).

Table 3.3 presents the average effective height of roughness elements obtained at the high tower locations of GS00 and GS10. For some months the standard deviations are high, suggesting high variance in aerodynamic roughness parameters during these periods, and also low standard deviations are apparent, thus suggesting low variances in roughness parameters for those specific months. This may be explained partly by changes in wind direction with regard to roughness elements and changes in vegetation condition. The high effective heights of roughness elements observed at GS00 as compared to GS10 may be partly explained by the fact that in general the vegetation in the hardveld area is taller and more diverse in terms of shape and size as compared to the sandveld area where GS10 is located. A further explanation stems from the fact that the hardveld is characterized by a rugged topography as compared to the largely flat sandveld area where GS10 is situated. The large standard deviations in effective heights of roughness elements, observed at GS00 as compared to GS10, largely reflect this distinct difference between the hardveld and sandveld landscape characteristics. Table 3.4 presents the average effective heights of roughness elements (largely vegetation) at various monitoring sites of GS01-GS08, the results are in the same order of magnitude as GS10 h_{eff} averages, suggesting a similar evolution of aerodynamic roughness parameters.

The derivation of λE using temperature profiles and the surface energy balance also requires knowledge of the scalar roughness height of heat transfer (z_{oh}), mainly for the calculation of H. A widely used parameter for comparing z_{om} and z_{oh}, is expressed by Owen and Thompson (1963) as $kB^{-1}=\ln(z_{om}/z_{oh})$ where B^{-1} is a dimensionless inverse Stanton number. Various semi empirical parameterizations for computation of kB^{-1} for a savanna, vineyard and bare soil are compared by Verhoef et al. (1997). But none of these parameterizations was able to compute the correct kB^{-1} values for savanna (partially vegetated surfaces). More recently, Su et al. (2001) evaluated two kB^{-1} models, a model of Blümel (1999) and the extended model of Massman (1999) on three surfaces cotton, shrubs and grass.

Table 3.3. Monthly average values of effective height of roughness elements derived at near-neutral conditions based on GS00 and GS10 wind speed measurements; The number in parenthesis is the standard deviation; *n* is the number of observations and ** indicates no information

Month	GS00 2001 h_{eff} (m)	n	GS00 2002 h_{eff} (m)	n	GS00 2003 h_{eff} (m)	n	GS10 2003 h_{eff} (m)	n	GS00 2004 h_{eff} (m)	n	GS10 2004 h_{eff} (m)	n
January	**	**	**	--	9.73(3.96)	6	**	--	9.13(2.94)	5	1.87(0.71)	21
February	**	**	13.5(1.64)	4	9.52(4.13)	59	**	--	7.48(3.43)	10	1.92(0.73)	16
March	**	**	10.89(5.03)	8	9.32(4.10)	66	**	--	10.99(3.70)	64	2.31(0.42)	12
April	**	**	7.30(3.65)	47	9.42(3.77)	45	**	--	14.41(1.16)	32	1.92(0.76)	14
May	**	**	8.82(3.14)	25	9.01(2.95)	23	**	--	**	--	2.25(0.44)	15
June	**	**	8.20(3.76)	34	9.26(3.12)	10	**	--	7.21(3.81)	10	1.76(0.40)	8
July	**	**	8.51(4.29)	13	7.73(3.36)	12	**	--	7.92(4.79)	27	2.14(0.77)	4
August	**	**	11.78(4.19)	16	9.56(4.19)	36	**	--	9.72(3.54)	52	2.56(0.11)	6
September	8.27(3.90)	18	9.94(3.45)	16	9.89(3.82)	44	**	--	9.23(3.82)	56	1.88(0.71)	9
October	8.14(3.53)	34	9.35(2.87)	17	7.41(3.14)	22	**	--	10.38(1.88)	11	2.04(0.43)	10
November	9.57(5.70)	12	7.35(4.37)	18	8.20(4.63)	13	2.09(0.45)	14	9.98(4.62)	46	2.07(0.39)	20
December	14.61(0.90)	5	6.70(3.34)	6	8.74(4.34)	23	1.98(0.57)	17	3.50(-)	1	2.68(-)	1

Table 3.4. Average values of effective height of roughness elements derived at near-neutral conditions based on mobile tower wind speed measurements at 2 m and 10 m heights at sites GS01-08; The number in parenthesis is the standard deviation and ** indicates no information

Station	GS01	GS01	GS02	GS02	GS03	GS03	GS04
Month/year	2002	2003	2002	2003	2002	2003	2003
January	**	**	**	**	**	1.78(0.51)	**
February	**	**	**	**	**	**	2.22(-)
March	**	**	**	**	**	**	**
April	**	**	**	0.54(-)	**	**	**
May	**	**	**	**	**	**	2.30(-)
June	**	1.81(0.52)	**	1.97(0.59)	**	**	**
July	**	**	**	1.04(0.44)	**	1.91(-)	1.16(0.17)
August	**	**	**	**	**	**	**
September	**	**	**	**	**	**	**
October	2.55(0.17)	**	**	**	**	**	**
November	2.61(0.15)	**	**	**	2.42(0.19)	**	**
December	**	**	2.05(0.39)	**	**	**	**
**	**	**	**	**	**	**	**
Station	GS05	GS06	GS06	GS07	GS07	GS08	GS08
Month/year	2003	2002	2003	2002	2003	2002	2003
January	**	**	**	**	**	**	1.97(0.55)
February	1.48(0.18)	**	**	**	**	**	**
March	**	**	**	**	1.74(0.36)	**	1.68(0.26)
April	**	**	1.51(0.42)	**	**	**	**
May	2.08(0.06)	**	**	**	**	**	**
June	**	**	**	**	2.63(0.07)	**	2.22(0.25)
July	**	**	**	**	**	**	**
August	2.13(-)	**	**	**	**	**	**
September	**	**	**	**	**	**	**
October	**	2.39(0.37)	**	**	**	2.60(0.10)	**
November	**	**	**	2.59(0.22)	**	**	**
December	**	**	**	**	**	1.89(0.70)	**

They found out that the model of Massman (1999) was superior in estimation of kB^{-1} values for a shrub surface over the Blümel (1999) model. Since the shrub environment represents a partially vegetated surface that closely resembles the study area, the Massman (1999) model has been adopted. In the current study, kB^{-1} values were computed according to

$$kB^{-1} = \frac{kC_d}{4C_t \dfrac{u_*}{u(h_{ws})}(1-e^{-n_{ec}/2})} f_c^{\,2} + kB_s^{-1} f_s^{\,2} \qquad (3.21)$$

where, n_{ec} is the within canopy wind speed profile extinction coefficient formulated as; $n_{ec}=C_dLAI_c/(2u_*^2/\ u(h_{ws})^2)$, C_d is the drag coefficient of the foliage elements assumed to take a value of 0.2, LAI_c is the one sided leaf area index defined for the total area, $u(h_{ws})$ is the horizontal wind speed at the top of the canopy, f_c is the fractional canopy coverage and f_s is its complement. C_t is the heat transfer coefficient of the leaf, and kB_s^{-1} is calculated according to; $kB_s^{-1}=2.46(Re_*)^{0.25}$-ln(7.4) where Re_* is the roughness Reynolds number expressed as; $Re_*=h_su_*/v_a$ with h_s the roughness height of the soil, and it is assumed to take a value of 0.009 m. The kinematic viscosity of the air v_a is given by $v_a =1.327\text{x}10^{-5}(P_o/P_a)(T_a/T_o)^{1.81}$, with P_a and T_a the ambient pressure and temperature and P_o=101.3kPa and T_o =273.15K. Once z_{om} and kB^{-1} values are known then z_{oh} can be derived from

$$z_{oh} = z_{om}/\exp\!\left(kB^{-1}\right)$$

(3.22)

The input requirements and parameters of Equation 3.21 used for the high tower monitoring sites are presented in Table 3.5.

Table 3.5. Input requirements for the kB^{-1} model and the parameters used for the high tower monitoring sites of GS00 and GS10

Symbols (unit)	Variables and parameters	GS00 data (hardveld)	GS10 data (sandveld)
u (ms^{-1})	Wind speed at reference height	Actual measurements	Actual measurements
T_a (°C)	Air temperature at reference height	Actual measurements	Actual measurements
P_a (kPa)	Surface air pressure	90.2	87.7
h_{ws} (m)	Maximum measurement height	18	18
LAI_c (-)	Leaf area index per total area	0.0075	0.0084
f_c	Fractional foliage cover	0.27	0.27
C_t	Heat transfer coefficient of the leaf	0.01	0.01

The *TP* method will not work when no temperature differences (no gradient) are observed between two measurement heights, a situation that was occasionally encountered in the present research

60

work. Once H is known then AET can be calculated from the surface energy balance equation by applying as input, also G_o and R_n. R_n was post processed (using Equation 3.1) from separately measured radiation balance components at GS00 and GS10 locations, and G_o estimates were obtained as 0.5 and 0.1 of R_n, for nighttimes and daytimes respectively.

Penman-Monteith approach

A physically realistic way to determine the partitioning of H and λE, is the Penman-Monteith approach. A problem with this approach is that it is complicated, and several input parameters are needed which are difficult to obtain. According to this model actual evapotranspiration is calculated as

$$\lambda E = \frac{\Delta_T (R_n - G_o) + \rho_a C_p \left(\dfrac{e_s - e_a}{r_a} \right)}{\Delta_T + \gamma \left(1 + \dfrac{r_s}{r_a} \right)} \qquad (3.23)$$

where λE [MJ m^{-2} day^{-1}] is latent heat flux (for actual evapotranspiration), R_n (MJ m^{-2} day^{-1}) is net radiation, G_o [MJ m^{-2} day^{-1}] is soil heat flux, γ [kPa $^{\circ}$C^{-1}] is the psychrometric constant, C_p [kJ Kg^{-1} $^{\circ}$C^{-1}] is the specific heat capacity of air taken as 1013 kJ Kg^{-1} $^{\circ}$C^{-1}, Δ_T [kPa $^{\circ}$C^{-1}] is the rate of change of the saturation vapour pressure with temperature, e_s [kPa] is the saturation vapour pressure, ρ_a is mean air density at constant pressure, e_a [kPa] is the actual vapour pressure, r_s [s m^{-1}] and r_a [s m^{-1}] are surface and aerodynamic resistances respectively. *Subsequently, the AET in mm/day is expressed as AET=0.408 λE, in which 0.408 is a conversion factor and λE is express by* Equation 3.23.

A similar assessment of AET as per Equation 3.23 is by far more challenging because of the difficulty in obtaining resistance parameters. The difficulty in using Equation 3.23 refers mainly to the definition of spatio-temporal variables such as r_a and r_s. The difficulties related to the derivation of r_a from Equation 3.5 were already emphasized. Besides r_a, the *P-M* model involves one more difficulty in the definition of such a variable as r_s. Several attempts

were made in the literature to evaluate r_s by means of empirical rules (e.g. O'Toole and Real, 1986). One such an attempt is the so-called Jarvis type models (Jarvis, 1976: Stewart, 1988: De Rooy and Holtslag, 1999), in which stomatal (canopy) resistance is expressed as a minimum r_s multiplied by a series of independent stress functions combined in a multiplicative way, through which each function is representing the influence of each factor. The main weakness of Jarvis type models is the assumption that environmental factors operate independently (Monteith, 1995). Another way in which r_s can be estimated, is through the inversion of the Penman-Monteith equation (Equation 3.24), in which the actual evapotranspiration is considered as a known input parameter (Gash and Stewart, 1975), obtained by other methods (e.g. the TSEB and BSEB approaches).

$$r_s = \frac{\rho_a C_p (e_s - e_a) + r_a (\Delta_T (R_n - G_o) - \Delta_T \lambda E - \gamma \lambda E)}{\gamma \lambda E} \qquad (3.24)$$

Here, the notations are as described earlier. Obviously, this approach cannot be used for determination of AET. The surface resistance can also be estimated by substitution of stand transpiration (T_p: expressed as vapour flux density) derived from sap flow measurements in place of E in the inverted Penman-Monteith equation (Equation 3.24). However, this procedure is practically valid only for dry season estimates of T_p when the assumption $E=T_p$ can be made.

3.6 Results and discussion

Evapotranspiration is a major component of the water balance, and as such is used as input in groundwater recharge models which are used in groundwater resources evaluation and management.

All the radiation balance components were monitored only at GS00 and GS10. Additionally, $S\downarrow$ was monitored in GS08. The diurnal course of net radiation on a clear-sky is typically bell-shaped during daytime, with maxima around midday and minimum values at nighttime (Figure 3.2). However, when there is overcast, the bell-shaped temporal pattern will be interrupted, and can take various forms

depending on the persistence of the overcast. Additionally, data analysis revealed that the net radiation is basically high during the summer and low during the winter season, with high daily variability in summer as compared to the winter season. Therefore, monitoring of radiation components especially shortwave incoming radiation is vitally necessary for reliable estimates of R_n for evapotranspiration assessment in the Kalahari. This study showed that the R_n derived according to Equation 3.2 is a reasonable and cost effective (net radiometer is typically several times more expensive than the shortwave radiometer) approximation, since the *PET* obtained by using such R_n, explains 80% of the variance of *PET* obtained by using R_n determined directly from measured, site specific net radiation components at GS00 and GS10 sites. The maintenance of the instruments is important for the radiation data quality assurance. All the radiometer domes of this study were occasionally cleaned to remove dust and bird droppings to minimize erroneous readings. Besides, the relative accuracy of radiometer devices was continuously monitored by comparing the measured (less spatially variable) incoming shortwave radiations at GS00, GS08 and GS10 to keep good quality data.

Relative humidity (*RH*) and air temperature are important inputs in the assessment of *AET* and *PET*. *RH* and air temperature within the study area are less spatially variable, but highly temporally variable. The large diurnal variations which are associated with both variables (Figure 3.3) in the Kalahari, emphasize the significance for their proper monitoring so that reliable evapotranspiration estimates can be achieved. The less spatial variability is mainly manifested by the high coefficients of determination (R^2) presented in Table 3.1. However, *RH* is more vulnerable to error than air temperature because of sensor calibration drift, accumulation of dust and moisture on the sensor including occupation by insects. Therefore, it needs to be calibrated at least once a year, and regularly cleaned to remove any undesirable artefacts. In the current study the integrity of *RH* and air temperature was controlled during mobile tower campaigns by comparing readings of the permanent *RH/T* monitoring sites with the *RH/T* readings of the mobile tower. Any significant deviations in such comparison would then reflect abnormalities with one or more

sensors. This procedure for assessing the integrity of *RH* and air temperature is "strongly recommended" by Allen (1996).

Wind speed measurements are critical for the evapotranspiration assessment. In the current study the reliability of wind speed measurements was monitored by employing additional anemometers at permanent wind speed monitoring sites during mobile tower campaigns, in this case significant deviations in anemometer readings should reflect some abnormalities with one or both sensors. Both, *PET* and *AET* require wind speed measurements above the roughness elements i.e. above the top canopy level in case of *PET* at least one and in case of *AET* at least two of such measurements. In the study area these conditions were fulfilled only at the two reference towers of GS00 and GS10 where *PET* and *AET* could have been defined directly. In the other sites such as GS01-08, only *PET* was defined indirectly using the mobile tower and the good wind speed correlations between 2 m wind speed measurements at different distant locations and between 2 m and 10 m at the same location.

The correlation coefficients of the regression models turned out to be surprisingly high as for the usually weakly correlated wind speed measurement. This was likely due to the homogeneous wind characteristics in the Kalahari sandveld resulting from short and quite sparse vegetation having aerodynamically uniform wind characteristics. The lack of two wind speed and two *RH/T* measurements above the canopy level did not permit the calculation of *AET* at GS01-08 sites. This however was not critical because *PET* is typically sufficient as input for groundwater models. Moreover once the wind profiles for GS01-08 are established, for example by using multilevel wind speed mobile tower, then *AET* can be estimated even by backward data extrapolation.

The experience of the current research showed that single point measurement of soil heat flux cannot represent the entire footprint area because of surface and subsurface inhomogeneity. The surface inhomogeneity was caused by variations in fractional vegetation cover (related to sparse vegetation) and in leaf area index (related to vegetation species diversity) resulting in canopy shadows and canopy

light interception, which can obscure radiative heating of bare soil surfaces; there is, at all times, no unique soil surface temperature that could be defined for the entire footprint area. The subsurface inhomogeneity was caused by variability of thermal conductivity of soils which are largely dependent on soil moisture condition. For the above mentioned reasons, the soil heat flux measurements obtained by soil heat flux plates and soil temperature sensors at GS00 and GS10 sites were not used for estimation of G_o according to Equation 3.9. Instead, common empirical relationships that define G_o as $0.5R_n$ for nighttimes and $0.1R_n$ for daytimes without dependence on soil properties were used, since both surface temperature and thermal gradient of the soil reacts to R_n.

The potential evapotranspiration was estimated for all ADAS locations (Figure 3.1) in the study area using a combination of measured and regressed data input. Figure 3.5 illustrates the spatial and temporal variability of *PET* for five days of November 2003. The *PET* in all the monitoring sites is in the same order of magnitude for each specific day. This indicates that in the study area, *PET* does not vary much spatially, instead is remarkably temporally variable.
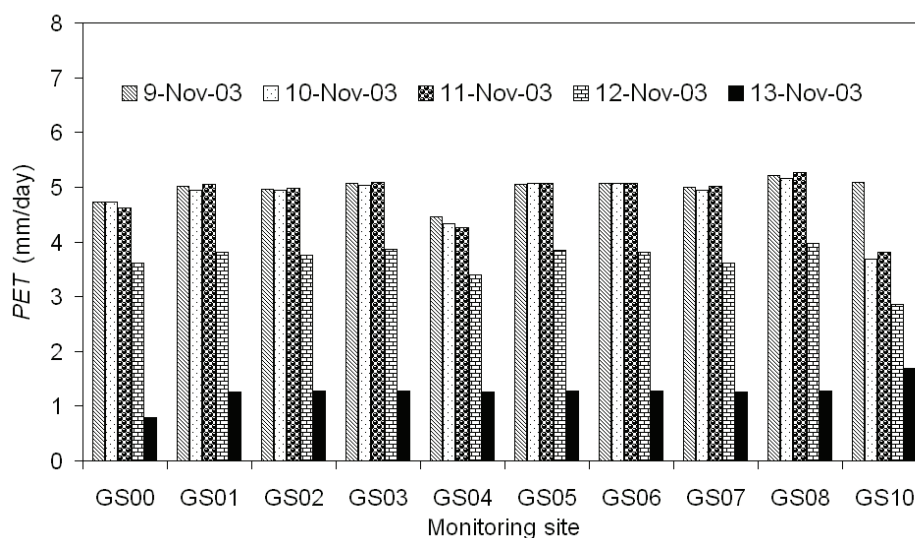
Figure 3.5. Daily *PET* in all monitoring sites (GS00–GS10) for five subsequent days, 9-13 November 2003

Table 3.6 analyzes further the spatial variability of *PET*. This variability is due to the variability in the input parameters used for *PET* calculation. As mentioned, in the study area the relative humidity and air temperature are monitored at all ADAS locations. The short-wave incoming radiation that is available in GS00, GS08 and GS10 locations is spatially invariable so it does not influence spatial variability of *PET*. The most critical wind speed input, was only permanently available at GS00, GS08 and GS10 due to budgetary constraints. At GS01-07 the wind speed input was available only temporarily from the 'mobile tower' which made it possible to establish the regression models with GS08 and later with GS10 that turned out to be surprisingly good in the Kalahari but would not necessarily be that good elsewhere.

Table 3.6. Minimum (Min.) and maximum (Max.) *PET* rates for GS01-GS10

	2002 daily *PET* (mm/day)		2003 daily *PET* (mm/day)		2004 daily *PET* (mm/day)	
Monitoring tower	**Min. rate**	**Max. rate**	**Min. rate**	**Max. rate**	**Min. rate**	**Max. rate**
GS00	0.1	5.8	0.2	5.8	0.2	6.1
GS01	1.0	6.0	0.7	5.9	1.0	5.9
GS02	1.1	6.0	0.8	5.8	1.0	5.7
GS03	1.1	6.0	0.8	5.9	1.1	5.9
GS04	1.0	6.0	0.8	5.4	1.1	5.8
GS05	1.1	6.1	0.8	5.9	1.0	6.0
GS06	1.1	6.0	0.8	5.9	1.0	5.9
GS07	1.1	5.6	0.8	5.8	1.0	5.8
GS08	1.1	6.3	0.8	6.1	0.9	6.1
GS09	0.1	6.0	**	**	**	**
GS10	**	**	**	**	0.3	5.0

Figures 3.6 and 3.7 illustrate daily variability of evapotranspiration in one year (2004) for GS00 and GS10. The temporal variations in daily *AET* with the BSEB and TSEB methods are evident in Figures 3.6 and 3.7. These variations are in the same order of magnitude for GS00 and GS10 and range from 0.1 to 3.5 mm/day. The results are in the same order of magnitude as those obtained through a remote sensing based energy balance solution by Timmermans and Meijerink (1999) that ranged from 1.5 to 3 mm/day. The seasonal trends in actual evapotranspiration of both sites are characterized by higher actual

evapotranspiration rates in the hot and humid summer and lower in the cold and dry winter periods. The higher evapotranspiration rates in summer are obviously related to increased availability of water for evapotranspiration, higher ambient temperatures and higher solar radiation.

Apart from a few data loss discontinuities in Figures 3.6 and 3.7, the majority of discontinuities in the time series analysis of TSEB AET are where the temperature differences between two measurement heights were zero. In such a situation the *TP*-profile method (and hence the TSEB approach) runs into problems, which is a more prevalent case in dry periods. Moreover, the results of the TSEB approach (Figure 3.7) at GS10 site, for some winter days give evapotranspiration estimates that exceed the potential rates obtained with Equation 3.4. This indicates the uncertainty of the sensible heat flux derivation by using temperature profiles over the dry Kalahari sandveld. A further observation is that the unrealistic TSEB estimates are more prevalent in the dry winter season rather than in the relatively wet summer season and in GS10 rather than in GS00. Perhaps the TSEB approach is more sensitive to reduced moisture conditions as in GS10 winter peak rather than in GS00 where there is more access to moisture because of direct groundwater evapotranspiration.
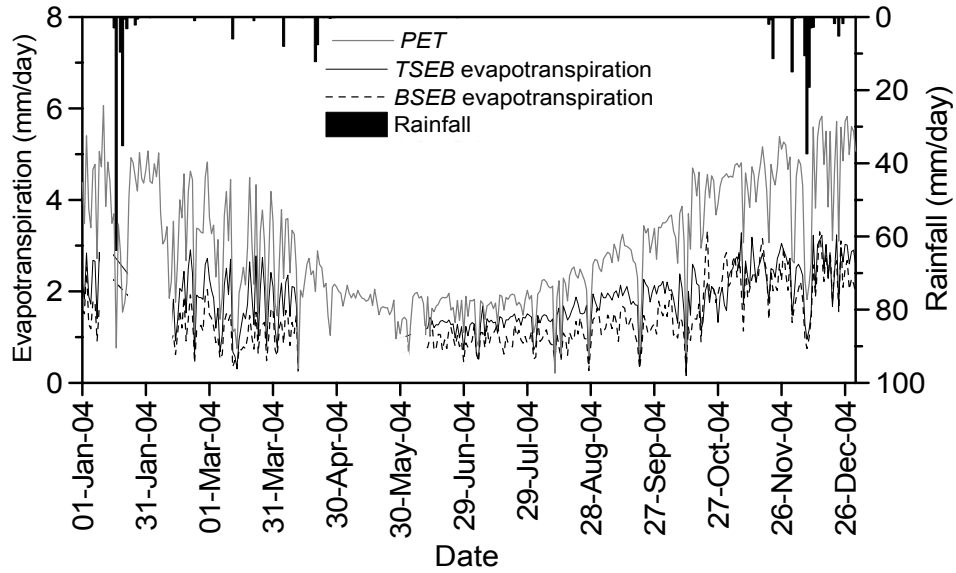
Figure 3.6. Evapotranspiration estimates at GS00 site for year 2004; rainfall is also shown
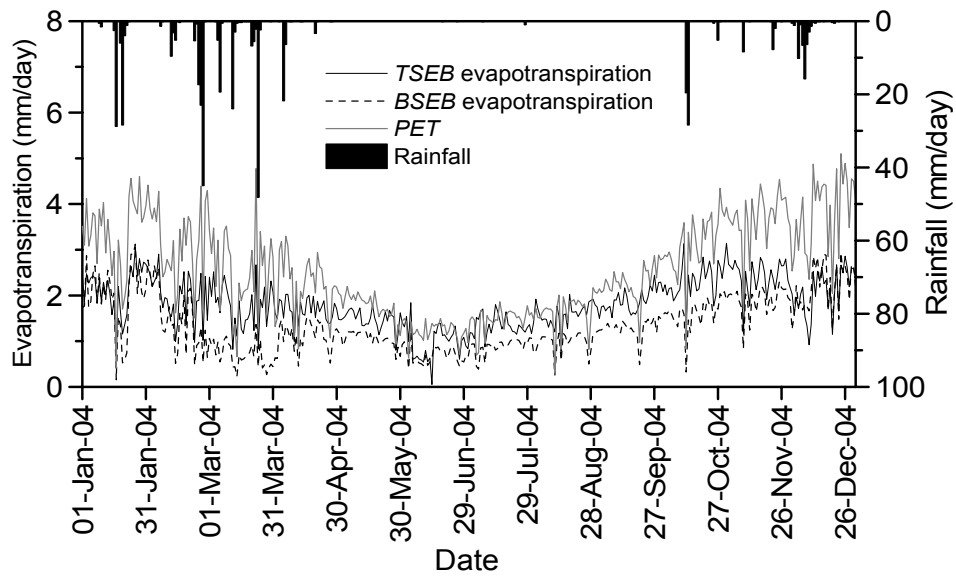
Figure 3.7. Evapotranspiration estimates at GS10 site for year 2004; rainfall is also shown

During data analysis, it was observed that, the *TP* method underestimated the sensible heat flux, and therefore resulted in high residual latent heat flux (evapotranspiration) obtained as a solution of the surface energy balance equation. Furthermore, both aerodynamic and thermal parameters need to be determined more accurately if the intention is to improve the accuracy and reliability of TSEB approach estimation of actual evapotranspiration. For example, data on wind direction must be obtained to reliably estimate aerodynamic parameters. In addition, suitable atmospheric stability correction functions must be defined experimentally for the study area.

In the present study, the difficulty in estimation of roughness parameters must have compounded the problem of uncertainty in the estimation of the sensible heat flux. The lack of independent measurements of the sensible heat flux (e.g. from scintillometers or eddy correlation) makes it impossible to investigate the reliability of the parameters that cannot be measured directly in the present investigation. The reliability of the temperature profile method for sensible heat flux estimation needs to be investigated with independent measurements of sensible heat flux, so that the difficult-to-get parameters can be evaluated through comprehensive assessment.

The experiment with the use of a constant r_s in the *P-M* approach for estimation of *AET* revealed that the best quality of fit (indicated by the coefficient of determination, R^2), that could be obtained in testing a wide range of r_s values (ranging from 110-600 s m^{-1}), as input to resemble BSEB *AET* (assuming that BSEB is reliable) could not exceed 50% of explained variance. The BSEB approach results were used in the experiment because they are lower and therefore, more likely actual evapotranspiration estimates than estimates derived from TSEB approach. Figure 3.8 illustrated the resulting bias (*P-M* estimated *AET* minus BSEB *AET*) of an undertaking when a constant r_s of 270 s m^{-1} was assumed. The resulting large bias of the experiment which ranges from -1.2 to 1.8 put in question the forward applicability of the *P-M* formula for *AET* calculations applying common r_s by "lump, most likely" estimate of this value.
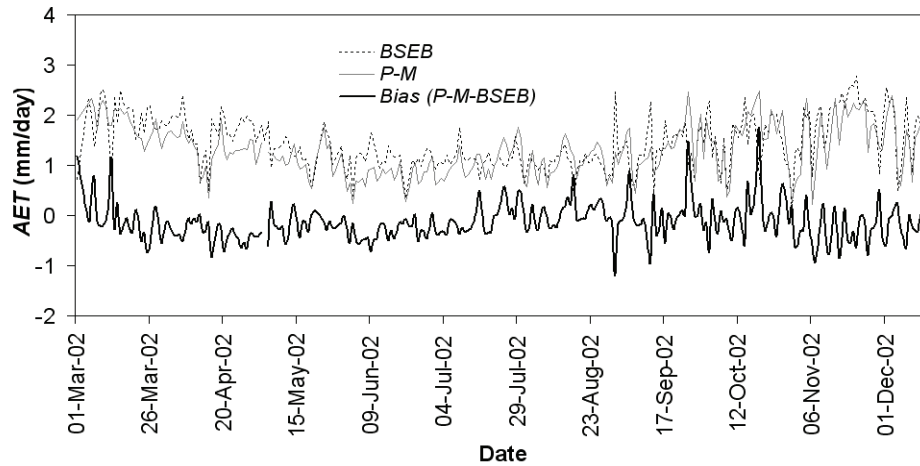
Figure 3.8. GS00 time series of BSEB *AET* **and** *P-M* **estimated** *AET* **and bias between the two**

Table 3.7 presents the annual rainfall, *PET* and *AET* obtained with BSEB and TSEB methods at GS00 (for the years 2002-2004) and at GS10 (for year 2004). The comparison of rainfall with *AET* (Table 3.7) shows that *AET* substantially exceeds the rainfall. The large *AET* at GS00 could be explained by substantial groundwater evapotranspiration (i.e. groundwater root extraction and upward advective-diffusion (Lubczynski, 2000) at the relatively shallow groundwater table (often <10 m)), but the substantially larger *AET* than rainfall at GS10 in the Kalahari sandveld is difficult to explain. The GS10 location is where the groundwater table is at approximately 76 m depth, so the high rates of groundwater evapotranspiration under such thick unsaturated zone are unlikely even knowing about the existence of tree species in the Kalahari, which are able to extend their roots to great depth in search for permanent water bodies. This is because the scale of such process is restricted to the limited deep rooted species such as *B. albitrunca* and *A. erioloba,* and because extensive advective-diffusive upward water movement from depth of more than 70 m is not experimentally confirmed, and is not likely. The most likely explanation is that both BSEB and TSEB methods overestimated the *AET* either because of the algorithmic problem in the circumstances of dry Kalahari conditions or because the applied *AET* assessment approaches account for additional water e.g. from

dew or from hydraulic lift, that does not originate directly from rain. This problem requires further investigation.

Table 3.7. Annual rainfall and annual evapotranspiration for GS00 and GS10; BSEB and TSEB *AET* are presented in two columns, the first column representing a sum of the available daily *AET* estimates (without daily values corresponding to periods when *AET* could not be resolved as explained above) and the second column representing a sum of the calculated *AET* (as in the first column) and of the extrapolated *AET* values for the periods with data gaps using *AET* correlation with *PET* for which 70% of the variance in *PET* was explained by *AET* (for either BSEB or TSEB). The latter adjusted column can be considered as a likely representation of the annual *AET* provided that the correlation with *PET* was appropriate.

Site	Year	Annual rainfall (mm)	TSEB *AET* (mm)	TSEB *AET* + Est. (mm)	BSEB *AET* (mm)	BSEB *AET* + Est. (mm)	*PET* (mm)
GS00	2002	215	509	609	481	558	1068
	2003	312	573	623	526	569	1073
	2004	408	504	624	389	492	1077
GS10	2004	462	655	661	480	486	922

3.7   Conclusions

1. *PET* is highly temporally but less spatially variable in the Kalahari study area; it ranges from 0.1-6.3 mm/day. The surprisingly good correlations between half-hourly wind speed measurements in the Kalahari sandveld facilitated the use of a mobile tower for calculation of Penman-Monteith *PET*, not only in the reference towers with complete input data but also in other eight (GS01-08) ADAS locations where such data was not available.

2. *AET* obtained in the study area by microclimatic methods such as BSEB and TSEB, ranges from 0.1 to 3.5 mm/day. This result in annual totals that exceeds the total rainfall sum, so the most likely conclusion is that TSEB and BSEB overestimated the *AET*, TSEB because of underestimation of sensible heat flux and BSEB because the temperature and relative humidity gradients are very

small particularly in dry conditions at large measurement heights, and therefore difficult to measure reliably (Gieske, 2003).

3. The physically based Penman-Monteith *AET* approach, unfortunately, still suffers an unsolved problem of determination of the temporally variable surface resistance, thus limiting its direct-use in *AET* calculations. More accurate *AET* monitoring schemes such as eddy correlation and scintillometry will often be too expensive to be justified in regional groundwater projects.

4. There is not available as yet, a direct estimation method of groundwater evapotranspiration, which represents fraction of total evapotranspiration. The only way is through modelling of fluxes, which if not supported by extensive soil moisture monitoring of the entire depth of unsaturated zone, may result in uncertain results.

5. While using saturated-unsaturated models in groundwater management, the scientific benefit of using actual evapotranspiration as model input to characterise the fluctuations with time instead of *PET*, is minimal unless a much more advanced methodology is used. In general, focusing on monitoring of *PET* in combination with soil moisture transport modelling seems preferable.

6. The recommended setup for *PET* monitoring in groundwater related projects, involves one anemometer and one relative humidity/temperature sensor per monitoring location and at least one pyranometer per entire monitoring network, for spatially invariant shortwave incoming radiation. Besides, in groundwater monitoring projects, *PET* monitoring should be facilitated by groundwater table and rainfall measurements and optionally by unsaturated zone profile measurements (soil moisture and soil matric pressure) and by sap flow measurements of most abundant trees.

Chapter 4 Kalahari tree transpiration estimated by sap flow technique

4.1 Introduction

The main components of the water balance of the Kalahari are formed by rainfall and evapotranspiration. Almost all the rainfall infiltrates into the sandy subsurface and returns subsequently to the atmosphere by evaporation. The outcome of the previous investigations in the Kalahari under comparable conditions suggested that only about 5 mm escapes this process in the upper soil layers and percolates downward to deeper layers and possibly to the saturated zone (De Vries et al., 2000). However, there are indications that deep rooting trees are able to extract water from deeper parts of the unsaturated zone and possibly from the capillary fringe above the water table at depths of more than 70 m (Chapter 5). This implies that eventually the calculated deep percolation of about 5 mm/yr may be taken up by these trees, which means that the actual net groundwater recharge of the aquifer is less than the estimated 5 mm. This is in accordance with the estimated regional groundwater discharge of the order of 1 mm or less (De Vries, 1984; De Vries et al., 2000)

Kalahari trees are well adapted to dry water stress conditions. Some of them have extremely deep roots (Canadell et al., 1996; Le Maitre et al., 2000) that allow them to reach groundwater and remain green throughout the dry seasons. The significance of the transpiration process and the continuously increasing demand for groundwater supply in water limited ecosystems such as the Kalahari poses a problem of groundwater competition; therefore it deserves great attention particularly in the context of sustainability of groundwater resources.

Various thermal-based techniques are now available for estimating transpiration by measuring tree sap flow (Swanson, 1994; Granier et al., 1996a; Smith and Allen, 1996; Köstner et al., 1998; Wullschleger et al., 1998). The spatio-temporal measure of transpiration called

stand transpiration can be derived through scaling methods (Hatton et al., 1995; Hatton and Wu, 1995; Oren et al., 1998a). The scaling methodology requires *in situ* evaluation of sap velocities and sapwood areas for the different sizes of trees of the same species. Such an approach has been used to estimate stand transpiration in plantations (Hatton and Vertessy, 1990) and in native forests where one, or two dominant species were measured (Granier et al., 1990; Köstner et al., 1992; Cermák et al., 1995; Martin et al., 1997; Granier et al., 2000), typically for a period of few weeks or months only.

The long-term monitoring of transpiration can contribute to an improved understanding of the behaviour of the savanna ecosystem and in providing input data for the hydrological water balance. It can also be an important input for the establishment of the overall water balance since the surface energy balance based algorithms for actual evapotranspiration do not provide sufficient accuracy in water limited ecosystems as indicated in Chapter 3. Despite its importance, the long-term monitoring of water uptake by vegetation in water limited ecosystems such as the Kalahari has been carried out by only a limited number of studies and typically on one species only. The most notable is a two-year sap velocity monitoring of the *Quercus rotundifolia* tree in southern Portugal by David et al. (2004). The present study in contrast to other studies, presents long-term (>2 years) sap flow monitoring over nine natural, savanna tree species, not only in the form of individual temporal sap flow variability per tree but also as temporal variability of transpiration in eight randomly selected plots in the Kalahari.

This chapter investigates (i) the seasonal variability of transpiration for various Kalahari trees; (ii) the relationship between Kalahari trees species transpiration and meteorological conditions and (iii) the spatio-temporal variability of transpiration in selected plots.

4.2 Material and methods

Stand (plot) transpiration can be estimated on the basis of sap flow measurements of individual trees (Hatton and Vertessy, 1990). In this study the sap flow measurements were carried out with the

thermal dissipation probe (TDP) method (Granier, 1987) because of its simplicity, high degree of accuracy, reliability and relatively low cost (Lu et al., 2004).

4.2.1 Sap flow measurement principles and assumptions

Sap flow (Q_s) is a product of sap velocity (v) often referred also as sap flux density and sap wood area (A_x) or more precisely, the conductive (hydro-active) xylem area. Unfortunately, no field method exists as yet to measure Q_s directly therefore Q_s is typically defined through separate measurements of v and A_x as

$Q_s = vA_x$ (4.1)

where Q_s is typically expressed in L/day.

The applied TDP method has been widely used for measuring sap velocity in a number of environments (Granier et al., 1990; Diawara et al., 1991; Granier and Loustau, 1994; Loustau et al., 1996; Loustau et al., 1998; Köstner, 2001; Lundblad and Lindroth, 2002; Sellami and Sifaoui, 2003). According to Granier (1987), v is typically expressed in cm/hr, and can be estimated from the continuously measured temperature difference (ΔT) between two sensor probes, the downstream (upper) heated with constant power of 0.2 W and upstream (lower) non-heated probes, both inserted to a depth of ~2 cm into the sapwood structure and at a distance of 10-15 cm from each other. The ΔT measurements are referenced to ΔT_{max} which is the maximum temperature difference between two probes in a given period, assuming that no sap flow occurs.

$v = 0.0119[(\Delta T_{max} - \Delta T)/ \Delta T]^{1.231}$ (4.2)

For most tree species, ΔT is typically higher in the night and lower during the day due to the cooling effect of convective heat dissipation by sap flow.

The normalised sap flow Q_n of individual trees, typically expressed in L/d/m^2 and seldom in mm/d, can be estimated by

$$Q_n = Q_s / A_c \tag{4.3}$$

where A_c in [m^2] is the projected ground area of a tree crown. The Q_n, particularly when expressed in mm/d, can give a misleading impression that Q_n is a hydrological flux representing areal transpiration, which is not the case because Q_n represents Q_s per its corresponding canopy area. Q_n is useful in comparing water withdrawal efficiency per unit area of the canopy.

Individual Q_s measurements of trees can be scaled up to plot level tree transpiration (T_p) using the following equation (e.g. Pataki and Oren, 2003)

$$T_p = \Sigma Q_s / A_p \tag{4.4}$$

where T_p [LT^{-1}] is mean stand (plot) level transpiration and A_p is the area of the plot. T_p represents a hydrological flux, which if taken over a sufficiently large and representative area (A_p), can be directly compared with other fluxes such as rain, evapotranspiration etc.

The difference between Q_n and T_p is that Q_n takes into account only the spaces within the canopy, whereas T_p also takes into account the spaces between canopies in sap flow scaling.

While undertaking the long-term sap flow monitoring of largely diverse savanna trees, several assumptions had to be invoked, of which the following are critical: (i) sap velocities of sample trees represent different size classes of trees in the Kalahari; (ii) the variations of sap velocity in space are implicitly captured in the variability of sap velocity of the measured sample trees; (iii) the water flux at the sensor location reflects water transpired by leaves i.e. stem capacitance, radial, circumferential and axial sap velocity variations are neglected.

4.2.2 Tree assessment

The assessment of sap flow (Q_s) of individual trees refers to monitoring of temporal variability of sap velocity (v) on various tree species and to the assessment of conductive sap wood area (A_x).

Monitoring of sap velocity

The long-term Kalahari monitoring of tree sap velocities was carried out with TDP type of sensors manufactured by *Umweltanalytische Produkte* (UP) in Germany. The UP monitoring system consists of three sensor pairs (probes) connected in series. Each system is powered through a 12V current regulator using 0.125 A (3 x 0.2W for probes and 0.9W for regulator). At each monitoring sites, two of such systems were installed. The considerable current demand of 0.125 A was continuously supplied through high quality, *Sonnenshein 130Ah* sealed lead-acid, rechargeable batteries placed in a special container, which was buried in the ground to avoid vandalism. At all the monitoring locations, the batteries were exchanged with charged ones every two weeks. All the measurements were sampled every 30 seconds and averaged values stored every 30 minutes by *Skye DataHog2* loggers.

The sap velocity monitoring was carried out between November 2001 and January 2004, in seven monitoring sites of GS01-07 (Figure 3.1) and on nine tree species present in the surrounding of the sites: *A. erioloba, A. fleckii, B. albitrunca, B. africana, D. cinerea, L. nelsii, O. pulchra, S. longipedunculata* and *T. sericea*. Refer to Appendix A for example photographs of species. Every TDP sensor pair was inserted in different trees, except at GS03 where two probes were installed into one tree. The trees were selected to provide coverage of various tree species but also because of different biometric characteristics. The tree selection was also constrained by the length of the TDP cable that limited the measuring distance of the trees from the recording logger because of the minimum voltage (at the sensor side) threshold constrained by manufacturer at ~11.6 V. In the selection of the trees, non-healthy individuals with irregular stems were excluded.

Table 4.1. Biometric characteristics of the trees selected for sap velocity monitoring in plots 01-07; the first four characters of the tree code (GS0*CH*) represent the plot and monitoring site number; the last three characters represent the logger channel number.

Plot name	Selected tree	Tree code	Stem diameter (cm)	Crown diameter (m)	Tree height (m)
GS01	*A. fleckii*	GS01CH6	15.2	4.95	4.8
	B. africana	GS01CH8	20.1	5.1	5.8
	A. fleckii	GS01CH5	14.6	5.8	4.7
	A. fleckii	GS01CH7	10.8	4.8	5.0
	O. pulchra	GS01CH4	3.2	1.1	2.0
	O. pulchra	GS01CH9	6.7	2.3	2.7
GS02	*S. longipedunculata*	GS02CH6	22.6	6.6	7.2
	O. pulchra	GS02CH4	7.0	1.6	2.5
	S. longipedunculata	GS02CH9	15.3	5.3	4.4
	S. longipedunculata	GS02CH7	20.1	5.2	5.5
	S. longipedunculata	GS02CH5	26.4	6.4	8.8
	S. longipedunculata	GS02CH8	19.9	3.8	5.3
GS03	*B. albitrunca*	GS03CH4	12.4	2.5	5.0
	B. albitrunca	GS03CH5	12.4	3.1	4.0
	B. albitrunca	GS03CH6	11.8	2.7	5.4
	A. erioloba	GS03CH7	35.7	10.1	8.8
	A. erioloba	GS03CH9	29.3	6.7	7.8
GS04	*L. nelsii*	GS04CH7	25.1	4.9	6.4
	O. pulchra	GS04CH5	15.6	3.3	3.3
	L. nelsii	GS04CH9	26.1	5.6	7.5
	L. nelsii	GS04CH6	20.4	6.2	4.9
	L. nelsii	GS04CH8	24.2	6.0	7.3
	L. nelsii	GS04CH4	26.3	6.6	7.0
GS05	*A. erioloba*	GS05CH9	10.8	3.3	3.2
	T. sericea	GS05CH4	8.9	3.3	3.3
	T. sericea	GS05CH5	5.7	2.8	2.2
	T. sericea	GS05CH6	8.6	3.7	2.4
	D. cinerea	GS05CH8	10.5	3.9	3.0
	B. albitrunca	GS05CH7	27.7	5.8	5.3
GS06	*T. sericea*	GS06CH9	8.9	8.4	2.6
	T. sericea	GS06CH5	10.5	4.8	3.1
	D. cinerea	GS06CH6	6.4	3.7	2.9
	B. albitrunca	GS06CH4	9.5	1.7	2.4
	B. albitrunca	GS06CH7	15.0	2.6	4.3
	B. albitrunca	GS06CH8	29.3	5.3	5.4
GS07	*A. fleckii*	GS07CH5	15.1	5.6	4.3
	A. fleckii	GS07CH4	9.5	3.3	4.0
	A. fleckii	GS07CH7	7.0	4.0	2.2
	T. sericea	GS07CH6	10.5	4.1	4.1
	T. sericea	GS07CH9	3.5	2.2	3.1
	A. fleckii	GS07CH8	14.3	6.2	5.0

In total 41 trees were selected and Table 4.1 present the biometric characteristics of those trees. Stem diameters were measured at 0.5 m above the ground level, which in the Kalahari environment guaranteed the absence of branches between the sensor location and the ground level. The stem diameters and canopy diameters were defined as averages from the two perpendicular stem and canopy diameters measured by a calliper and a calibrated tape respectively (always in North-South and East-West directions).

In each tree that was selected for sap velocity measurement, TDP sensors were always installed on the southern side of the stem, to minimize thermal effects of sunshine. All the sensors were installed at a height of 0.5 m above the ground level, i.e. the same height as the stem diameter measurement height. At each selected tree, small branches, sprouting leaves and the first loose bark were removed from the stems below the sensors' installation height. After which, two 2.1 cm deep holes (10 cm apart), were drilled into sapwood and two 2.1 cm long aluminium tubes provided by the supplier were inserted into the created holes with a special insertion tool for a depth of 2 cm into the sapwood (xylem) structure. Finally, the two TDP probes covered with a thin layer of silicon grease (to enhance thermal contact and prevent moisture from entering the space between sensors and aluminium tubes) were inserted into the aluminium tubes already inserted in the tree stems (Figure 4.1). The TDP method is generally sensitive to the influence of external atmospheric conditions, therefore thermo-isolating *Terrostat* paste was applied around needles and radiation protection shields were wrapped over TDP probes to insulate the measuring probes from the impact of external conditions.
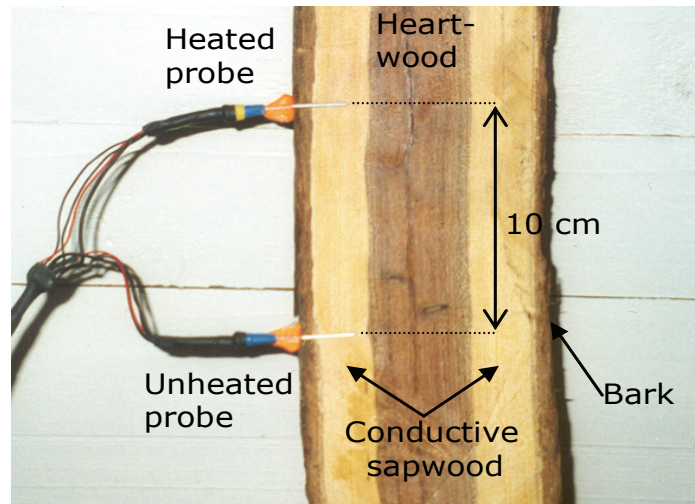
Figure 4.1. Installation of TDP (in *Acacia fleckii*)

At each monitoring site, all the TDP sensor measurements were recorded by 15-bit resolution *DataHog2 Skye* logger allowing for accurate voltage measurements with gain ranging from 0 to 2 mV. Such accuracy is particularly important for TDP measurements of ΔT because, the change of 1 $^{\circ}$C refers to the thermocouple voltage change of only 40μV. In addition to the TDP monitoring, the same *DataHog2* loggers also recorded microclimatic variables such as air temperature, relative humidity and wind speed, all at 2 m height above the ground surface. These observations were made for potential evapotranspiration assessment as described in Chapter 3. At GS08, GS00 and GS10 (Figure 3.1) where measurements for potential evapotranspiration were carried out (see Chapter 3), no sap velocity measurements were done but additional incoming shortwave radiation was monitored to complement other, *PET*-related microclimatic measurements. Besides, at all the monitoring sites, rainfall was measured using *Wallingford* type tipping bucket rain gauges. In all this monitoring, data was stored at 0.5 hr frequency.

The performance of the TDP sensors was checked every two weeks while changing batteries and in case of sensor failures, new sensors were installed to replace those that deteriorated with time. There was no marked difference between the sap velocity measurements of replacement TDP sensors in all cases.

Determination of conductive sapwood area

The sapwood area (A_x) used in this study to calculate sap flow (Q_s) according to Equation 4.1, was estimated on the basis of biometric upscaling functions (BUF) defined through more than 200 whole-tree-cutting and dye-tracing experiments described in Lubczynski et al. (2006, in prep.). Through those experiments, BUF were established by regression functions between A_x and stem areas (A_s) and between A_x and canopy areas (A_c). The selection of the whole tree-cutting and dye tracing method by the current study was made for the following reasons: (1) Kalahari trees turned out to be too hard to use hand increment borers; (2) a number of species in contrast to what is presented in Figure 4.1, had hardly distinguishable contrast between sapwood and heartwood; (3) whole tree-cutting and dye tracing method is still considered the most reliable in A_x (Lu et al., 2004); (4) determination of BUF on the basis of cut tree experiments is a one-time procedure that once done for given species, allows later to estimate A_x in non-invasive way.

For the assessment of A_x in this study, BUF of nine species was needed: *A. erioloba, A. fleckii, B. albitrunca, B. africana, D. cinerea, L. nelsii, O. pulchra, S. longipedunculata* and *T. sericea*. Except of *S. longipedunculata* for which the BUF was defined in this study, all other BUF were obtained from Lubczynski et al. (2006, in prep.) as specified in Table 4.2.

Table 4.2. Biometric upscaling functions (BUF) for estimation of conductive xylem area; A_x and A_s (stem area) are in cm^2, A_c (canopy area) is in m^2; the first eight equations are from Lubczynski et al. (2006, in prep.), and the last one is from the current study.

Tree species	Tree Species symbol	No. of observations. (n)	Regression equation	R^2
A. erioloba	*Ae*	23	$A_x = (4\times10^{-5} A_s + 0.0002)\times10^4$	0.93
A. fleckii	*Af*	11	$A_x = (6\times10^{-5} A_s + 0.0009)\times10^4$	0.94
B. albitrunca	*Ba*	11	$A_x = (8\times10^{-5} A_s - 0.0002)\times10^4$	0.99
B. africana	*Bua*	33	$A_x = (5\times10^{-5} A_s + 0.0003)\times10^4$	0.90
D. cinerea	*Dc*	23	$A_x = (3\times10^{-5} A_s + 0.00002)\times10^4$	0.95
L. nelsii	*Ln*	11	$A_x = (7\times10^{-5} A_s - 0.0004)\times10^4$	0.99
O. pulchra	*Op*	17	$A_x = (170\times10^{-5} A_c - 0.0037)\times10^4$	0.92
T. sericea	*Ts*	32	$A_x = (4\times10^{-5} A_s - 0.0004)\times10^4$	0.86
S. longipedunculata	*Sl*	30	$A_x = (8\times10^{-5} A_s)\times10^4$	0.98

4.2.3 Plot assessment

In order to analyze spatio-temporal variability of T_p in the Kalahari, eight quadratic plots of 30x30 m were demarcated, at the monitored locations of GS01-07 and at the additional location of GS08 site not equipped with TDP sensors (Figure 3.1) but with tree species for which both v and A_x was derived from other locations. In each plot all tree species were classified and their biometric properties were measured. i.e. stem diameter and crown diameter in the same way as for sap velocity monitored trees. In total, 720 trees were identified and measured in eight plots of GS01-08. Table 4.3 presents the plot biometric characteristics such as plot-total stem areas ($A_s{}^p$), plot-total crown areas ($A_c{}^p$) and total number of trees, all classified per species and per plot ($n_o{}^p$).

Table 4.3. Number of trees per species (n_o^p [-]), their stem (A_s^p [cm^2]) and crown (A_c^p [m^2]) areas for each plot; (see Table 4.2 for species symbols)

Plot	Notation	Ae	Af	Ba	Bua	Dc	Ln	Op	Sl	Ts	Totals
GS01	A_s^p	0	5612.1	0	1855.5	7424.4	0	1384.9	0	1787.3	18064
	A_c^p	0	94.7	0	119.8	87.1	0	67.1	0	150.5	519
	n_o^p	0	85	0	8	78	0	24	0	37	232
GS02	A_s^p	0	797.9	0	662.4	0	0	2102.1	2500.5	191.1	6254
	A_c^p	0	39.6	0	62.5	0	0	100	157.4	47.4	499
	n_o^p	0	5	0	21	0	0	69	12	9	116
GS03	A_s^p	2001.5	585	343.2	0	3588.9	0	0	0	389	6908
	A_c^p	134.6	40.8	18.2	0	235.4	0	0	0	46.2	475
	n_o^p	4	5	3	0	16	0	0	0	7	35
GS04	A_s^p	0	66.9	185.7	0	2694.4	17090.3	297.1	0	247.4	20582
	A_c^p	0	26.6	6.5	0	201.2	689	15.6	0	40.1	979
	n_o^p	0	1	2	0	15	46	4	0	7	75
GS05	A_s^p	223.2	46.2	602.6	0	112.4	0	0	0	2004.2	2989
	A_c^p	25.8	7.2	26.4	0	18.2	0	0	0	432	510
	n_o^p	5	2	1	0	1	0	0	0	62	71
GS06	A_s^p	0	0	1998.6	0	7968	326.3	0	0	236.8	10530
	A_c^p	0	0	38.3	0	91.4	35.9	0	0	94.1	260
	n_o^p	0	0	12	0	13	10	0	0	5	40
GS07	A_s^p	0	5068	0	0	1053.4	0	246.2	0	375.6	6743
	A_c^p	0	636.2	0	0	129.4	0	10.8	0	52.6	829
	n_o^p	0	60	0	0	11	0	3	0	7	81
GS08	A_s^p	0	730.4	0	97.5	647.3	0	326.3	0	1038.3	2840
	A_c^p	0	78.1	0	78.1	160.2	0	11.9	0	201.2	530
	n_o^p	0	13	0	1	14	0	6	0	36	70

4.3 Results and discussion

4.3.1 Sap velocity

Main monitoring constraints and uncertainties

Although TDP sap velocity (*v*) measurement method is assumed to be of high degree of accuracy and reliability (Lu et al., 2004), there are many potential sources of uncertainty in using this method.

All thermal methods of sap velocity measurements refer to a selected part of the sapwood area; in case of heat pulse method it is a "point" measurement (Hatton et al., 1995), in case of TDP method it is a "section" measurement and in the case of Cermák et al. (1973) method it is a "sector" measurement. In all cases, the acquired measurement results are integrated (extrapolated) over the entire sapwood area, which when considering spatial (radial, circumferential and axial) heterogeneity of the velocity field are also dependent on the species type, and as such creates an integration error (Wullschleger and King, 2000; Lu et al., 2004). The radial variability of the sap velocity field in tree stems has been demonstrated in a number of studies such as Phillips et al. (1996), Jimenez et al. (2000), Lu et al. (2000), Nadezhdina et al. (2002) and Ford et al. (2004).

In this study most of the sap velocity measurements were carried out with only one sap velocity sensor (TDP) per tree. This was mainly because of the following reasons: 1) having more sensors per tree was not critical for the main objectives of this study (plot transpiration assessment) because: (a) the temporal variability of the sap velocity did not require multi-sensor installation in the measured tree because the eventual error related to heterogeneity of the flux density field was assumed to be time invariant; (b) the error in measuring only one, representative sap velocity measurements per tree (instead of many of them), is anyhow lower than the errors in the evaluation of A_x and the scaling up of individual sap flows; 2) other sap velocity measurements in the same study area (Lubczynski

et al., 2006; in prep.) indicated relatively low variability of sap velocity per species regardless of the biometric characteristic of trees; 3) considering limited funds, it was worthwhile to measure more trees rather than using many TDP installations on individual trees.

Sap velocity measurements can also be affected by natural thermal gradient (NTG) as presented by Do and Rocheteau (2002 a,b). The NTG can either result in underestimation or overestimation of the sap velocity and also has relatively small effect on the calculated sap velocity when considering its use for plot level tree transpiration upscaling which is affected by additionally, more critical errors (e.g. errors made in the estimation of conductive sapwood area and in upscaling of individual sap flows to plot transpiration and even to the errors related to the heterogeneity of the flux density field when having limited amount or even one sap velocity sensor per tree). Therefore, a combination of budgetary constraints and the above aspects meant that the NTG assessment was not critical for the current study. Other uncertainties related to sap velocity measurements and data processing using TDP method are described in Clearwater et al. (1999) and in Lu et al. (2004).

Seasonal trends of sap velocities

The long-term, seasonal evolution of daily average sap velocity for all the 41 monitored trees are presented in Figure 4.2 from 11 November 2001 to 14 January 2004. The seasonal trend of increasing daily average sap velocity in the wet summer and decreasing daily average sap velocity in dry winter is "driven" mainly by: (i) seasonal changes of solar radiation and air temperature (daily average sap velocity pattern follows the seasonal trend of solar radiation and air temperature); (ii) Increased driving force of transpiration due to abundance of leaves; (iii) soil moisture availability. The effect of soil moisture on stomatal conductance is well documented (Oren et al., 1998b; Harris et al., 2004); the reduction in soil moisture affects the dynamics of the water flux in stems, and increases the contribution of water stored in the stem with regard to canopy transpiration.

Seasonal variability of daily average sap velocity between trees of different species is noticeable in Figure 4.2. Particularly distinct is the difference between species such as *S. longipedunculata* and *L. nelsii* that drastically decreases daily average sap velocity to minimum during the dry season in contrast to species such as *B. africana, D. cinerea, T. sericea, B. albitrunca* and *A. fleckii* that maintain water uptake through out the year only reducing its quantity. Figure 4.2 also shows that the nine tree species differ not only in daily average sap velocity pattern but also in daily average sap velocity rate. For example, wet season maximum daily average sap velocity ranges from ~4 cm/hr for *S. longipedunculata* to <0.1 cm/hr for some *A. erioloba*. This order of magnitude in daily average velocity are consistent with separate measurements made by Lubczynski et al., (2006; in prep.) within the study area and were also confirmed experimentally in the field by D. Chavarro and J. Roy (unpublished data) using a pump and a digital recorder.

However, the order of magnitude in the daily average sap velocity is much lower than those reported in the literature from climatically moderate ecosystems (e.g. by Phillips et al., 1996; Lambs and Muller, 2002; Nadezhdina et al., 2002; Larcher 2004; Bovard et al., 2005). They are also much lower than those reported by Donaldson (1969: cited in web page:http://www.met.gov.na/programmes/napcod/bush%20encr/ch3.pdf) for the Molopo area in Namibia with conditions similar to those of the present study. Variations in sap velocity within one tree were also observed in tree species of Miomo woodland in Tanzania where sap velocity was highest at a depth of 0.5 cm below the cambium and lowest at 2.5 cm depth (Nyadzi et al., 2003). The latter depth is nearly that of this study. It is possible that in the present study with uncertainities related to the use of a single *TDP* per tree, the sap velocity is underestimated, because high velocity xylem vessels might not have been intercepted. The fact that this actually happens is proved by the breakthrough time in the tracer experiments of Chapter 5. On the other hand, the occurrence of low velocity vessels can also be expected. The presence of high velocity xylem vessels were also observed in nuclear magnetic resonance images of stems by D. Chavarro and J. Roy (unpublished data) within

the framework of the Kalahari Research Project (KRP). Other sources of uncertainty have been discussed earlier.

In general, different trees of the same species, regardless of their growing stage, show similar daily average sap velocity pattern as indicated in Figures 4.2(c), 4.2(e), 4.2(f), 4.2(g) and 4.2(i). Notwithstanding the above, however, some differences in daily average sap velocity rate and pattern can also be discerned in Figure 4.2. For example, in Figure 4.2(b) the average sap velocity of GS05CH9 *A. erioloba* tree in GS05 was substantially higher than in the *A. erioloba* trees in GS03. Also the temporal daily average sap velocity pattern of GS05CH9 was quite different from the other two GS03 trees. As already mentioned, the difference between *A. erioloba* trees at different locations can probably be attributed to the difference in root water accessibility. Other differences, particularly between the individuals of the same species at the same plot location can be caused by: (i) different conditions in 'capturing' water from the subsurface resulting from local inhomogeneities of the Kalahari sand; (ii) different canopy exposures to the sun; (iii) the complexity of eco-physiological responses of trees (e.g. interception) due to the complex interactions of physical and physiological phenomena, and to the numerous surfaces, mostly leaves, that exchange matter and energy with the atmosphere (Köstner et al., 1998); (iv) local heterogeneity of the flux density field (position of the probe with respect to the flux density field, tree xylem health etc.); (v) influence of NTG; (vi) errors in sap velocity data processing e.g. ΔT_{max} drift.
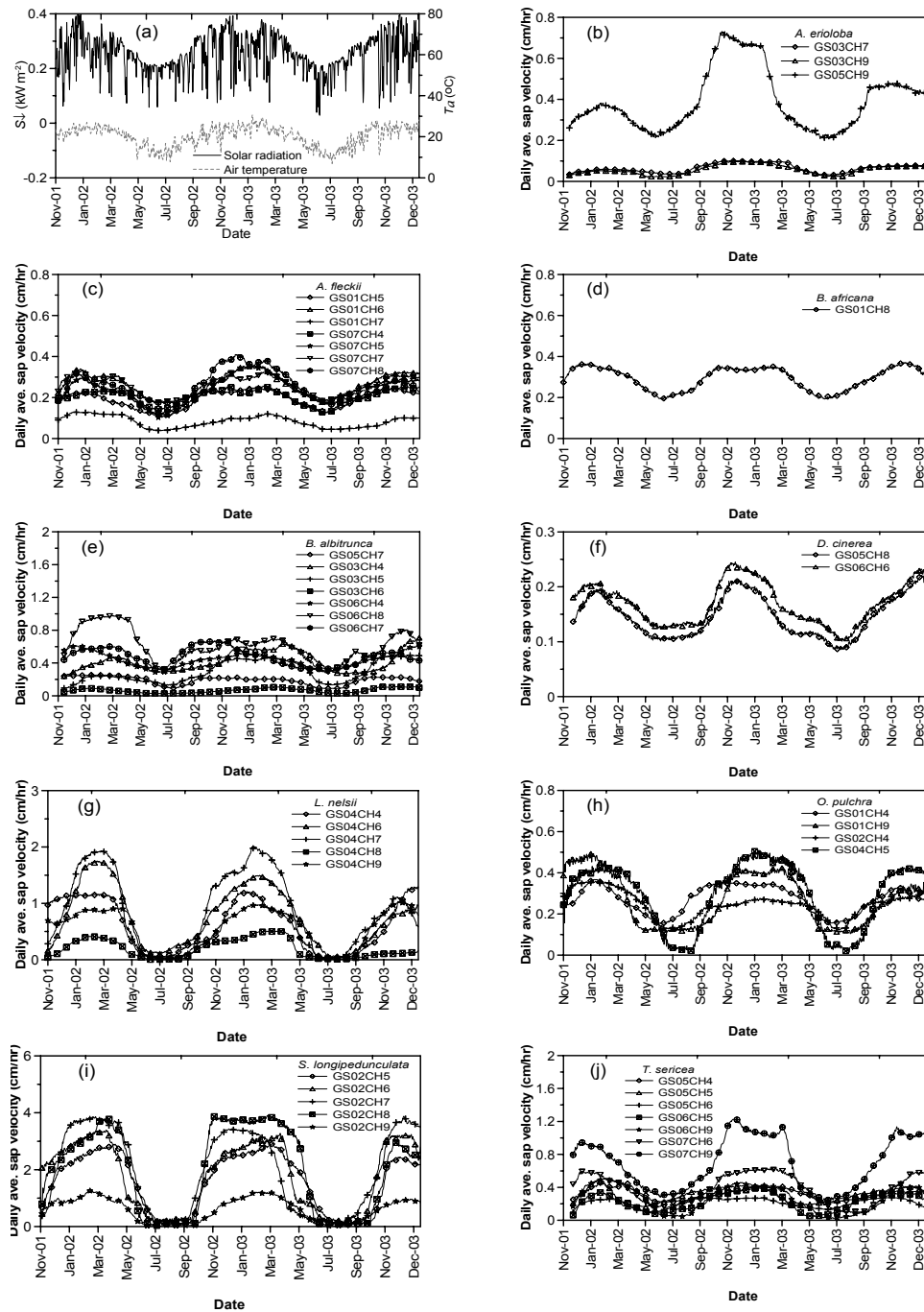
Figure 4.2. Seasonal trends of daily average (ave.) sap velocity (*from (b) until (j)*) in cm/hr in relation to (a) incoming shortwave radiation (*S↓*) and (b) air temperature (*T_a*); see also Appendix B

4.3.2 Conductive sapwood area

Estimation of the conductive sapwood area (A_x) is critical because it is used in the calculation of Q_s (Equation 4.1) and hence in the calculation of T_p (Equation 4.4). As mentioned the conductive xylem area was defined using cut-and-dye tracing of the whole tree method which is still considered as the most reliable and direct assessment of the conductive sapwood area (Lu et al., 2004). The A_x necessary for upscaling of individual tree sap flows of various tree species into the GS01-GS08 plots (Figure 3.1) was not estimated on the trees in the selected eight plots, but predicted by statistical regression equations (BUF) between stem sizes and sapwood areas, as defined by Lubczynski et al. (2006, in prep.), except for the *S. longipedunculata* for which the BUF was defined in this study (Table 4.2). This was permitted because over 90% of the variance in A_x of the tree species could be well explained by the BUF. In the case of *O. pulchra,* sap velocity with canopy area was used instead of stem size, because the latter relation had a much lower R^2 (0.66).

The use of BUF for calculation of individual Q_s in the monitored plots is advantageous because trees in the plot can be reserved for future assessments when the technology of Q_s assessment will have improved.

4.3.3 Sap flow and normalized sap flow

The following range of sap flow values (in L/day) were obtained in the monitored trees:

0-18.75	for five *L. nelsii* trees
0.01-0.60	for seven *T. sericea trees*
0.01-0.78	for three *A. erioloba trees*
0.02-0.12	for two *D. cinerea* trees
0.02-0.75	for four *O. pulchra* trees
0.04-33.16	for five *S. longipedunculata* trees
0.05-12.68	for seven *B. albitrunca* trees
0.06-0.99	for seven *A. fleckii* trees
0.73-1.42	for one *B. africana* tree

In estimating Q_s the eventual errors in v and A_x have to be taken into account. In this study, as in most of sap flow assessment studies, one of the most critical issues in estimating Q_s was the problem of radial heterogeneity of the sap flow field. In all 41 monitored trees, the sensors were installed in the external part of the conductive sapwood (right behind the bark) while A_x was estimated as total conductive sapwood area. Whenever xylem annulus was thicker than the length of the TDP probe (2.1 cm), the calculated Q_s was estimated by multiplying sap velocity (integrated over the length of the TDP probe) by the total area of the xylem annulus. In such cases the eventual error is dependent on the difference (heterogeneous) between the flow field that is not penetrated by the sensor from that which has been penetrated. Nevertheless, due to the averaging of sap velocity along the sensor length, the TDP method has a greater advantage over "point" measurements (e.g. heat pulse method) because it has relatively low sensitivity to spatial variations in sap flux density caused by micro-variation in xylem structure (Lu et al., 2004).

The monitored sap velocity seems to differ significantly within the tree species, but A_x clearly depends on the biometry of trees, therefore Q_s directly depends on the growing stage of the trees within certain species. Regardless of the tree species type, Q_s is typically larger for more grown (larger) trees than for less grown (smaller) trees. Therefore, Q_s cannot be used for direct comparison of transpiration ability among different species. A better indicator in this respect is the normalized sap flow (Q_n). According to Equation 4.3, Q_n represents the individual tree transpiration (per canopy area), i.e. the amount of sap flow $Q_s=vA_x$ per projected (on the ground surface) canopy area (A_c). The highest Q_n values are therefore found in trees which are characterized by high Q_s with relatively low A_c, which indicates high transpiration efficiency per unit area of the canopy.

In this study Q_n was calculated for all 41 monitored trees according to Equation 4.3. For each tree, A_x (estimated by regression equations in Table 4.2) was multiplied by the monitored velocity (in Figure 4.2) and divided by corresponding crown area (A_c), computed from crown diameters in Table 4.1. This resulted in the daily average, temporally variable Q_n presented in Figure 4.3, which largely resembles the

90

temporally variable pattern of daily average sap velocity (Figure 4.2). This is because Q_n is obtained by multiplication of sap velocity (v) by the temporally invariant factor A_x/A_c (assumed constant within the time period of the current study).

The Q_n differences between individual trees of the same species are larger than similar differences in the daily average sap velocity. They are likely attributed to: (i) transpiration edge effect due to high positive heat advection from a cleared (or bare) area towards the forest edge (as demonstrated by Giambelluca et al., 2003), (ii) differences in crown positions with respect to other crowns (trees exposed or sheltered, and (iii) leaf area index (*LAI*). Granier et al. (1996b) working in a natural rainforest in the Amazon basin and Giambelluca et al. (2003) working in a small tropical forest patch of northern Vietnam concluded that well exposed trees transpired more than poorly exposed trees, and transpiration rates decreased with distance from the forest's edge. Barradas et al. (2005) also made a similar observation in young apricot trees in Spain.
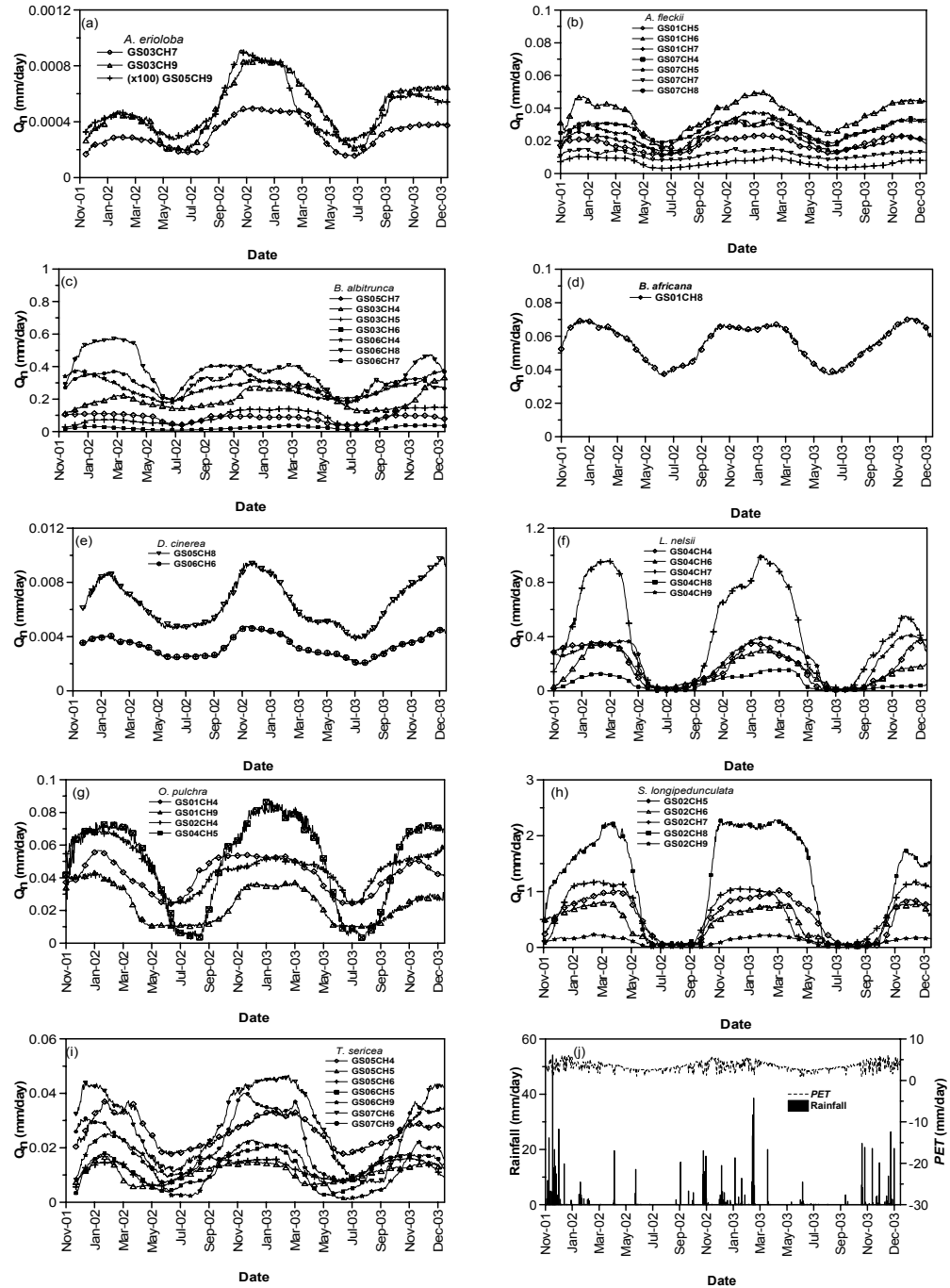
Figure 4.3. Normalised sap flow (*Q_n*), potential evapotranspiration (*PET*) and rainfall; see also Appendix C

4.3.4 Plot level tree transpiration

The plot level tree transpiration (T_p) was calculated in this study according to Equation 4.4 taking into account trees only (transpiration of under-story was not considered). The T_p was defined by upscaling of sap flow measurements in eight plots marked as GS01-08. Each plot provided temporal variability of transpiration whereas the differences between the plots illustrated spatial variability of transpiration.

Upscaling of sap flow measurements into plot level

Upscaling of sap flow measurements into plot level tree transpiration (T_p) was carried out based on long-term averages of sap velocity measurements (except for *B. africana* since only one tree was measured) calculated for each measured species. The obtained species-specific long-term average sap velocities were multiplied by species-specific estimates of conductive xylem areas derived from BUF regression equations (Table 4.2) based on their total stem areas (or total crown areas in case of *O. pulchra*) within the plot. According to Equation 4.4, the sap flows of all individual trees of the plots were then summed and divided by the plot area (900 m^2), to give estimates of the transpiration per plot in the form of fluxes [L/T]. An example of the entire calculation procedure is illustrated in Table 4.4 for a (randomly selected) day of 1 April 2002.

As mentioned T_p assessment was carried out in eight plots, seven of them (GS01-07) equipped with automated sap velocity monitoring sensors and the last one GS08 without such monitoring. The case of the GS08 plot shows that the upscaling does not necessarily need to take place exactly where the sap velocity measurements are done but can be done in any selected plots of similar soil and climatic condition (preferably not very far from the location where measurements are done) provided sap velocity measurements and BUF are available for all the tree species at the assessed plot (without measurements).

93

Table 4.4. An example of plot tree transpiration calculation for one day of 1 April 2002; where $\bar{v}_s$ - the daily average sap velocity of all the trees per analyzed species in cm/hr; A_x - conductive xylem area [cm^2]; Q_s - total plot sap flow for tree species analyzed [l/day]; T_{sp} species plot transpiration [mm/day] so that $T_p=\Sigma T_{sp}$; *Ae – A. erioloba*; *Af – A. fleckii*; *Ba – B. albitrunca*; *Bua – B. africana*; *Dc – D. cinerea*; *Ln – L. nelsii*; *Op – O. pulchra*; *Sl – S. longipedunculata*; *Ts – T. sericea*

Plot	Notation	Ae	Af	Ba	Bua	Dc	Ln	Op	Sl	Ts	Totals
	$\bar{v}_s$	0.14	0.22	0.42	0.3	0.16	1.12	0.31	2.88	0.33	6
GS01	A_x	0	3376.3	0	930.8	2227.5	0	1103.7	0	710.9	8349
	Q_s	0	17.83	0	6.7	8.55	0	8.21	0	5.63	47
	T_{sp}	0	0.0198	0	0.0074	0.0095	0	0.0091	0	0.0063	0.0521
GS02	A_x	0	487.8	0	334.2	0	0	1663	2000.4	72.4	4558
	Q_s	0	2.58	0	2.41	0	0	12.37	138.27	0.57	156
	T_{sp}	0	0.0029	0	0.0027	0	0	0.0137	0.1536	0.0006	0.1735
GS03	A_x	802.6	360	272.6	0	1076.9	0	0	0	151.6	2664
	Q_s	2.7	1.9	2.75	0	4.14	0	0	0	1.2	13
	T_{sp}	0.003	0.0021	0.0031	0	0.0046	0	0	0	0.0013	0.0141
GS04	A_x	0	49.2	146.5	0	808.5	11959.2	228.5	0	99.4	13291
	Q_s	0	0.26	1.48	0	3.1	321.46	1.7	0	0.79	329
	T_{sp}	0	0.0003	0.0016	0	0.0034	0.3572	0.0019	0	0.0009	0.3653
GS05	A_x	91.3	36.7	480.1	0	33.9	0	0	0	797.7	1440
	Q_s	0.31	0.19	4.84	0	0.13	0	0	0	6.32	12
	T_{sp}	0.0003	0.0002	0.0054	0	0.0001	0	0	0	0.007	0.013
GS06	A_x	0	0	1596.9	0	2390.6	224.4	0	0	90.7	4303
	Q_s	0	0	16.1	0	9.18	6.03	0	0	0.72	32
	T_{sp}	0	0	0.0179	0	0.0102	0.0067	0	0	0.0008	0.0356
GS07	A_x	0	3049.8	0	0	316.2	0	146.8	0	146.2	3659
	Q_s	0	16.1	0	0	1.21	0	1.09	0	1.16	20
	T_{sp}	0	0.0179	0	0	0.0013	0	0.0012	0	0.0013	0.0217
GS08	A_x	0	447.2	0	51.7	194.4	0	165.3	0	411.3	1270
	Q_s	0	2.36	0	0.37	0.75	0	1.23	0	3.26	8
	T_{sp}	0	0.0026	0	0.0004	0.0008	0	0.0014	0	0.0036	0.0088

The main errors associated with the calculation of plot tree transpiration (T_p) are of multi-source nature. Some errors are inherent from sap velocity measurements, data processing and from the velocity averaging process, while others originate from the field estimation of conductive sapwood areas and from the upscaling process according to biometric upscaling functions (BUF). Additionally, some other errors are related to plot size restriction e.g. some trees especially those situated close to plot boundaries may extend their roots to draw water from beyond the boundaries of the plot.

Spatio-temporal variability of plot tree transpiration

The seasonal course of plot tree transpiration (T_p) for the selected eight plots of GS01-08 is shown in Figure 4.4. The T_p pattern is generally similar to the daily average sap velocity pattern in Figure 4.2, but more smoothed than the daily average sap velocity pattern (as a result of averaging effect). T_p reflects the seasonal trend of potential evapotranspiration (*PET*) and temperature (Figure 4.4). The temporal variability of T_p is seasonally cyclic, very similar from one year to the other within the monitoring period. Unfortunately in the presented monitoring period there was no climatically-extreme year (e.g. a severe drought) that could clarify to which degree climatic factors could influence T_p.

The differences in plot tree transpiration between different plots at any given time can be explained by: (i) differences in amount of trees per plot; (ii) differences in tree species-composition that influences the variations in sap velocity and conductive xylem area; (iii) differences in growing stage of the trees which influences sapwood area; (iv) differences in climatic factors, mainly differences in rainfall amounts, leading to differences in soil moisture availability to active roots; (v) differences in soil type and its degree of heterogeneity that influences the root access to soil moisture and eventually groundwater; (vi) by errors in estimating T_p.

Spatial variability of tree transpiration can be analyzed by comparing different records of T_p in the eight (GS01-08) plots as in Figure 4.4.

95

Most of the plots indicate T_p <0.05 mm/d with exception of GS04 where T_p goes up to 0.4 mm/d in the hot wet summers and GS02 where T_p goes up to 0.18 mm/d. In GS04 this is likely due to a large quantity of sizeable *L. nelsii* trees, which are characterized by high sap velocity rates in summer ($\approx$1 cm/hr) season (Figure 4.2) and large conductive sapwood areas as presented in Table 4.4. In GS02 high T_p is likely due to a relatively high contribution of *S. longipedunculata* characterized by the highest summer sap velocity rates reaching up to 4 cm/hr. The dominant tree species of GS04 and GS02 such as *L. nelsii* and *S. longipedunculata* are characterized by high summer sap velocity and extremely low sap velocity in the winter season (high amplitude). The lowest T_p are observed in GS03, GS05 and GS08 plots; they vary in range from less than 0.01 mm/d in winter to $\sim$0.02 mm/d in summer. This low T_p is mainly due to the low contribution of the individual trees inside these plots.
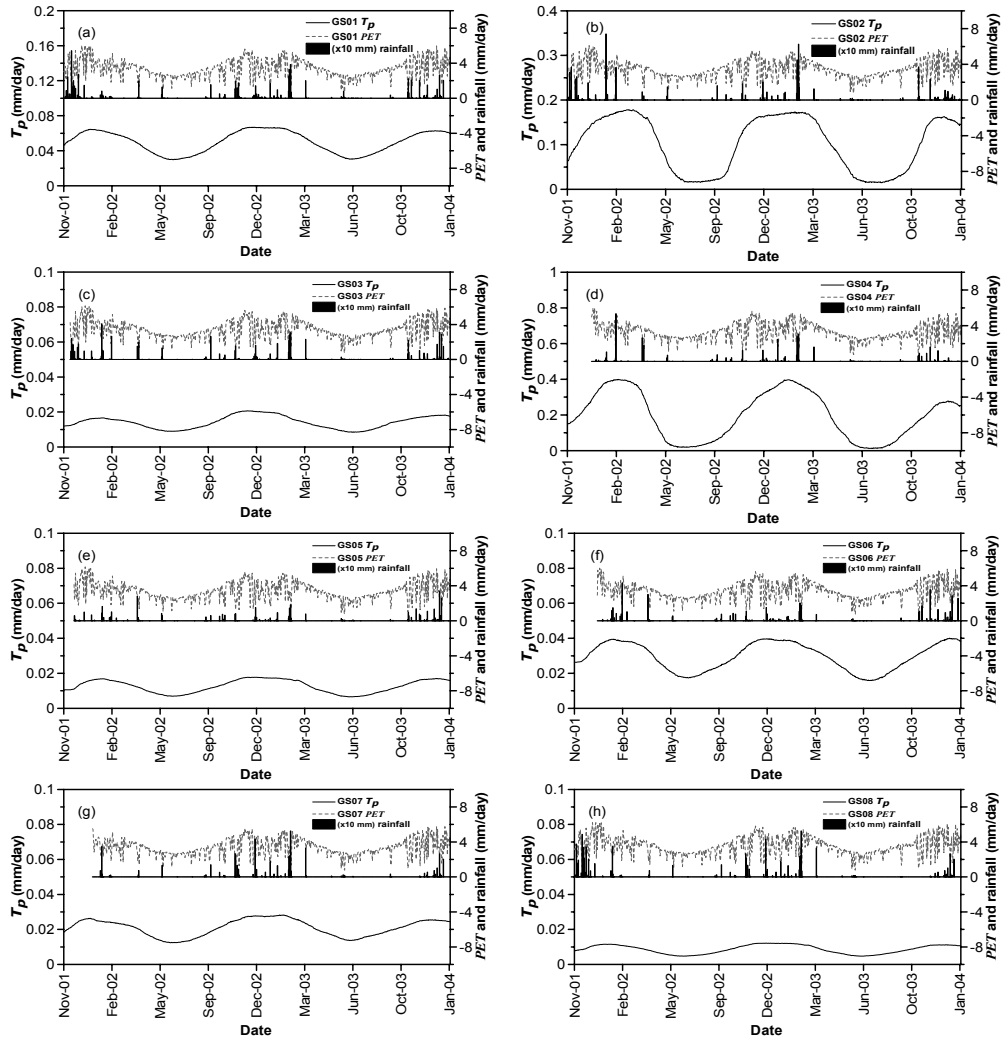
Figure 4.4. Plot tree transpiration in relation to *PET* and rainfall

The quickest and probably the most convenient way of presenting spatio-temporal variability of T_p is demonstrated in Figure 4.5. This graph presents T_p for six selected clear-sky days covering some of the variability within one full hydrological year in all eight plots. Figure 4.5 emphasizes the large differences in T_p among the plots. It also shows that the high transpiration rate was associated with a high variability of T_p.

Figure 4.5. Daily plot level tree transpiration for the six selected clear-sky days

Annual transpiration versus PET and rainfall

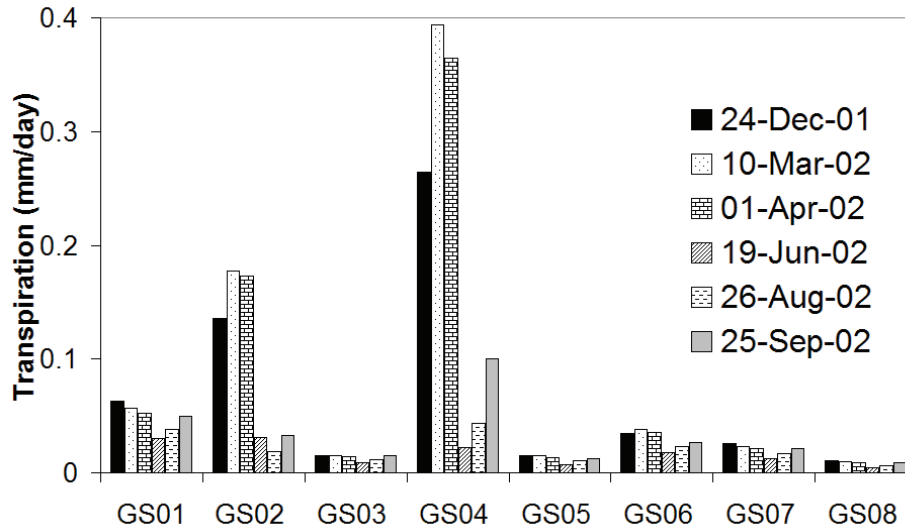Table 4.5 presents the annual plot level tree transpiration (T_p) and the corresponding rainfall and potential evapotranspiration (*PET*) for three hydrological years. The *PET* was calculated according to the Penman-Monteith equation as discussed in Chapter 3. The missing fragments of T_p from 1 September 2001 to 10 November 2001 and from 15 January 2004 to 31 August 2004, necessary to compare fluxes of full hydrological years (Table 4.5), were estimated by linear regression models (for each plot) using daily air temperature records. The quality of fit (R^2) of those regression models ranged from 70-79%. Similar regression models using daily incoming shortwave radiation yielded $R^2 < 30\%$ and were therefore not used. The rainfall monitoring in GS01-07 plots had started only at the end of 2001, so for the sake of completeness of the annual rainfall of the hydrological year 2001/2, the missing records since 1 September 2001 were obtained from GS08 since it has daily rainfall records that dates back to 1999.

The annual T_p [mm/yr] largely varies between plots from 3 mm/yr in GS08 to 71 mm/yr in GS04, both in the 2002/3 hydrological year. For most of the plots T_p represents less than 10% of the rainfall except for GS04 for which it ranges from 13 to 15% of rainfall, in wetter years of 2001/2 and 2003/4 and up to 32% of rainfall in the relatively dry year of 2002/3. Why is the T_p contribution higher in a year with less rainfall (less water available) than in years with more rainfall? Comparison of T_p with rainfall for all the plots and all the three years (Table 4.5) shows that lower rainfall in 2002/3 did not result in lower T_p than in the other two wetter years; in the cases already mentioned (such as GS04) and also GS07, it was even higher. This proves that Kalahari trees are drought resistant and able to extract water from deeper layers, in which the soil moisture content is not directly dependent on seasonal rainfall like in the upper soil layers.

Table 4.5. Annual plot tree transpiration, rainfall and *PET* for three hydrological years[*]; hydrological year is a period starting from first September and ending with the thirty-first of August

Plot no.	2001/2 (mm/yr)			2002/3 (mm/yr)			2003/4 (mm/yr)		
	T_p	Rainfall	*PET*	T_p	Rainfall	*PET*	T_p	Rainfall	*PET*
GS01	17	428	1192	19	318	1213	18	653	1170
GS02	34	477	1201	36	325	1224	39	511	1172
GS03	5	494	1207	5	260	1233	5	529	1191
GS04	64	477	1209	71	223	1218	62	418	1087
GS05	4	465	1198	5	158	1219	5	468	1181
GS06	10	514	1201	11	195	1221	11	479	1187
GS07	7	497	1211	8	372	1228	7	434	1180
GS08	3	497	1236	3	372	1274	3	431	1205

Table 4.5 shows that rainfall is by far higher than transpiration by trees and much lower than *PET*. The Kalahari study area is flat and sandy so there is nearly no surface runoff while infiltration is substantial. The average recharge however proved to be very low. Estimates by De Vries et al. (2000) gives groundwater recharge values for the Kalahari of less than 5 mm/yr. The isotope study presented in Chapter 6, indicated stable isotopic enrichment of soil moisture extending down to ≈ 4 m depth. This in combination with large infiltration and low recharge suggests that a major part of the infiltrated rainfall water is directly evaporated and transpired by shallow rooted vegetation (grasses, bushes and some tree species)

from the upper ≈4 m layer and only a small part is transpired by trees. An even smaller amount escapes evapotranspiration and is converted to recharge.

The Kalahari with its thick sandy cover, high infiltration rate, and high evapotranspiration and groundwater tables in excess of 40 m deep represents a special environment with regard to tree growth and transpiration. Even simple field reconnaissance shows that within the gray winter landscape of leafless trees, there are some trees e.g. *B. albitrunca* and *A. erioloba* that remain freshly green throughout the dry season. Other species e.g. *T. sericea* and *L. nelsii* start flowering in the end of the dry season. Where do they get water from? Traces of extremely deep Kalahari tree rooting systems of *B. albitrunca* and *A. erioloba* has already been proved by Jennings (1974) and is extensively confirmed by the present study (Chapter 5). The quantity of sap flow water measured in the tree stems, depending on the tree species, can partly originate from groundwater and partly from the unsaturated zone. This means that the calculated T_p values (Table 4.5) can be partly attributed to the direct root water uptake from the aquifer. This is of particular concern since transpiration rates are in the same order of magnitude or higher than the groundwater recharge of Kalahari as defined by De Vries et al. (2000). This explains the very low groundwater discharge, estimated in the order of 1 mm/yr (De Vries 1984; De Vries et al., 2000). It is evident that safe yield or sustainable production of groundwater is very low. Almost all available water from rainfall is being used by the natural vegetation.

4.4 Summary and conclusions

The TDP sap flow evaluation method, applied under Kalahari conditions, proved to be a good and robust tool in assessing temporal variability of tree transpiration. The seasonal courses of sap velocity and other transpiration-related variables (sap flow and normalised sap flow) follow the seasonal trend of air temperature and potential evapotranspiration, i.e. high in wet summer and low in dry winter.

There is variability in sap velocity between trees of different species; this variability refers not only to large differences in average velocity rates but also to the seasonal distribution that varies both in amplitude and in pattern.

Trees of the same species also show variability of sap velocity. This was particularly distinct when comparing individuals from different plots and less distinct for individuals of the same plot. Such variations are mainly attributed to differences in soil moisture availability and microclimatic influences associated with plot exposure.

There is a large variability in tree composition between the eight selected plots responsible for plot tree transpiration differences ranging from 3 mm/yr (GS08) to 71 mm/yr (GS04). These differences demonstrate the spatial variability of transpiration in the Kalahari.

The plot tree species composition determines not only the spatial but also the temporal variability of plot tree transpiration (T_p) that differs substantially in rates among the eight plots. For example, in the GS04, T_p varies from nearly 0 mm/d in the dry winter season to 0.4 mm/d in the wet summer season, while in GS03, GS05 and GS08, T_p does not even exceed 0.02 mm/d.

It is remarkable that there seems to be no relation between tree transpiration and rainfall in the Kalahari; with nearly 100% more rainfall in 2003/4 than in 2002/3, the transpiration remained in the same order of magnitude. This probably means that trees mainly extract water from deeper layers ($>\approx 4$ m) of which the moisture content is hardly subjected to inter-annual variations of rainfall (see also Chapters 5 and 6). In an average plot, tree transpiration accounts for less than 10% of the total rainfall in a hydrological year, except for the GS04 plot where T_p ranges from 13 to 32% of the total rainfall depending on the wetness of the hydrological year.

The relatively large T_p in plots as compared to the calculated transport of moisture below the main root zone, which is in the order of a few mm/yr, and the extremely deep rooting systems of certain

tree species with the potential to extract groundwater from the saturated zone, suggest that the net groundwater recharge that determines sustainability of groundwater resources in most Kalahari regions can be zero in periods of low rainfall.

Despite the fact that all the transpiration related components such as sap velocity, sap flow, normalised sap flow and T_p were affected by various types of TDP assessment errors, they provided a consistent and valuable insight in the temporal variability of sap velocity and transpiration mainly because the majority of these errors have a systematic nature. For monitoring of the temporal variability of transpiration, one properly working TDP installed per tree seems to be sufficient, although more of them would be certainly useful in contributing to the reduction of the heterogeneity effect. This method, however, as any other thermal sap flow method, requires intensive maintenance.

The accuracy of estimating the sapwood area (A_x) has obviously no impact on temporal variability of T_p. It is critical, however, in estimating individual sap flows and in upscaling process. Unfortunately, there is not as yet an efficient and accurate method to evaluate the conductive sapwood area. The most reliable method of tree-cutting and dye-tracing was used in this study (not shown) although for environmental reasons it is not recommended in general. The best perspectives in this respect are in the application of non-invasive methods, which however are still at an experimental stage.

Chapter 5 Rooting depth investigation

5.1 Introduction

Rooting patterns and rooting depths of vegetation are commonly unknown, so that the vegetation's ability to reach deep water tables is generally poorly understood. The different rooting systems that exist in nature are the results of both genetically and environmentally determined characteristics. As a consequence, root systems may show a wide variation both between and among species, depending on site conditions, the presence of neighbouring plants, developmental stage and genotype. Studies on root distributions are usually concerned with root length as a function of depth because of its role in the absorption of nutrients and water. Therefore, root length distributions are often used in groundwater flow models to define the sink term in the water balance. The importance of the description of rooting depth and rooting pattern for modelling root water uptake in hydrological models has been emphasized by Feddes et al. (2001). In the case of groundwater recharge studies in areas where the groundwater table is far below the main root zone, it is essential to know at which depth infiltrating water is beyond the reach of the roots.

There is increasing evidence that some plant species are able to send their roots deep into the unsaturated zone in search for water and nutrients. This pattern is observed in plants that maintain their growth for years with little or no rainfall. Canadell et al. (1996) summarised the information about the maximum rooting depths of vegetation types on a global scale. By grouping all species across biomes, with exclusion of croplands, they computed mean maximum rooting depths of 7.0±1.2 m (n=82) for trees, 5.1±0.8 m (n=69) for shrubs, and 2.6±0.1 m (n=85) for herbaceous plants. Furthermore, they also observed that plants from the drier environments or in environments with long dry periods showed the deepest rooting system. This observation was further emphasised by Schenk and

Jackson (2005), when mapping the global distribution of deep roots in relation to climate and soil variables.

Phillips (1963) reported maximum rooting depths of 50 m for *Prosopis sp*. in Arizona, whereas Le Houérou (1972) in Morocco mentioned depths of 60 m for *Ziziphus lotus (L)*. Jennings (1974) reported having found living roots at a depth of 68 m in a borehole in Central Kalahari (at Phuduhudu) in which the water level was at 141 m. Haase et al. (1996) injected a chemical tracer above the phreatic surface at depths of 16 and 28 m in alluvial fan deposits in the semi-arid part of Spain, and found that the tracer was taken up by *Retama sphaerocarpa* after at most one day, implying that the rooting system of this shrub species was equal or deeper than the tracer placement depths.

Since Jennings (1974) findings in the Botswana Kalahari, no work has been undertaken to confirm the deep rooting depths of vegetation in the semi-arid Botswana Kalahari until the present study. This study was, among others, initiated because groundwater recharge and water balance analyses in the Kalahari by De Vries et al. (2000) had given indirect evidence of groundwater extraction from depths of more than 50 m. The aim of the present investigation was to ascertain by direct measurements from what depths in the unsaturated zone and/or from the capillary fringe above the water table the roots take up water. Therefore, (following Haase et al., 1996), lithium chloride (LiCl) was injected as tracer at the bottom of boreholes, drilled especially for that purpose to various depths above the local water table, in the area with deep Kalahari sand and in the area with shallow hard rock (hardveld). Only at one location of the hardveld area was the tracer applied below the phreatic water table. Subsequently, the tracer content in young (immature) tree leaves was analyzed for 14 consecutive days following the subsurface injection, to detect the depths from which water was extracted by the trees in the vicinity of the boreholes. Lithium was used because of the following reasons: 1) it occurs only in small quantities in the natural environment, 2) it is soluble in water such that it can be transported in solution and 3) it can be taken up by plants without adverse effects on their growth, if present at low concentrations. Lithium ion was

found to be toxic to experimental plants by Kent (1941) and Wallace et al. (1977), but such observation was not made by Sayre and Morris (1940) and Martin et al. (1982). More examples of lithium ion toxicity in plants can be found in Bradford (1966). Unfortunately, no information of lithium toxicity is available for Kalahari trees, although being glycophytes they are expected to be affected at high concentrations.

5.2   Field tracing experiment

In September 2003 eighteen holes were drilled by down-the hole-hammering (percussion drilling) in the Serowe study area. Of these 18 drill-holes, four holes were located in the hardveld (east of the escarpment) and the rest in the Kalahari sandveld (Figure 5.1).
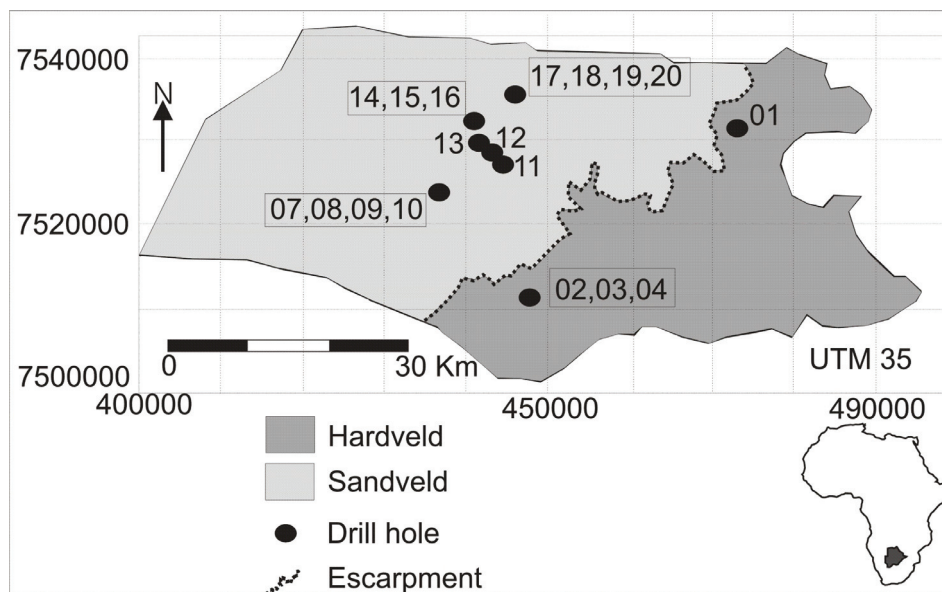

Figure 5.1. Spatial distribution of drill holes (numbers represent drill hole identification**)**

Of the four drill-holes located in the hardveld, one terminated in a phreatic sandstone aquifer (Drill-hole no. 01) and the remaining three holes ended in superficial deposits and weathered material above the

Stormberg basalts. All other 14 drill-holes, situated in the Kalahari sandveld, ended in the Kalahari sediments (predominantly sand).

The drill-holes were lined with Polyvinyl Chloride (PVC) pipes with an internal diameter of 100 mm which contained perforations at known depths, to allow water to leak out to surrounding sediments. The perforated section of the PVC pipes (screen) was 3 m long in all drill-holes, and formed the lower part of the pipes, placed at the bottom of each drill-hole. These perforations explain the little refilling with sand that was observed in some of the pipes in April 2004 as presented in Table 5.1.

On the 7th and 8th of April 2004, water was poured down the drill-holes to produce a wet area in the surrounding sediments. The amount of added water in each drill-hole was equal to the volume of the perforated part of the pipe that was not refilled by sediments. The primary objective was to increase water flow in the adjacent sediments, so as to facilitate tracer movement after insertion in each individual hole. This was done a day before tracer application to the hole, to allow sufficient time for water to seep into the surrounding sediments.

During clear-sky sunny days of 8th and 9th April 2004, at the end of the wet season (when there is enough crown volume for repeated foliage sampling), the volumes of LiCl solution as presented in Table 5.1 were added to the drill-holes. This was achieved by lowering small containers filled with LiCl, attached to a plastic cord into the pipe. The added LiCl was slowly diluted with water, with a volume approximately equal to the volume of the sediment 'unfilled' screen, i.e. the section of the PVC pipe with 'free' perforations. In this way, leakages were only possible at perforations and not at any other location above the perforations. The average concentrations of Li^+, (if uniformly diluted within the sediments) are also given in Table 5.1.

Each tracer test site was at a distance that varied from 1.3 - 8.1 m from the tree to be sampled as shown in Table 5.2. The biometric parameters (crown area, stem area and height) of the selected tree are also presented in Table 5.2. In total 19 trees were measured,

representing seven tree species of *A. erioloba, A. fleckii, B. albitrunca, D. cinerea, S. longipedunculata, T. sericea,* and *Z. mucronata*. Refer to Appendix A for example photographs of the species.

Table 5.1. Depths of drill-holes, groundwater tables and amounts of added lithium chloride; * represent actual water level measurements. For the remaining (dry) holes the groundwater *(Gw)* level was estimated by interpolation from nearby boreholes

Drill hole no.	Sept. 2003 terminal depth (m)	April 2004 hole depth (m)	Depth refilled with sediments (m)	*Gw* level (m. b. g. l.)	Total sediment free screen volume (l)	Mass of lithium chloride applied (g)	Vol. of water added for dilution (l)	Average Li$^+$ concen-tration (mg/l)
01	11	11	0	*8	23.6	4950	85.7	-
02	31	31	0	36	23.6	4950	85.7	9456
03	23	23	0	36	23.6	4950	85.7	9456
04	18	17	1	36	15.7	3300	57.1	9462
07	23	23	0	78	23.6	4950	85.7	9456
08	18	17.6	0.4	78	20.4	3300	71.3	7577
09	18	16	2	78	7.9	1650	28.6	9445
10	38	38	0	78	23.6	4950	85.7	9456
11	58	57.5	0.5	79	19.6	3300	68.9	7841
12	43	43	0	79	23.6	4950	85.7	9456
13	43	43	0	79	23.6	4950	85.7	9456
14	73	73	0	80	23.6	4950	85.7	9456
15	73	73	0	80	23.6	4950	85.7	9456
16	50	50	0	80	23.6	4950	85.7	9456
17	63	63	0	76	23.6	4950	85.7	9456
18	43	42.2	0.8	76	17.3	3300	61.8	8742
19	33	31.7	1.3	77	13.4	1650	45.1	5990
20	23	21.1	1.9	76	8.6	1650	30.9	8742

Samples of twigs were taken from each of the selected trees before application of LiCl to be used as controls. Sampling was repeated each day for two weeks, after LiCl application. Foliage samples of young leaves were collected randomly (no sampling height measurements were undertaken) at twig tops that were facing the drill hole in the outer part of the canopy. The samples were dried at

80°C in an oven, after which they were ground, weighed, and ashed in a furnace at 430°C, digested in 1 ml of 10% HNO_3. The concentration of Li^+ in the extract was measured by an ICP-OES (Perkin Elmer Optima 3000XL Inductively Coupled Plasma-Optical Emission Spectrometry). The analytical precision of Li^+ was 0.1 µg Li^+ g^{-1} dry mass (1 standard deviation) based on 35 blind duplicate pairs.

Table 5.2. Biometric properties of monitored trees and drill hole related details; the selected trees were neither flowering nor fruiting

Species	Tree code	Drill hole no.	Depth to top of filter (m)	Distance from drill hole (m)	Tree height (m)	Stem diameter at 50 cm height (m)	Average canopy diameter (m)
Z. mucronata	T1	01	8	5	13	0.92	17.4
A. fleckii	T2	02	28	5.2	4	0.18	6.3
D. cinerea	T3	03	20	4	3.2	0.64	7.7
T. sericea	T4	04	15	3.9	3	0.19	3.4
B. albitrunca	T5	07	20	8.1	6	0.45	7.6
A. fleckii	T6	08	15	2.4	4	0.23	8.7
A. fleckii	T7	09	15	4.1	4.5	0.2	10.1
A. erioloba	T8	10	35	3.6	5	0.38	8.1
B. albitrunca	T9	10	35	2.1	4.8	0.37	4.7
A. erioloba	T10	11	55	3.2	9	0.47	10.9
A. erioloba	T11	12	40	4.6	7.5	0.13	2.5
B. albitrunca	T12	13	40	2.2	6	0.33	6.3
A. erioloba	T13	14	70	1.3	5	0.19	3.7
B. albitrunca	T14	15	70	3.1	7	0.43	5.9
A. erioloba	T15	16	47	3	6	0.21	2.7
S. longipedunculata	T16	17	60	7	3.4	0.5	5.0
S. longipedunculata	T17	18	40	1.9	6.5	0.28	5.7
S. longipedunculata	T18	19	30	3.3	8	0.19	5.2
A. erioloba	T19	20	20	4.1	4	0.28	7.1

In the study area four micrometeorological stations of GS00 and GS02-04 were installed to obtain rainfall and potential evapotranspiration (*PET*) data as discussed in Chapter 3. The rainfall and PET data were acquired from GS00 monitoring site in case of DH 01 drill hole, GS02 for the case of DH 17-20 drill holes, GS03 for the case of DH 11-16 drill holes and GS04 for the case of drill holes DH 07-10. During the field tracing experiment significant rainfall was

recorded at the hardveld site near drill-hole DH 01 (Figure 5.2) whilst the Kalahari sandveld sites (DH 07-20) had minimal rainfall. The potential evapotranspiration was higher at the Kalahari sites than at the hardveld DH 01 site during the field experiment.
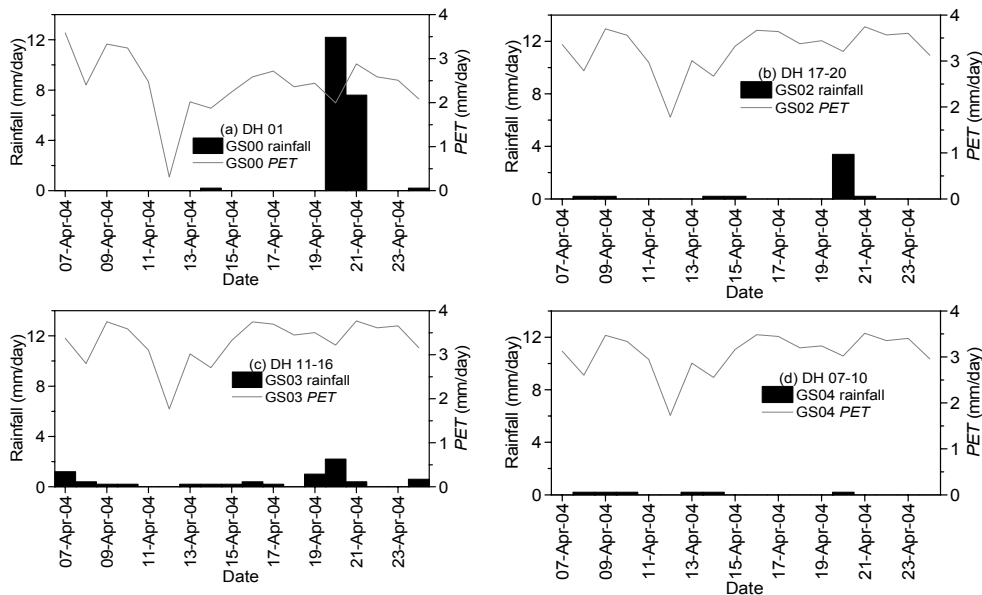

Figure 5.2. Rainfall and *PET* for 7-24 April 2004 at drill hole (DH) sites

5.3   Results

A general trend of increasing concentrations of Li^+ in the foliage with time, is taken as evidence of the existence of roots at the tracer placement depth in the nearby drill hole. Figures 5.3-5.5 presents the temporal evolution of Li^+ concentrations in monitored trees for a period of 15 days after tracer application; the results are shown by grouping species. The depth of tracer insertion is indicated near the tree code for clarity and the Li^+ concentration at day-0 was taken as the background value because this foliage sample was taken before tracer injection on the same day.

All trees in the vicinity of the injected drill holes show a clear and surprisingly fast response, which proves the transport of the tracers

from depths of at least the bottom of the respective drill holes. In the cases of T13 and T14 this means depths of more than 70 m. Exceptional high concentrations were observed in T6, T11 and T19 with injection depths of 15, 40 and 20 m respectively. Large variations occur in Li^+ concentrations in leaves within an individual tree and among trees of the same species, and also the time of peak concentration varies.
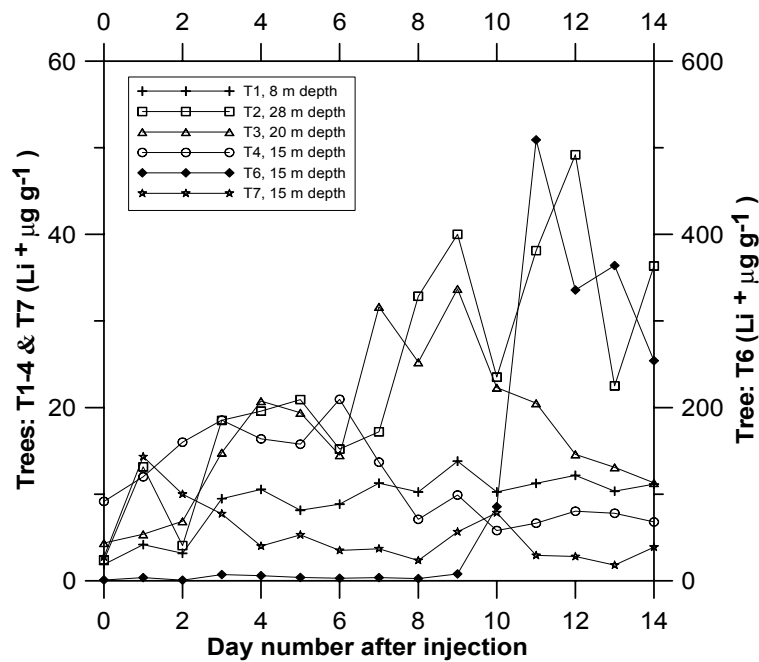

Figure 5.3. Temporal pattern of Li^+ **concentration in** *Z. mucronata* **(T1),** *A. fleckii* **(T2, T6 and T7),** *T. sericea* **(T4) and** *D. cinerea* **(T3).**
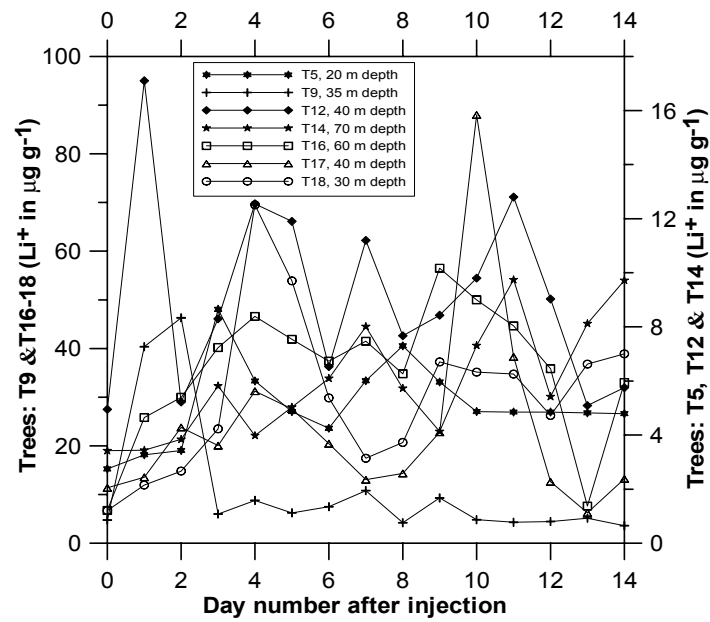
Figure 5.4. Temporal pattern of Li⁺ concentration in *B. albitrunca* (T5, T9, T12 and T14) and *S. longipedunculata* (T16-T18).
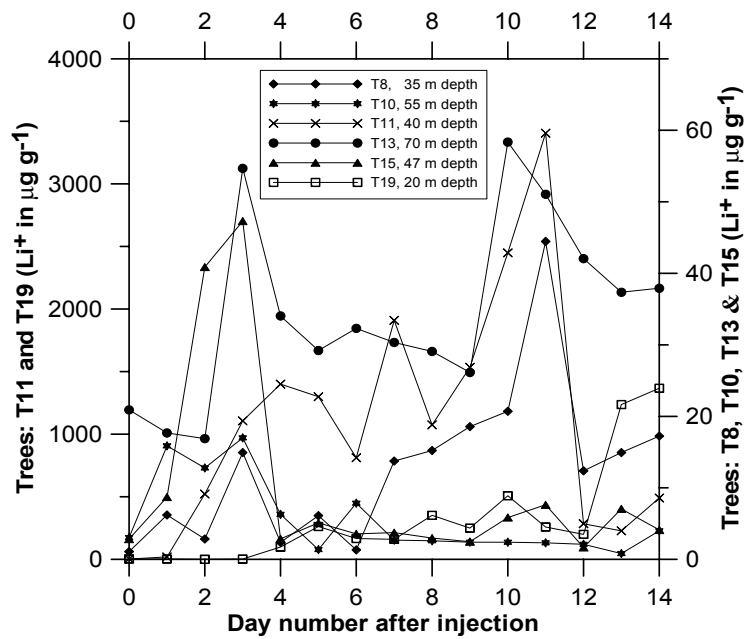

Figure 5.5. Temporal pattern of Li⁺ concentration in *A. erioloba*.

5.4 Discussion and conclusion

As mentioned, all 19 experiments showed an increase in tracer contents of samples taken from the canopy, suggesting uptake of water by deep roots. However, another process also could explain the observed phenomena. In principle, soil water can also have moved upwards from injection depths to more shallow root systems by the high suction gradients that were induced by the wetting of the soil. The second option, however, is considered very unlikely because of the very low hydraulic conductivity values of the moisture contents (3-5 mass %, Selaolo, 1998) in the undisturbed sandy material around the wetted locations. Evaporation-induced fluxes calculated by Coudrain-Ribstein et al. (1998) under similar conditions (as for the tracer placement depths of the present investigations), ranged from 0.1-3 mm/yr, which would result in an upward tracer movement with ascending water of less than 1 mm for a period of 15 days. An upward transport of less than 1 mm is also consistent with a water flux of 3 mm/yr as provided by Enfield et al., 1973 (cited by Scanlon, 1994) for a similar environment in the Hanford area. Moreover, the presence of deep roots in the study area was also confirmed in seven 10 m deep shaft excavations that were made during installation of soil moisture sensors within the framework of the present study.

The observed response of the trees after inserting the tracer was more irregular than expected. Expected was an increase of the tracer in the canopy after one or a few days, followed by a steady level. The observed pattern was often different and indicates complex moisture movement in the root zone due to irregular distribution, dispersion and diffusion of moisture and solution, because of soil heterogeneity, in combination with variation in root activity and distance of the various root components to the tracer solution.

It may also reflect the destructive nature of sampling by cutting twigs, despite a strict sampling protocol. These cuttings might have caused variation in transpiration rates and accumulation of the tracer in the different branches, including minor decreases in concentrations between day-1 and day-3 in a few cases (e.g. in T13). Another possible explanation is that the toxicity of Li^+ was so high that the

112

leaves were dead and thrown off or the Li^+ was leached from the canopy by rainfall (in some cases) as demonstrated by Tamm (1951). The leaching of mineral nutrients from trees by rain has also been reported in a number of studies such as Muoghalu and Johnson (2000). However, no symptoms of toxicity or massive leaf shedding were observed during the current experiments. Additionally, the observed variations may also be related to the sampling procedure since the leaves were not sampled at the same location (i.e. one point) and at the same height in the outer canopy.

There are more factors that can influence the observed variation in responses. By-pass flow through fractures or dead root tunnels would rapidly reduce the amount of water available for diffuse expansion of moisture around the well and could explain a strong initial peak. Selaolo (1998) concluded in his groundwater study (in a similar environment) that by-pass flow equalled diffuse flow in the recharge process. As presented in Chapter 4, sap flow measurements were made in the same area and in the same tree species as used in the tracer studies, but for much longer periods of time. The results also show much temporal variations, which are not understood as yet. They may be related to physiological properties (e.g. changes in metabolism, transport within the plant etc.) that could overshadow the above possible explanations; e.g. Jacobson et al. (1960) reported that in barley plants Ca^{2+} inhibits the absorption of Li^+ over the entire pH range.

Fluctuations in meteorological conditions will also play an important role. During data analysis, weak correlations were found between foliage Li^+ concentrations and meteorological variables (air temperature, relative humidity, solar radiation and rainfall). The weak correlation possibly indicates that the temporal variations in foliage Li^+ concentrations are unrelated to variations in meteorological variables. However, peaks of Li^+ concentrations in some trees (T6 on day 11 in Figure 5.3; T8 and T11 on day 11 in Figure 5.5; T12 on day 11 and T14 on day 11 in Figure 5.4) coincided with rainfall (Figure 5.2), which could be an indication of rapid percolation, followed by a redistribution of the Li^+ plume around the insertion well, and thus facilitating uptake by roots further away from the insertion well or it

simply reflect increase in (stem) conductivity within the tree as a result of increased water availability.

Similar appreciable variations in foliar concentrations of potassium were observed by Ernst (1975) in trees in the Miombo woodland in south Central Africa and by Tolsma et al. (1987) in trees in a semi-arid savanna ecosystem (in the hardveld) in Botswana.

Furthermore, although sap velocity measurements were made in the same tree species in Chapter 4, they cannot explain the observed fast Li^+ transfer from root to shoot. They represent average sap velocities which are much lower than the velocity in some high velocity xylem vessels which could be responsible for the fast ascend of Li^+ to the leaves (at twig tops). The existence of high velocity xylem vessels were confirmed by D. Chavarro and J. Roy (unpublished data) in nuclear magnetic resonance images within the framework of the Kalahari Research Project (KRP). In their experiment it was also observed that within a few hours the dye circulated from a container to the tip of leaves much more rapidly than can be explained by the Granier relationship (i.e. Equation 4.2). The velocities which can explain the fast Li^+ ascend from tracer placement depths to the canopy tops is estimated to be in the order of 0.1-3 m/hr. This order of magnitude of velocity is consistent with maximum sap velocities reported by Larcher (2004).

By extending roots to deep horizons, trees are able to explore a significant depth of soil for water and nutrients. This aspect is important for the survival of vegetation in the semi-arid Kalahari environment, particularly during rainless periods. In the event of hydraulic lift, particularly in the height of the dry season, it is possible that vegetation with shallow root systems could be thriving primarily on water released at shallow subsurface by trees with deep root systems, which are evidently able to extract water from deep horizons. Hydraulic lift has now been demonstrated in nearly 50 plant species, most of the new examples with this ability are for Mediterranean climate species, but they also come from arid and cool temperate regions, and from seasonally dry tropical and subtropical habitats (Jackson et al., 2000).

114

A recent example of hydraulic lift is reported by Kurz-Besson et al. (2006) in *Quercus suber* in a savanna type Mediterranean ecosystem. Another example by Ludwig et al. (2003) was reported in *A. tortilis* in northern Tanzania in a savanna type ecosystem that is associated with a semi-arid climatic zone. Furthermore, deep roots can explain the occurrence of trees that show positive signs of continuous transpiration by green leaves, even during the height of the dry season, a condition that is observed in most Kalahari trees. Future work must explore the occurrence of hydraulic lift among Kalahari tree species, and if the process is active, its influence on soil water dynamics and vegetation should also be explored.

Chapter 6 Determination of the origin of water used by savanna vegetation

6.1   Introduction

The natural abundances of stable isotopes of water vary within soil, plant and atmosphere continuum. These variations have been explored in a number of water transport and water use studies, e.g. Dawson and Ehleringer (1991),Walker and Richardson (1991), Brunel et al. (1991), Ehleringer and Dawson (1992), Thorburn et al. (1992), Mensforth et al. (1994), Midgley et al. (1994), Synder and Williams (2000) and Lamontagne et al. (2005). Additionally, the stable isotopes of water have been used to estimate transpiration (Calder et al., 1992) and evapotranspiration (Brunel et al., 1997). Furthermore, isotope techniques have been developed to estimate long-term bare soil evaporation (Barnes and Allison, 1988).

The occurrence of deep rooting savanna vegetation has been mentioned in several studies e.g. Canadell et al. (1996) and Scott and Le Maitre (1998), Schenk and Jackson (2005), and by the current study where roots have been traced up to depths of 70 m as presented in Chapter 5. Therefore, it is expected that with scarcity of water near the surface, the commonly observed dry season transpiration of savanna vegetation relies not only on uptake of water from unsaturated zone layers but also from the groundwater table (i.e. close to the capillary fringe). Depth of water uptake may be assessed from the oxygen or hydrogen isotopic composition of sap-flow, rainwater, soil and groundwater. The seasonal variability of $\delta^{18}O$ or δ^2H of rains, combined with the enrichment of superficial drying layers in ^{18}O or ^2H can lead to isotope gradients between superficial and deep soil water reservoirs. Therefore groundwater often shows a different isotopic composition than soil water in the overlying superficial layers. Because water extraction by roots does not discriminate between water with different isotopes, the isotopic composition of xylem water is expected to reflect the water source, or the mixing of several sources. There is strong evidence from

literature that trees are able to shift from one source to another depending on the developmental stage or on seasonal factors. For instance, Midgley et al. (1994) in South Africa showed that plantation trees that normally depend on surface and unsaturated zone water shifted to groundwater during the drought. In Arizona, in contrast, Synder and Williams (2000) showed that *Salix gooddingii* used groundwater in favour of water in the upper soil layers during the summer rainy period.

Sap flow measurements and sampling for isotopes (during rainless days) in the trees were undertaken between December 2002 and August 2003. The investigated species include *A. erioloba, A. fleckii, A. karoo, B. albitrunca, S. longipedunculata and Z. mucronata.* Refer to Appendix A for example photographs of the species. *Z. mucronata and A. karoo* were monitored in the hardveld area where groundwater tables are shallow (<20 m) and the rest were monitored in the Kalahari sandveld where the groundwater table lies at great depth (>50 m). The monitoring period began in the wet season (when the main extraction is expected from shallow layers) and continued through the dry season with an expected shift to water extraction from greater depth. The key objective was to investigate the origin of water used by vegetation in general, and particularly with respect to the possible uptake of water from the deep groundwater basins during the dry season by deep root systems.

6.2   Site description

In the Serowe study area 11 microclimatic monitoring sites were installed in the framework of the present study (GS00-10), but the current investigations of isotopic compositions of soil and xylem water were carried out at four microclimatic monitoring sites of GS00-GS03 (Figures. 2.1 and 3.1). Table 6.1 presents the site specific details of these investigated areas. Three sites (GS01-03) are located in the Kalahari sandveld and one (GS00) is situated in the hardveld. The geomorphologic settings of the GS00 site are different from those of the GS01-03 sites, which is also reflected by soil texture. The annual rainfall for a period spanning from 1 January 2002-31 December 2003 at all sites was similar, but with lower *PET* at GS00 as compared to

the other sites. The average groundwater depth was less in the GS00 area than in the GS01-03 area.

Table 6.1. Site specific details of study areas; rainfall, *PET* and groundwater depth information were derived from an existing monitoring network discussed in Chapters 2 ,3 and 7.

	GS00	GS01	GS02	GS03
Number of sampled trees	2	1	1	2
Sampled trees	*A. karoo* and *Z. mucronata*	*A. fleckii*	*S. longipedunculata*	*B. albitrunca* and *A. erioloba*
Tree density (trees ha^{-1})	1500	1300	1000	200
Soil texture	Loamy sand	sand	sand	sand
Geomorphologic setting	Flood plain	Sand plateau	Sand plateau	Sand plateau
Average groundwater depth (m)	11	57	76	80
Annual rainfall 2002/2003 (mm/yr)	215/315	211/371	291/355	273/331
Annual *PET* 2002/2003 (mm/yr)	1068/1071	1199/1219	1210/1227	1216/1241

6.3 Materials and methods

6.3.1 Theory

The use of stable isotopes of water for the determination of the origin of water transpired by vegetation depends on the principle that the isotopic composition of water in the plant is the same as that of the source from which the water is extracted. In case of more possible sources, the isotopic composition of water in the plant can be expected to be a mixture. The present study concentrates on the identification of the depths from which water is extracted in the different seasons by trying to match the isotope composition of the xylem water in the tree with the isotope composition of water at different depths in the subsurface. The soil moisture content below

which no extraction by trees can take place (the permanent wilting point) must be defined *a priori* to exclude the influence of soil water from such dry horizons. However, the study might also give evidence of the occurrence of vegetation that can extract soil moisture below the 'normal' permanent wilting point, defined at a suction of 1.47 MPa.

The basic assumptions underlying this approach can be summarized in five conditions (Brunel et al., 1994):

(1) No isotopic fractionation occurs during water extraction by the roots. The absence of fractionation in water uptake by roots has been demonstrated by Walker and Richardson (1991) and Thorburn et al. (1992) under laboratory and green house conditions, and under field conditions by Brunel et al. (1994). This assumption has been validated for a number of vegetation species in various parts of the world (Thorburn et al., 1992). The only exception demonstrated so far is for a coastal mangrove (Lin and Sternberg, 1993).

(2) Xylem water isotopic composition within the plant does not change significantly except near the leaf. According to Brunel et al. (1997) mixing of xylem water within branches and leaves has not been observed in studies involving trees.

(3) No major errors are associated with the sampling of isotopes or in the extraction and analysis of water from plants and soil.

(4) The isotopic composition of the soil is laterally homogeneous within the rooting area (Brunel et al., 1997).

(5) Time delays associated with transport of isotopes through the plant are considered to be negligible and the xylem does not store water from a previous period.

6.3.2 Methods

The concentration of stable isotopes of water in both soil and plants were measured, along with analysis of soil moisture content. Samples of soil, xylem and groundwater were taken in summer (December 2002 - April 2003) and winter (June 2003 - August 2003) to encompass different soil moisture regimes.

120

Vegetation, groundwater and soil sampling

Xylem water was sampled at mid-day by collecting twig samples of 10-30 mm diameter from the canopy using pruning shears. The twigs were stripped of bark, cut into 50 mm lengths, placed into glass vials and then sealed with parafilm. Groundwater samples were collected in 5 ml water-tight glass bottles from adjacent boreholes using a submersible pump, powered by a small generator. Well bore storage was removed prior to collection of groundwater samples. Soil samples were collected by hand-augering to depths ranging from 3.1-10.1 m (depending on the limit of a hand-auger and/or ability to penetrate hard horizons), with samples taken every 1 m, every time augering a new hole at the same location near the sampled trees. The collected soil samples were placed in 500 ml glass jars, and then sealed with a paraffin wax, to exclude evaporation. The soil samples were later used for soil water extraction, grain size analysis and gravimetric moisture content determinations.

The lack of deep sampling into the unsaturated zone is assumed to be less problematic for the current study since Selaolo (1998) showed that ^{18}O and ^2H isotopic composition of soil moisture remains fairly stable below 3-4 m in the Kalahari, and usually approaches that of the groundwater zone below. The upper 4 m represents the main root zone where the main exchange of water between the atmosphere and the soil takes place.

Water extraction and isotopic analysis

Water was extracted from plant and soil samples using vacuum distillation (Obakeng et al., 1997). The extracted xylem and soil water samples were analysed by the isotope laboratory of the Quaternary Dating Research Unit (QUADRU) at the Council for Scientific and Industrial Research (CSIR) in Pretoria. At the CSIR, ^{18}O was analyzed as carbon dioxide using the H_2O-CO_2 equilibration technique and Deuterium as hydrogen gas after reduction of the water with zinc (Coleman et al., 1982). The mass spectrometer used for the analysis of ^{18}O and ^2H was the VG SIRA 24EM. The results of the isotopic analysis are reported as per mil (parts per thousand) relative to the

Vienna Standard Mean Ocean Water (V-SMOW). The analytical precision of ^{18}O and ^{2}H analysis was 0.1 and 1‰ respectively. The relative abundance δ [‰] values were calculated according to the following standard expression

$$\delta = 1000[(R_l/R_{std})-1] \tag{6.1}$$

where, R_l is the ratio of the heavy isotope to the light isotope in a sample and R_{std} is the same ratio in the standard (V-SMOW).

Permanent wilting point water content estimation

Under natural conditions, water is removed from the soil principally by direct evaporation or by transpiration. However, transpiration ceases and plants wilt at certain soil water suction as they are no longer able to draw water from the soil, termed the *permanent wilting point* (PWP). It has been widely accepted that the permanent wilting point for most plants is reached at a suction of 1.47 MPa, but more recently much higher suctions have been reported in the literature. For example, Scott and Le Maitre (1998) reported that in the Kalahari some desert deciduous shrubs occasionally shed their leaves at 10 MPa.

In the present study, the soil moisture at permanent wilting point at the four study sites was estimated, so that based on soil moisture profiles the influence of such horizons on the xylem isotope composition could be taken into consideration. In order to estimate soil moisture contents at the permanent wilting point suction of 1.47 MPa, a soil moisture characteristic curve was developed for Kalahari sediments. This curve was based on *in situ* (at the GS02 site) soil moisture and matric pressure measurements at 1 m depth by *ECHO-20* and *EQ2 equitensiometer* sensors, respectively. The results are expressed by the empirical formula:

$$\theta_s = 0.0326 \Psi_s{}^{-0.029} \tag{6.2}$$

where, Ψ_s [kPa] is the soil matric pressure and θ_s [m^3m^{-3}] is the volumetric soil moisture content. By using Equation 6.2, the following

122

assumptions are implicitly made: (i) a nonhysteretic soil redistribution process is assumed for Kalahari sand, (ii) the equation is valid in all Kalahari soil profiles, by assuming the Kalahari soil to have high homogeneity as confirmed by extensive soil testing (D. Rossiter, unpublished data) and as reported by Porporato et al. (2003).

For the hardveld soil profiles no suction data were available for developing a soil moisture characteristic curve, instead soil texture was used to estimate the moisture content at wilting point, based on the classification of water retention properties presented by Rawls and Brakensiek, 1983 (cited by Lubczynski and Roy, 2005).

Using Equation 6.2 and a suction of 1.47 MPa as input, the gravimetric soil moisture content at permanent wilting point for Kalahari sediments was estimated to be 1.6 %. For the more heterogeneous and more loamy hardveld area, a value of 0.055 cm^3 cm^{-3} was estimated for the permanent wilting point as defined at 1.47 MPa , which resulted in a gravimetric moisture content of 3.5%. This value was obtained by making use of site-specific soil texture information of site GS00 as presented in Table 6.1, and the Rawls and Brakensiek (1983) water retention properties classification. Following Selaolo (1998) an average bulk density of 1.55 g cm^{-3} was used in all cases for converting volumetric moisture contents to gravimetric moisture contents (in %) for similar Kalahari soils.

Tree water use

In order to obtain information about the water use of each sampled tree, sap velocity monitoring was carried out using the Granier's Thermal Dissipation Probe method (Granier, 1987). The data was acquired using *Umweltanalytische Produkte* (UP) sensors and stored by *Skye DataHog2* loggers at GS01-03 sites (as described in Chapter 4) and the *Delta-2e* logger at GS00 site, sampling data every 30 seconds and storing 30 minutes averages of the samples. Refer to Figure 3.1 for location of the sites.

Sap velocity was calculated according to Granier (1987), considering the thermal difference between probes occurring at times of positive

(ΔT) and zero flow (ΔT_{max}). In order to calculate sap flow the sap velocity of individual trees were multiplied by the estimated conductive xylem areas, derived from species specific biometric functions obtained from Table 4.2 (Chapter 4). The water use of each tree (normalized sap flow) was calculated according to Equation 4.3.

6.4 Results and discussion

6.4.1 Rainfall and tree transpiration

Figure 6.1 presents daily rainfall of the study sites and the water use for each sampled tree for the period December 2002 –August 2003. It is evident that the water use (i.e. consumption) of the monitored trees was high during summer and decreased during winter months, which is a typical seasonal trend for Kalahari trees as indicated in Chapter 4. The rainfall events between sampling days for isotopic analyses may be expected to have influenced the soil moisture isotopic composition and hence the isotopic compositions of water transpired by vegetation. Due to equipment failure the sap flow data for two trees (*A. karoo* and *Z. mucronata*) monitored at the GS00 site is unavailable, but a similar water use trend can also be expected for these trees.

6.4.2 Overview of groundwater, soil and tree xylem water isotope data

The isotopic composition of xylem water for the various trees under investigation is presented in Figure 6.2. Only the ^{18}O isotopic data are given because the analytical precision of ^{18}O is better than that of ^{2}H. The following conclusions can be obtained from the diagrams:

The isotopic composition of xylem water in the Kalahari trees is temporally slightly variable for each tree and between different tree species at the same location. The isotope composition in the xylem at sites GS02 and GS03 closely reflects the more or less constant isotope composition of soil moisture below a depth of about 3 m, which is below the upper zone where the soil moisture content is mainly below wilting point and where the ^{18}O content is enriched by

124

soil evaporation. Water extraction is obviously predominantly from the deeper soil moisture zone and/or from groundwater. Xylem water in *S. longipedunculata* at GS02 in December 2002 shows an inexplicable low [18]O content; this might be an analysis error.
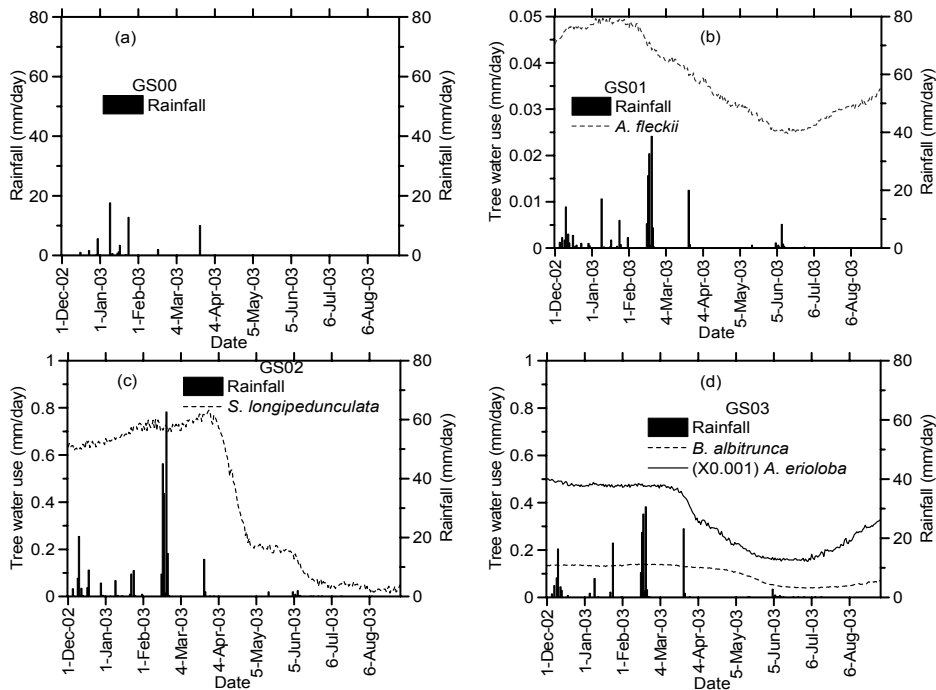

Figure 6.1. Daily rainfall at GS00-03 sites and water use (sap flow normalised by crown area) of *A. erioloba, A. fleckii, B. albitrunca* and *S. longipedunculata*

Xylem water at site GS01, in contrast, shows clearly an [18]O content above that of soil moisture and groundwater below a depth of 3 m. This suggests a considerable extraction of water from the upper, isotopically enriched, soil layers by *A. fleckii*. This might indicate that this tree is able to exert a higher suction than the defined wilting point at 1.47 MPa.

Site GS00 at the hardveld shows a slightly different situation. The upper 4 m of the soil was permanently above wilting point during the measuring period, and the xylem water of *A. karoo* and *Z. mucronata* clearly reflects the isotopic concentration of that upper soil layer. This

relatively high soil moisture content of the upper soil, in spite of a lower rainfall in comparison with the Kalahari sites, is due to the loamy nature of the soil at the hardveld area.

Very little information is currently available to determine the water source strategy for most tree species found in the Kalahari. As observed elsewhere some trees may only revert to groundwater use when all other sources are not available (Zencich et al., 2002). While groundwater may constitute a small proportion of water use by some Kalahari trees, it is probably still important for their long-term survival because in this region annual *PET* is much larger than rainfall. Therefore, it would be desirable to compare water sourcing strategies of trees between wet and dry years.

The ^{18}O content of groundwater in the Kalahari is more depleted in ^{18}O than soil moisture (Figure 6.2). The explanation is that groundwater is most probably replenished both by diffuse percolation of soil moisture and by more direct percolation through by-pass flow after high intensity rainfall showers, which normally show a more depleted character than moderate rainfall. Soil water below 4 m will be slightly enriched (compared to rainwater) through infiltration from the upper soil horizon where direct evaporation and isotope enrichment takes place.

The isotopic composition of groundwater from the Ntane sandstone aquifer in the Kalahari area as well as in the hardveld area was fairly uniform at each specific location through out the monitoring period as depicted in Figure 6.3. The isotopic composition of the groundwater at all sites lies on the Global Meteoric Water Line (G-MWL), but the groundwater at GS00 site is more depleted isotopically than the groundwater at other sites. The figures suggest a trend in isotopic enrichment of groundwater from east to west, from GS00 to GS02/ GS03. This trend most likely reflects differences in residence times of water in the aquifer since isolation from the atmosphere. The most depleted water correspond with the part of the aquifer that is relatively shallow with rapid infiltration through weathered hard rock and fractures at short distance from the groundwater divide (GS00 and GS01), while the least depleted groundwater of GS02-03 is

126

further away from the groundwater divide and corresponds to a thick unsaturated zone with lower infiltration fluxes of a more diffuse nature from unsaturated zone moisture that has been subjected to isotopic enrichment through evaporation.

The isotope figures of Kalahari groundwaters as depicted in Figure 6.3 are comparable with earlier studies in the Letlhakeng-Botlhapatlou and Central Kalahari area, some 300 km to the south (Selaolo, 1998; De Vries et al., 2000). The deviation of the slope of the Central Kalahari Meteoric Water Line (CK-MWL) from the Global Meteoric Water Line is most probably due to the fact that the CK-MWL was based on a limited number of monthly averaged rainwater samples. This procedure resulted in monthly averaged ^{18}O figures of rainwater between -6 ‰ and 0. High intensity rainfall events, which are responsible for most of groundwater recharge normally shows a more depleted signature, and thus explains the depleted character of the Kalahari as well as the hardveld groundwaters.
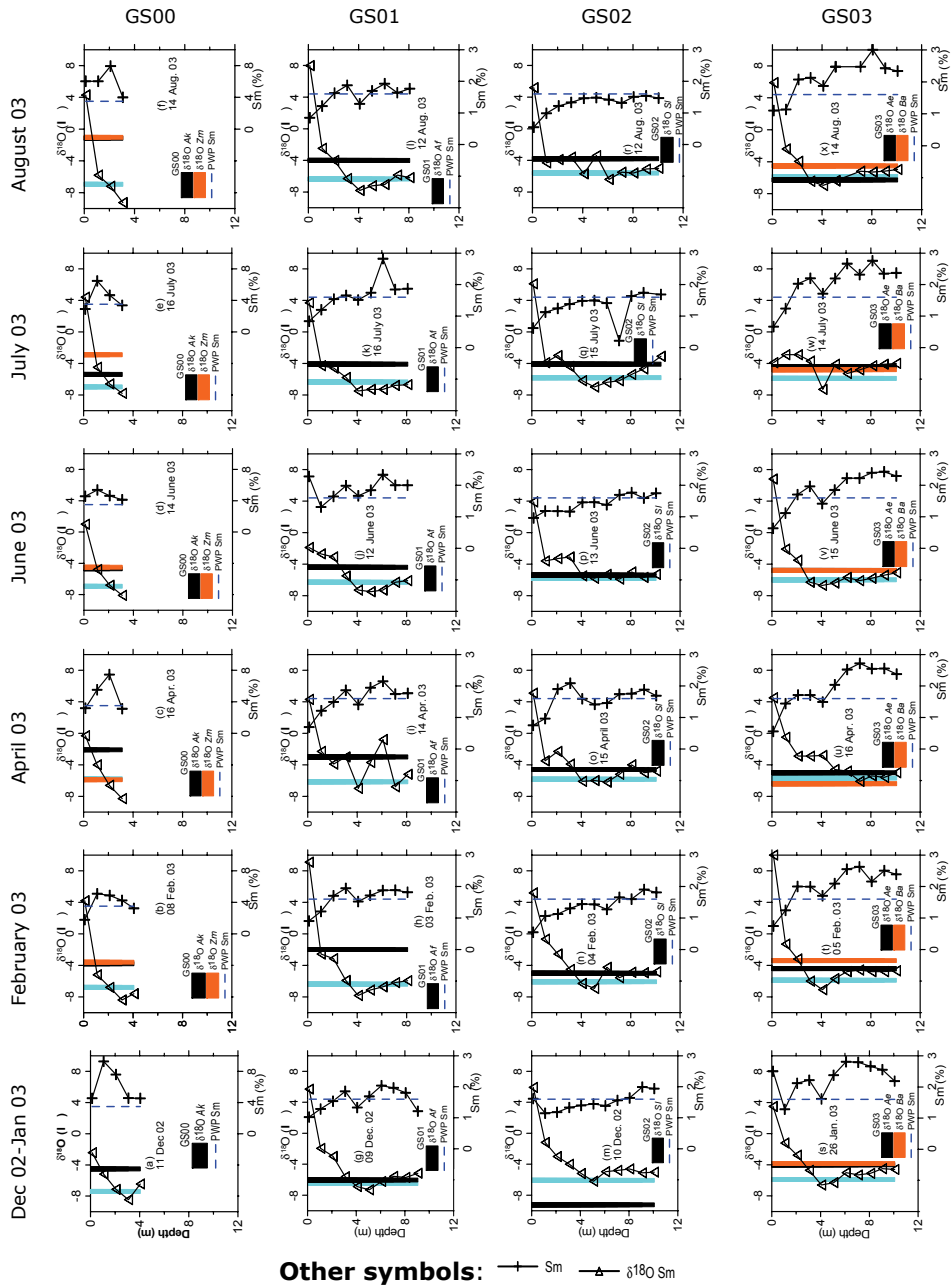
127

Figure 6.2. **18O content of soil water (Sm), groundwater (Gw-shown as light blue bars), and xylem water of *A. karoo (Ak), Z. mucronata (Zm), A. fleckii (Af), S. longipedunculata (Sl), A. erioloba* (Ae) and *B. albitrunca (Ba)* (also shown as black and light brown bars). Soil moisture at permanent wilting point (PWP Sm) is also shown as a dotted dark blue line.**
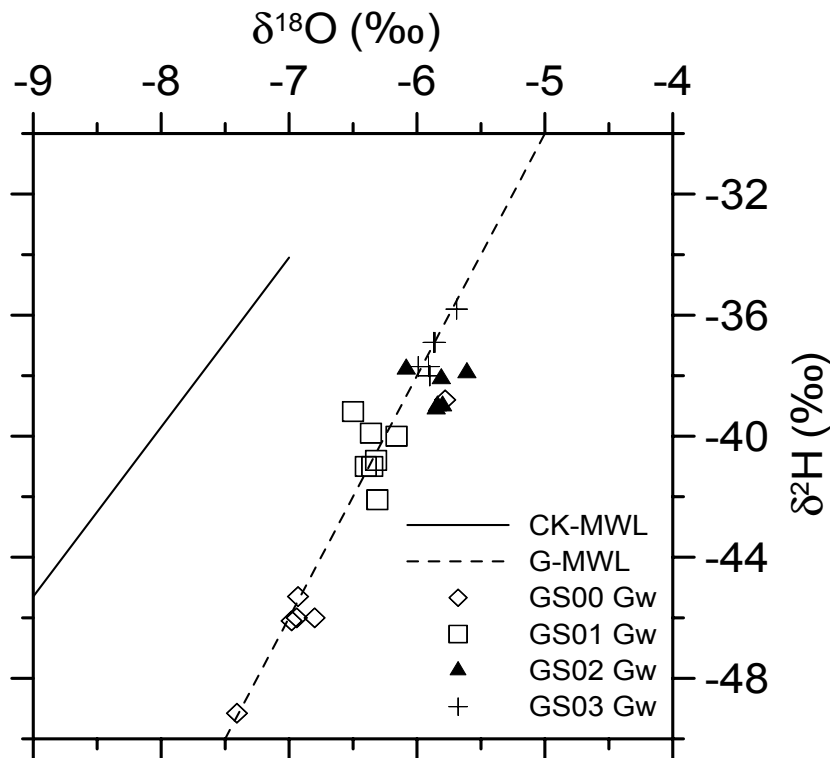
Figure 6.3. Isotopic composition of groundwater (Gw) at GS00–03 sites. CK-MWL refers to Central Kalahari Meteoric Water Line derived from Selaolo (1998) and G-MWL refers to the global meteoric water line (Craig, 1961).

6.5   Conclusions

1. Water extraction by *A. karoo* and *Z. mucronata* at GS00 was mainly from the upper 4 m.

2. Except for 9 December 2002, water extraction by *A. fleckii* was mainly from the upper 4 m at GS01, indicating that *A. fleckii* can exert a higher suction than 1.47 MPa or it has more roots in the shallow subsurface.

3. Water extraction by *S. longipedunculata* at GS02 was mainly from the horizons much deeper than 4 m, most probably caused by the

fact that the soil moisture above 4 m was generally below the wilting point.

4. Water extraction by *A. erioloba* and *B. albitrunca* at the GS03 site was mainly from below 4 m depth, also at this site most probably because the soil moisture above 4 m was generally below wilting point.

Future studies in the Kalahari should establish the possible role of hydraulic lift in water use strategies of Kalahari trees. This effort must be accompanied by the use of applied tracers for identifying the origin of water used by trees since stable isotopes of water result in a non-uniqueness solution when many possible sources of water are present. Moreover, the isotopic composition of rainwater from the present study should be investigated.

Chapter 7 Soil moisture regimes, groundwater level fluctuations and groundwater recharge

7.1   Introduction

Quantification of the rate at which water is replenished in an aquifer (groundwater recharge) is a critical matter for many desert regions, particularly in case of large settlements such as the Serowe area, where water demand is increasing, due to growing human and livestock populations. Therefore evaluating the net replenishment of the aquifer is vital to sustainability and optimal management of the groundwater resources. Net replenishment or net groundwater recharge is defined as the water flux that passes through the unsaturated zone and reaches the aquifer minus the amount that is extracted from the aquifer by deep rooting vegetation and/or upward vapour-liquid transport. Net groundwater recharge equals net groundwater discharge plus or minus change in storage. A number of factors affect recharge of groundwater: Hydraulic conductivity, soil porosity and soil texture, geomorphic conditions, type of vegetation, rainfall intensity and its seasonal distribution are some examples of such factors.

Groundwater recharge is difficult to measure directly, but can be estimated by tracers. Other methods are based on numerical models of the physical process of infiltration. Such models are calibrated on experimental data and measurements, such as groundwater table fluctuations, soil moisture fluctuations and hydraulic properties of the subsurface. Recent studies are, for instance, by Fazal et al. (2005) who applied a conceptual model, calibrated by genetic algorithm to estimate recharge using groundwater level measurements in four catchments of Miyakojima Island of Japan, and by Ladekarl et al. (2005) who applied a numerical simulation model to estimate groundwater recharge for two natural ecosystems covered with oak and heather using soil moisture measurements. Determination of recharge from lumped water balance studies as the difference

between rainfall, evapotranspiration and surface runoff is normally not suitable for (semi) arid areas because the recharge component is normally very small and in the same order of magnitude, or even smaller than the errors in rainfall and evapotranspiration determinations.

Groundwater recharge can be subdivided into direct or diffuse recharge, and indirect recharge from concentrated surface water in depressions or (ephemeral) streams. Overviews of groundwater recharge studies are found in Lerner et al. (1990), Simmers (1997) and in a special issue of the Hydrogeology Journal, vol. 10, no. 1 of 2002.

Studies on groundwater recharge from Botswana and South Africa are, among others, given by Bredenkamp (1988a,b), Van Tonder and Kirchner (1990), Bredenkamp et al. (1995), Gieske (1992), Selaolo (1998) and De Vries et al. (2000).

7.2   Problem statements

The study of soil moisture transport and groundwater recharge in a semi-arid area with variable savanna vegetation and variable depths to groundwater table is complex (e.g. Scanlon et al., 1997) because by-pass flow and water vapour transport complicate the process, whereas low moisture contents make it difficult to measure accurately the variations that determine the transport processes. Therefore, in order to obtain more information on the above aspects, within the present study of water extraction by trees, the test sites were well instrumented with sensors to monitor soil moisture and groundwater level fluctuations.

In this part of the thesis the result of *in situ* soil water monitoring at eight 'undisturbed' sites are presented; it includes an evaluation of soil moisture transport and the recharge process through a thick unsaturated zone. The results are considered preliminary and merely indicative because the monitoring period is too short to predict long-term recharge and there are gaps in the dataset.

7.3   Materials and methods

7.3.1 Field monitoring, sampling and laboratory analyses

Monitoring of vadose zone moisture and matric pressure

In the study area seven matric pressure-moisture profiles at seven monitoring locations of GS01-GS07 (Figure 3.1) were installed. Each profile consisted of four dielectric *ECHO 20* soil moisture sensors and four gypsum block matric pressure sensors installed ≈ 2 m apart from each other at 2 m, 4 m, 6 m and 8 m below ground surface (m b.g.s.). The data acquisition and data storage were controlled by *Skye DataHog2* loggers, sampling data at various sensor-dependent sampling times and storing it at a uniform interval of half an hour.

In order to investigate if recharge occurs at large depth through Kalahari sand, an additional deep matric pressure profile was also installed at the GS10 location (Figure 3.1) characterized by absence of basalt and unconfined aquifer conditions (Table 7.4). The deep profile consists of 15 gypsum block matric pressure sensors distributed logarithmically with increasing depth interval starting at 0.25 m and ending at 76 m b. g. s., just at the groundwater table level. Additionally, and 2 m away from the deep soil matric pressure profile, a shallow soil matric pressure profile consisting of 6 ceramic blocks called *Watermarks* was installed down-hole, at corresponding shallow depths of 0.25, 0.5, 1, 2, 4 and 7 m. The GS10 data acquisition and data storage was controlled by the multi-channel *Delta-2e* logger, also sampling data at various sensor-dependent sampling times and storing it at a uniform interval of half an hour.

At all sites where unsaturated zone moisture and matric pressure were monitored, a tipping-bucket rain gauge (calibrated to record 0.2 mm/tip) was used for monitoring the amount of incident rainfall. Additionally, rainfall was also monitored at GS00 and GS08 sites at an interval of half an hour. The various rainfall and soil moisture/matric pressure measuring devices used within the current study are presented in Table 7.1.

Table 7.1. Soil moisture and rainfall sensor types and their locations in the study area

Monitored variable	Sensor type	Measuring range or sensitivity	Location
Rainfall	Raingauge ARG100	0.2 mm/tip	GS00-08,GS10
Soil moisture	ECHO-20	0.0004-0.4 m^3m^{-3}	GS01-07
Matric pressure	Watermark 200SS	0-200 cBar	GS10
Matric pressure	Gypsum GPSY1	50-1500 cBar	GS01-07,GS10

All profiles, except GS05, showed uniformity in grain sizes in samples from different depths. They consist of ≈90% sand (63-2000µm), ≈6% silt (2-63µm) and ≈4% clay (<2µm). At GS05, however, the silt composition was rather high: ≈ 13% silt, ≈85% sand and ≈2% clay fractions at all depths. In all profiles soil samples were collected up to a depth of 10 m.

Calibration of sensors

The monitoring of all soil moisture and matric pressure sensors was carried out by recording voltage drops related to the electrical resistance of the materials surrounding the installed sensors. Therefore, calibration equations were used to derive the equivalent entity (soil moisture or matric pressure). Tables 7.2 and 7.3 present calibration equations that were used in the present investigation. The calibration equations used for *ECHO-20* probes were developed in the laboratory by adding incrementally known amounts of water on field soil samples and recording the corresponding voltages. After which the data was fitted by a linear model to give the associated equations as presented in Table 7.2. The calibration equations (Table 7.3) for *Gypsum GSPY1* and *Watermark 200SS* sensors were obtained from data provided by the instrument dealer (*Skye instruments).*

Table 7.2. Calibration equation for *ECHO-20* sensors at four soil depth intervals; x is voltage in millivolts, θ_s is soil moisture in $m^3 m^{-3}$ and n is number of observations

Sensor	Soil depth interval (m)	Calibration equation for GS01-04 and GS06-07 soil profiles	R^2	n	Calibration equation for GS05 soil profile	R^2	n
Echo-20	1-2	$\theta_s=0.0006x-0.214$	0.98	18	$\theta_s= 0.0004x - 0.1497$	0.92	18
Echo-20	3-4	$\theta_s=0.0006x-0.218$	0.97	18	$\theta_s= 0.0001x - 0.0544$	0.98	14
Echo-20	5-6	$\theta_s=0.0006x-0.210$	0.97	19	$\theta_s= 0.0002x - 0.0864$	0.94	19
Echo-20	7-8	$\theta_s=0.0006x-0.214$	0.98	20	$\theta_s= 0.0003x - 0.0995$	0.96	16

Table 7.3. Calibration equations for *watermark 200SS* and *Gypsum GPSY1 sensors*; x is voltage in millivolts, Ψ_s is matric pressure in bars and n is number of observations

Sensor	Calibration equation	R^2	n
Gypsum GPSY1	$\Psi_s= 3E\text{-}07x^2 + 0.0008x + 0.103$	0.99	51
Watermark 200SS	$\Psi_s= 4E\text{-}07x^2 + 0.0002x + 0.052$	0.99	41

Monitoring of groundwater

Groundwater monitoring in the study area consists of 17 well measurement points equipped with automated groundwater table recorders (AGTR). The AGTR records the pressure above the sensor suspended in groundwater. Of the 17 AGTRs, one was a differential (automatically compensating for barometric pressure) AGTR installed by the Department of Water Affairs, and 16 were absolute (compensated by the external barometric pressure measurement) AGTRs installed at shallow level within the framework of the current study. Additionally, two loggers installed in boreholes 5336 and 8403 were available for measuring barometric pressure, for removal of barometric influence. All AGTRs were programmed to acquire data at one-hour interval. This data was then periodically retrieved with a normal *laptop* computer.

The stratigraphy of the boreholes and the types of AGTRs in these boreholes are presented in Table 7.4. Out of the 17 monitored

boreholes, five boreholes have no basalt intermediate layer between the upper Kalahari beds and the underlying Ntane sandstone aquifer. The rest are associated with variable thickness of Stormberg basalt as depicted in Table 7.4. The role of basalt in water flow is essentially two fold: it may act as an impeding layer when fresh and un-fractured or facilitate vertical infiltration flow when weathered or fractured. Lithological descriptions by WCS (1998) and SGC (1988), suggest that the basalt is generally weathered in the top few ($\approx$<5 m) meters, and becomes fresh at greater depths.

Extensive information concerning hydraulic properties of the Ntane sandstone aquifer and the Stormberg basalt is provided in reports by SGC (1988) and WCS (1998). The storage coefficients for boreholes were derived from the WCS (1998) groundwater model for the study area. Therefore, the storage coefficients in Table 7.4 are average values from a modelling calibration that was initially based on distributed storage coefficients from pumping test results of SGC (1988) and WCS (1998).

Table 7.4. Stratigraphy, storage coefficients (S) and installed AGTR types of monitored boreholes; DI250 is 'Barodiver', DI240 and DI241 are 'mini-Divers' and TP-2A is 'Tirtalog logger'

Bh no.	GS site	Distance of borehole from GS site (km)	Kalahari beds thickness (m)	Stormberg basalt thickness (m)	Ntane sandstone thickness (m)	Flow conditions	Average depth to water level (m)	S	AGTR type
8403	GS00	0.1	0	0	unknown	unconfined	8	0.04	DI250, TP-2A
4139	GS00	19	0	24	>48	confined	24	0.04	DI241
8449	GS01	0.07	24	28	>118	confined	57	0.04	DI240
4147	GS01	10	0	71	73	confined	51	0.04	DI241
4743	GS02	0.05	75	0	>63	unconfined	76	0.04	DI241
5309	GS03	0.4	55.6	0	43.4	unconfined	79	0.04	DI241
5310	GS04	0.5	39.2	0	48.6	unconfined	72	0.04	DI241
5306	GS04	16	0	0	50.8	unconfined	36	0.04	DI241
5312	GS05	6	36.9	48.8	88.9	confined	80	0.04	TP-2A
5337	GS05	9	43.6	32	91.7	confined	103	0.04	DI240
5343	GS05	0.09	59.7	37	>103.2	confined	100	0.03	DI241
5314	GS06	5	41.4	49.1	53.1	confined	72	0.04	DI241
5336	GS06	0.1	24	33.3	48.8	confined	94	0.03	DI250, DI-241
5326	GS07	0.05	57.5	50.7	119.4	confined	108	0.07	DI240
4742	GS07	4.5	45	57	>53	confined	102	0.06	DI240
8472	GS08	0.2	24	70	>90	confined	94	0.04	Troll SP 4000
8493	GS08	1	26	68	>92	confined	94	0.01	DI241
4743	GS10	0.005	75	0	>63	unconfined	76	0.04	DI241

7.3.2 Recharge estimation methods

There are many sophisticated models and indirect methods for estimating groundwater recharge. However, due to lack of sufficient and coherent field data and model parameter values in most cases, it is difficult to apply physically based models (based on Richard's equation) such as HYDRUS (Šimůnek et al., 1998) and SWAP (Van Dam et al., 1997) for calculation of groundwater recharge. As mentioned earlier (Chapter 3) the main problem is to find adequate

parameters for the effects of roots (in the sink term) and how to capture or represent the by-pass flow component. Among different indirect techniques, the lumped water balance is widely used for assessing recharge. However, application of the water balance under semi-arid condition is not straightforward because the recharge component is very small in comparison to the other components, and therefore very susceptible to small inaccuracies in the determination of the basic components.

Another type of approach is the use of tracers to determine mass transport or to trace the movement of soil water. This methodology was applied by the GRES phase II project to assess groundwater recharge in the Letlhakeng-Botlhapatlou area, some 300 km, south of the present study area (Selaolo, 1998; De Vries et al., 2000).

Due to the difficulty in the parameterisation of the thick unsaturated zone the estimation of recharge in this study is based on three simple approaches: (i) a linear reservoir (LINRES) approach of De Vries et al. (2000), (ii) the classical water table fluctuation (WTF) approach and (iii) a one-dimensional lumped parameter hydrological model (EARTH) of Van der Lee and Gehrels (1990).

The practical advantage of the three methods is their simplicity and insensitivity to the mechanisms of recharge, and hence they are suitable for situations where spatio-temporal scales are much longer than they could feasibly be studied with process based models such as SWAP and HYDRUS. Additionally, because of their insensitivity to the actual recharge mechanisms they are not restrained by

preferential flow (Healy and Cook, 2002). Furthermore, their recharge values can represent integrated values over large areas; this is a great advantage as compared to methods that depend on unsaturated zone measurements (Healy and Cook, 2002).

Linear reservoir approach (De Vries et al., 2000)

The extent to which prevailing climatic conditions influence the groundwater regime is to a large extent governed by basic hydraulic properties of the groundwater flow system. The basic hydraulic properties are a combination of the hydraulic properties of the unsaturated zone and the geometric properties of the groundwater flow system. Generally, the specific groundwater drainage resistance and the storage factor can characterize these basic hydraulic properties. According to De Vries (1974), on the regional scale of a drainage basin groundwater level change is controlled by groundwater recharge and groundwater discharge (q_d) to surface drainage networks. Therefore, when an external stress q_r (recharge rate) is considered on the aquifer system the following linear-reservoir approach can be applied (De Vries et al., 2000)

$$q_r = \frac{h_t - h_o e^{-\alpha_c t_{da}}}{(1 - e^{-\alpha_c t_{da}})\gamma_d} \tag{7.1}$$

Where $\alpha_c = 1.5(\gamma_d S_y)^{-1}$ is the reaction factor or reservoir outflow recession constant [T^{-1}] obtained from the recession curve according to Equation 7.2, γ_d is the specific groundwater drainage resistance [T], S_y is the specific yield, h_t presents, the head above the drainage base at the beginning of a recession at time (t) equals t and h_o is the height above the drainage base at the end of a recession ($t=0$) as illustrated in Figure 7.1. t_{da} is time [T] interval between $t=0$ and $t=$t, i.e. duration of water level rise (Figure 7.1).
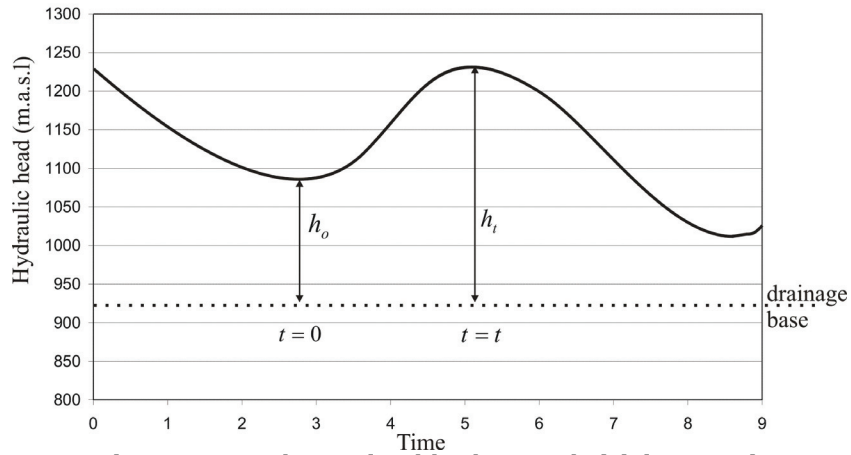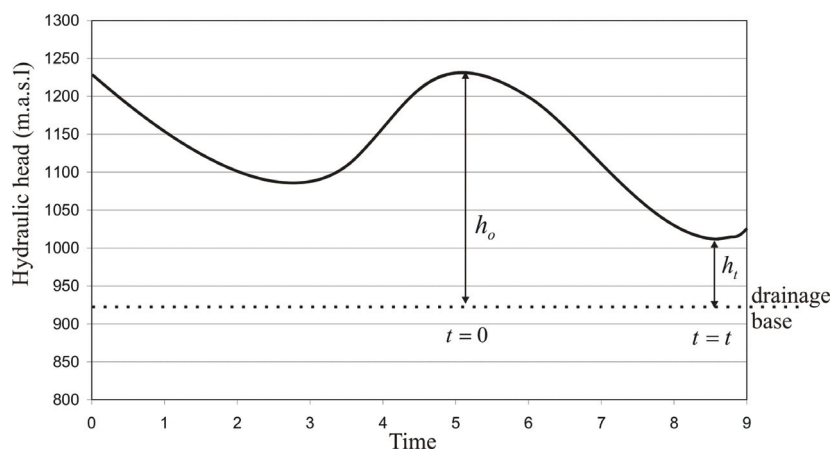
Figure 7.1. Schematized hydrograph (rising part)

The α_c in Equation 7.1 above is calculated from the recession part of a hydrograph according to

$$\alpha_c = -\ln\left(\frac{h_t}{h_o}\right)\Big/ t_{dr} \qquad\qquad (7.2)$$

where h_o is present head above the drainage base at the beginning of a recession at time $t=0$ and h_t is the height above the drainage base at the end of a recession ($t=$t) as illustrated in Figure 7.2. t_{dr} is time [T] interval between $t=0$ and $t=$t, i.e. duration of the recession (Figure 7.2).

Figure 7.2. Schematized hydrograph (recession part)

Under steady state conditions q_r equals the groundwater discharge (q_d) to the drainage base on a regional scale, such that as t_{da} tends to positive infinity then Equation 7.1 reduces to

$$q_d = \frac{\bar{h}}{\gamma_d} \qquad (7.3)$$

where $\bar{h}$ is the average head above the discharge base at the divide and γ_d is the specific drainage resistance expressed as

$$\gamma_d = \frac{D_L^{\;2}}{2T_{ss}} \qquad (7.4)$$

where D_L is distance between the divide and the drainage base and T_{ss} is the average regional transmissivity.

Water table fluctuation method

The WTF method is based on the assumption that water level rises are caused by rainfall recharging the aquifer. If the water table rise is known then recharge can be inferred according to

$$q_r = S_y \frac{\Delta h}{\Delta t} \qquad (7.5)$$

Where, q_r is recharge, Δh is the recharge related change in water table height occurring in the time interval Δt and S_y is the specific yield. The determination of reliable estimates of S_y is a critical matter, since S_y is essentially time dependent. E.g. Healy and Cook (2002) points out that the field and laboratory determinations of S_y are largely dependent on the duration of such tests, with long duration tests yielding greater S_y values. Additionally, the storage coefficient for a falling water table is more or less constant but for a rising water table the storage coefficient depends on the initial soil moisture content.

Estimating Δh can however, be problematic because rainfall is not the only factor that can cause the water table to rise. While evaluating recharge from groundwater fluctuations, all other causes of the water

table rise need to be filtered out, e.g. the so-called Lisse effect (Week, 2002) due to compressed air (Healy and Cook, 2002). Other causes of water level changes that are not related to recharge and discharge include periodic impacts such as: Ocean tides, earth tides or atmospheric tides and extraction by pumping. Additionally, the WTF approach encounters problems by predicting no recharge under situations of high attenuation of the moisture transport, where the rate of water movement away from the water table is equal to the steady recharge rate, and thus no water level rise would be observed.

In fact the WTF approach is focused on short periods during which recharge exceeds discharge.

One dimensional lumped parameter model (EARTH)

For application of a model based on the physical process of infiltration, the present study focuses on a practical approach that uses a series of linearly coupled modules that represent some element of physical reality. This type of modelling has been applied in groundwater hydrology by e.g. Thiery (1988), Finch (1998), Disse (1999) and Fazal et al., (2005).

In the present study, the Extended model for Aquifer Recharge and soil moisture Transport through the unsaturated Hard rock (EARTH) of Van der Lee and Gehrels (1990) is used for one dimensional simulation of recharge and groundwater level fluctuations because most of the model parameters could be estimated directly or indirectly from a combination of available field data and data from the literature, as in Table 7.5. However, the model does not account for lateral groundwater flow and direct groundwater extraction.

A detailed description of the model is provided by Van der Lee and Gehrels (1990). Only an overview is presented here for clarity. The EARTH model consists of four reservoirs, which perform the following specific functions: (i) *Maximum Interception Loss* module that calculates the amount of precipitation retained by vegetation, depression storage and loss to evaporation, which together determines the effective rainfall or precipitation excess that

142

infiltrates; (ii) *Soil Moisture Storage* module that distributes infiltration water into actual evapotranspiration, percolation and soil moisture storage; (iii) *Linear Reservoir Routing* module that controls the time that percolating water takes to reach the water table at variable depths; (iv) *Saturated flow* module that calculates groundwater level rise using the recharge or in its absence, it calculates the groundwater recession.

Input data

The standard EARTH model uses continuous daily rainfall and potential evapotranspiration (*PET*) data, 11 soil and groundwater related parameters (Table 7.5) as input, soil moisture measurements and observed groundwater level fluctuations for its calibration. As output the EARTH model calculates continuous daily groundwater levels, actual evapotranspiration, aquifer recharge, percolation, ponding, surface runoff and soil moisture.

Table 7.5. Soil and groundwater related parameters of EARTH model and their derivations in the present study

Parameter	Symbol	Derivation of parameter
Maximum soil moisture content (mm)	S_m	Soil texture, bulk density as input in Rosetta program
Residual soil moisture content (mm)	S_r	Soil texture, bulk density as input in Rosetta program
Initial soil moisture content (mm)	S_i	Calibration
Soil moisture at field capacity (mm)	S_{fc}	Calibration
Maximum surface storage (mm)	$SUST_{max}$	Field observations
Maximum interception loss (mm)	I_c	Maximum interception recommended for most land cover types by Pitman (1973)
Saturated conductivity (mm/day)	K_s	Soil texture, bulk density as input in Rosetta program
Unsaturated recession constant (day)	UnR_c	Calibration
Number of linear reservoirs (-)	n_r	Calibration
Storage coefficient (-)	S	Pumping tests of WCS (1998) and SGC(1988)
Saturated recession constant (day)	R_c	Groundwater level observations

The maximum soil moisture content (S_m), residual soil moisture content (S_r) and saturated hydraulic conductivity (K_s) were estimated from soil texture and bulk density information using the *Rosetta* program (Schaap et al., 1999; 2001). *Rosetta* is a computer program for estimating soil hydraulic parameters with hierarchical pedotransfer functions (PF). It is able to estimate van Genuchten (1980) water retention parameters and saturated hydraulic conductivity.

Pedotransfer functions normally show appreciable scatter as shown by Wagner et al. (2001). However, Zarkesh (2005) demonstrated that the van Genuchten (1980) water retention model gave realistic results when applied to a recharge scheme, and as such was adopted by the current study.

Based on Rosetta estimates S_m, S_r and K_s were fixed at 417 mm, 150 mm and 6804 mm/day respectively. The absolute value of S_r is not significant with regard to recharge; only the magnitude of the soil retention capacity (Soil moisture at field capacity (S_{fc}) minus S_r) is significant (Van der Lee and Gehrels, 1990). The Maximum surface storage was fixed at 0 mm for all observation locations. The Maximum interception loss was fixed at 1.5 mm based on Pitman (1973)'s recommendation for maximum interception of most land cover types. The storage coefficients were obtained from Table 7.4. The remaining parameters were obtained by calibration.

For each observation location calibration was performed in two stages: unsaturated zone calibration and saturated zone calibration. The purpose of the unsaturated zone calibration was to constrain the estimated actual evapotranspiration (AET) between dry season plot tree transpiration (T_p) and potential evapotranspiration (PET). The calibration was undertaken such that the S_{fc} and initial soil moisture content (S_i) were adjusted manually so that the EARTH model calculated actual evapotranspiration estimates for the dry season, closely approached the dry season plot tree transpiration estimates (presented in Chapter 4). In other words the actual evapotranspiration estimates obtained by the simulation model were constrained between the dry season plot-tree transpiration and the corresponding PET calculated according to Equation 3.4 (Chapter 3).

144

The soil moisture was not used in the unsaturated zone calibration because of the large spatial and temporal variations in the measurements.

The one-dimensional simulation modelling was undertaken with the information of 13 observation locations situated in the Kalahari sandveld. This simulation (exercise) was not carried out for the hardveld sites because the constraining plot tree transpiration data was not available and moreover, plot tree transpiration of the eight selected Kalahari plots (see Chapter 4) could not be simply extrapolated to the hardveld observation points (boreholes).

The EARTH model as standard allows for calibration of groundwater levels and soil moisture, but in this study the model is constrained by a combination of groundwater levels and dry season transpiration. *This is the first study in Botswana to constrain a hydrological model using measured tree transpiration data*. The underlying assumption of this approach is that dry season actual evapotranspiration closely resembles dry season plot tree transpiration in the height of the dry season, since most grasses and shrubs are dormant, and therefore have negligible contribution to evapotranspiration loss, and soil evaporation is also expected to be insignificant. The present approach circumvents the need for detailed soil storage parameters which would be nearly impossible when dealing with a thick unsaturated zone (i.e. large scale processes). Once the unsaturated zone calibration has been achieved, calibration of the saturated zone was done manually by adjusting the unsaturated recession constant, the saturated recession constant and the number of reservoirs (n_r) until a close match of observed and simulated groundwater levels was reached, after which the fit was improved by optimization of the two recession constants.

Model efficiency

There is no direct observation of recharge, say from a lysimeter study. Therefore, the coefficient of determination (R^2) and the mean square errors (*MSE*) of observed and estimated heads for an

observation location were used in this study to evaluate the goodness of the calibration fit. The *MSE* is defined as

$$MSE = n^{-1} \sum_{i=1}^{n} \left(h_i - \hat{h}_i \right)^2 \qquad (7.6)$$

where, n is the total of observation days, h_i and $\hat{h}_i$ are the observed and estimated heads respectively for the *i*th day. The *MSE* helps to determine the degree of scatter of the estimated data with regard to the initial mean of the variance or standard deviation.

7.4 Analysis of field data

This section describes the dynamics of soil moisture, matric pressure and groundwater level (piezometric) fluctuations.

7.4.1 Soil moisture content

Soil moisture content was measured with *ECHO-20* sensors at seven profiles (GS01-07) to study temporal and spatial behaviour. Figure 7.3 illustrates the temporal variability of the soil moisture content for GS01-07 profiles. The following observations can be made from Figure 7.3:
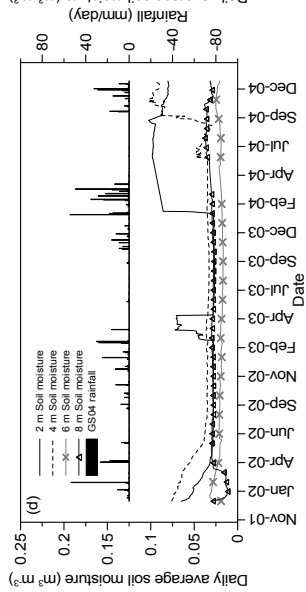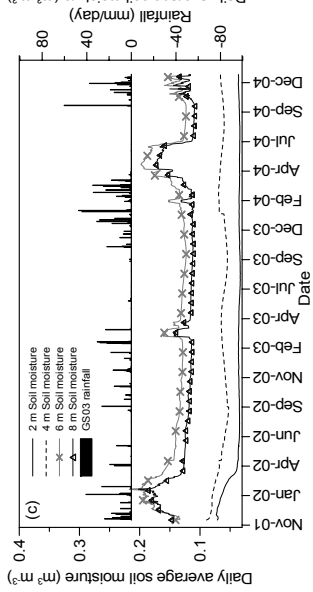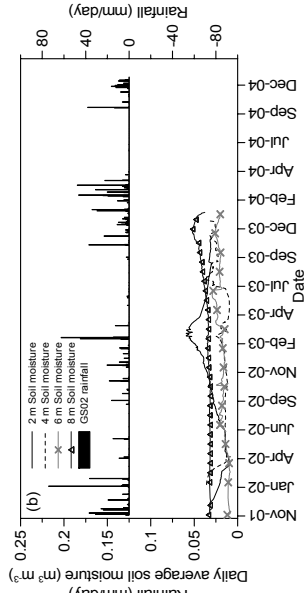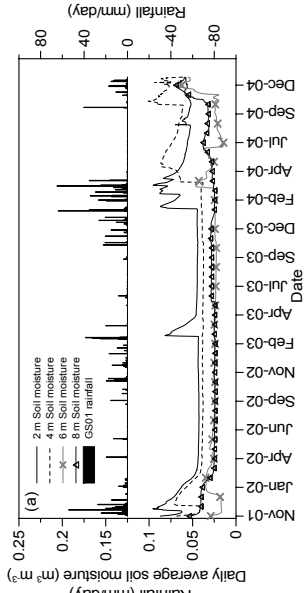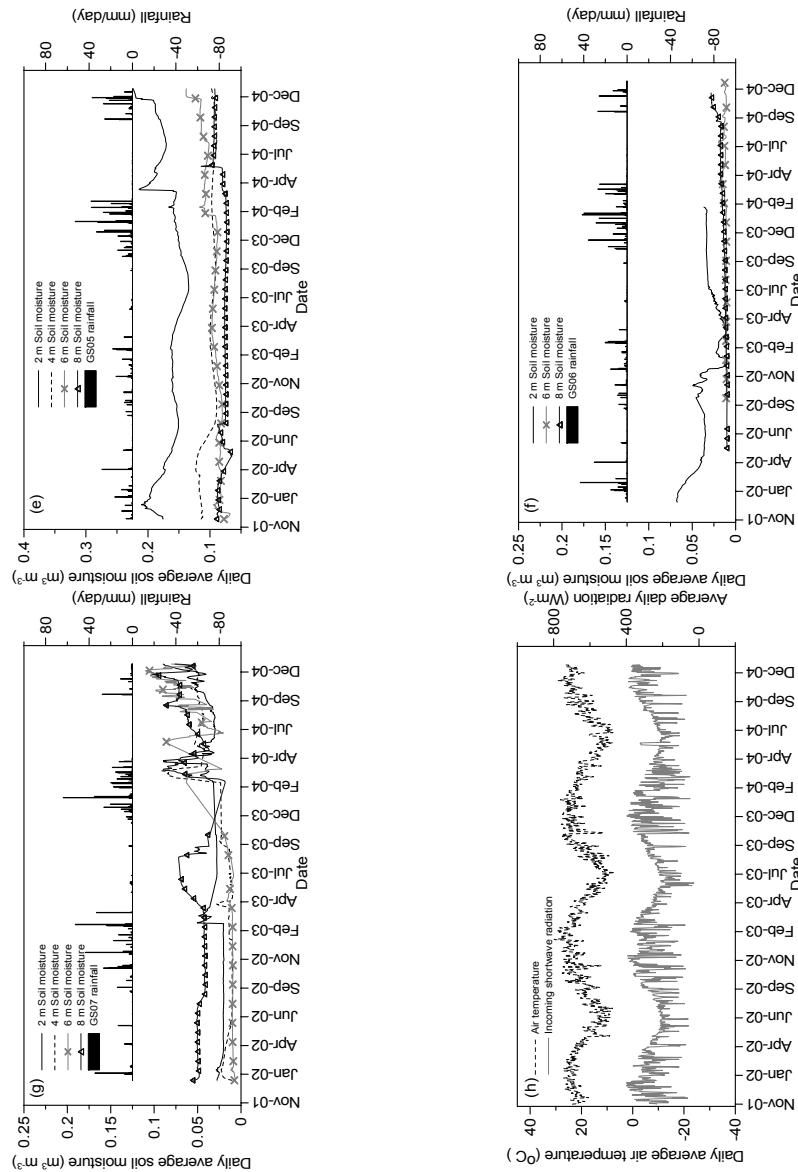
Figure 7.3. Temporal variability of soil moisture monitored *in situ* at various depths at GS01-07 sites; Daily rainfall, incoming shortwave radiation and air temperature are also shown

- Rainwater can propagate up to a depth of 8 m in response to seasonal rainfall, and infiltration occurs primarily in response to summer rainfall.

148

- The low winter rainfall often results in soil moisture increase for several months because of low evapotranspiration, caused by reduced ambient temperatures (Figure 7.3(h)) and low solar radiation (Figure 7.3(h)) in winter.

- The summer soil moisture increases are short-lived (< one month) due to increased evapotranspiration.

- The temporal variability in soil moisture decreases with depth at GS01, GS05 and GS06 profiles (Figure 7.3(a), 7.3(e) and (7.3f)), i.e. large soil moisture variability is observed at shallow depths as compared to deeper horizons. However, this feature is not apparent at GS02-04 and GS07 site profiles (Figure 7.3(b-d) and 7.3(g)).

- Situations exist, whereby soil moisture increase occurs at greater depths, prior to increases at shallow depths (e.g. GS01-03 and GS05 profiles), thus suggesting that the water by-passed the soil store of the upper horizons to reach the deeper soil store.

- Notwithstanding the above observations, in some cases, data from GS01 and GS05 profiles indicate progressive increases in soil moisture with depth after major rainfall events thus suggesting diffuse flow in these cases. Furthermore, the decrease in soil moisture was generally much slower at 2 m at GS05 than GS01 site profile, suggesting differences in hydraulic properties.

- GS04 soil moisture content at 4 m, 6 m and 8 m depth remained fairly constant for a greater part of the monitoring period suggesting that rain derived soil moisture by-passes the location of the *ECHO-20* sensors or that soil moisture is lost by evapotranspiration before reaching the sensors.

7.4.2 Temporal and vertical variations of soil matric pressure (mp) at GS10 site

At the GS10 site, one profile is based on the *Watermark 200SS* sensors, placed at intervals up to 7 m depth (see Figure 7.4(a)). Another profile is based on *GPSY1 gypsum* blocks, at the same intervals, up to 7 m depth (see Figure 7.4(b)), and this profile was extended with larger intervals at depths from 11 m up to the average groundwater level of 76 m (see Figure 7.4(c)); the 'deep' profile. The distance between the *Watermarks 200SS* and *GPSY1* profiles was 2 m.

Other seven gypsum block soil matric pressure (mp) profiles at GS01-07 sites were installed experimentally on *Datahog2* loggers by applying an external *Direct Current-Alternating Current* (DC-AC) interface. Their results were spurious most likely due to polarization problem (Strangeways, 1983) as a result of long current excitation (≈ 1s) and unchangeable power of the *Datahog2* logger, and as such were considered unreliable and were removed from the analysis. The two matric pressure profiles at GS10 that operated on *Delta-2e* logger are discussed below. Figure 7.4(a) starts from November 2003 primarily to facilitate comparison of the dynamics of soil matric pressure (as a manifestation of soil moisture variation) at the shallow profile with those of the deep profile presented by Figure 7.4(b-c). The following observations can be made from Figure 7.4;

- Infiltrating rainwater propagated down to 7 m in the shallow profile (Figure 7.4(a)) and reached a depth of 22 m in the deep profile (Figure 7.4(b-c)).
- Infiltration in the upper 22 m occurs primarily in response to summer precipitation.
- At depths of 29, 37 and 46 m (Figure 7.4(c)), there is steady decrease in soil matric pressure, indicating drying conditions.
- In general, soil moisture at 56 and 66 m is fairly stable throughout the monitoring period.
- The soil matric pressure at 76 m with values slightly lower than zero reflects most likely close contact with groundwater; the groundwater table in the neighbouring 4743 borehole was at 76 m below the ground surface. It has to be mentioned however that gypsum blocks are reported as accurate only between -0.5 and -15 bars i.e. -50 and -1500 kPa (Hayes and Tight, 1995) and therefore the three deepest sensors' results are uncertain.
- *Watermarks* and *Gypsum* blocks appear to be more sensitive to temporal variability of soil moisture than the *ECHO-20* soil moisture sensors.
- Matric pressure values from *Watermarks* and *Gypsum* blocks are in the same order of magnitude, but the temporal record at the two profiles is not identical for the upper layers.
- It seems that a matric pressure of -1.5 bar (-150 kPa) is normal for average conditions of the area between the active zone of downward and upward flow and the zone of capillary water above the water table.
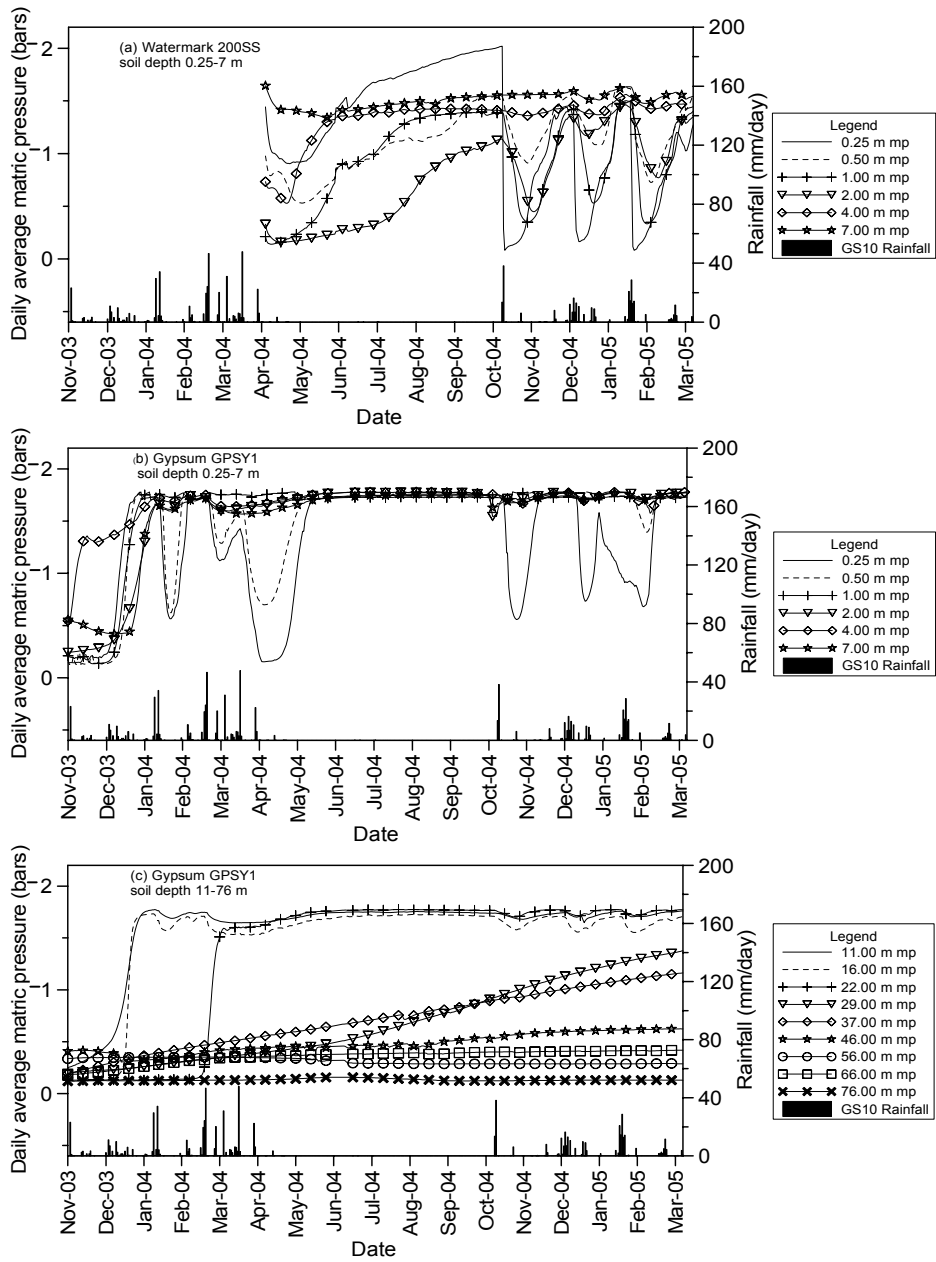
150

Figure 7.4. Temporal variability of soil matric pressure (mp) monitored *in situ* at various depths at shallow (0.25-7 m) GS10 profile and deep (0.25-76 m) GS10 profile; Daily precipitation is also shown

Figure 7.5 displays the soil matric pressure (mp) as a function of depth for the GS10 site. Figure 7.5(a) represents a typical profile during the wet season and ending up in the dry season, whereas Figure 7.5(b) represents a typical dry season profile, which ends up in the wet season. The first remarkable feature of the graphs is the low levels of soil matric pressure displayed between 0.5 m and 22 m depth, even for the wet conditions following rainfall events. The penetration of earlier surface infiltration from previous rainfall events (shown in Figure 7.4) to depths exceeding 2 m after 24 March 2004 is quite apparent (in Figure 7.5).
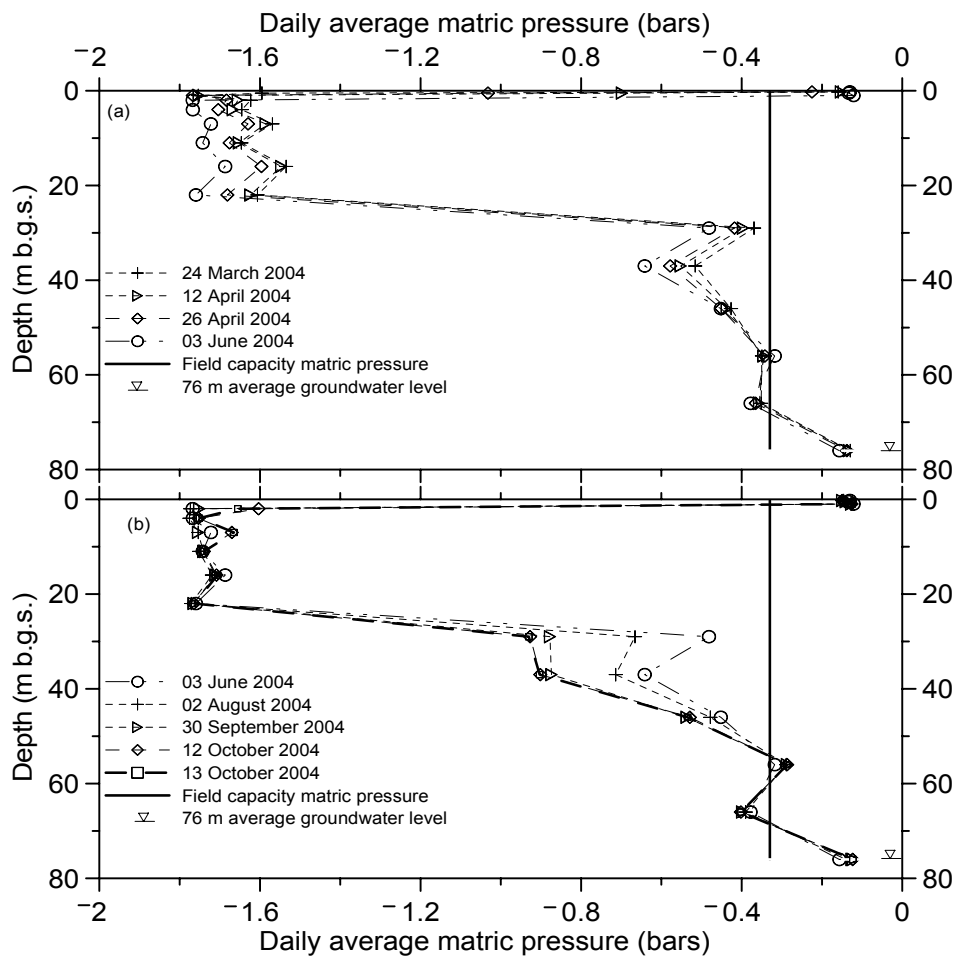
Figure 7.5. GS10 soil matric pressure profile for selected days, a) wet to dry season and b) dry to wet season

Between 29 m and 46 m in Figure 7.5(a), it shows that the profile is drying, that is soil matric pressures were generally on the decrease from 24 March 2004 to 03 June 2004, and while below about 52 m soil matric pressures appeared to be more or less stable. A similar feature is also observed in Figure 7.5(b), where soil matric pressures were generally on the decrease between 29 m and 46 m from 03 June 2004 to 13 October 2004, while below about 52 m soil matric pressures appeared to be more or less stable.

Another remarkable feature of Figure 7.5 is the sharp increase in matric pressure between $\approx$22 m and $\approx$29 m, indicating a shift from dry to moist conditions. Additionally, the important feature of Figure 7.5 is that the moisture conditions between 29 m and 52 m, are migrating towards low matric pressures, an indication that the profile is drying at this location. The presence of small drying and wetting fluctuations below 52 m is difficult to explain in terms of recent rainfall events, perhaps is an artefact of measuring equipment or influence of deep rooting systems.

7.4.3 Observed groundwater level fluctuations

Annual groundwater level fluctuations in the sandveld during the observation period range from $\approx$0.02 to $\approx$0.6 m, but can be significantly higher in the hardveld area ($\approx$ 3 m).

The increase in gas pressure as a result of high intensity rainfall events, which could lead to Lisse effects, was considered irrelevant for the case of the present study because groundwater tables are basically deep (>8 m), and well out of the limits of the Lisse effect (<1.3 m; Week, 2002). The effects of pumping and lateral flow were minimized or avoided by the careful selection of the field sites. All sites are far away from pumping infrastructure and are situated in areas of low hydraulic gradient. Barometric pressure influence was removed from groundwater level signals using data from the barometric AGTR installed primarily to measure barometric pressure. The groundwater level observations in the study area do not reveal earth or atmospheric tides. Ocean tides are obviously not to be expected.
The combined effects of evaporation from the water table, which may be caused by thermal vapour transport (Walvoord et al., 2002a) or upward liquid flow, and/or transpiration by deep rooting trees,

regional pumping and lateral outflow to the aquifer boundaries, implies that the water table is falling between recharge events.

The effect of the presence of a basalt confining layer on water level changes is examined by comparing groundwater levels of boreholes where basalt is present with those where it is absent. Based on this approach, boreholes were divided into four groups as follows; (A) boreholes in which Kalahari beds are present and basalt is absent (Figure 7.6), (B) boreholes in which Kalahari is absent and basalt is present (Figure 7.7), (C) boreholes in which both Kalahari beds and basalt are absent (Figure 7.8), (D) boreholes in which both Kalahari beds and basalt are present (Figure 7.9). For location see Table 7.4 and Figure 3.1.
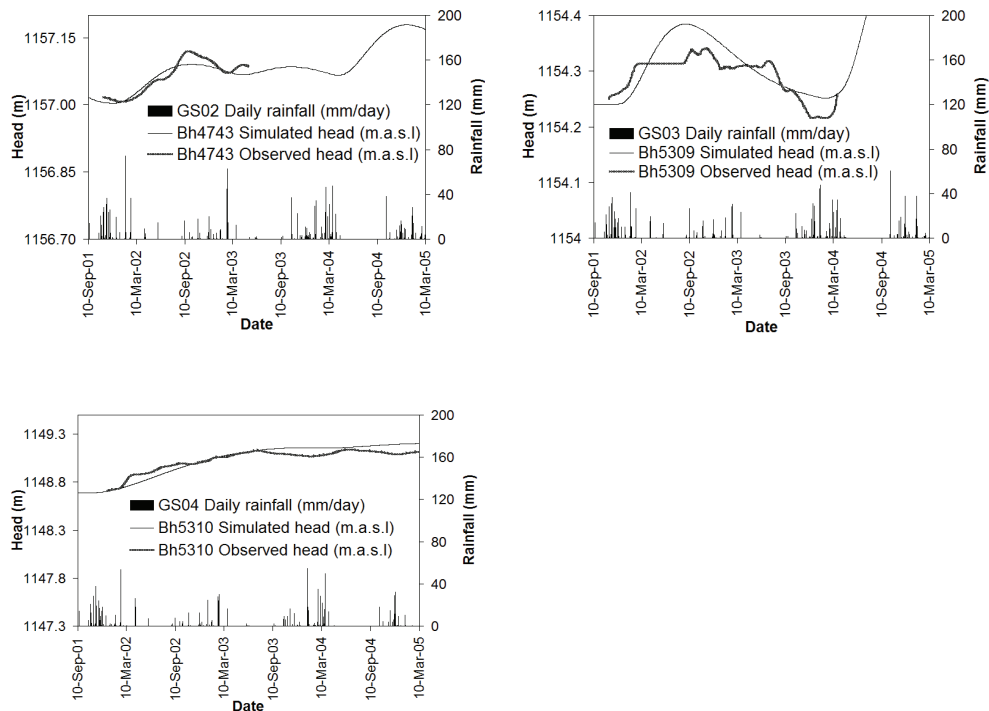
Figure 7.6. Groundwater level fluctuations in boreholes (Bh) in which Kalahari beds are present and the basalt is absent (Type A); Rainfall and EARTH model simulated heads are also shown

Figure 7.6 illustrates hydrometric data for boreholes 4743, 5309 and 5310. Groundwater levels were only monitored up to 11 May 2003 and 25 March 2004 at 4743 and 5309 respectively, because the

pressure transducer failed after that time. The following observations can be made from Figure 7.6:

- Water levels at 4743 and 5310 depict a rising trend during the monitoring period.
- All hydrographs show no immediate response to wet season rainfall; at 4743 there is a clear association between rainfall clusters and groundwater level rises with a lag of about 6 months.
- The pattern of groundwater level responses is different for each borehole, despite similar geological conditions.

- Generally groundwater level responses to seasonal rainfall are very low in all boreholes; amplitudes are in order of 20 cm.
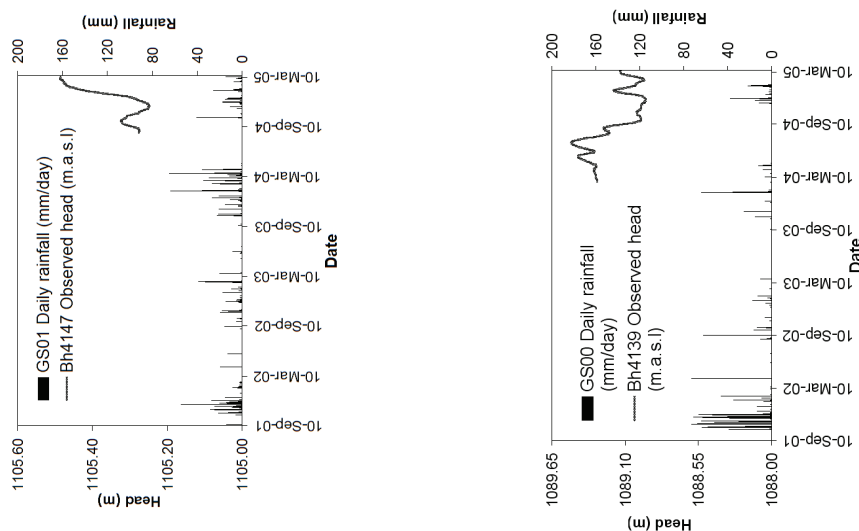
Figure 7.7. Groundwater fluctuations in boreholes (Bh) in which Kalahari cover is absent and basalt is present (Type B); Rainfall is also shown

Figure 7.7 presents the piezometric level fluctuations for 4147 and 4139. The pattern of responses is much faster and more attenuated as compared to responses for boreholes depicted by Figure 7.6. Despite the short duration of the monitoring period, the pattern of responses is evidently different between the two boreholes, for 4147 the piezometric head shows an increasing trend between 10 September 2004 and 10 March 2005, while that of 4139 is fairly

stable within the same time interval. This merely reflects the heterogeneity in hydraulic properties of the basalt. The observations in these two boreholes indicate a fast infiltration through fractures of the basalt. This process will be more important for 4139 than 4147 where the basalt thickness is in the order of 24 m (i.e. relatively thin), while that of 4147 is 70 m thick.
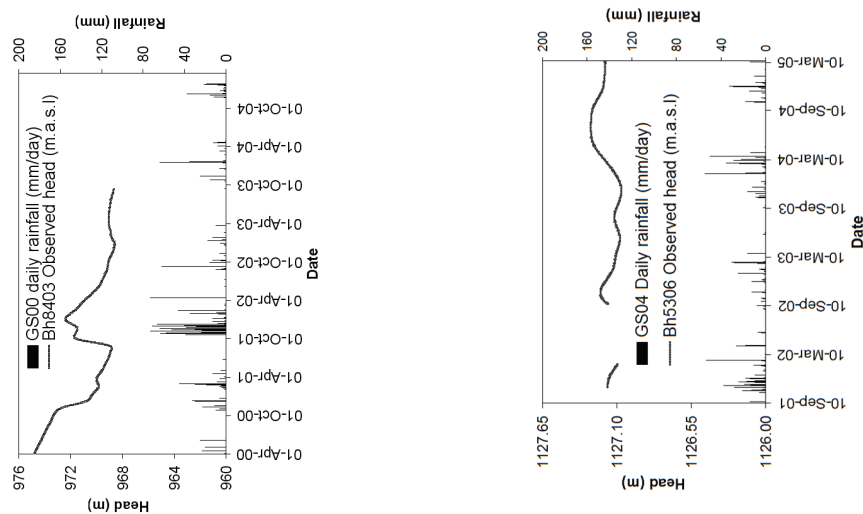

Figure 7.8. Groundwater fluctuations in boreholes (Bh) in which both Kalahari cover and basalt are absent (Type C); Rainfall is also shown

Figure 7.8 illustrates hydrometric data for boreholes 5306 and 8403 where the Ntane sandstone aquifer is covered by a thin veneer of superficial deposits. Groundwater levels were only monitored up to 13 September 2003 at 8403, because the pressure transducer failed after that time. This makes comparison of responses between the two boreholes much more difficult. Despite this shortcoming the following observations can be made from this figure:

- Water level shows a slower response in 5306 than in 8403.
- Larger water level changes are observed in 8403 than in 5306.
- The hydrographs show variable response to wet season rainfall.

The temporal evolution of piezometric level fluctuations at locations where both Kalahari beds and Stormberg basalt are present is shown in Figure 7.9. The following boreholes represent these locations:

156

8472, 4742, 8493, 5326, 5312, 5314, 5343, 5336, 5337 and 8449. Boreholes 4742, 5312, 5326 and 8472 were monitored for a short duration. In the case of 4742 and 5326 the water level declined below the bottom of the borehole, making it impossible to continue with monitoring at this location. For borehole 8472, the Department of Water Affairs did not make more data available. As for 5312 the monitoring was started late, as an additional effort to expand the existing monitoring network. Some of the observed piezometric levels are declining with spatially variable decline rates, e.g. 4742, 5326, 8449 and 8493; in other boreholes the piezometric levels appear to

be fairly stable. This perhaps is a general manifestation of regional pumping in the area because boreholes that are fairly stable are much further away from the pumping infrastructure as compared to those that show continuous decline in levels. All hydrographs show delayed response to wet season rainfall, with different delay periods.

A combination of a pronounced seasonal response and short-term records makes it difficult to detect any long-term trend in the groundwater hydrographs. Some manually collected long-term water level data were available from 1988-2001 for twelve boreholes. Though there is uncertainty about the quality of this data, it appears that the 1988-2001 groundwater levels were higher for seven boreholes than those recorded between 2001 and 2005 by the current study. In the remaining five boreholes the levels remained approximately constant. Since 2001 most boreholes (where basalt is absent, therefore representing unconfined conditions) have shown an inter-annual water level rise in the range of 2 cm/yr to 300 cm/yr, although there is considerable variation from year to year.

The large-scale seasonal fluctuation characteristics of the groundwater hydrographs, simply reflects the delay in attenuation of moisture in the overlying sediments, which appears to be not much dependent on the thickness of the unsaturated zone (Figure 7.10(a)) and geological conditions, since no obvious relationship could be found between the magnitude of water (piezometric) level response and unsaturated zone thickness on the one hand and similar geological conditions (Figures 7.6-7.9) on the other. However, the

geomorphological setting of a borehole may play a significant role in terms of the magnitude of water level response as illustrated in Figure 7.8 by boreholes 8403 and 5306. Borehole 8403 is mainly positioned at or close to the dissected edge of the escarpment and lies in the vicinity of numerous ephemeral streams. Concentration of rainwater and rapid indirect infiltration through stream beds resulted in a very pronounced seasonal response in this borehole. On the contrary, borehole 5306 is located in a relatively flat area with no streams in its vicinity or some form of depression through which it could have received focused recharge. Additionally, there is no obvious relation between inter-annual water level change and annual rainfall (Figure 7.10(b)). This suggests that the long-term water level trend is influenced by a combination of both local and regional components of recharge.
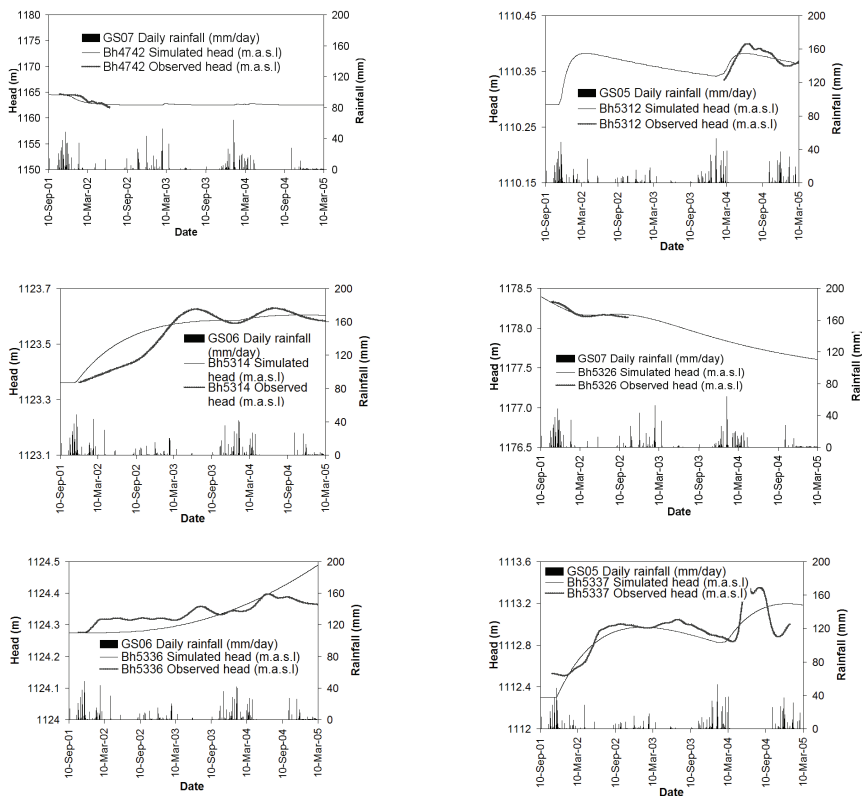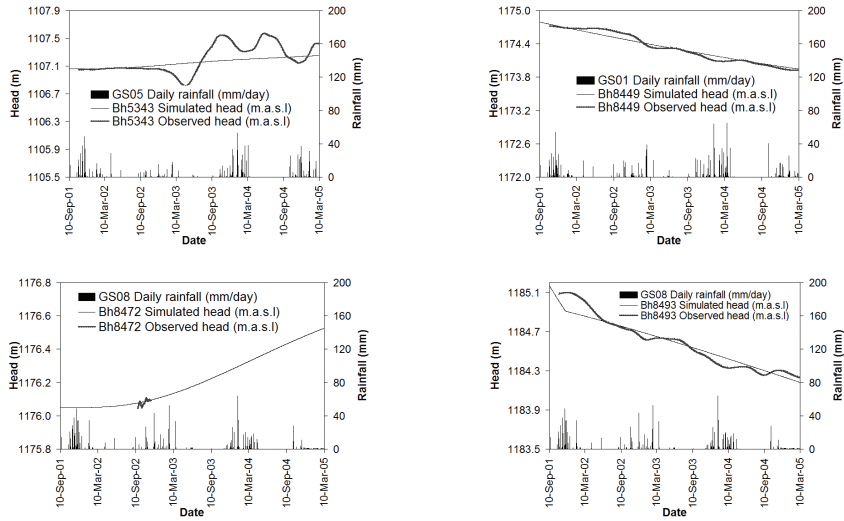
Figure 7.9. Groundwater fluctuations in boreholes (Bh) in which both Kalahari and basalt are present (Type D). Rainfall and EARTH model simulated heads are also shown
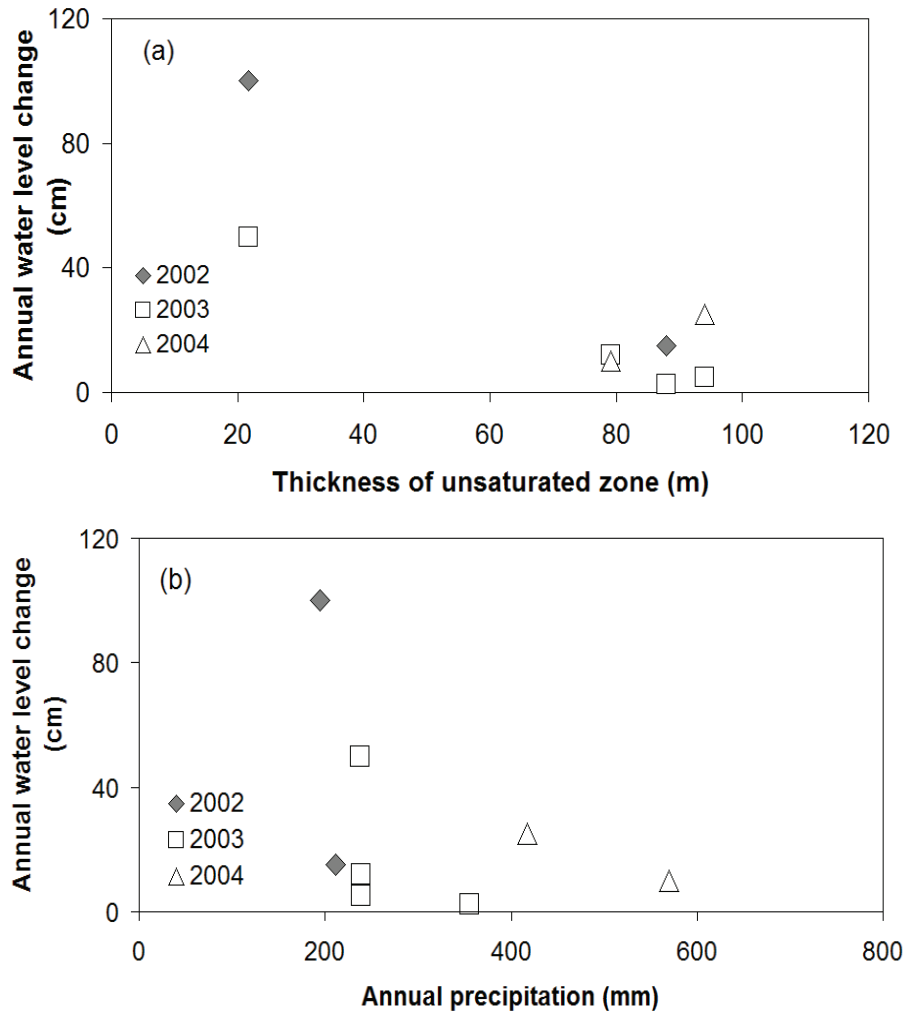
Figure 7.10. Relationship between annual groundwater water level change (data from boreholes presented in Table 7.6) for years 2002-2004 and (a) unsaturated zone thickness, (b) annual precipitation

7.5 Estimates of groundwater recharge

In this section three recharge estimation approaches are applied: (1) The linear reservoir approach (LINRES), (ii) the water table fluctuation approach (WTF) and (iii) the infiltration transport model (EARTH).

160

7.5.1 LINRES and WTF approaches

The selection of boreholes for applying the LINRES and WTF methods was based on (i) the availability of a well formed hydrograph which is suitable for the fitting of a recession curve and (ii) the existence of unconfined flow conditions that permitted the use of the specific yield storage parameter that is required as input by both methods.

In applying the LINRES approach, a drainage base of 925 m a. s. l. was assumed for all boreholes. For the westerly directed flow regimes the Makgadikgadi pans (situated some 150 km north of Serowe; Figure 1.2) were taken as drainage base, since the groundwater table slopes from the divide (near the escarpment) to near surface at the Makgadikgadi pans. For the easterly directed flow regimes the discharge base was taken as topographic elevation at the eastern limit of the Ntane sandstone aquifer where it wedges out and reaches near surface. The underlying assumption for the LINRES method is that rainfall is uniform over the whole basin, which is probably not really the case.

Table 7.6 presents the annual average groundwater recharge estimates obtained by the linear reservoir approach (LINRES) and water table fluctuation (WTF) approaches for four boreholes. The table indicates that recharge ranged from 2-150 mm/yr at the observation locations. However, no recharge was calculated at 5309 because the hydrograph was not well formed and therefore difficult for the recession curves to be fitted despite the fact that flow conditions were unconfined at this location. The high recharge estimates at 8403 are a result of focused recharge in a streambed. The recharge estimates of the WTF are in the same order of magnitude as estimates of the LINRES approach.

Table 7.6. Annual recharge (q_r) estimates of WTF and LINRES; - indicates no information

Observation location	2000/01 q_r (mm/yr)		2001/02 q_r (mm/yr)		2002/03 q_r (mm/yr)		2003/04 q_r (mm/yr)	
	WTF	LINRES	WTF	LINRES	WTF	LINRES	WTF	LINRES
8403	150	150	40	43	43	44		
5306	-	-	-	-	4	4	16	16
4743	-	-	8	8	2	2	-	-
5310	-	-	-	-	9	9	5	5

7.5.2 One-dimensional modelling with EARTH

The EARTH model is considered to be a good choice for three reasons: i) in this model absolute values of soil parameters are not as important as their relative magnitudes. This aspect of the model provided a unique opportunity to estimate some soil parameters of the model based on a combination of field data and literature as described in Table 7.5; (ii) the possibility to constrain the model between dry season plot tree transpiration (representing the lower limit of actual evapotranspiration) and *PET* (representing an upper limit of actual evapotranspiration); and (iii) model calibration using groundwater (piezometric) levels also provided an additional advantage.

Model calibration

Figures 7.6 and 7.9 show plots of observed and simulated heads for the 13 observation locations that were simulated with EARTH. In Figures 7.6 and 7.9 all data that was available between 10 September 2001 and 10 March 2005 was included in the model calibration effort. Calibrated model parameters for different observation locations of the study area are shown in Table 7.7. This table shows that in the study area the soil retention capacity ($SRC=S_{fc}-S_r$) varied between 130 mm and 219 mm. Table 7.7 also shows that the coefficient of determination (R^2) and mean square error (*MSE*) are variable, indicating different matching between simulated and observed heads. Because R^2 depends on the data scatter, it may be possible to have lower R^2 value with good prediction, e.g. Bh5343 has R^2=44%, but a

better *MSE* (0.04 m^2/day) than BH4742 with R^2=82% but with a rather high *MSE* of 0.4 m^2/day. The generally low *MSE* values (close to zero) obtained indicate that the present models have a good potential for estimating recharge distribution.

Model verification was not undertaken because the data was considered too short for such verification to make sense. Additionally, the commonly used split-sample test technique provides only a limited verification of lumped parameter models, and point measurements of state variables cannot be used because of small scale heterogeneity, which cannot be simply extended to large scale processes.

Table 7.7. Calibrated model parameter and model efficiency for different observation locations; notation is given in Table 7.5, I_c, S_m, S_r, $SUST_{max}$ and K_s were fixed at 1.5 mm, 417 mm, 150 mm, 0 mm and 6804 mm/day respectively. Storage coefficients were obtained from Table 7.4.

Observation location	Model parameters					Model efficiency	
	S_i (mm)	S_{fc} (mm)	UnR_c (day)	n_r (-)	R_c (day)	R^2 (%)	*MSE* (m^2/day)
4742	150.00	280.00	10	7	55	82	0.4
4743	184.00	300.00	125	3	50	89	0.001
5309	151.75	295.00	100	3	60	60	0.002
5310	299.00	300.00	465	2	288	92	0.01
5312	275.00	300.00	1055	1	36	77	0.0002
5314	299.00	300.00	3250	1	280	80	0.008
5326	150.00	369.00	67	4	682	96	0.004
5336	299.00	300.00	1275	3	1555	71	0.0009
5337	150.00	298.00	435	1	400	70	0.04
5343	295.00	299.00	600	3	86	44	0.04
8449	190.00	300.00	5000	2	5700	97	0.07
8472	154.00	299.10	650	3	720	50	0.0003
8493	153.00	299.05	4220	1	1515	94	0.07

Estimated recharge

Table 7.8 presents a summary of estimated actual evapotranspiration (*AET*) and simulated recharge for three hydrological years ranging from 1 September 2001 to 31 August 2004. Annual recharge estimates range from 0-37 mm/yr, and represent <20% of the annual rainfall. In some observation locations the estimated recharge

is more than the annual plot level tree transpiration while for other locations recharge estimates are smaller than the annual plot level tree transpiration.

Recharge seems to be highly spatially and temporally variable in the study area as suggested by Figure 7.11. Furthermore, when comparing recharge estimates derived by the one dimensional EARTH simulation modelling and other recharge estimation methods (WTF and LINRES) presented in Table 7.6 (with exception of 8403 that receive focused recharge), the annual estimates are in the same order of magnitude, although generally higher in the former. The average annual groundwater recharge seems to be in the order of 10-20 mm (Table 7.8).
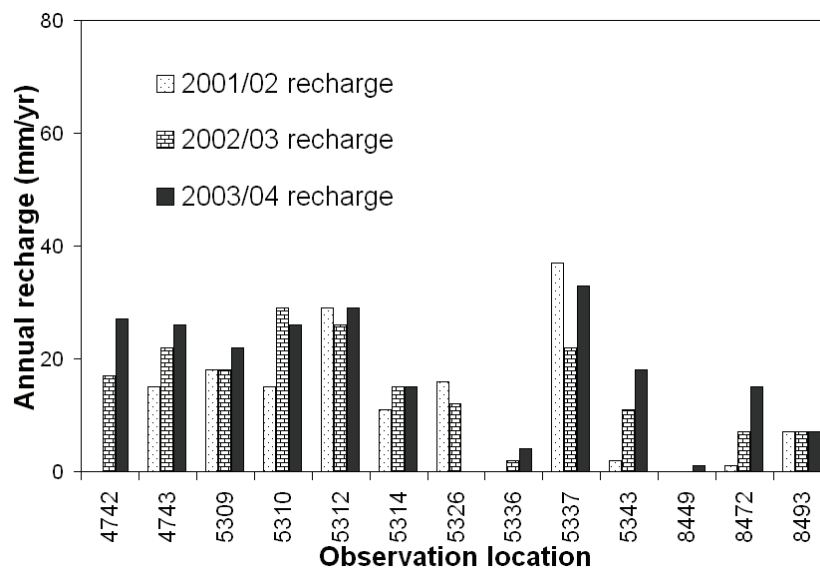
Figure 7.11. Spatial variability of recharge (EARTH) for three hydrological years

Table 7.8. Potential evapotranspiration (*PET*) from Chapter 3, plot-tree transpiration (*T_p*) from Chapter 4, rainfall (*P*), actual evapotranspiration (*AET*) from EARTH modelling and groundwater recharge (*q_r*) from EARTH modelling for three hydrological years; Obs. stands for observation location, - means not calculated

| | 2001/02 | | | | | 2002/03 | | | | | 2003/04 | | | | |
| | (mm/yr) | | | | | (mm/yr) | | | | | (mm/yr) | | | | |
Obs.	*PET*	*Tp*	*P*	*AET*	*qr*	*PET*	*Tp*	*P*	*AET*	*qr*	*PET*	*Tp*	*P*	*AET*	*qr*
4742	1211	7	497	375	0	1228	8	372	256	17	1180	7	434	260	27
4743	1201	34	477	346	15	1224	36	325	222	22	1172	39	511	283	26
5309	1209	5	494	315	18	1218	5	260	193	18	1087	5	529	286	22
5310	1209	64	477	381	15	1218	71	223	154	29	1087	62	418	253	26
5312	1198	4	465	333	29	1219	5	158	96	26	1181	5	468	273	29
5314	1201	10	514	390	11	1221	11	195	128	15	1187	11	479	301	15
5326	1211	7	497	343	16	1228	8	372	277	12	1180	7	434	289	0
5336	1201	10	514	390	0	1221	11	195	128	2	1187	11	479	301	4
5337	1198	4	465	255	37	1219	5	158	95	22	1181	5	468	270	33
5343	1198	4	465	345	2	1219	5	158	96	11	1181	5	468	271	18
8449	1192	17	428	265	0	1213	19	318	216	0	1170	18	653	330	1
8472	1236	3	497	269	1	1274	3	372	274	7	1205	3	431	284	15
8493	1236	3	497	268	7	1274	3	372	274	7	1205	3	431	284	7
Averages	-	13	-	-	12	-	15	-	-	15	-	14	-	-	17

From Table 7.8 it is noticeable that the sum of the estimated actual evapotranspiration and the groundwater recharge do not equal the rainfall amount at all observation locations; this difference mainly emphasizes the difficulty in the estimation of actual evapotranspiration and hence the calculation of the groundwater recharge as the difference between rainfall and actual evapotranspiration.

7.6   Estimation of net groundwater recharge

Under steady state conditions the net groundwater recharge is equal to the outflow (discharge). If the groundwater divide is taken at 1170 m a. s. l. at the eastern fringe of the Kalahari (near Serowe), at a distance of ≈150 km to the discharge base at Makgadikgadi pans (925 m a. s. l.), and assuming a regional average transmissivity of 500 m^2/day, a regional net groundwater recharge of 4 mm/yr is obtained by applying Equations 7.3-7.4. Since the recharge seems to be in the order of 15 mm/yr on average (Table 7.8), it can be concluded that about 11 mm/yr of this substantial recharge is

extracted by deep rooting vegetation which has been demonstrated to reach depths in excess of 70 m (Chapter 5). This agrees rather well with the calculated plot tree transpiration.

7.7   Discussion and conclusion

Soil moisture transport depicts a complicated pattern, which is characterised by a combination of diffuse and by-pass flow components. The deepest soil profile (76 m) at GS10 suggests that soil moisture (in the form of liquid flow) during the period of observation only reached up to 22 m (see Figure 7.4(b-c)). This might reflect removal of percolate through soil water extraction by deep roots. It is also possible that soil moisture response at greater depth is masked by attenuation processes in combination with a lack of sufficient resolution of the instrument's signal. Loss of water by isothermal vapour flux as demonstrated by Walvoord et al. (2002a, b), or upward liquid flow as indicated by Scanlon (2000) and Scanlon et al. (2003) is not likely because the environments studied by Scanlon (2000), Walvoord et al. (2002a, b) and Scanlon et al. (2003) were much drier than the Kalahari. Another remarkable feature of the GS10 deep profile (Figure 7.5) is the sharp increase in matric pressure between ≈22 m and ≈29 m, indicating a shift from dry to moist conditions. The explanation might be a high clay content below 29 m, and a continuous capillary connection (as proposed by Coudrain-Ribstein et al., 1998) of this zone with the water table or residual moisture from previous major rainfall events (such as the exceptionally high 2000 rainfall events, see Chapter 2) which is currently in the process of drying up. The first explanation of a high capillary rise is not likely because of the very low capillary flux (≈2×10^{-11} cm/day) in dry coarse sand, which would result in an extremely low flow velocity.

This observation also brings into focus the question of how widespread is recharge in the Kalahari. Perhaps it is confined to locations where preferential flow is important. For instance, the rises in groundwater level that were observed some 5 m away from the deep GS10 profile in the neighbouring borehole 4743, supports the

argument of preferential flow close to the hole or some distance away from it. This is consistent with the findings made by Selaolo (1998) in

a similar environment. Through tracer studies he concluded that the diffuse and by-pass flow components were equally represented in most soil profiles.

Another aspect is concentrated recharge in years with above average rainfall. Long-term rainfall data (1986-2004) of Serowe (provided by the Department of Meteorological Services) reveals that there were 11 years of below average annual rainfall (≈440 mm), and eight years of above average rainfall. Exceptionally, high rainfall events were observed in 1988, 1995 and in 2000 in the most recent years, possibly leading to increased recharge. A case example is the 2000 cyclonic depression (Cyclone Eline) that led to wide spread floods across Southern Africa and increased groundwater levels in the Kalahari (Water Surveys Botswana, 2001; Sibanda, 2006). In general, from 2001, the region experienced a succession of years with below average rainfall.

Hydrograph records from monitored boreholes show very different behaviour, with some boreholes showing little change during the monitoring period while others appear to be markedly affected by periods of high or low rainfall. This basically reflects both recharge heterogeneity and lateral variations in flow or differences in attenuation through the thick unsaturated zone, so that small water level fluctuations might be an indication for steady infiltration throughout the year.

Despite the different groundwater level fluctuation patterns caused by the differences in attenuation or rock heterogeneity, spatial rainfall distribution (Chapter 2) and because of effects of regional pumping, most groundwater (piezometric) level fluctuations show temporal close correlation with inter-annual rainfall variations. Such a close correlation was also observed in the western Kalahari by Chilume (2001) and Rahube (2003) in the same aquifer with even much thicker unsaturated zones (>80 m) of Kalahari sediments. Therefore,

the observed water level rise is taken as manifestation of the arrival of rainwater from the recent rainfall events to the aquifer.

The calculations of groundwater recharge were based on groundwater level data and specific yield in the case of WTF and LINRES approaches. Additional recharge estimates were obtained by one dimensional simulation modelling with EARTH using more data such as *PET* (Chapter 3), tree transpiration (Chapter 4) and a number of model parameters in addition to groundwater level data and storage coefficients. Although, there were soil moisture measurements they were not used in EARTH model calibration because they were uncertain, representing small scale processes. Field data consistently show that vadose zone properties measured at vertical scales of 0.01-0.1 m vary significantly at scales of 0.1-1 m (Zhang, 2002 and Rubin, 2003).

A high correlation (*r*=0.84) was observed between annual rainfall and annual actual evapotranspiration, but much weaker correlation (*r*<0.5) with other fluxes such as tree transpiration and direct groundwater recharge estimates. This is to be expected since rainfall and evapotranspiration are the main components in the water balance and hence the high correlation. The lack of strong correlation between other fluxes mainly emphasise the complexity of the dynamics of fluxes in the semi-arid Kalahari environment.

Apart from local and focused recharge in depressions and fractures, the average annual groundwater recharge according to the present study is in the order of 5-20 mm (Based on estimates from Kalahari sandveld in Table 7.6 and Table 7.8). The EARTH model recharge results obtained for this Kalahari sandveld are higher than the recharge estimates of the Ntane sandstone aquifer obtained by chloride mass balance calculations in the area around Letlhakeng-Botlhapatlou (LB), at the Kalahari fringe, 300 km to the south, under comparable environmental conditions. In that area groundwater recharge estimates range from 4-12 mm/yr (Selaolo, 1998; De Vries et al., 2000). Also in the southern area, but further to the east, under conditions comparable to the present study area, to the area east of the escarpment, recharge values in the range of 10-25 mm/yr were

168

determined (Gieske, 1992; Beekman et al., 1996). The difference between the present study and the other mentioned studies is that this study is focused on local conditions, which results in high

variability in recharge values, whereas the other studies are more of a regional character and represents averages for a longer time span. It should be emphasized that these figures are only of an indicative nature.

The calculated annual plot-tree transpiration by deep rooting trees is in the order of 10-20 mm on average. Subtraction of this component from the calculated groundwater recharge of 5-20 mm, result in a net groundwater recharge of the order of 0-10 mm, which is of the same order of magnitude as the calculated regional annual groundwater discharge of about 4 mm.

Chapter 8 Summary and conclusions

8.1 Introduction and problem statement

The Botswana Kalahari can be characterized as a flat steppe and savanna with rather dense vegetation on a mantle of thick sand cover. Rainfall is concentrated in the hot summer season and is of the order of 400 mm/yr. Infiltration rate is high and almost all rainwater infiltrates and is subsequently removed by evapotranspiration. Surface runoff only occurs very locally in dry valleys in periods of extremely high rainfall.

The question if groundwater is replenished under present day conditions has been a matter of debate for a long time. Research in the eastern fringe of the Kalahari in the 1990s resulted in an average annual recharge figure in the order of 5-10 mm under an average rainfall of 450 mm in an area with a groundwater table between 20 and 100 m (Selaolo, 1998; De Vries et al., 2000). However, there is evidence that the total regional groundwater discharge is less than the total amount of percolate that reaches the groundwater zone, and the question was raised if deep rooting trees could be able to reach the groundwater table and extract groundwater that previously had escaped evapotranspiration from the main root zone in the upper 4 m.

Therefore the present study was initiated with the aims:
(1) To investigate the rooting depth of large trees, to find the horizons from which the trees extract their water and to determine the seasonal water fluxes through their xylem. These problems were approached by the use of applied tracers, environmental tracers and sap flow measurements, at several locations and within different tree species.
(2) To determine rainfall, potential and actual evapotranspiration from micrometeorological observations at different sites, and to analyze the temporal and spatial variability of these important components of the water balance.

(3) To monitor seasonal variations and propagation of soil moisture and to estimate groundwater recharge from a combination of groundwater level fluctuations, rainfall and evapotranspiration data.

8.2   Study area

The investigations were conducted in Serowe area (Chapter 1), which is located at the fringe of the Kalahari, in the Central District of Botswana. The study area of about 2690 km^2 straddles two different, but typical Botswana environments that are separated by an escarpment: the sandveld with deep Kalahari sand, to the west, and the hardveld with hard rock at shallow depth, to the east. The climate is semi-arid, with annual potential evapotranspiration (1350-1450 mm/yr) far exceeding annual rainfall (400-500 mm/yr). Groundwater table depths are less than 40 m in the hardveld, and more than 20 m at the sandveld. The study concentrated on the sandveld area.

As a result of the lack of permanent surface water bodies, residents of Serowe village (at the eastern flank of the escarpment) are largely dependent on groundwater resources that are mainly replenished by the scant and erratic rainfall, of which only a small quantity escapes water consumption by the rather dense savanna vegetation.

8.3   Rainfall series

Annual average rainfall in the study area was 437 mm for the observation period 1925-2004, with a minimum of 119 mm and a maximum of 970 mm. Precipitation is largely restricted to the summer period from October to April. Precipitation is mainly of a convective nature and most rainwater comes down during storm events in typical quantities of the order of 20-50 mm.

Chapter 2 focused on rainfall variability within the study area. Based on data from 11 rain gauges (10 installed for the current study and one from the Department of Meteorological Services), it has been shown that within the study area, rainfall is spatially highly variable but that rainfall at un-gauged locations can be reasonably estimated by the observations from the most near gauged location.

8.4 Evapotranspiration assessment

In Chapter 3, potential evapotranspiration (*PET*) was analysed with the Penman-Monteith equation. Actual evapotranspiration (*AET*) was estimated with the Bowen ratio surface energy balance (BSEB) and the temperature profile surface energy balance (TSEB) approaches. The calculations were based on microclimatic monitoring data obtained from 11 automated monitoring sites (GS00-10).

The Penman-Monteith *PET* in the Kalahari indicated large temporal variability, ranging from 0.1 to 6.1 mm/d. The *AET* obtained with BSEB and TSEB approaches ranged from 0.1 to 3.5 mm/d. On average annual time scale, the calculated actual evapotranspiration exceeds the annual rainfall, and thus the present methods overestimate the evapotranspiration. The overestimation is likely attributed to algorithm problems of the surface energy balance. In addition, direct root extraction from the aquifer at greater depths is likely to be restricted to the deep rooters (such as *B. albitrunca, A. erioloba* and *S. longipedunculata*) and also extensive advective-diffusive upward water movement from depths in excess of 70 m is unlikely (Chapter 4). However, it is taken that the obtained *PET* data are useful as input for water transport modelling and for further analysis of spatial and temporal variability.

In order to analyze *PET* spatially and to provide input for hydrological models, an attempt was made to derive *PET* not only at monitoring locations where the complete *PET* data input was available (e.g. GS00 and GS10), but also at those monitoring sites where wind speed was not recorded. For that purpose, a 10 m high mobile tower was shifted between those locations not equipped with anemometers (GS01-07) and the obtained data was correlated with the wind speed data of permanent stations. The obtained correlations were surprisingly good, due to the homogeneous wind speed characteristic in the Kalahari. These interrelations finally made the estimation of *PET* distribution possible, which for the same reason as wind speed, turned out to be also spatially homogeneous.

More accurate AET determination methods of practical nature are required because eddy correlation and scintillometry are often too expensive to be justified in regional groundwater projects.

8.5   Tree transpiration assessment

Tree transpiration was monitored in the study area, for a period of more than two years, using TDP tree sap velocity measurements at seven sites (GS01-07), on 5-6 trees at each site. In total 41 measurements were carried out on the selected nine tree species. The individual tree sap flows were temporally variable, with higher flows in wet summer seasons than in dry winter seasons. In order to estimate tree transpirations on plot level scale, the sap flow measurements were upscaled to seven 30x30m plots, surrounding the GS01-07 monitoring sites. Tree plot transpiration was additionally calculated by extrapolation for site GS08, where no sap flow monitoring equipment was installed, using the biometric upscaling functions obtained for each tree species and the average (except for *B. africana* in which a single tree was measured) sap velocity measurements for each species.

The daily plot tree transpiration, varied from nearly zero in the dry season to 0.4 mm/d in the wet season. The annual plot tree transpiration calculated for the eight plots, pointed at low variability of inter-annual tree transpiration, but high spatial variability among the plots, ranging from 3 to 71 mm/yr per plot. Since annual rainfall is of the order of 440 mm, this means that more than 350 mm/yr is lost by transpiration of grass and shrubs as well as from direct evaporation from the upper shallow subsurface layers and from interception. The annual plot level tree transpiration did not show a direct dependency on the yearly rainfall, suggesting that trees mainly use water from much deeper layers instead of soil water from the upper shallow layers. This hypothesis was confirmed by analysis of the depth from which soil water was extracted by the trees, with the help of environmental isotopes (^{2}H and ^{18}O) (Chapter 6).

174

8.6   Rooting depth investigation

In Chapter 5, the rooting depths of 19 trees in the Kalahari sandveld and hardveld were investigated in native savanna habitat; groundwater table depths in these areas range from 8 m to more than 70 m. The rooting depths were explored by putting lithium chloride as a tracer in deep boreholes; subsequently, young (immature) leaves of nearby trees were analysed during consecutive days to detect and monitor the uptake of the tracer.

Represented in this experiment were seven variously-aged tree species (*A. erioloba, A. fleckii*, *B. albitrunca*, *D. cinerea, S. longipedunculata*, *T. sericea* and *Z. mucronata*)*.* The trees were able to absorb the tracer within a few days from varied placement depths, ranging from 8-70 m. This means that the mentioned tree species can develop roots to depths of more than 8-70 m in order to reach deep sources of moisture in water-scarce ecosystems such as the Kalahari desert.

8.7   Determination of water sources used by vegetation

The stable isotopic signature of xylem water for six trees and the associated isotopic composition in soil and groundwater at four sites were investigated in Chapter 6. The objective of the investigation was to identify the depths from which water was extracted by trees, particularly during the dry season. The results show a range of isotopic signatures, indicating that most of the Kalahari trees such as *A. erioloba*, *B. albitrunca* and *S. longipedunculata* made predominantly use of soil water that was extracted from depths of more than 3 m (that is below the main root zone of shrubs and grasses). There is, however, evidence that *A. fleckii, A. karoo* and *Z. mucronata* also made use of more shallow water, which in the case of *A. fleckii* meant extraction under suctions that exceeded the permanent wilting point of 1.47 MPa.

8.8   Soil moisture regimes, groundwater level fluctuations and groundwater recharge

Natural groundwater recharge characteristics for the study area have been evaluated in Chapter 7 using rainfall, evapotranspiration, soil moisture and groundwater level observations, acquired by various methods. The sensors used for soil moisture observations were connected to data loggers that also controlled and stored data for evapotranspiration (Chapter 3) and sap flow analysis (Chapter 4).

Soil moisture and matric pressure profiles showed the occurrence of diffuse as well as preferential flow components in rainwater infiltration. The deepest soil profile (76 m) at GS10 indicated that downward soil moisture transport during the period of observation only reached up to 22 m. This might reflect removal of percolate by soil water extraction by deep roots up to 22 m b.g.s. This observation brings into focus the question of how widespread recharge in the Kalahari is. Perhaps it is confined to a few locations where preferential flow is important, such as depressions where rainwater accumulates, and/or areas with high permeability, for instance where fractures in hard rock or duricrust at or near the surface facilitates fast infiltration. The lack of significant variation in soil moisture signals at greater depths can also be explained as residual moisture from earlier major rainfall events, otherwise it could be an artefact of measuring equipment or influence of deep rooting systems.

Groundwater level response to rainfall vary from site to site; the differences in reaction depend mainly on site-specific differences in topographic features, vegetation characteristics, soil physical properties and local aquifer hydraulic characteristics. Groundwater level fluctuations in boreholes in this study were used to assess groundwater recharge. Three recharge estimation approaches were applied: linear reservoir (LINRES), water table fluctuation (WTF) and EARTH lumped parameter model. LINRES and WTF make use of the estimated change in aquifer storage, whereas EARTH is based on a combination of modelling of rainfall, evapotranspiration, moisture transport and groundwater level fluctuations. The EARTH model in

this study was calibrated by estimated model parameters in combination with dry season tree transpiration data, acquired through sap flow measurements, and by groundwater level observations. Soil moisture measurements were not directly used in this modelling exercise because they represent small scale processes that cannot be easily extended to large scale processes.

It is evident that groundwater level fluctuation will be reduced by high attenuation of the seasonal water flux, because the flux will then approach a steady state. Accordingly, the aforementioned methods will under such conditions underestimate the groundwater flux to the water table. On the other hand, a strong reaction of the groundwater table can be the result of local conditions of focused recharge by accumulation of water at the surface and/or preferential flow. Thus regionalized recharge figures based on boreholes which produce a clear reaction on rainfall might be too high.

LINRES and WTF recharge estimates gave comparable results, but EARTH resulted in higher values. The outcome of the recharge calculation ranges between 0 and 150 mm/yr; the latter extreme value is from a location with focused infiltration in an ephemeral stream valley on the hardveld. An overall groundwater recharge average seems to be in the order of 15 mm/yr. Since the overall regional groundwater discharge out of the considered region is estimated at 4 mm/yr, this means that groundwater extraction by deep rooting trees is of the order of 10 mm/yr.

Although the applied methods suffer from a lack of adequate data as well as from conceptual uncertainties, the results are in the order of magnitude which is not much different from previous investigations with chloride mass balances and isotopic tracers, under comparable conditions in the Kalahari, 300 km to the south. In that area groundwater recharge values in the range from 4-12 mm/yr were obtained (Selaolo, 1998; De Vries et al., 2000). It should be noticed that tracer studies normally give, in contrast to the methods used in this study, recharge values that represent average conditions on a longer time scale; in the Kalahari generally tens of years.

8.9   Conclusions

The main conclusion is that this study has proved that several tree species in the Kalahari desert are able to extend their roots to great depths, of more than 70 m locally, and to extract soil water and/or groundwater from such depths. This means that water which has escaped evapotranspiration in the main root zone (the upper 4 m), and has percolated to greater depths or even has reached the groundwater table, can still be subjected to evapotranspiration. These findings are to be taken into consideration in groundwater recharge studies and evaluation of sustainable resources in (semi-)arid areas. Additionally, this shows that a better understanding of moisture dynamics and water consumption in connection with climatic data in general, is essential for a sustainable use of the Kalahari environment and its resources.

8.10   Further research

Future research in the Kalahari should, apart from continuous general recharge investigations and monitoring, focus on water consumption by the various types of vegetation and on the partitioning of transpired water between water that is extracted from different depths of the unsaturated zone and that which originates from the saturated zone. This approach will likely provide important information on groundwater transpiration in areas with a deep groundwater table. Additionally, there is a need to investigate the existence of hydraulic redistribution (hydraulic lift and hydraulic descent[4]) and vapour transport processes, since the role of these features has not yet been taken into consideration in the Botswana Kalahari. The existence and importance of these processes have been indicated by several studies e.g. Burgess et al. (1998), Schulze et al. (1998), Walvoord et al. (2002a, b), Ludwig et al. (2003), Hultine et al. (2004) and Kurz-Besson et al. (2006).

---

[4] Hydraulic descent is the vertical transfer of water from wet shallow layers to relatively dry deep layers resulting from root water transport and efflux to the soil.

Samenvatting (Summary in Dutch)

Bodemvocht regime en evapotranspiratie aan de rand van de Botswaanse Kalahari, in het bijzonder met betrekking tot diep wortelende vegetatie

Het grootste deel van de Botswaanse Kalahari kan gekarakteriseerd worden als een tamelijk vlakke savanne met een dichte gras- en struikvegetatie en wisselende concentraties aan bomen. De ondergrond bestaat vrijwel geheel uit een pakket matig fijne eolische en fluviatiele zanden van Tertiaire tot recente ouderdom, waarvan de dikte toeneemt van ca. 10 meter aan de randen tot meer dan 100 m in het centrum van het gebied. Het Kalahari zand ligt op de Karoo afzettingen, die voornamelijk bestaan uit zandsteen, basalt en schalies van Paleozoïsche tot Mesozoïsche ouderdom. De Karoo gesteenten vormen de voornaamste watervoerende laag; de Kalahari zanden bevatten nagenoeg geen verzadigd grondwater, afgezien van lokale grondwatervoorkomens rond grote pannen (depressies). Oppervlakte afstroming uit de Kalahari ontbreekt, en het grondwater in dit afgesloten grondwaterbekken draineert naar het topografisch laagste gebied, de Makgadikgadi zoutpannen.

De jaarlijkse neerslag varieert van gemiddeld 450 mm aan de oostelijke begrenzing van de Kalahari tot 350 mm in het centrum. Lagere hoeveelheden van ca. 250 mm worden gevonden in het uiterste zuidwesten, dat een woestijn-karakter heeft, terwijl naar het uiterste noordoosten de regenval toeneemt tot 650 mm /jaar. De neerslag valt gedurende de hete zomerperiode en is geconcentreerd in kort durende perioden met convectieve buien van enkele tientallen millimeters. Vrijwel alle neerslag die niet direct verdampt, infiltreert in de goed doorlatende zanden en wordt tijdelijk opgeslagen in de bovenste 4 m van het profiel, dat min of meer samenvalt met de dichte wortelzone van de grassen en lage struiken. Van daaruit wordt het meeste water vervolgens door evapotranspiratie via de vegetatie weer aan de atmosfeer afgegeven, terwijl een klein deel infiltreert naar de diepere ondergrond.

179

Tot aan het einde van de 20^e eeuw is er discussie geweest over de vraag of het grondwater onder de Kalahari, dat zich tussen de 20 en 100 m diepte bevindt, al dan niet onder de huidige klimatologische omstandigheden wordt aangevuld, en zo ja, in welke mate (De Vries and Von Hoyer, 1988). In de jaren negentig van de vorige eeuw is daarom door de Botswaanse Geologische Dienst en de Amsterdamse Vrije Universiteit een uitgebreid onderzoek gedaan in het oostelijk deel van de Kalahari naar de grootte van de aanvulling van het grondwater. De conclusie hiervan was dat de grondwatervoeding in orde van grootte varieert van ca. 10 mm/jaar aan de rand van de Kalahari tot 1 mm/jaar in het centrum (De Vries et al., 2000). De vraag rees echter, wat gebeurt er verder met dit water dat zich op grote diepte (> 20 m) bevindt, aangezien de gemiddelde grondwater afvoer uit de Kalahari minder dan 1 mm/jaar lijkt te bedragen. Als hypothese is toen geopperd dat mogelijk een deel van het infiltrerende regenwater, dat vanuit de wortelzone naar beneden percoleert, uiteindelijk op grotere diepten door diep wortelende bomen (zoals acacia soorten) als bodemvocht en/of grondwater zou worden onttrokken.

In dit proefschrift wordt het watergebruik (transpiratie) van deze bomen, en hun rol in de bodemvocht en grondwaterbewegingen, nader onderzocht in een gebied van 2690 km^2 in het oostelijk deel van de Kalahari, ten westen van de plaats Serowe. De grondwaterdiepte neemt in dit gebied toe van 8 m beneden maaiveld aan de rand, tot meer dan 70 m naar het westen. De gemiddelde jaarlijkse neerslag over de periode 1925-2004 bedroeg 437 mm. De gemiddelde potentiële verdamping werd bij eerder klimatologisch onderzoek bepaald op 1350-1450 mm/jaar.

De worteldiepte van 19 verschillende bomen werd onderzocht door via 19 boorgaten, die in de nabijheid van deze bomen waren geboord, lithiumchloride als tracer (merkstof) in de ondergrond te brengen. Dit gebeurde op diepten tussen 8 m en 70 m, afhankelijk van de locale diepte van de grondwaterspiegel. Binnen enkele dagen bleek de tracer terug te vinden in de takken en bladeren van de onderzochte bomen. Hiermee was ondubbelzinnig aangetoond dat deze bomen inderdaad tot de betreffende diepten kunnen wortelen (dat wil zeggen

soms tot meer dan 70 m) en van daaruit water kunnen onttrekken (Hoofdstuk 5).

Met sapstroommetingen, die gedurende 2 jaar zijn uitgevoerd, werd het watergebruik in 41 bomen van negen verschillende species bepaald (Hoofdstuk 4). De metingen vonden plaats op zeven verschillende experimentele (natuurlijke) proefvelden, waarna de uitkomsten werden geëxtrapoleerd over een gebied van 30 x 30 m rond deze velden. Dit leverde een jaarlijkse bijdrage door de gezamenlijke bomen aan de verdamping, die varieerde van 3 mm tot 71 mm tussen de proefgebieden onderling. Het gemiddelde over de zeven gebieden bedroeg 18 mm/jaar. Aangezien de totale verdamping niet veel minder kan zijn dan de totale regenval, betekent dit dus dat de bijdrage van de bomen aan het totale watergebruik van de vegetatie in het onderzochte gebied in orde van grootte varieert van 1-20%.

Om een indruk te krijgen van de diepten vanwaar uit het water aan de ondergrond door de bomen wordt onttrokken, werd voor zes bomen, op vier velden, de relatieve concentraties aan de natuurlijke isotopen ^{18}O en ^{2}H in het xyleem-water bepaald. Daarnaast werd in de ondergrond, nabij deze bomen, de concentraties van genoemde isotopen in het bodemvocht en het grondwater onderzocht. Hieruit bleek dat het grootste deel van het door de bomen onttrokken water afkomstig is van diepten van meer dan 4 m, dus van dieper dan de wortelzone van de grassen en struiken (Hoofdstuk 6).

Neerslag, potentiële en werkelijke verdamping werden bepaald voor de jaren 2002, 2003 en 2004 op 11 velden met behulp van zelf registrerende instrumenten in meetmasten en ter beschikking staande faciliteiten voor automatische opslag en bewerking van informatie. Het doel van dit onderzoek was de variabiliteit van neerslag en verdamping in ruimte en tijd te analyseren.

Analyse van de neerslaggegevens laat zien dat, voor onderlinge afstanden tot 10 km, de correlatie coëfficiënt tussen de dagelijkse neerslaghoeveelheden hoger is dan 0.8. Voor afstanden van meer dan

20 km neemt deze correlatie coëfficiënt af tot 0.6 (en soms minder), (Hoofdstuk 2).

De potentiële verdamping (*PET*) is bepaald via de Penman-Monteith methode, terwijl de werkelijke (of actuele) verdamping (*AET*) is gemeten via de 'Bowen ratio surface energy balance' methode en de 'Temperature profile surface energy balance' methode. De resultaten lieten een variatie in *PET* van 0.1 – 6.1 mm/dag zien, terwijl *AET* een variatie te zien gaf van 0.1 – 3.5 mm/dag. De variaties betreffen vooral een fluctuatie in de tijd; regionaal bleek het gebied tamelijk homogeen. De berekende jaarsom van de werkelijke verdamping (*AET*) volgens deze methoden overschreed de totale neerslag. De conclusie is dan ook dat de metingen een overschatting van de totale verdamping hebben opgeleverd (Hoofdstuk 3).

Voorts is met behulp van de stijging van de grondwaterstand na regenperioden, een schatting gemaakt van de grondwateraanvulling. Daarnaast is de infiltratie van het regenwater in de ondergrond beneden de wortelzone gemodelleerd via het 1-dimensionale infiltratiemodel EARTH. Dit model is gebaseerd op de neerslag, verdamping en grondwaterstandsfluctuaties, waarbij de resultaten van de sapstroommetingen werden gebruikt voor calibratie (Hoofdstuk 7). Deze berekeningen, die slechts betrekking hebben op een periode van 3 jaar, en op slechts enkele locaties zijn uitgevoerd, leverden een orde van grootte van 15 mm/jaar voor de grondwateraanvulling. Wordt hiervan de grondwateronttrekking door de diep wortelende bomen afgetrokken, dan verkrijgt men de netto grondwatervoeding. Er van uitgaande dat gemiddeld over langere tijd een evenwicht heerst tussen netto grondwater*aanvoe*r en grondwater*afvoer*, dan is de netto grondwateraanvulling gelijk aan de gemiddelde regionale grondwaterafstroming. Deze regionale grondwaterafstroming werd in het onderzochte gebied, op basis van de gemiddelde horizontale doorlaatcapaciteit van de watervoerende laag en de hydraulische gradiënt, geschat op een orde van grootte van enkele millimeters per jaar.

Conclusie: De bomen in de Kalahari kunnen met hun wortels het grondwater volgen tot diepten van meer dan 70 m. De bijdrage van

182

deze bomen aan de totale evapotranspiratie van de savanne vegetatie bedraagt in orde van grootte 15 tot 20 mm per jaar. Deze totale evapotranspiratie kan bij afwezigheid van oppervlakteafvoer, slechts weinig lager zijn dan de totale regenval. Het feit dat de diepe wateronttrekking door de bomen in dezelfde orde van grootte ligt als de berekende diepe percolatie van het neerslagwater, verklaart de geringe netto voeding en afstroming van het grondwater. Verder wijst de betrekkelijk geringe transpiratie (watergebruik) door de bomen, en het feit dat dit water voornamelijk van grotere diepten afkomstig is, op een dominante positie van de lagere vegetatie in de competitie voor het gebruik van het beschikbare water.

References

Abtew, W., 1996: Evapotranspiration measurements and modelling for three wetland systems in south Florida. Water Resources Bulletin 32 (3), 465-473.

Allen, R.G., 1996: Assessing integrity of weather data for reference evapotranspiration estimation. Journal of Irrigation and Drainage Engineering 122, 97-106.

Allen R.G. Pereia L.S. Raes D. and Smith, M., 1998: Crop evapotranspiration-guidelines for computing crop water requirements. FAO Irrigation and Drainage Paper 56, Rome; 52-55.

Angus, D.E. and Watts, P.J., 1984: Evapotranspiration-How good is the Bowen ratio method? Agricultural Water Management 8, 133-150.

Arnold, J.G., Srinivasan, R., Muttiah, R.S. and Williams J.R., 1998: Large area hydrologic modeling and assessment, Part I. Model development. Journal of American Water Resources Association 34, 73-89.

Arntzen, J., Fidzani, H. and Tacheba, G., 1996: Communal rangelands in Botswana: less subsistence, more commerce and fewer beneficiaries. GCTE subsistence rangelands workshop, Gaborone, p. 17.

Barnes, C.J. and Allison, G.B., 1988: Tracing of water movements in the unsaturated zone using stable isotopes of hydrogen and oxygen. Journal of Hydrology 100, 143-176.

Barradas V.L., Nicolás, E. Torrecillas, A. and Alarcón J.J., 2005: Transpiration and canopy conductance in young apricot (*Prunus armenica L.*) trees subjected to different PAR levels and water stress. Agricultural Water Management 77, 323-333.

Bastiaanssen, W.G.M., Menenti, M., Feddes, R.A. and Holtslag, A.A.M., 1998a: A remote sensing surface energy balance algorithm for land (SEBAL). 1. Formulation. Journal of Hydrology 212-213, 198-212.

Bastiaanssen, W.G.M., Pelgrum, H., Wang, J., Ma, Y., Moreno, J.F., Roerink, G.J. and van der Wal, T., 1998b: A remote sensing surface energy balance algorithm for land (SEBAL). Part 2. Validation. Journal of Hydrology 212-213, 213-229.

Beekman, H.E., Gieske, A. and Selaolo, E.T., 1996: GRES: Groundwater recharge studies in Botswana 1987-1996. Botswana Journal of Earth Science 3, 1-17.

Bhalotra, Y.P.R., 1987: Climate of Botswana, Part 2: Elements of Climate. Department of Meteorological Services, Ministry of Works, Transport and Communications: Botswana. p. 104.

Black, T.A., Gardner, W.R., and Thurtell G.W., 1969: The prediction of evaporation, drainage, and soil water storage of a bare soil. Proceedings of the soil science society of America 33, 655-660.

Blaney, H.F., and Criddle, W.D., 1950: Determining water requirements in irrigated areas from climatological and irrigation data. Technical paper no. 96, US Department of Agriculture, Soil Conservation Service, Washington, DC., USA, p. 44.

Blümel, K., 1999: A simple formula for estimation of the roughness length for heat transfer over partly vegetated surfaces, Journal of Applied Meteorology 38, 814-829.

Botswana National Water Master Plan Review (BNWMPR), 2006: Sociology and demography: Final report to the Department of Water Affairs, Ministry of Minerals, Energy and Water Resources, vol. 2, 1-85.

Bovard, B.D., Curtis, P.S., Vogel, C.S., Su, H.B., Schmid, H.P., 2005: Environmental controls on sap flow in a northern hardwood forest. Tree Physiology 25, 31-38.

Bowen, I.S., 1926: The ratio of heat losses by conduction and by evaporation from any water surface. Physical Review 2nd series 26(6), 779-787.

Bradford, G.R., 1966: Lithium. In: Diagnostic Criteria for Plants and Soils. Ed. H.T. Chapman. University of California, Riverside, p. 793.

Bredenkamp, D.B., 1988a: Quantitative estimation of groundwater recharge in dolomite. In: Proceedings NATO advanced research workshop on Estimation of Natural Recharge of Groundwater (ed. By I. Simmers), Reidel, Dordrecht, The Netherlands, p. 449-460.

Bredenkamp, D.B., 1988b: Quantitative estimation of groundwater recharge in the Pretoria-Rietnedale area. In: Proceedings NATO advanced research workshop on Estimation of Natural Recharge of Groundwater (ed. By I. Simmers), Reidel, Dordrecht, The Netherlands, p. 461-476.

Bredenkamp, D.B., Botha, L.J., Van Tonder, G.J. and Van Rensburg, H.J., 1995: Manual on quantitative estimation of groundwater recharge and aquifer storativity. Water Research Commisson, Republic of South Africa. p. 363.

Brunel, J.P., Walker, G.R., Dighton, C.D. and Kenneth-Smith, A.K., 1991: Using stable isotopes of water to trace plant water uptake. In: Stable isotopes in plant nutrition, soil fertility and environmental studies, proceedings of an international symposium, October 1990. IAEA-FAO, Vienna, 543-561.

Brunel, J.P., Walker, G.R., and Kenneth-Smith, A.K., 1994: Field validation of isotopic procedures for determining sources of water used by plants in a semi-arid environment. Journal of Hydrology 167, 351-368.

Brunel, J.P., Walker G.R., Dighton, J.C. and Monteny, B., 1997: Use of stable isotopes of water to determine the origin of water used by vegetation

186

and to partition evapotranspiration. A case study from HAPEX-Sahel. Journal of Hydrology 188-189, 466-481.

Brutsaert, W., 1982: Evaporation into the atmosphere. D. Reidel Company, Dordrecht, The Netherlands, p. 299.

Bureau de Recherches Geologiques et Minieres (BRGM), 1991: Evaluation of groundwater resources: Letlhakeng-Botlhapatlou groundwater project. Final report to Geological Survey Department, Ministry of Mineral Resources and Water Affairs. p. 215.

Bureau de Recherches Geologiques et Minieres (BRGM), 1993: Recharge study, Evaluation of groundwater resources: Mmamabula groundwater resources investigation. Phase II-Khurutshe area. Final report to Geological Survey Department, Ministry of Mineral Resources and Water Affairs. p. 80.

Burgess, S.S.O., Adams, M.A., Turner, N.C. and Ong, C.K., 1998: The redistribution of soil water by tree root system. Oecologia 115, 306-311.

Calder, I.R., Swaminath, M.H., Kariyappa, G.S., Srinivasalu, N.V., Srinivasa Murty, K.V. and Mumtaz, J., 1992: Deuterium tracing for the estimation of transpiration from trees. Part 3. Measurement of transpiration from *eucalyptus* plantation, India. Journal of Hydrology 130, 37-48.

Canadell, J., Jackson R.B., Ehleringer, J.R., Mooney, H.A., Sala, O.E. and E.-D. Schulze, 1996: Maximum rooting depth of vegetation types at the global scale, Oecologia 108, 583-595.

Carney, J.N., Aldiss, D.T. and Lock, N.P., 1994: The Geology of Botswana, Bulletin 13. Department of Geological Survey. Ministry of Minerals, Energy and Water Affairs, Lobatse, Botswana, p. 113.

Cermák, J., Deml, M. and Penka, J.M., 1973: A new method of sap flow rate determination in trees. Biol. Plant 15, 171-178.

Cermák, J., Cienciala, E., Kucera, J., Lindroth, A., Bednárová, E., 1995: Individual variation of sap flow rate in large pine and spruce trees and stand transpiration: a pilot study at the central NOPEX site. Journal of Hydrology 168, 17-27.

Chilume, J.C., 2001: Hydrogeological assessment of the south western Karoo basin, a case study from Lokalane, Botswana. ITC MSc thesis, Enschede, The Netherlands. p. 91.

Choudhury, B.J. 1997: Global pattern of potential evapotranspiration calculated from the Penman-Monteith equation, using satellite and assimilated data. Remote Sensing of the Environment 61, 64-81.

Clearwater, M.J., Meinzer, F.C., Andrade, J.L., Goldstein, G. and Holbrook, N.M., 1999: Potential errors in measurement of non-uniform sap flow using heat dissipation probes. Tree Physiology 19, 681-687.

Coates-Palgrave, K., 2002: Trees of Southern Africa. C. Struik Publishers, Capetown. South Africa.

Coleman M.C., Shepherd, T.J., Durham, J.J., Rouse J.D. and Moore, G.R., 1982: Reduction of water with zinc for hydrogen isotope analysis. Analytical Chemistry 54, 993-995.

Conway, J. and Van Bavel, C.H.M., 1967: Evaporation from wet soil surface calculated from radiometrically determined surface temperatures. Journal of Applied Meteorology 6, 650-655.

Coudrain-Ribstein, A., Pratx, B., Talbi, A. and Jusserand, C., 1998: Is evaporation from phreatic aquifers in arid zones independent of the soil characteristics?, Earth and Planetary Sciences 326, 159-165.

Craig, H., 1961: Isotopic variations in meteoric waters. Science 113, 1702-1703.

David, T.S., Ferreira, M.I., Cohen, S., Pereira, J.S. and David J.S., 2004: Constraints on transpiration from an evergreen oak tree in southern Portugal. Agricultural and Forest Meteorology 122, 193-205.

Dawson, T.E. and Ehleringer, J.R., 1991: Streamside trees that do not use stream water. Nature 350, 335-337.

Dawson, T.E., 1993: Hydraulic lift and plant water use: implications for water balance, performance and plant-plant interactions. Oecologia 95, 565-574.

Dawson, T.E., 1996: Determining water use by trees and forests from isotopic, energy balance and transpiration analyses: the roles of tree size and hydraulic lift. Tree Physiology 16, 263-272.

De Bruin, H.A.R. and Holtslag, A.A.M., 1982: A simple parameterization of the surface fluxes of sensible and latent heat during daytime compared with Penman-Monteith Concept. Journal of Applied Meteorology 21, 1610-1621.

De Bruin, H.A.R., Van den Hurk, B.J.J.M. and Kohsiek, W., 1995: The scintillation method tested on a dry vineyard area. Boundary Layer Meteorology 76, 25-40.

Dekker, G.B., Jongewaard, T. and Beekman, H.E., 1997: Groundwater recharge and resources assessment evaluation in the Botswana Kalahari-Groundwater resource study of the Lehututu area. GRES II Project. Technical report, Department of Geological Survey; University of Botswana and Vrije Universiteit Amsterdam.

De Rooy, W.C. and Holtslag, A.A.M., 1999: Estimation of surface radiation and energy flux densities from single level weather data. Journal of Applied Meteorology 38, 526-540.

De Vries, J.J., 1974: Groundwater flow systems and stream nets in the Netherlands: a groundwater - hydrological approach to the functional relationship between the drainage system and the geological and

climatical conditions in a Quaternary accumulation area, PhD thesis, Vrije Universiteit, Amsterdam, The Netherlands, p. 226.

De Vries J.J., 1984: Holocene depletion and active recharge of the Kalahari groundwaters- A review and an indicative model. Journal of Hydrology 70, 221-232.

De Vries, J.J. and Von Hoyer, M., 1988: Groundwater recharge studies in the semi-arid Botswana- a review. In: "I. Simmers (editor), Estimation of natural groundwater recharge" NATO ASI series C222, Reidel, Dordrecht, p. 339-348.

De Vries, J.J., Selaolo, E. T. and Beekman, H. E., 2000: Groundwater recharge in the Kalahari, with reference to paleo-hydrologic conditions, Journal of Hydrology 238, 110-123.

Diawara, A., Loustau, D. and Berbigier, P., 1991: Comparison of two methods for estimating the evaporation of a *Pinus pinaster* stand; sap flow and energy balance with sensible heat flux measurements by an eddy covariance method. Agricultural and Forest Meteorology 54, 49-66.

Dingman, S.L., 1994: Physical Hydrology. Macmillan College Publishing Co., New York, USA, p. 575.

Disse, M., 1999: Validation of a simple model to determine regional evapotranspiration and groundwater recharge rates. Phys. Chem. Earth (B) 24(4), 325-330.

Do, F. and Rocheteau, A., 2002a: Influence of natural temperature gradients on measurements of xylem sap flow with thermal dissipation probes. 1. Field observations and possible remedies. Tree Physiology 22, 641-648.

Do, F. and Rocheteau, A., 2002b: Influence of natural temperature gradients on measurements of xylem sap flow with thermal dissipation probes. 2. Advantages and calibration of a non-continuous heating system. Tree Physiology 22, 649-654.

Ecosurv Botswana, 1998: Vegetation mapping and ground truthing for radar imagery. Ecosurv , 30 September 1998, Gaborone, Botswana. p. 23.

Ehleringer, J.R., and Dawson, T.E., 1992: Water uptake by plants: perspectives from stable isotopes. Plant Cell and Environment 15, 1073-1082.

Ernst, W., 1975: Variation in the mineral contents of leaves of trees in miombo woodland in South Central Africa. Journal of Ecology 63. 801 -808.

Farr, J.L., Cheney, C.S., Baron, J.H. and Peart, R.,J., 1981: GS 10 project evaluation of underground water resources, final report, Department of Geological Survey, Lobatse, Botswana, pp 292.

Fazal, M.A., Imaizumi, M., Ishida, S., Kawachi, T. and Tsuchihara T., 2005: Estimating groundwater recharge using the SMAR model calibrated by genetic algorithm. Journal of Hydrology 303, 56-78.

Feddes, R.A., Hoff, H., Bruen, M., Dawson, T., de Rosnay, P., Dirmeyer, P., Jackson, R.B., Kabat, P., Kleidon, A., Lilly, A. and Pitman, A.J., 2001: Modeling root water uptake in hydrological and climate Models. Bulletin of the American Meteorological Society 82 (12), 2797-2809.

Finch, J.W., 1998: Estimating direct groundwater recharge using simple water balance model sensitivity to land surface parameters. Journal of Hydrology 211 (3), 112-125.

Ford, C.R., McGuire, M. A., Mitchel, Teskey, R.O., 2004: Assessing variation in the radial profile of sap flux density in *Pinus* species and its effects on daily water use. Tree Physiology 24, 241-249.

Foster, S.S.D., Bath, A.H., Farr, J.L. and Lewis, W.J., 1982: The likelihood of active groundwater recharge in the Botswana Kalahari. Journal of Hydrology 55, 113-136.

Freeze, R.A. and Cherry, J.A., 1979: Groundwater. Prentice-Hall, U.S.A. p. 604.

French, A.N., Schmugge, T.J. and Kustas, W.P. 2000: Estimating surface fluxes over the SGP site with remotely sensed data. Physics Chemistry Earth B 25(2), 167-172.

Gaabake, G.G., 1997: GRES with respect to general water resources needs in Botswana, paper presented at the Groundwater Recharge Evaluation Studies (GRES) Symposium, Gaborone, Botswana, November 3-4, 1997.

Gash, J.H.C. and Stewart, J.B. 1975: The average surface resistance of a pine forest derived from Bowen ratio measurements. Boundary-Layer Meteorology 8, 453-464.

Gehrels, J.C., 1999: Groundwater level fluctuations, separation of natural from anthropogenic influences and determination of groundwater recharge in the Veluwe area, the Netherlands, PhD thesis, Vrije Universiteit Amsterdam, The Netherlands, p. 269.

Giambelluca, T.W., Zieger, A.D., Nullet, M.A., Truong, D.M. and Tran, L.T., 2003: Transpiration in a small tropical forest patch. Agricultural and Forest Meteorology 117, 1-22.

Gieske, A., 1992: Dynamics of groundwater recharge; a case study in the semi arid eastern Botswana. PhD thesis, Vrije Universiteit Amsterdam, p. 290.

Gieske, A.S.M., 2003: Operational solutions of actual evapotranspiration. In: I. Simmers, 2003, Understanding water in a dry environment, Hydrological process in arid and semi arid zones, International

Association of Hydrogeologists, ISBN 90 5809 618 1, Balkema, Lisse, The Netherlands. p. 65-114.

Granier, A., 1987: Evaluation of transpiration in a Douglas-fir stand by means of sap flow measurements. Tree Physiology 3, 309-320.

Granier, A., Bobay, V., Gash, J.H.C., Gelpe, J., Saugier, B. and Shuttleworth, W.J., 1990: Vapour flux density and transpiration rate comparisons in a stand of maritime pine (*Pinus pinaster* Ait) in Les Landes forest. Agricultural and Forest Meteorology 51, 309-319.

Granier, A. and Loustau D., 1994: Measuring and modelling the transpiration of a maritime pine canopy from sap flow data. Agricultural and Forest Meteorology 71, 61-81.

Granier, A., Biron, P., Breda, N., Pontailler, J.-Y and Saugier, B., 1996a: Transpiration of trees and forest stands: short and long term monitoring using sap flow methods, Global Change Biology 2, 265-274.

Granier, A., Huc, R. and Barigah, S.T., 1996b: Transpiration of natural rain forest and its dependence on climatic factors. Agricultural and Forest Meteorology 78, 19-29.

Granier, A., Biron, P. and Lemoine D., 2000: Water balance, transpiration and canopy conductance in two beech stands. Agricultural and Forest Meteorology 100, 291-308.

Haase P., Pugnaire F.I., Fernández E.M., Puigdefábregas J., Clark S.C. and Incoll L.D., 1996: An investigation of rooting depth of the semi-arid shrub *Retama sphaerocarpa* (L.) Bioss. By labelling groundwater with a chemical tracer. Journal of Hydrology 177, 23-31.

Hamon, W.R., 1961: Estimating potential evaporation, In: Division, Journal of the Hydraulics (ed.), Proceedings of the American Society of Civil engineers, 107-120.

Hargreaves, G.H. and Samani, Z.A., 1985: Reference crop evapotranspiration from temperature. Applied Engineering in Agriculture 1(2), 96-99.

Harris P.P., Huntingford, C., Cox, P.M., Gash, J.H.C. and Malhi, Y., 2004: Effect of soil moisture on canopy conductance of Amazonian rainforest. Agricultural and Forest Meteorology 122, 215-227.

Hayes J.P. and Tight D.C., 1995: Applying electrical resistance blocks for unsaturated zone monitoring at arid sites, pp. 387-399. In: Handbook of vadose zone characterization and monitoring, edited by Wilson, L.G., Everett, L.G. and Cullen S.J., 1995, CRC press, p. 752.

Hatton T.J., and Vertessy, R.A., 1990: Transpiration of plantation *Pinus Radiata* estimated by the heat pulse method and the Bowen ratio, Hydrological Processes 4, 289-298.

Hatton, T.J., Moore, S.J. and Reece, P.H., 1995: Estimating stand transpiration in a *Eucalyptus populnea* woodland with the heat pulse

method: measurement errors and sampling strategies. Tree Physiology 15, 219-227.

Hatton, T.J. and Wu, H., 1995: Scaling theory to extrapolate individual tree water use to stand water use. Hydrological Processes 9, 527-540.

Healy, W.R. and Cook P.G., 2002: Using groundwater levels to estimate recharge. Hydrogeology Journal 10, 91-109.

Hernandez, A.R., 2002: Mapping of woody vegetation in arid zones-a multi-sensor analysis, a case study in the Serowe area, Botswana. MSc. thesis. Library of the International Institute for Geo-information Science and Earth Observation (ITC), Enschede, The Netherlands, p. 71.

Hultine, K.R., Scott, R.L., Cable, W.L., Goodrich, D.C. and Williams, D.G., 2004: Hydraulic redistribution by a dominant warm-desert phreatophytes: seasonal patterns and response to precipitation pulses. Functional Ecology 18, 530-538.

Jackson, R.B., Sperry, J.S. and Dawson T.E., 2000: Root water uptake and transport: using physiological processes in global predictions. Trends in Plant Science Perspectives 5(11), 482-488.

Jacobson, L., Moore, D.P., Hannapel and R.J., 1960: Role of calcium in the absorption of monovalent cations. Plant Physiology 35, 352-358.

Jarvis, P.G., 1976: The interpretation of the variations in leaf water potential and stomatal conductance found in canopies in the field. Philosophical Transactions of the Royal Society of London, Ser. B 273, 593-610.

Jennings, C.M.H., 1974: The hydrogeology of Botswana. PhD thesis, University of Natal, South Africa, p. 873.

Jensen, M.E., and Haise, H.R., 1963: Estimating evapotranspiration from solar radiation. Journal of Irrigation and drainage Division, ASCE 89 (LR4), 15-41.

Jensen, M.E., Burman, R.D. and Allen, R.G., 1990: Evaporation and irrigation water requirements, ASCE Manual 70, New York, USA, p. 332.

Jimenez, M.S., Nadezhdina, N., Cermak, J., Morales, D., 2000: Radial variation in sap flow in five laurel forest tree species in Tenerife, Canary Islands. Tree Physiology 20, 1149-1156.

Katjiua, M.L.J. and Ward, D., 2006: Resistance and tolerance of *Terminalia sericea* trees to simulated herbivory damage under different soil nutrient and moisture conditions. Journal of Chemical Ecology 32, 1431-1443.

Kent, N.L., 1941: Absorption, translocation and ultimate fate of lithium in the wheat plant. New Phytologist 40, 291-298.

Kocke N.L., Heerman, D.F. and Duke H.R., 1985: Measurement of evaporation and plant transpiration for irrigated corn. In: proceedings

by specialty conference on advances in irrigation and drainage; surviving external pressures. ASCE: New York, NY: 55-62.

Köstner, B.M.M., Schulze, E.-D., Kelliher, F.M., Hollinger, D.Y., Byers, J.N., Hunt, H.E., McSeveny, T.M., Meserth, R., Weir, P.L., 1992: Transpiration and canopy conductance in a pristine broad-leafed forest of *Nothofagus*: an analysis of xylem sap flow and eddy correlation measurements. Oecologia 91, 350-359.

Köstner, B., Granier, A. and Cermák, J., 1998: Sap flow measurements in the forest stands: methods and uncertainties. Ann. Sci. For. 55, 13-27.

Köstner, B., 2001: Evaporation and transpiration from forests in Central Europe-relevance of patch-level studies for spatial scaling. Meteorology and Atmospheric Physics 76, 69-82.

Kurz-Besson, C., Otieno, D., Lobo do Vale, R., Siegwolf, R., Schmidt, M., Herd, A., Nogueira, C., Soares David, T., Soares David, J., Tenhunen, J., Santos Pereira, J. and Chaves, M., 2006: Hydraulic lift in Cork Oak trees in a savannah-type Mediterranean ecosystem and its contribution to the local water balance. Plant and Soil 282, 361-378.

Kustas, W.P., Choudhury B.J., Kunkel, K.E. and Gay, L.W., 1989: Estimate of the aerodynamic roughness parameters over an incomplete canopy cover of cotton. Agricultural and Forest Meteorology 46, 91-105.

Kustas, W.P. and Norman, J.M., 1999: Evaluation of soil and vegetation heat flux predictions using a simple two-source model with radiometric temperatures for partial canopy cover. Agricultural and Forest Meteorology 94, 13-29.

Ladekarl, U.L., Rasmussen, K.R., Christensen, S., Jensen, K.H. and Hansen, B., 2005: Groundwater recharge and evapotranspiration for two natural ecosystems covered with oak and heather, Journal of hydrology 300, 76-99.

Lambs, L. and Muller, É., 2002: Sap flow and water transfer in the Garonne River riparian woodland, France. Annals of Forest Science 59, 301-315.

Lamontagne, S., Cook, P.G., O'Grady, A. and Eamus, D., 2005: Groundwater use by vegetation in a tropical savanna zone (Daly river, Australia). Journal of Hydrology 310 (1-4), 280-293.

Larcher, W., 2004: Physiological Plant Ecology. 4th ed. Springer, Berlin. p. 513.

Le Houérou, H.N., 1972: Africa-the Mediterranean region. In: C.M. Mckell, J. P. Blaisdell and J.R. Goodings (Eds.) Wildland shrubs-their Biology and Utilization. USDA Forest Service, Ogden, UT. pp. 26-36.

Le Maitre, D.C., Scott, D.F. and Colvin, C., 2000: Information on the interactions between groundwater and vegetation relevant to South

African conditions: A review. In: Past achievements and Future Challenges, Balkema, Rotterdam, 959-961.

Lerner, D.N., Issar, A.S. and Simmers, I., 1990: Groundwater recharge; a guide to understanding and estimating natural recharge. IAH series vol. 8, Heise, Hannover, Germany. p. 345.

Lin, G. and Sternberg, L. da S. L., 1993: Hydrogen isotopic fractionation by plants roots during uptake in coastal wetland plants. In: J.R. Ehleringer, Hall, A.E. and G.D. Farquhar (eds), Stable isotope and plant carbon/water relations. Academic press, New York.

Lloyd, C.R., Culf, A.D., Dolman, A.J. and Gash, J.H.C., 1991: Estimates of sensible heat flux from observations of temperature fluctuations. Boundary Layer Meteorology 57, 311-322.

Loustau, D., Berbigier, P., Roumagnac, P., Arruda-Pacheco, C., David, J.S., Fereira, J.S., Pereira, J.S. and Tavares, R., 1996: Transpiration of a 64-year-old maritime pine stand in Portugal. (1) seasonal course of water flux through maritime pine. Oecologia 107, 33-42.

Loustau, D., Domec, J.-C. and Bosc, A., 1998: Interpreting the variations in xylem sap flux density within the trunk of maritime pine (*Pinus pinaster* Ait.): application of a model for calculating water flows at tree and stand levels. Annals of Forest Science 55, 29-46.

Lu, P., Muller, W.J. and Chacko, E.K., 2000: Spatial variations in xylem sap flux density in the trunk of orchard-grown, mature mango trees under changing soil water conditions. Tree Physiology 20, 683-692.

Lu, P., Urban, L. and Z. Ping, 2004: Granier's thermal dissipation probe (TDP) method for measuring sap flow in trees: theory and practice. Acta Botanica Sinica 46(6), 631-646.

Lubczynski M.W., 2000: Ground water evapotranspiration-underestimated component of groundwater balance in a semi- arid environment- Serowe case Botswana. In: Past achievements and Future Challenges, Balkema, Rotterdam, 199-204.

Lubczynski, M. and Roy, J., 2005: MRS contribution to hydrogeological system parameterization. Near Surface Geophysics 3 (3), 131-139.

Lubczynski M.W., Obakeng O., Fregoso A., Mapanda W. Ziwa C., Keeletsang, M., Gelens M., de Gier A. and Chavarro, D., 2006: Dry season assessment of transpiration of woody savannah vegetation in the Kalahari estimated by sap flow technique. *In preparation*.

Ludwig, F., Dawson, T.E., Kroon, H., Berendse, F. and Prins, H.H., 2003. Hydraulic lift in *Acacia tortilis* trees on an East African savanna. Oecologia 134, 293-300.

Lundblad, M. and Lindroth, A., 2002: Stand transpiration and sap flow density in relation to weather, soil moisture and stand characteristics. Basic and Applied Ecology 3, 229-243.

Magombedze, L.M., Frengstad, B. and Lubczynski, M.W. 2004: Spatial variation of groundwater recharge in a semi-arid environment: Serowe, Botswana. In: Water resources of arid areas: proceedings of the international conference on water resources of arid and semi arid regions of Africa WRASRA, August 3-6th, 2004, Gaborone, Botswana. / ed. by Stephenson, D., Shemang, E.M., Chaoka, T.R. Rotterdam: Balkema, 2004. pp. 271-278.

Makkink G.F., 1957: Testing the Penman formula by means of lysimeters. Journal of the Institution of Water Engineers 11, 277-288.

Martin, M.P.L.D., Snaydon, R.W. and Drennan, D.S.H., 1982. Lithium as a non-radioactive tracer for roots of intercropped species. Plant and Soil 64, 203-208.

Martin, T.A., Brown, K.J., Cermák, J., Ceulemans, R., Kucera, J., Meinzer, F.C., Rombold, J.S., Sprugel, D.G. and Hinckley, T.M., 1997: Crown conductance and tree and stand transpiration in a second-growth *Abies amabilis* forest. Canadian Journal of Forest Res. 27, 797-808.

Massman, W.J., 1997: An analytical one-dimensional model of momentum transfer by vegetation of arbitrary structure. Boundary Layer Meteorology 83, 407-421.

Massman, W.J., 1999: A model study of kB^{-1} for vegetated surfaces using 'localized near field' Langrangian theory. Journal of Hydrology 223, 27-43.

Mazor, E., Verhagen, B.Th. and Sellschop, J.P.F., 1974: Kalahari groundwaters: Their hydrogen, carbon and oxygen isotopes. In "Isotope techniques in groundwater hydrology", IAEA, Vienna, I: 203-225.

Mazor, E., Verhagen, B.Th., Sellschop , J.P.F., Jones, M.T., Robins, N.E., Hutton, L. and Jennings, C.M.H., 1977: Northern Kalahari groundwaters: Hydrologic, isotopic and chemical studies at Orapa, Botswana. Journal of Hydrology 34: 203-234.

Mazor, E., 1982: Rain recharge in the Kalahari-a note on some approaches to the problem. Journal of Hydrology 55: 137-144.

McAneney, K.G., Green, A.E., and Astill, M., 1995: Large-aperture scintillometry; the homogeneous case, Agriculture and Forest Meteorology 76, 149-162.

Mensforth, L.J., Thorburn, P.J., Tyerman, S.D. and Walker, G.R., 1994: Sources of water used by riparian *Eucalyptus camaldulensis* overlying highly saline groundwater. Oecologia 100, 21-28.

Midgley, J.J., Talma, S., Scott, D., Olbrich, B. and van Wyk, G.F., 1994: Analysis of stable isotopes of xylem water from plantation trees in E. Transvaal and Zululand, indicate they utilized ground water during drought of 1992. South African Forestry Journal 170, 33-36.

Monteith, J.L., 1965: Evaporation and the environment, the state of movement of water in living organisms, XIXth symposium. Cambridge University Press, Swansea.

Monteith, J.L., 1995: Accommodation between transpiring vegetation and the convective boundary layer. Journal of Hydrology 166, 251-263.

Morton, F.I., 1994: Evaporation research-a critical review and its lessons for the environmental sciences. Critical reviews in Environmental Science and Technology 24 (3), 237-280.

Muoghalu, J.I. And Johnson, S.O., 2000: Interception, pH and solid content of rainfall in a Nigerian lowland rain forest. African Journal of Ecology 38, 38-46.

Nadezhdina, N., Cermák, J., Ceulemans, R., 2002: Radial patterns of sap flow in woody stem of dominant and understorey species: scaling errors associated with positioning of sensors. Tree Physiology 22, 907-918.

Nyadzi, G.I., Janssen, B.H., Otsyina, R.M., Booltink, H.W.G., Ong, C.K. and Oenema, O., 2003: Water and nitrogen dynamics in rotational woodlots of tree species in western Tanzania. Agroforestry Systems 59, 229-230.

Obakeng, O.T.O., Beekman, H.E., Meijer, H.A.J., Kers, B.A.M., and Van Elswijk, R.C., 1997: Groundwater recharge and resources assessment in the Botswana Kalahari-Moisture extraction for chemical and isotopic analysis. Groundwater recharge and evaluation study (GRES) II project: Technical report, Department of Geological Survey, Lobatse, Botswana. p. 85.

Obakeng, O.T., 2000: Groundwater recharge and vulnerability: a case study at the margins of the south - east central Kalahari sub-basin, Serowe region, Botswana. MSc thesis, Enschede, The Nethernads. p. 125.

Oren, R., Philips, N., Katul, G., Ewers, B.E. and Pakati, D.E., 1998a: Scaling xylem sap flux and soil water balance and calculating variance: a method for partitioning water flux in forests. Ann. Sci. For. 55, 191-216.

Oren, R., Ewers, B.E., Philips, N., Todd, P. and Katul, G., 1998b: Soil moisture affects canopy conductance at depths delineated with local water balance.Ecol. Appl.

O'Toole, J.C. and Real, J.G., 1986: Estimation of aerodynamic and crop resistances from canopy temperature. Agronomy Journal, 78, 305-310.

Owen, P.R. and Thomson, W.R., 1963: Heat transfer across rough surfaces. Journal of Fluid Mechanics 15, 321-334.

Pataki, D.E. and Oren, R., 2003: Species differences in stomatal control of water loss at the canopy scale in a mature bottomland deciduous forest. Advances in Water Resources 26, 1267-1278.

196

Penman H.L., 1948: Natural evaporation from open water, bare soil and grass. Proceedings of the Royal Society of London 193, 120-145.

Peters, S.W.M., 1995: Energy and water balance modelling of a semi-arid area using remote sensing. PhD thesis. Vrije Universiteit Amsterdam. p. 256.

Phillips, N., Oren, R. and Zimmermann, R., 1996: Radial patterns in sap flow in non-, diffuse- and ring-porous tree species. Plant, Cell and Environment 18, 983-990.

Phillips, W.S., 1963: Depth of roots in soil. Ecology 44: 424-429.

Pitman, W.V., 1973: A mathematical model for generating monthly rivers flows from meteorological data in South Africa. Report number 2/73. Hydrological Research Unit, Department of Civil Engineering, University of Witwatersrand, South Africa.

Porporato, A., Laio, F., Ridolfi, L., Caylor, K.K., and Rodriguez-Iturbe, I., 2003: Soil moisture and plant stress dynamics along the Kalahari gradient. Journal of Geophysical Research 108 (D3), 4127, doi: 10.1029/2002JD002448.

Priestley C.H.B. and Taylor, R.J., 1972: On the assessment of surface heat fluxes and evaporation using large scale parameters. Monthly weather review 100, 81-92.

Rahube, T.B., 2003: Recharge and groundwater resources evaluation of the Lokalane - Ncojane basin Botswana using numerical modelling. ITC MSc. Thesis, Enschede, The Netherlands. p. 113.

Raupach, M.R., 1994: Simplified expressions for vegetation roughness length and zero plane displacement as functions of canopy height and area index. Boundary-Layer Meteorology 71, 211-216.

Rubin, Y., 2003: Applied Stochastic Hydrogeology. Oxford University Press, Oxford, UK. p. 391.

Sayre, J.D. and Morris, V.H., 1940: The lithium method of measuring the extent of corn root systems. Plant Physiology 15, 761–764.

Scanlon, B.R., 1994: Water and heat fluxes in the desert soils. Water Resources Research 30 (3), 709-719.

Scanlon, B.R., Tyler, S.W. and Wierenga, P.J., 1997: Hydrologic issues in arid, unsaturated systems and implications for contaminant transport. Reviews of Geophysics 35(4), 461-490.

Scanlon, B.R., 2000: Uncertainties in estimating water fluxes and residence times using environmental tracers in an arid unsaturated zone. Water Resources Research 36 (2), 395-409.

Scanlon B.R., Keese, K., Reedy, R.C., Šimůnek, J. and Andraski, B.J., 2003: Variations in flow and transport in the thick desert vadose zones in response to paleoclimate forcing (0-90 kyr): Field measurements,

modeling and uncertainties. Water Resources Research 39(7), 1179, doi:10.1029/2002WR001604,2003.

Schaap, M.G., Leij, F.J. and van Genuchten. M.Th., 1999: A bootstrap-neural network approach to predict soil hydraulic parameters. In: van Genuchten, M.Th., F.J. Leij, and L. Wu (eds), Proc. Int. Workshop, Characterization and Measurements of the Hydraulic Properties of Unsaturated Porous Media, 1237-1250, University of California, Riverside, CA.

Schaap, M.G., Leij, F.J. and van Genuchten. M.Th., 2001: ROSETTA: a computer program for estimating soil hydraulic parameters with hierarchical pedotransfer functions. Journal of Hydrology 251, 163-176.

Schenk, H.J. and Jackson, R.B., 2005: Mapping the global distribution of deep roots in relation to climate and soil characteristics. Geordema 126, 129-140.

Scholes, R.J., Parsons, D.A.B., Kamuhuza, A., Davis, G., Ringrose, S., Gambiza, J., and Chileshe, E., 1997: The Kalahari transect: Research on global change and sustainable development in Southern Africa. International Geosphere-Biosphere Programme (IGBP) report 42, Stockholm, Sweden.

Schroeder, P.R., Dozier, T.S., Zappi, P.A., McEnroe, B.M., Sjostrom, J.W., and Peyton. R.L., 1994: The hydrologic evaluation of landfill performance (HELP) model: Engineering Documentation for version 3. EPA/600/R-94/168b. Washington D.C.: U. S. Environmental Protection Agency Office of Research and Development.

Schulze, E.-D., Caldwell, M.M., Canadell, J., Mooney, H.A., Jackson, R.B., Parson, D., Scholes, R., Sala O.E., and Trimborn, P., 1998: Downward flux of water through roots (i.e. inverse hydraulic lift) in dry Kalahari sands. Oecologia 115, 460-462.

Scott, D.F. and Le Maitre, D.C., 1998: The interaction between vegetation and groundwater: research priorities for South Africa, Report to the Water Research Commission project K5/730, CSIR Division of Water, Environment and Forestry Technology, Stellenbosch, 1-87.

Selaolo, E.T., 1998: Tracer studies and groundwater recharge assessment in the eastern fringe of the Botswana Kalahari, The Letlhakeng-Botlhapatlou Area. PhD thesis, Vrije Universiteit Amsterdam, The Netherlands. p. 229.

Sellami, M.H. and Sifaoui, M.S., 2003: Estimating transpiration in an intercropping system: measuring sap flow inside the oasis. Agricultural Water Management 59, 191-204.

Shuttleworth, W.J., 1993: Evaporation, In: Maidment, D.R. (Ed.), 1993, Handbook of Hydrology, McGraw-Hill, New York. p. 650.

198

Sibanda, T., 2006: Groundwater recharge estimation and modelling of the Nyamandhlovu aquifer, Mid Zambezi basin, Zimbabwe. UNESCO-IHE MSc. Thesis, Institute for Water Education, Delft, The Netherlands. p. 123.

Simmers, I. (ed.), 1997: Recharge of phreatic aquifers in (semi-) arid areas. IAH series, vol. 19. Balkema, Rotterdam, The Netherlands. p. 255.

Šimůnek, J., Šejna, M. and van Genuchten, M.Th., 1998: The HYDRUS-1D software package for simulating the one dimensional movement of water of water, heat and multiple solutes in variably saturated media. Version 2.0, IGWMC-TPS-70, International Groundwater Modeling Centre, Colorado School of Mines, Golden, Colorado, p. 251.

Smith, D.J. and Allen, S.J., 1996: Measurement of sap flow in plant stems. Journal of Experimental Botany 47, 1833-1844.

Smith, R.A., 1984: The Lithostratigraphy of the Karoo Supergroup in Botswana. Bulletin 26, Department of Geological Survey: Botswana. p. 239.

Snyder, K.A. and Williams D.G., 2000: Water sources used by riparian trees vary among stream types on the San Pedro river, Arizona. Agricultural and Forest Meteorology 105, 227-240.

Stewart, J.B., 1988: Modelling surface conductance of pine forest. Agricultural and Forest Meteorology 43, 19-35.

Strangeways, I.C., 1983: Interfacing soil moisture gypsum blocks with a modern data logging system using a simple, low cost, DC method. Soil Science 136(5), 322-324.

Stull, R.B., 1988: An introduction to boundary layer Meteorology. Kluwer Academic Publishers, p. 670.

Su, Z., Schmugge, T.,Kustas, W.P. and Massman, W.J., 2001: An evaluation of two models for estimation of the roughness height for heat transfer between the land surface and the atmosphere. Journal of Applied Meteorology 40 (11), 1933-1951.

Su, Z., 2002: The surface energy balance system (SEBS) for estimation of turbulent heat fluxes. Hydrology and Earth Systems Sciences 6(1), 85-99.

Swanson, R.H., 1994: Significant historical developments in thermal methods for measuring sap flow in trees. Agricultural and Forest Meteorology 72, 113-132.

Swedish Geological Company (SGC), 1988: Serowe Groundwater Resources Evaluation Project, Final report, Ministry of Mineral Resources and Water Affairs, Department of Geological Survey, Lobatse, Botswana, p. 286.

Tamm, C.O., 1951: Removal of plant nutrients from tree crowns by rain. Physiologia Plantarum 4, 184 -188.

Thiermann, V., and Grassl, H., 1992: The measurement of turbulent surface layer fluxes by bichromatic scintillation. Boundary Layer Meteorology 58, 367-389.

Thiery, D., 1988: Forecast of changes in piezometric levels by a lumped hydrological model. Journal of Hydrology 97, 129-148.

Thomas, D.S.G. and Shaw, P.A., 1991: The Kalahari Environment. Cambridge University Press, p. 284.

Thom, A.S., and Oliver, H.R., 1977: On Penman's equation for estimating regional evaporation. Quarterly Journal of the Royal Meteorological Society 103, 345-357.

Thorburn, P.J., Walker, G.R., and Brunel, J.P., 1992: Extraction of water from Eucalyptus trees for analysis of deuterium and oxygen-18: laboratory and field techniques. Plant Cell and Environment 16, 269-277.

Thornthwaite, C.W., 1948: An approach towards a rational classification of climate. Geographical Review 38, 55-94.

Tillman, J.E., 1972: The indirect determination of stability, heat and momentum fluxes of atmospheric boundary layer from simple scalar variables during dry unstable conditions. Journal of Applied Meteorology 11, 783-792.

Timmermans, W. and Meijerink, A., 1999: Remotely sensed actual evapotranspiration; implications for groundwater management in Botswana. International Journal of Applied Earth Observation and Geoinformation 1(3/4), 222-233.

Tolsma, D.J., Ernst, W.H.O., Verweij, R.A. and Vooijs, R., 1987: Seasonal variation of nutrient concentrations in a semi-arid savanna ecosystem in Botswana. Journal of Ecology 75, 755-770.

Van Dam, J.C., Huygen, J., Wesseling, J.G. Feddes, R.A., Kabat, P., Van Walsum, P.E.V., Groenendijk, P. and Van Diepen, C.A., 1997: Simulation of water flow, solute transport and plant growth in the Soil-Water-Atmosphere-Plant environment. Theory of SWAP version 2.0, Report 71, Department of Water Resources, Wageningen Agricultural University, Wageningen, The Netherlands, p. 167.

Vanderklein, D.W., Wilkens, R.T., Cartier, A. and Lemke, R.W., 2004: Plant architecture and leaf damage in Bear Oak. I: Physiological responses. Northeastern Naturalist 11, 343-356.

Van der Lee, J. and Gehrels, J.C., 1990: Modelling aquifer recharge-introduction to the lumped parameter model EARTH. Free University of Amsterdam, The Netherlands, p. 30.

Van Genuchten, M.Th., 1980: A closed form equation for predicting the hydraulic conductivity of unsaturated soils. Soil Science Society of America Journal 44, 892-898.

Van Straten, O.J., 1955: The geology and groundwater of Ghanzi cattle route. Annual report, Geological Survey, Bechuanaland Protectorate, p. 28-39.

Van Tonder, G.J. and Kirchner, J., 1990: Estimation of natural groundwater recharge in the Karoo aquifers of South Africa. Journal of Hydrology 121, 395-419.

Verhagen, B.Th., Mazor, E. and Sellschop , J.P.F., 1974: Radiocarbon and tritium evidence for direct rain recharge to groundwaters in the northern Kalahari. Nature 249: 643-644.

Verhagen, B.Th., 1990: Isotope hydrology of the Kalahari: recharge or no recharge? Proc. ixth biennial conference at the University of Durban (South Africa), February 1989. In: Palaeoecology of Africa and the surrounding islands, (editor; Klausheine), 21: 143-158.

Verhoef, A., de Bruin, H.A.R. and van den Hurk, B.J.J.M., 1997: Some practical notes on the parameter for sparse vegetation. Journal of Applied Meteorology 36, 560-572.

Vörösmarty, C.J., Federer, C.A. and Schloss, A.L., 1998: Potential evapotranspiration functions compared on US watersheds: Possible implications for global-scale water balance and terrestrial ecosystems modeling. Journal of Hydrology 207,147-169.

Vugts, H.F., Waterloo, M.J., Beekman, F.J., Frumau, K.F.A. and Bruijnzeel, L.A., 1993: The temperature variance method: a powerful tool in the estimation of actual evaporation rates. IAHS publ. No. 216, 251-260.

Wagner, B., Tarnawski, V.R., Hennings, V., Müller, U., Wessolek G. and Plagge, R., 2001: Evaluation of pedo-transfer functions for unsaturated soil hydraulic conductivity using an independent dataset. Geoderma 102, (3-4), 275-297.

Walker, C.D. and Brunel J.-P., 1990: Examining evapotranspiration in a semi-arid region using stable isotopes of hydrogen and oxygen. Journal of Hydrology 118, 55-75.

Walker, C.D. and Richardson, S.B., 1991: The use of stable isotopes of water in characterizing the sources of water in vegetation. Chemical Geology, Isotope Geoscience section 94, 145-158.

Wallace, A., Romney, E.M., Cha, J.W. and Chaudhry, F.M., 1977: Lithium toxicity in plants. Communication in Soil Science and Plant Analysis 8, 773–780.

Wallace, J.S., Lloyd, C.R. and Sivakumar M.V.K., 1993: Measurement of soil, plant and total evapotranspiration from millet in Niger. Agricultural and Forest Meteorology 63, 149-169.

Walvoord, M.A., Plummer, M.A, Phillips, F.M. and Wolfsberg, A.V., 2002a: Deep arid system hydrodynamics. 1. Equilibrium states and response

times in thick desert vadose zones. Water Resources Research, 38(12), 1308, doi:10.1029/2001WR000824.

Walvoord, M.A., Phillips, F.M., Tyler, S.W. and Hartsough, P.C., 2002b: Deep arid system hydrodynamics. 2. Application to paleohydrologic reconstruction using vadose profiles from the northern Mojave Desert. Water Resources Research, 38(12), 1291, doi:10.1029/2001WR000825.

Warrington, S., Cottam, D.A. and Whittaker, J.B., 1989: Effects of insect damage on photosynthesis, transpiration and SO_2 uptake by sycamore. Oecologia 80, 136-139.

Water Surveys Botswana, 2001: Monitoring of groundwater pollution. Morupule Power Station, Tender no. 2932/00. Annual Report 2000-2001. Report to Botswana Power Corporation. Variously paginated.

Week, E.P. 2002: The Lisse effect revisited. Ground Water 40, 652-656.

Wellfield Consulting Services (WCS), 1998: Serowe Wellfield 2 extension project. Final report to the Department of Water Affairs, Ministry of Minerals, Energy and Water Resources, variously paginated.

Wieringa, J., 1986: Roughness-dependent geographical interpolation of surface wind speed averages. Quarterly Journal of Royal Meteorological Society 112, 867-889.

Wieringa, J., 1993: Representative roughness parameters for homogeneous terrain. Boundary Layer Meteorology 63, 323-363.

Wullschleger, S.D., Menizer, F.C. and Vertessy, R.A., 1998: A review of whole plant water use studies in trees. Tree Physiology 18, 499-512.

Wullschleger, S.D. and King, A.W., 2000: Radial variation in sap velocity as a function of stem diameter and sap wood thickness in yellow poplar trees. Tree Physiology 20, 511-518.

Xu, C.Y. and Singh, V.P., 2002: Cross comparison of empirical equations for calculating potential evapotranspiration with data from Switzerland. Water Resources Management 16(3), 197-219.

Zarkesh, M.K., 2005: Decision support system for flood water spreading site selection in Iran. PhD thesis, Wageningen University. p. 259.

Zencich, S.J., Froend, R.H., Turner, J.V. and Gailitis V., 2002: Influence of groundwater depth on the seasonal sources of water accessed by Banksia tree species on a shallow, sandy coastal aquifer. Oecologia 131, 8-19.

Zhang, D., 2002: Stochastic methods for flow in porous media, coping with uncertainties. Academic Press, San Diego, USA. p. 350.

Zhou, X., Persaud, N. and Wang, H., 2005: Periodicities and scaling parameters of daily rainfall over semi-arid Botswana. Ecological Modelling 185, 371-378.

Appendices

Appendix A: Example photographs of all investigated species

A. karoo

A. erioloba

A. fleckii
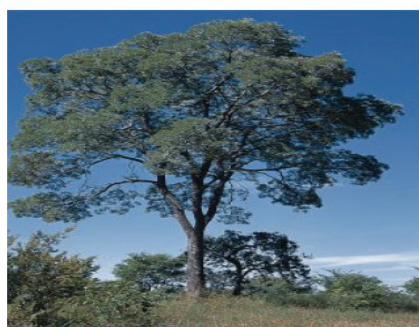
B. africana
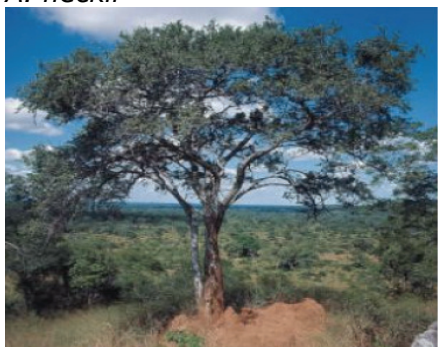
B. albitrunca

D. cinerea
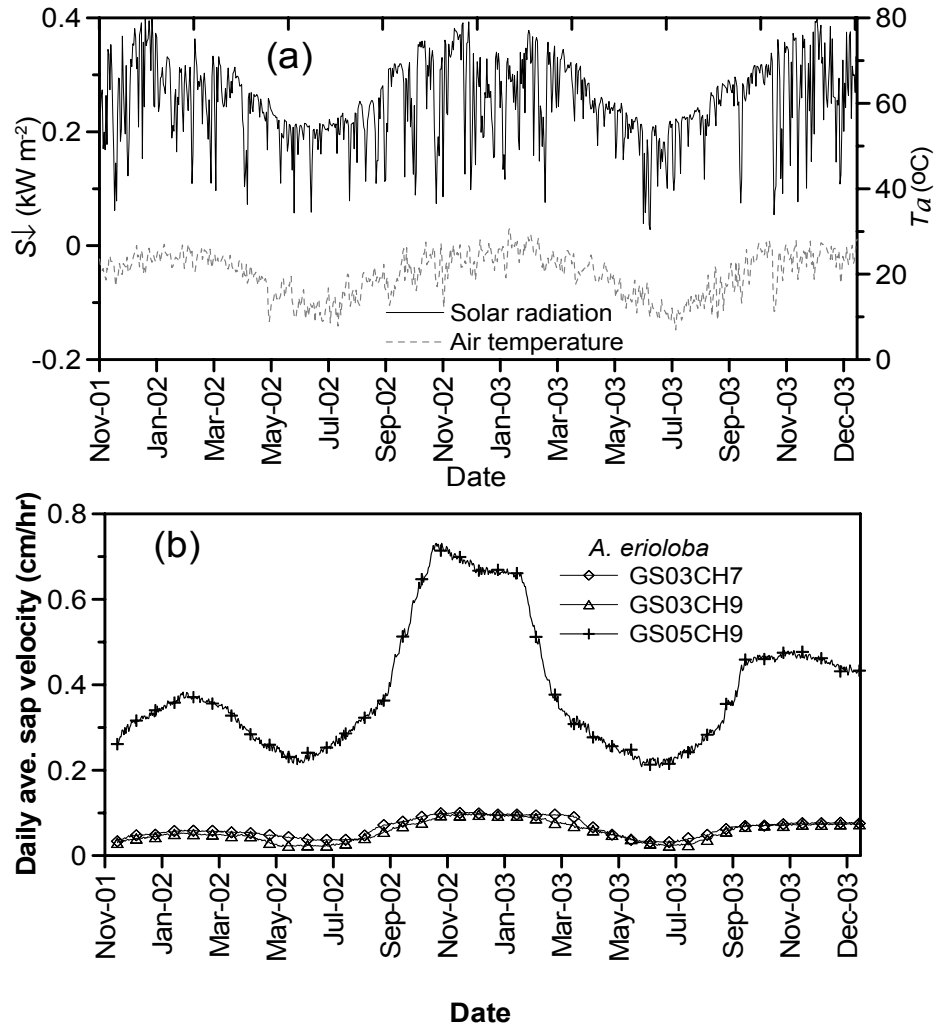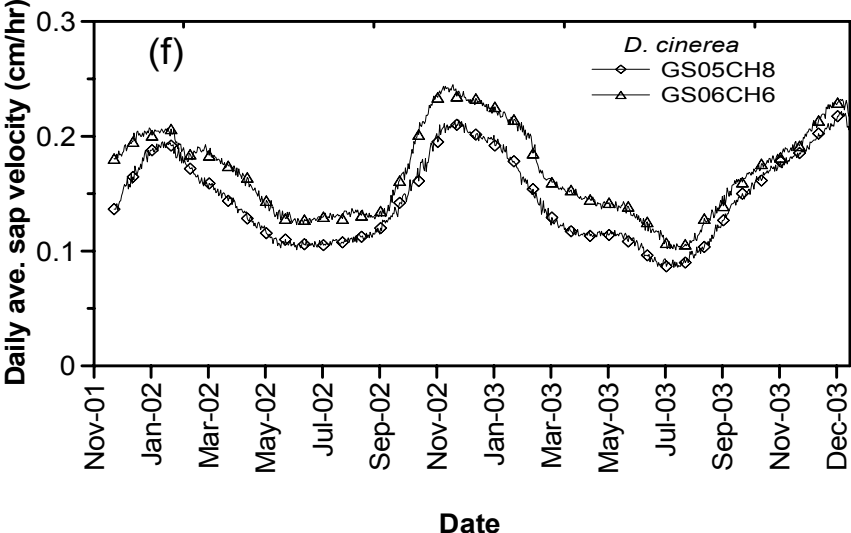
L. nelsi

O. pulcha
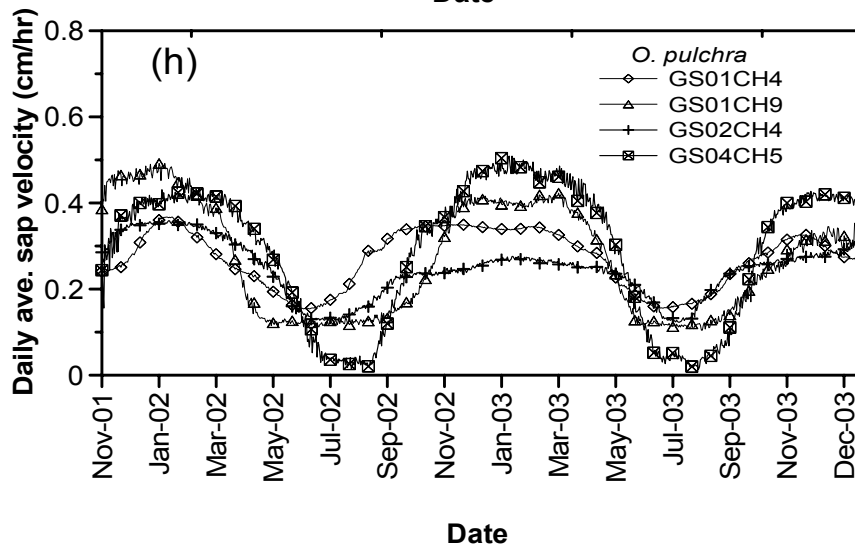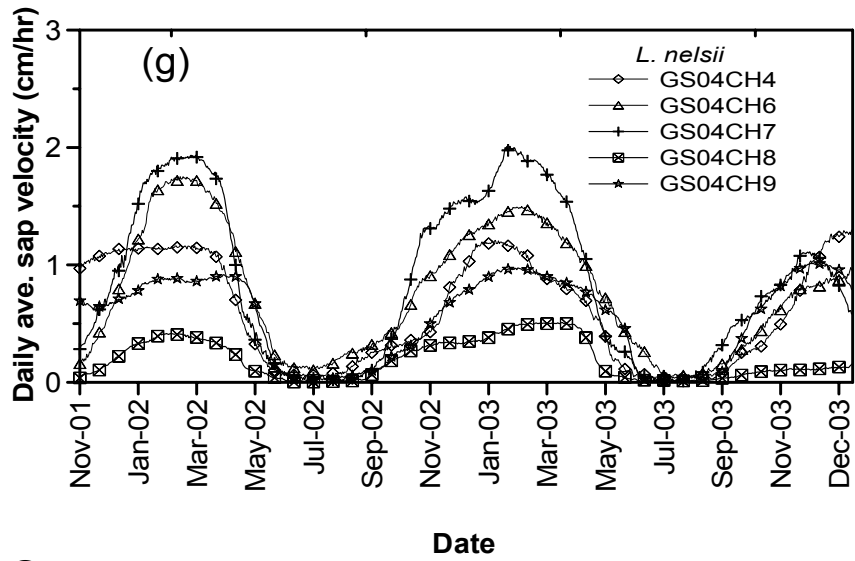

S. longipedunculata

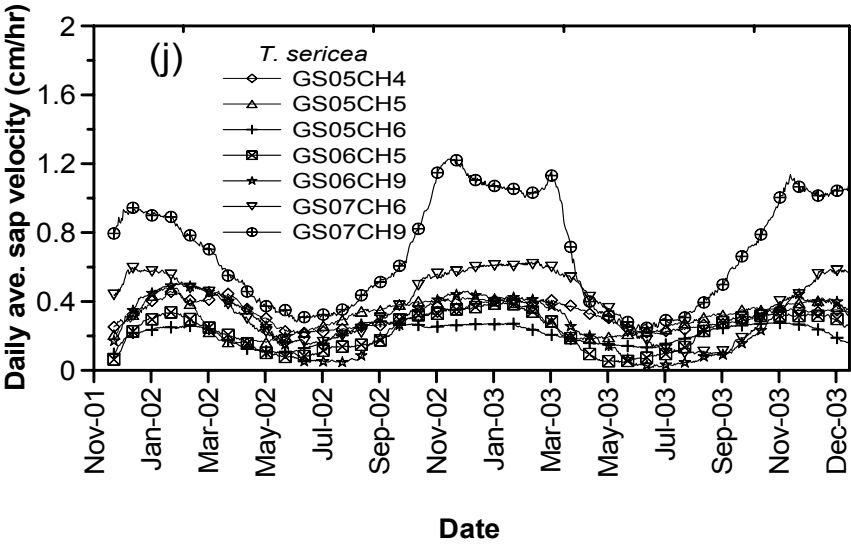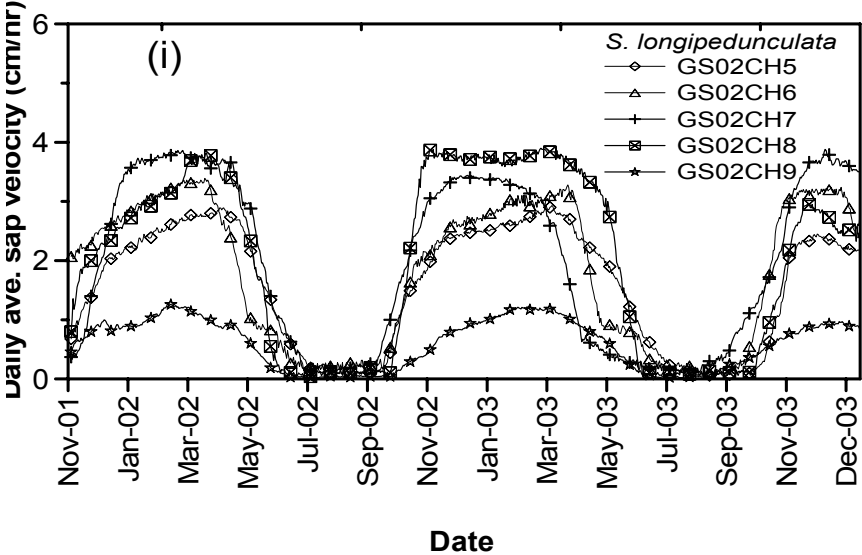*T. Sericea*

Z. mucronata

Appendix B: Seasonal trends of daily average (ave.) sap velocity (*from (b) until (j)*) in cm/hr in relation to (a) incoming shortwave radiation ($S\downarrow$) and (b) air temperature (T_a)
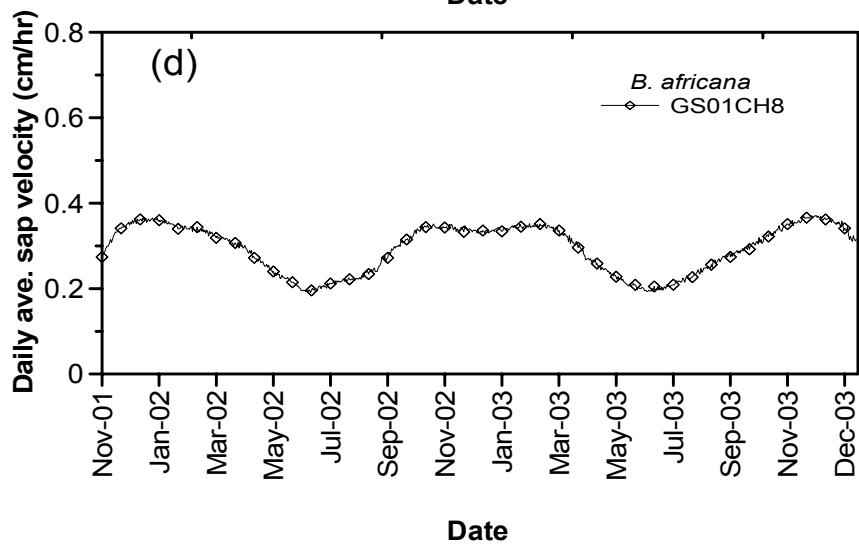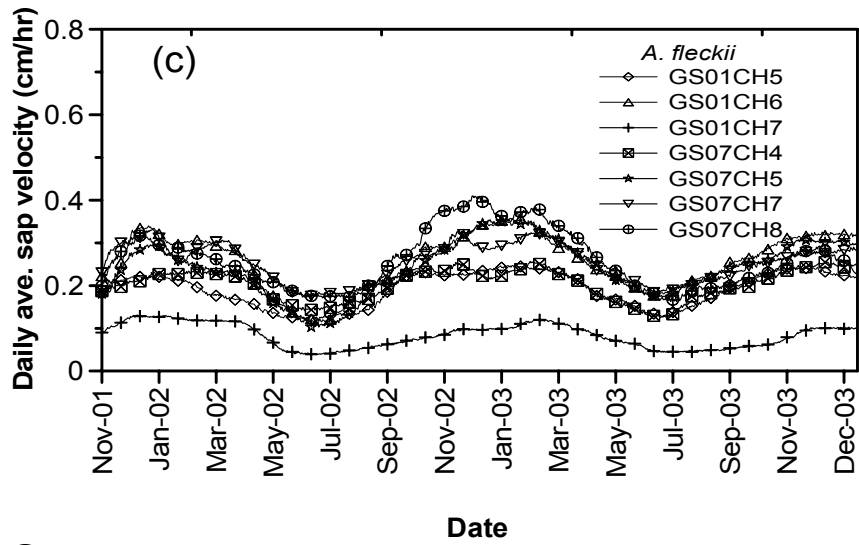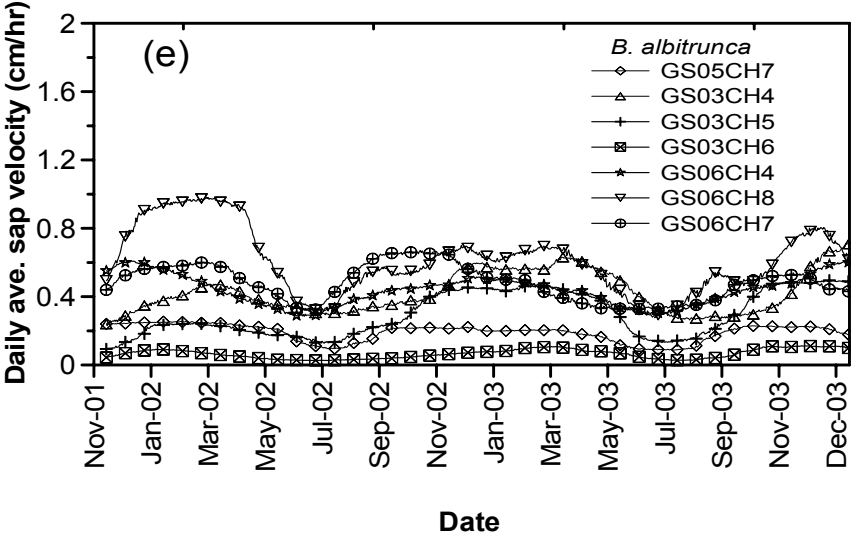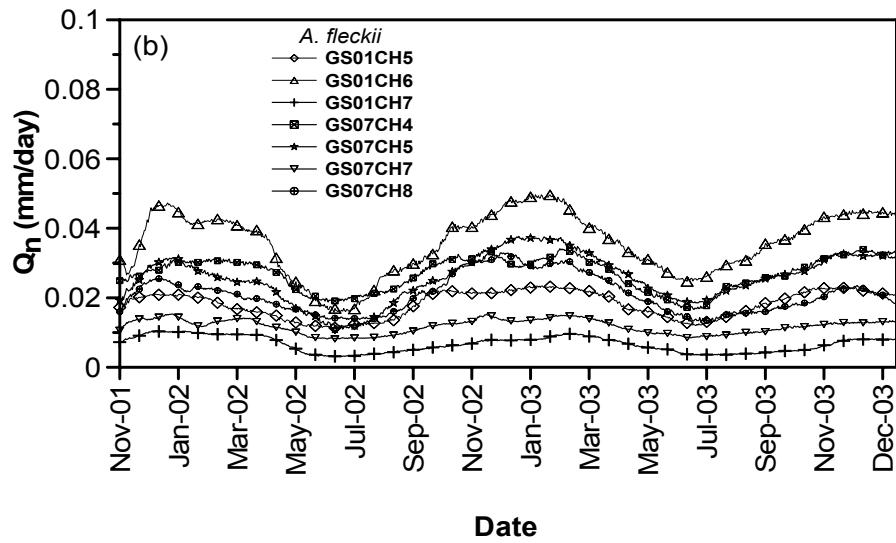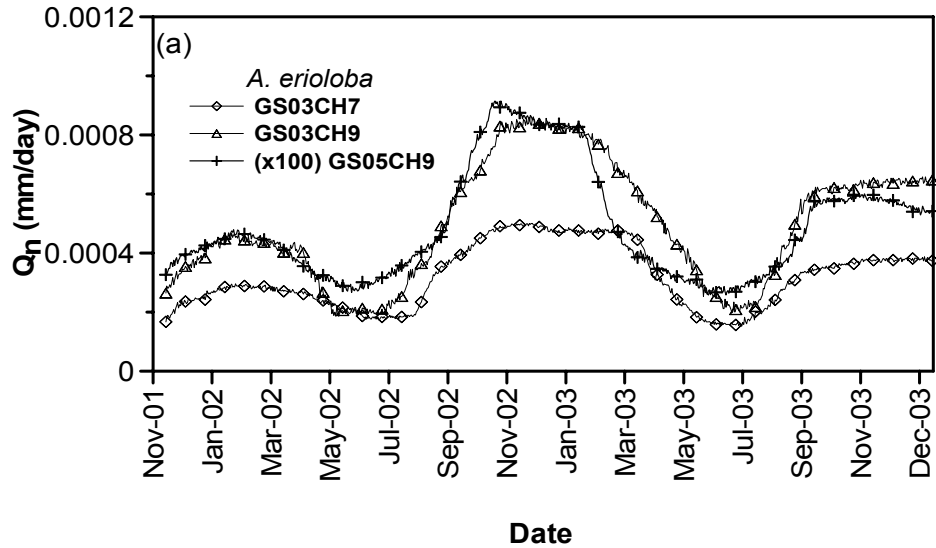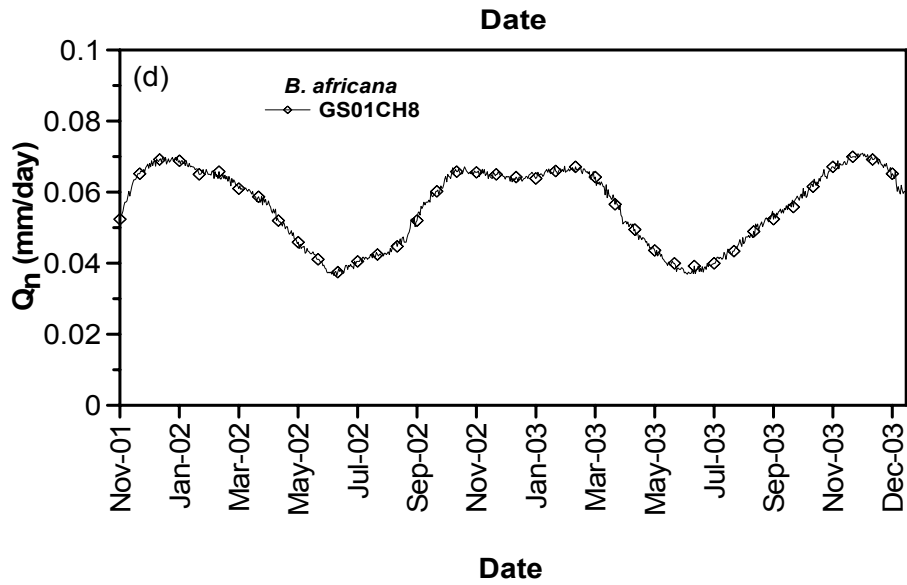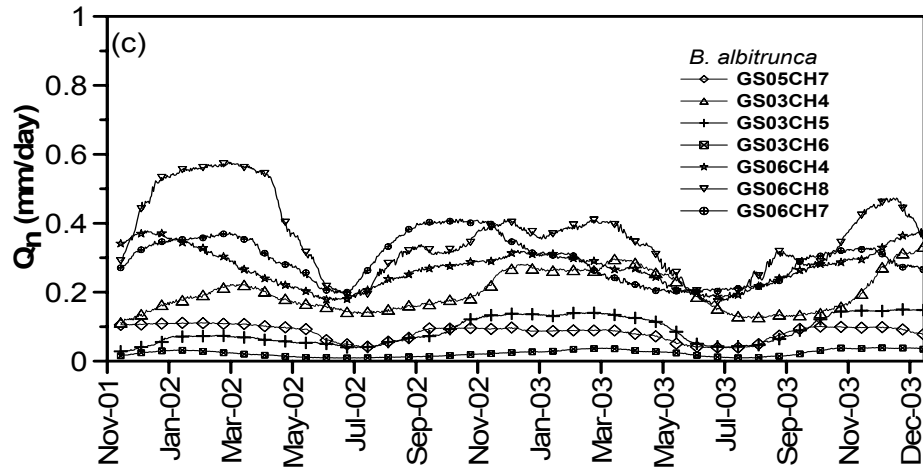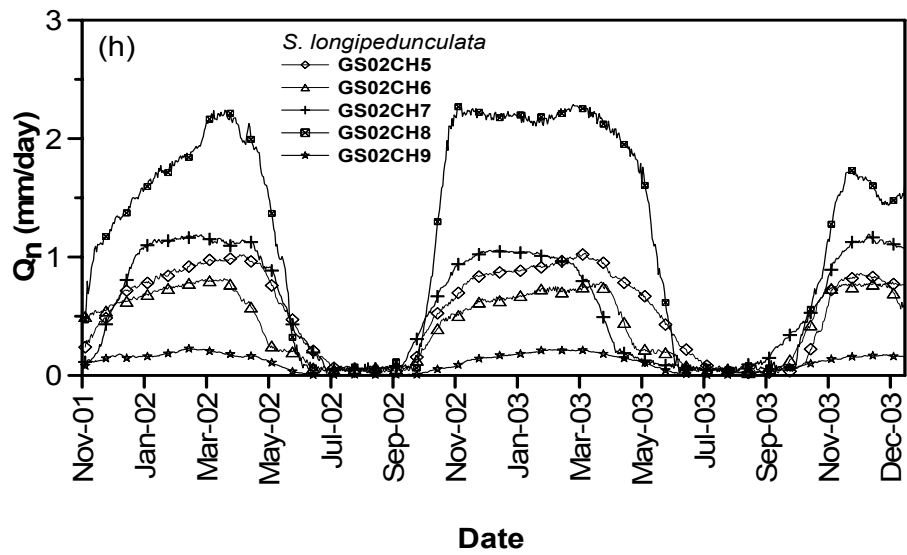
Appendix C. Normalised sap flow (*Q_n*), potential evapotranspiration (*PET*) and rainfall

Date

Date
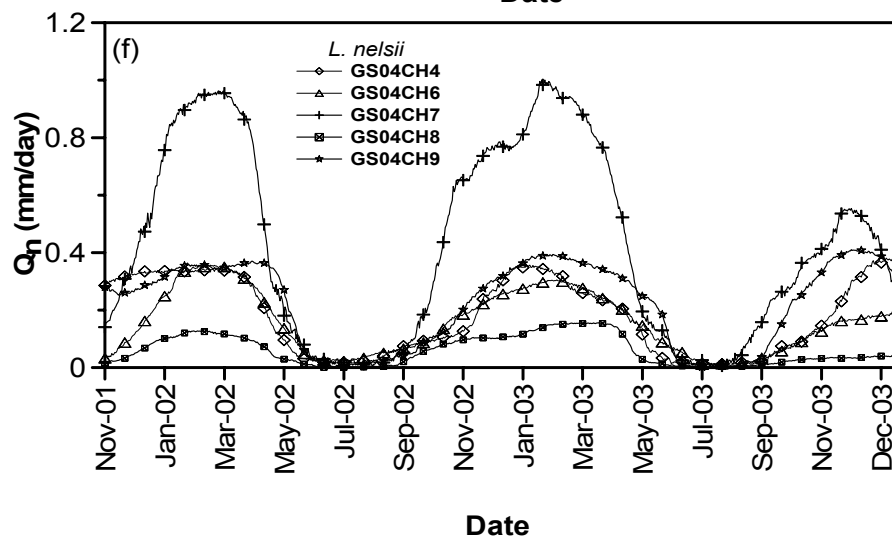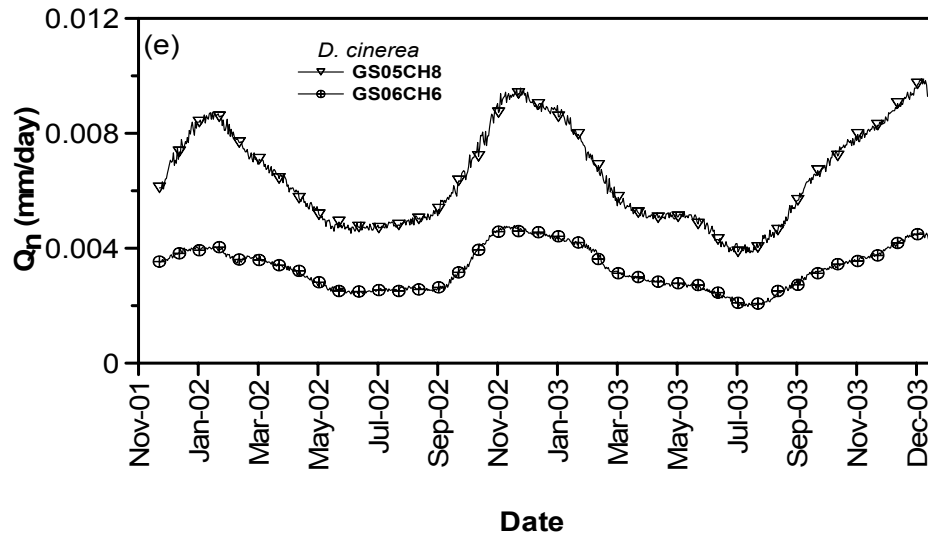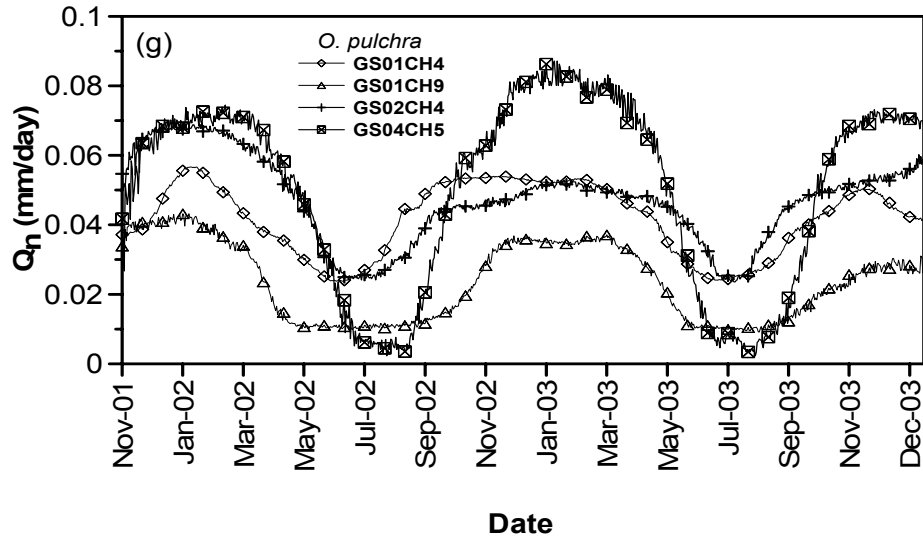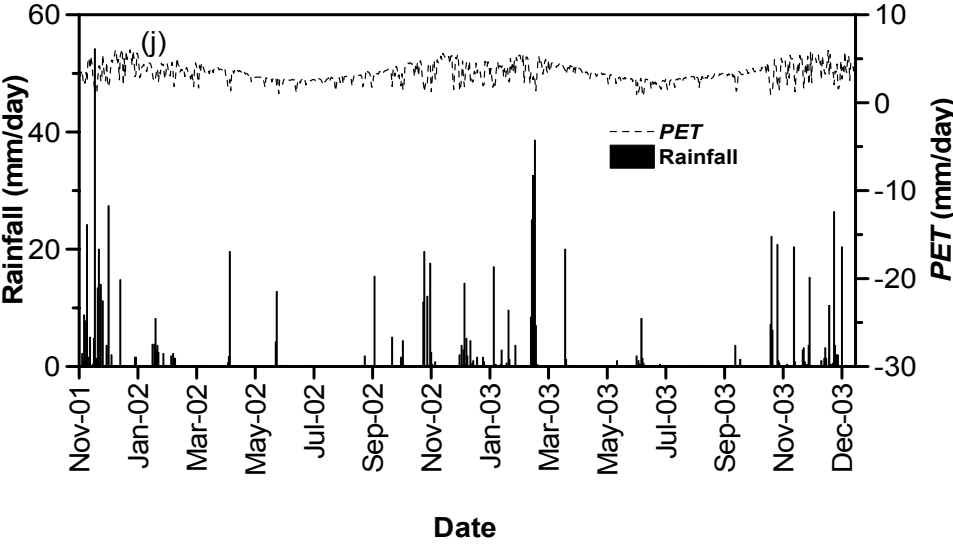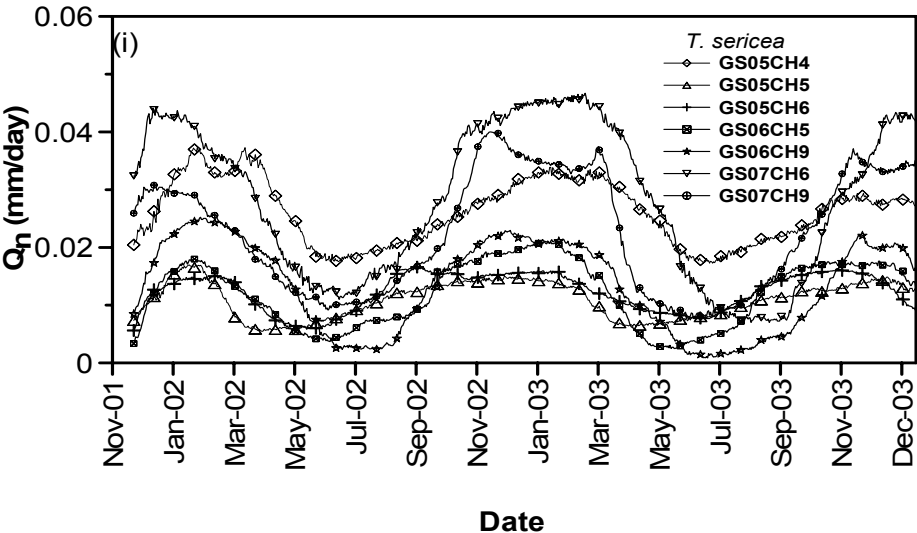
Curriculum vitae

Obolokile T. Obakeng is a Principal Hydrogeologist at the Department of Geological Survey (Botswana). He attended Letlhakane Primary School from 1978 to 1984. In 1985, he was admitted to Letlhakane Secondary School for Junior Certificate and Cambridge O' level studies which spanned from 1985 to 1989. In 1990 he participated in the national service (Tirelo Setshaba). From January 1991 to July 1991 he attended the Pre-Entry Science Course (PESC) programme at the University of Botswana (UB).

He earned a BSc. degree in Geology at UB in 1995, after which he joined the GRES II[5] project at the Department of Geological Survey from October 1995 to January 1997 as an Assistant Hydrogeologist, under the supervision of Dr. Hans E. Beekman. Within the framework of the GRES II project he studied Isotope Hydrology in 1996 at the Centre for Isotope Research at Rijksuniversiteit Groningen, in The Netherlands.

In February 1997, he was employed in the same post of Assistant Hydrogeologist into the permanent establishment of the Botswana Geological Survey. His main duties were mainly to carry out field and laboratory experiments, formulate and supervise groundwater exploration projects.

He returned to The Netherlands in October 1998 where he earned an MSc. degree (with distinction) in Water Resources in 2000 at the International Institute for Geo-information Science and Earth Observation (ITC), after which he continued with further research work leading to this PhD thesis.

---

[5] GRES II stands for **G**roundwater **R**echarge and **E**valuation **S**tudy phase II; it was a collaboration project between the Botswana Geological Survey, Vrije Universiteit Amsterdam and the University of Botswana.

ITC Dissertation List

1. **Akinyede** (1990), Highway cost modelling and route selection using a geotechnical information system
2. **Pan He Ping** (1990), 90-9003-757-8, Spatial structure theory in machine vision and applications to structural and textural analysis of remotely sensed images
3. **Bocco Verdinelli, G.** (1990), Gully erosion analysis using remote sensing and geographic information systems: a case study in Central Mexico
4. **Sharif, M**. (1991), Composite sampling optimization for DTM in the context of GIS
5. **Drummond, J.** (1991), Determining and processing quality parameters in geographic information systems
6. **Groten, S.** (1991), Satellite monitoring of agro-ecosystems in the Sahel
7. **Sharifi, A.** (1991), 90-6164-074-1, Development of an appropriate resource information system to support agricultural management at farm enterprise level
8. **Zee, D. van der** (1991), 90-6164-075-X, Recreation studied from above: Air photo interpretation as input into land evaluation for recreation
9. **Mannaerts, C.** (1991), 90-6164-085-7, Assessment of the transferability of laboratory rainfall-runoff and rainfall - soil loss relationships to field and catchment scales: a study in the Cape Verde Islands
10. **Ze Shen Wang** (1991), 90-393-0333-9, An expert system for cartographic symbol design
11. **Zhou Yunxian** (1991), 90-6164-081-4, Application of Radon transforms to the processing of airborne geophysical data
12. **Zuviria, M. de** (1992), 90-6164-077-6, Mapping agro-topoclimates by integrating topographic, meteorological and land ecological data in a geographic information system: a case study of the Lom Sak area, North Central Thailand
13. **Westen, C. van** (1993), 90-6164-078-4, Application of Geographic Information Systems to landslide hazard zonation
14. **Shi Wenzhong** (1994), 90-6164-099-7, Modelling positional and thematic uncertainties in integration of remote sensing and geographic information systems
15. **Javelosa, R.** (1994), 90-6164-086-5, Active Quaternary environments in the Philippine mobile belt
16. **Lo King-Chang** (1994), 90-9006526-1, High Quality Automatic DEM, Digital Elevation Model Generation from Multiple Imagery
17. **Wokabi, S.** (1994), 90-6164-102-0, Quantified land evaluation for maize yield gap analysis at three sites on the eastern slope of Mt. Kenya
18. **Rodriguez, O.** (1995), Land Use conflicts and planning strategies in urban fringes: a case study of Western Caracas, Venezuela

19. **Meer, F. van der** (1995), 90-5485-385-9, Imaging spectrometry & the Ronda peridotites

20. **Kufoniyi, O.** (1995), 90-6164-105-5, Spatial coincidence: automated database updating and data consistency in vector GIS

21. **Zambezi, P.** (1995), Geochemistry of the Nkombwa Hill carbonatite complex of Isoka District, north-east Zambia, with special emphasis on economic minerals

22. **Woldai, T.** (1995), The application of remote sensing to the study of the geology and structure of the Carboniferous in the Calañas area, pyrite belt, SW Spain

23. **Verweij, P.** (1995), 90-6164-109-8, Spatial and temporal modelling of vegetation patterns: burning and grazing in the Paramo of Los Nevados National Park, Colombia

24. **Pohl, C.** (1996), 90-6164-121-7, Geometric Aspects of Multisensor Image Fusion for Topographic Map Updating in the Humid Tropics

25. **Jiang Bin** (1996), 90-6266-128-9, Fuzzy overlay analysis and visualization in GIS

26. **Metternicht, G.** (1996), 90-6164-118-7, Detecting and monitoring land degradation features and processes in the Cochabamba Valleys, Bolivia. A synergistic approach

27. **Hoanh Chu Thai** (1996), 90-6164-120-9, Development of a Computerized Aid to Integrated Land Use Planning (CAILUP) at regional level in irrigated areas: a case study for the Quan Lo Phung Hiep region in the Mekong Delta, Vietnam

28. **Roshannejad, A.** (1996), 90-9009-284-6, The management of spatio-temporal data in a national geographic information system

29. **Terlien, M.** (1996), 90-6164-115-2, Modelling Spatial and Temporal Variations in Rainfall-Triggered Landslides: the integration of hydrologic models, slope stability models and GIS for the hazard zonation of rainfall-triggered landslides with examples from Manizales, Colombia

30. **Mahavir, J.** (1996), 90-6164-117-9, Modelling settlement patterns for metropolitan regions: inputs from remote sensing

31. **Al-Amir, S.** (1996), 90-6164-116-0, Modern spatial planning practice as supported by the multi-applicable tools of remote sensing and GIS: the Syrian case

32. **Pilouk, M.** (1996), 90-6164-122-5, Integrated modelling for 3D GIS

33. **Duan Zengshan** (1996), 90-6164-123-3, Optimization modelling of a river-aquifer system with technical interventions: a case study for the Huangshui river and the coastal aquifer, Shandong, China

34. **Man, W.H. de** (1996), 90-9009-775-9, Surveys: informatie als norm: een verkenning van de institutionalisering van dorp - surveys in Thailand en op de Filippijnen

35. **Vekerdy, Z.** (1996), 90-6164-119-5, GIS-based hydrological modelling of alluvial regions: using the example of the Kisaföld, Hungary

36. **Pereira, Luisa** (1996), 90-407-1385-5, A Robust and Adaptive Matching Procedure for Automatic Modelling of Terrain Relief

37. **Fandino Lozano, M.** (1996), 90-6164-129-2, A Framework of Ecological Evaluation oriented at the Establishment and Management of Protected Areas: a case study of the Santuario de Iguaque, Colombia

38. **Toxopeus, B.** (1996), 90-6164-126-8, ISM: an Interactive Spatial and temporal Modelling system as a tool in ecosystem management: with

two case studies: Cibodas biosphere reserve, West Java Indonesia: Amboseli biosphere reserve, Kajiado district, Central Southern Kenya

39. **Wang Yiman** (1997), 90-6164-131-4, Satellite SAR imagery for topographic mapping of tidal flat areas in the Dutch Wadden Sea

40. **Saldana-Lopez, Asunción** (1997), 90-6164-133-0, Complexity of soils and Soilscape patterns on the southern slopes of the Ayllon Range, central Spain: a GIS assisted modelling approach

41. **Ceccarelli, T.** (1997), 90-6164-135-7, Towards a planning support system for communal areas in the Zambezi valley, Zimbabwe; a multi-criteria evaluation linking farm household analysis, land evaluation and geographic information systems

42. **Peng Wanning** (1997), 90-6164-134-9, Automated generalization in GIS

43. **Lawas, C.** (1997), 90-6164-137-3, The Resource Users' Knowledge, the neglected input in Land resource management: the case of the Kankanaey farmers in Benguet, Philippines

44. **Bijker, W.** (1997), 90-6164-139-X, Radar for rain forest: A monitoring system for land cover Change in the Colombian Amazon

45. **Farshad, A.** (1997), 90-6164-142-X, Analysis of integrated land and water management practices within different agricultural systems under semi-arid conditions of Iran and evaluation of their sustainability

46. **Orlic, B.** (1997), 90-6164-140-3, Predicting subsurface conditions for geotechnical modelling

47. **Bishr, Y.** (1997), 90-6164-141-1, Semantic Aspects of Interoperable GIS

48. **Zhang Xiangmin** (1998), 90-6164-144-6, Coal fires in Northwest China: detection, monitoring and prediction using remote sensing data

49. **Gens, R.** (1998), 90-6164-155-1, Quality assessment of SAR interferometric data

50. **Turkstra, J.** (1998), 90-6164-147-0, Urban development and geographical information: spatial and temporal patterns of urban development and land values using integrated geo-data, Villaviciencia, Colombia

51. **Cassells, C.** (1998), 90-6164-234-5, Thermal modelling of underground coal fires in northern China

52. **Naseri, M.** (1998), 90-6164-195-0, Characterization of Salt-affected Soils for Modelling Sustainable Land Management in Semi-arid Environment: a case study in the Gorgan Region, Northeast, Iran

53. **Gorte B.G.H.** (1998), 90-6164-157-8, Probabilistic Segmentation of Remotely Sensed Images

54. **Tegaye, Tenalem Ayenew** (1998), 90-6164-158-6, The hydrological system of the lake district basin, central main Ethiopian rift

55. **Wang Donggen** (1998), 90-6864-551-7, Conjoint approaches to developing activity-based models

56. **Bastidas de Calderon, M.** (1998), 90-6164-193-4, Environmental fragility and vulnerability of Amazonian landscapes and ecosystems in the middle Orinoco river basin, Venezuela

57. **Moameni, A.** (1999), Soil quality changes under long-term wheat cultivation in the Marvdasht plain, South-Central Iran

58. **Groenigen, J.W. van** (1999), 90-6164-156-X, Constrained optimisation of spatial sampling: a geostatistical approach

59. **Cheng Tao** (1999), 90-6164-164-0, A process-oriented data model for fuzzy spatial objects
60. **Wolski, Piotr** (1999), 90-6164-165-9, Application of reservoir modelling to hydrotopes identified by remote sensing
61. **Acharya, B.** (1999), 90-6164-168-3, Forest biodiversity assessment: A spatial analysis of tree species diversity in Nepal
62. **Akbar Abkar, Ali** (1999), 90-6164-169-1, Likelihood-based segmentation and classification of remotely sensed images
63. **Yanuariadi, T.** (1999), 90-5808-082-X, Sustainable Land Allocation: GIS-based decision support for industrial forest plantation development in Indonesia
64. **Abu Bakr**, **Mohamed** (1999), 90-6164-170-5, An Integrated Agro-Economic and Agro-Ecological Framework for Land Use Planning and Policy Analysis
65. **Eleveld, M.** (1999), 90-6461-166-7, Exploring coastal morphodynamics of Ameland (The Netherlands) with remote sensing monitoring techniques and dynamic modelling in GIS
66. **Yang Hong** (1999), 90-6164-172-1, Imaging Spectrometry for Hydrocarbon Microseepage
67. **Mainam, Félix** (1999), 90-6164-179-9, Modelling soil erodibility in the semiarid zone of Cameroon
68. **Bakr, Mahmoud** (2000), 90-6164-176-4, A Stochastic Inverse-Management Approach to Groundwater Quality
69. **Zlatanova, Z.** (2000), 90-6164-178-0, 3D GIS for Urban Development
70. **Ottichilo, Wilber K.** (2000), 90-5808-197-4, Wildlife Dynamics: An Analysis of Change in the Masai Mara Ecosystem
71. **Kaymakci, Nuri** (2000), 90-6164-181-0, Tectono-stratigraphical Evolution of the Cankori Basin (Central Anatolia, Turkey)
72. **Gonzalez, Rhodora** (2000), 90-5808-246-6, Platforms and Terraces: Bridging participation and GIS in joint-learning for watershed management with the Ifugaos of the Philippines
73. **Schetselaar, Ernst** (2000), 90-6164-180-2, Integrated analyses of granite-gneiss terrain from field and multisource remotely sensed data. A case study from the Canadian Shield
74. **Mesgari, Saadi** (2000), 90-3651-511-4, Topological Cell-Tuple Structure for Three-Dimensional Spatial Data
75. **Bie, Cees A.J.M. de** (2000), 90-5808-253-9, Comparative Performance Analysis of Agro-Ecosystems
76. **Khaemba, Wilson M**. (2000), 90-5808-280-6, Spatial Statistics for Natural Resource Management
77. **Shrestha, Dhruba** (2000), 90-6164-189-6, Aspects of erosion and sedimentation in the Nepalese Himalaya: highland-lowland relations
78. **Asadi Haroni, Hooshang** (2000), 90-6164-185-3, The Zarshuran Gold Deposit Model Applied in a Mineral Exploration GIS in Iran
79. **Raza, Ale** (2001), 90-3651-540-8, Object-oriented Temporal GIS for Urban Applications
80. **Farah, Hussein** (2001), 90-5808-331-4, Estimation of regional evaporation under different weather conditions from satellite and meteorological data. A case study in the Naivasha Basin, Kenya

81. **Zheng**, **Ding** (2001), 90-6164-190-X, A Neural - Fuzzy Approach to Linguistic Knowledge Acquisition and Assessment in Spatial Decision Making

82. **Sahu, B.K.** (2001), Aeromagnetics of continental areas flanking the Indian Ocean; with implications for geological correlation and reassembly of Central Gondwana

83. **Alfestawi, Y.** (2001), 90-6164-198-5, The structural, paleogeographical and hydrocarbon systems analysis of the Ghadamis and Murzuq Basins, West Libya, with emphasis on their relation to the intervening Al Qarqaf Arch

84. **Liu, Xuehua** (2001), 90-5808-496-5, Mapping and Modelling the Habitat of Giant Pandas in Foping Nature Reserve, China

85. **Oindo, Boniface Oluoch** (2001), 90-5808-495-7, Spatial Patterns of Species Diversity in Kenya

86. **Carranza, Emmanuel John** (2002), 90-6164-203-5, Geologically-constrained Mineral Potential Mapping

87. **Rugege, Denis** (2002), 90-5808-584-8, Regional Analysis of Maize-Based Land Use Systems for Early Warning Applications

88. **Liu, Yaolin** (2002), 90-5808-648-8, Categorical Database Generalization in GIS

89. **Ogao, Patrick** (2002), 90-6164-206-X, Exploratory Visualization of Temporal Geospatial Data using Animation

90. **Abadi, Abdulbaset M.** (2002), 90-6164-205-1, Tectonics of the Sirt Basin – Inferences from tectonic subsidence analysis, stress inversion and gravity modelling

91. **Geneletti, Davide** (2002), 90-5383-831-7, Ecological Evaluation for Environmental Impact Assessment

92. **Sedogo, Laurent G.** (2002), 90-5808-751-4, Integration of Participatory Local and Regional Planning for Resources Management using Remote Sensing and GIS

93. **Montoya, Lorena** (2002), 90-6164-208-6, Urban Disaster Management: a case study of earthquake risk assessment in Carthago, Costa Rica

94. **Ahmad, Mobin-ud-Din** (2002), 90-5808-761-1, Estimation of Net Groundwater Use in Irrigated River Basins using Geo-information Techniques: A case study in Rechna Doab, Pakistan

95. **Said, Mohammed Yahya** (2003), 90-5808-794-8, Multiscale perspectives of species richness in East Africa

96. **Schmidt, Karin** (2003), 90-5808-830-8, Hyperspectral Remote Sensing of Vegetation Species Distribution in a Saltmarsh

97. **Lopez Binnquist, Citlalli** (2003), 90-3651-900-4, The Endurance of Mexican Amate Paper: Exploring Additional Dimensions to the Sustainable Development Concept

98. **Huang, Zhengdong** (2003), 90-6164-211-6, Data Integration for Urban Transport Planning

99. **Cheng, Jianquan** (2003), 90-6164-212-4, Modelling Spatial and Temporal Urban Growth

100. **Campos dos Santos, Jose Laurindo** (2003), 90-6164-214-0, A Biodiversity Information System in an Open Data/Metadatabase Architecture

101. **Hengl, Tomislav** (2003), 90-5808-896-0, PEDOMETRIC MAPPING, Bridging the gaps between conventional and pedometric approaches
102. **Barrera Bassols, Narciso (**2003), 90-6164-217-5, Symbolism, Knowledge and management of Soil and Land Resources in Indigenous Communities: Ethnopedology at Global, Regional and Local Scales
103. **Zhan, Qingming** (2003), 90-5808-917-7, A Hierarchical Object-Based Approach for Urban Land-Use Classification from Remote Sensing Data
104. **Daag, Arturo S.** (2003), 90-6164-218-3, Modelling the Erosion of Pyroclastic Flow Deposits and the Occurrences of Lahars at Mt. Pinatubo, Philippines
105. **Bacic, Ivan** (2003), 90-5808-902-9, Demand-driven Land Evaluation with case studies in Santa Catarina, Brazil
106. **Murwira, Amon** (2003), 90-5808-951-7, Scale matters! A new approach to quantify spatial heterogeneity for predicting the distribution of wildlife
107. **Mazvimavi, Dominic** (2003), 90-5808-950-9, Estimation of Flow Characteristics of Ungauged Catchments. A case study in Zimbabwe
108. **Tang, Xinming** (2004), 90-6164-220-5, Spatial Object Modelling in Fuzzy Topological Spaces with Applications to Land Cover Change
109. **Kariuki, Patrick** (2004), 90-6164-221-3, Spectroscopy and Swelling Soils; an integrated approach
110. **Morales, Javier** (2004), 90-6164-222-1, Model Driven Methodology for the Design of Geo-information Services
111. **Mutanga, Onisimo** (2004), 90-5808-981-9, Hyperspectral Remote Sensing of Tropical Grass Quality and Quantity
112. **Šliužas, Ričardas V.** (2004), 90-6164-223-X, Managing Informal Settlements: a study using geo-information in Dar es Salaam, Tanzania
113. **Lucieer, Arko** (2004), 90-6164-225-6, Uncertainties in Segmentation and their Visualisation
114. **Corsi, Fabio** (2004), 90-8504-090-6, Applications of existing biodiversity information: Capacity to support decision-making
115. **Tuladhar, Arbind** (2004), 90-6164-224-8, Parcel-based Geo-information System: Concepts and Guidelines
116. **Elzakker, Corné van** (2004), 90-6809-365-7, The use of maps in the exploration of geographic data
117. **Nidumolu, Uday Bhaskar** (2004), 90-8504-138-4, Integrating Geo-information models with participatory approaches: applications in land use analysis
118. **Koua, Etien L.** (2005), 90-6164-229-9, Computational and Visual Support for Exploratory Geovisualization and Knowledge Construction
119. **Blok, Connie A.** (2005), Dynamic visualization variables in animation to support monitoring of spatial phenomena
120. **Meratnia, Nirvana** (2005), 90-365-2152-1, Towards Database Support for Moving Object Data
121. **Yemefack, Martin** (2005), 90-6164-233-7, Modelling and monitoring Soil and Land Use Dynamics within Shifting Agricultural Landscape Mosaic Systems
122. **Kheirkhah, Masoud** (2005), 90-8504-256-9, Decision support system for floodwater spreading site selection in Iran
123. **Nangendo, Grace** (2005), 90-8504-200-3, Changing forest-woodland-savanna mosaics in Uganda: with implications for conservation

124. **Mohamed, Yasir Abbas** (2005), 04-15-38483-4, The Nile Hydroclimatology: impact of the Sudd wetland (Distinction)
125. **Duker, Alfred, A.** (2005), 90-8504-243-7, Spatial analysis of factors implicated in *mycobacterium ulcerans* infection in Ghana
126. **Ferwerda, Jelle, G.,** (2005), 90-8504-209-7, Charting the Quality of Forage: Measuring and mapping the variation of chemical components in foliage with hyperspectral remote sensing
127. **Martinez, Javier** (2005), 90-6164-235-3, Monitoring intra-urban inequalities with GIS-based indicators. With a case study in Rosario, Argentina
128. **Saavedra, Carlos** (2005), 90-8504-289-5, Estimating spatial patterns of soil erosion and deposition in the Andean region using Geo-information techniques. A case study in Cochabamba, Bolivia
129. **Vaiphasa, Chaichoke** (2006), 90-8504-353-0, Remote Sensing Techniques for Mangrove Mapping
130. **Porwal, Alok** (2006), 90-6164-240-X, Mineral Potential Mapping with Mathematical Geological Models
131. **Werff, Harald van der** (2006), 90-6164-238-8, Knowledge-based remote sensing of complex objects: recognition of spectral and spatial patterns resulting from natural hydrocarbon seepages
132. **Vlag, Daniël van de** (2006), 90-8504-384-0, Modeling and visualizing dynamic landscape objects and their qualities
133. **Joshi, Chudamani** (2006), 90-8504-470-7, Mapping cryptic invaders and invisibility of tropical forest ecosystems: *Chromolaena odorata* in Nepal
134. **Bandara, K.M.P.S.** (2006), 90-8504-406-5, Assessing irrigation performance by using remote sensing
135. **Dilo, Areti** (2006), 90-8504-461-8, Representation of and Reasoning with Vagueness in Spatial Information. A system for handling vague objects
136. **Debba, Pravesh** (2006), 90-8504-462-6, Sampling scheme optimization from hyperspectral data
137. **Huisman, Marco** (2006), 90-6164-246-9, Assessment of rock mass decay in artificial slopes
138. **Lemmens, Rob** (2006), 90-6164-250-7, Semantic interoperability of distributed geo-services
139. **Chacón Moreno, Eulogio** (2007), 90-8504-559-2, Ecological and spatial modeling: Mapping ecosystems, landscape changes, and plant species distribution in Llanos del Orinoco, Venezuela